A study of chemokine receptors and the immunological synapse

Richard Mark Robert Kasprowicz

PhD

University of York

Biology

February 2014

Abstract

Chemokine receptors play a central role in directing leukocytes to various tissues around the body by recognising chemotactic cues called chemokines. Upon entry into a tissue, infiltrating leukocytes from the blood stream encounter tissue resident cells, and in the case of T lymphocytes scan antigen presenting cells (APCs). Following antigen recognition, signalling components can be recruited into micro-scale domains at the interface of the APC-T cell conjugate, forming a structure known as the immunological synapse (IS). The chemokine receptors CCR5 and CXCR4 have been implicated in promoting IS formation through their recruitment to the T cell side of human APC-T cell interfaces. However, this is based primarily on studies with immortalized cell lines transfected with GFP-tagged chemokine receptors and does not take into account what happens on the APC side of the IS. Hence, the behaviour of endogenous CXCR4 and CCR5 during the formation of IS between primary T cells and APCs needs to be clarified.

Live cell microscopy and flow cytometry were employed to examine a previously uncharacterised macrophage-CD4+ T cell IS, formed *in vitro* between primary human blood isolated T cells and monocyte-derived macrophages (MDMs) pulsed with a superantigen (sAg). Under these conditions, MDM-CD4+ T cell conjugates displayed elevated T cell intracellular calcium responses. A fraction of these conjugates showed T cell receptor capping as well as ICAM1 and relocation of the Golgi apparatus towards the cell–cell interface, which suggests that the interactions between MDMs and CD4+ T cells lead to the formation of synapses and possibly kinapses.

Endogenous T cell surface CCR5 and CXCR4 molecules were found to cap at the MDM-CD4+ T cell IS, albeit infrequently. Yet, intracellular pools of T cell CCR5 receptors were consistently reported facing the IS interface and showed partial overlap with a marker of the *trans*-Golgi network, implying that intracellular CCR5 may translocate to the IS as a cargo in the Golgi. In contrast, on MDMs, cell surface CCR5 did not accumulate at the IS interface. FRAP analysis revealed that CCR5 molecules are relatively mobile at the surface of MDMs, and that CCR5 movement is affected by depletion but not sequestration of membrane cholesterol. These findings suggested that the non-accumulation of MDM CCR5 at the IS interface was not due to the restriction of lateral movement. Importantly, this work highlights cell-type differences in the behaviour of endogenous CCR5 receptors.

This thesis brings new insights into the roles of endogenous chemokine receptors in human leukocytes during antigen-dependent interactions and informs future research aiming to bridge the gap between mouse and human systems to study immune synapses.

Table of contents

List of figures

List of tables

Acknowledgements

Firstly, I would like to thank my supervisor Nathalie Signoret for giving me this opportunity. I have learnt an incredible amount throughout this process, both personally and professionally, and I extend to you my heartfelt thanks for being so supportive and for pushing me to be the best that I can be.

I am grateful to my training committee, Peter O'Toole and Mark Coles, for their guidance and scientific advice. I would also like to thank past members of the Signoret Lab; James Fox for teaching me all the basics in the lab and to Laura Bennett for helping me to become more organised.

I would like to thank all of the Imaging and Cytometry team at York for their assistance and training. In particular, I am indebted to Peter O'Toole for making this work possible on so many levels. I would also like to thank Jo Marrison and Ian Morrison for helping me get maximum sensitivity from the LSM780 and for putting up with my nagging to switch the hardware around every few weeks!

Thank you to everyone at the CII, for many stimulating discussions and for loaning me reagents. Many thanks in particular to Paul Pryor for your encouragement and cloning advice. I am much obliged to the Evans lab for allowing me to use their microscope to perform the calcium imaging study. I would also like to thank Julie Wilson for her programming and mathematical expertise in helping me to analyse my data.

I would like to thank my family and friends who have been immensely supportive, particularly my parents for your patience and understanding. Last, but certainly not least, to my fiancée Rowena for standing by me, and sometimes even for me, during this process. Only you will ever know what it has been. I am eternally grateful for all you have done.

Author’s declaration

All data presented in this thesis is original. All the work presented here was performed by Richard Kasprowicz, with the following exceptions: Appendix 1, which is a c script for piecewise linear regression written by Dr J. Wilson for this study (University of York, York, UK); data in Technical Appendix 1 & 2 in Chapter 5, which was acquired with the help of Sam Godden (MScBT).

Chapter 1: Introduction

1.1 The Chemokine System

1.1.1 Nomenclature and grouping

Chemokine receptors are members of the seven-transmembrane (7TM) receptor superfamily of G protein coupled receptors (GPCRs), which function to coordinate leukocyte trafficking. The chemokine ligands bound by these receptors are small proteins, mostly 70–80 amino acids in length (8–12 kDa), defined by a tertiary structure that is stabilised by disulphide bonds between key cysteine residues (Allen et al., 2007; Bachelerie et al., 2013). According to the number and position of N-terminal cysteine residues each chemokine is assigned to one of four major groups, termed C, CC, CXC and CX3C. Chemokine receptor nomenclature is reflective of this since receptors are generally restricted to binding chemokines from a particular group (Bachelerie et al., 2013). For example, the receptor CCR5 binds chemokine ligands belonging to the CC group and has been designated the number '5' for identification purposes. To date, 24 different chemokine receptors have been classified, including six atypical receptors (Bachelerie et al., 2013). Yet chemokines are far more numerous, meaning that the majority of chemokine receptors are promiscuous with regard to chemokine binding. This should not be interpreted as redundancy as even closely-related chemokines can have different agonistic effects on receptor function (Rot and von Andrian, 2004). Unrelated to their structurally-derived nomenclature, chemokines are also broadly categorised according to their function into inflammatory or homeostatic groups, which bind inducible or constitutively expressed receptors, respectively (Johnson et al., 2005). Experimentation in the present study concerns the inflammatory chemokine receptor CCR5 in particular and also the homeostatic chemokine receptor CXCR4.

1.1.2 Ligand-stimulated initiation of chemokine receptor signalling

1.1.2.1 Chemokine receptor structure

Chemokine receptors are proteins of 340–380 amino acids, which exist as 7TM helices arranged in a bundle connected by three extracellular loops (ECLs) and three intracellular loops (ICLs). The second ICL contains the DRY motif implicated in G protein binding that is conserved amongst all but the atypical chemokine receptors (Allen et al., 2007). The N-terminus is extracellular whilst the C-terminus is intracellular, and in the case of CCR5 contains cysteine residues, which can be palmitoylated to form an additional loop

(Oppermann, 2004) (**Fig.1.1**). In contrast, a consensus palmitoylation sequence is lacking in CXCR4 (Bachelerie et al., 2013). The crystal structures of CCR5 in complex with the human immunodeficiency virus (HIV)-entry inhibitor Maraviroc (residues 19–313; modifications: C-terminal truncation from F320; 54 residues of rubredoxin inserted into ICL3 between R223 and G227; point mutations, C58Y, G163N, A233D and K303E) and CXCR4 in complex with small molecule and cyclic peptide antagonists (residues 27–352; modifications: 160 residues of T4 lysozyme inserted into ICL3; point mutations, L125W) have been determined (Tan et al., 2013; Wu et al., 2010).

1.1.2.2 Chemokine binding

Chemokines comprise of an N-terminal region followed by a core domain comprised of an N-loop, a 3_{10} helix, a three-stranded β-sheet terminating in a C-terminal α-helix (Allen et al., 2007). Initial docking is mediated mostly by ionic interactions of the chemokine core domain with the receptor ECLs and N-terminus (Allen et al., 2007; Scholten et al., 2012). Distinct residues are critical for binding of different chemokines to ECL regions that often overlap, as demonstrated for CCR5 through the generation of systematic point mutations, which revealed that different amino acids of ECL2 are responsible for CCL3 and CCL5 binding (Blanpain et al., 2003). Following the initial docking step, concerted action of the receptor N-terminal domain and ECLs coordinate the chemokine N-terminus to interact with residues in the receptor transmembrane helical bundle (Allen et al., 2007; Blanpain et al., 2003; Scholten et al., 2012). As the intimate positioning implies, the N-terminal region of chemokines has been found to be critical in inducing chemokine receptor signalling (Allen et al., 2007). This is exemplified by deletion of the first eight N-terminal amino acids of CCL5, which ablates chemotaxis and calcium signalling in a monocytic cell line (Gong et al., 1996). Furthermore, addition of a methionine residue to the N-terminus of CCL5 was shown to induce a weak calcium signal and slow internalization, which is consistent with partial agonist activity, but led to functional antagonism (Mack et al., 1998; Proudfoot et al., 1999). Since then numerous other chemical modifications have been made to the N-terminal region of CCL5 to generate more potent functional antagonists (Gaertner et al., 2008), which highlight how the chemokine N-terminus contributes to the potency and regulation of signal transduction.

Chemokine binding stabilises a conformational arrangement of the transmembrane helices of the receptor, which enables signal transduction across the plasma membrane (PM) by permitting binding of intracellular machinery such as G proteins or kinases (Berro et al., 2013; Springael et al., 2007). However chemokine receptor coupling to G proteins can reciprocally influence the chemokine binding. Allosteric binding of different proteins

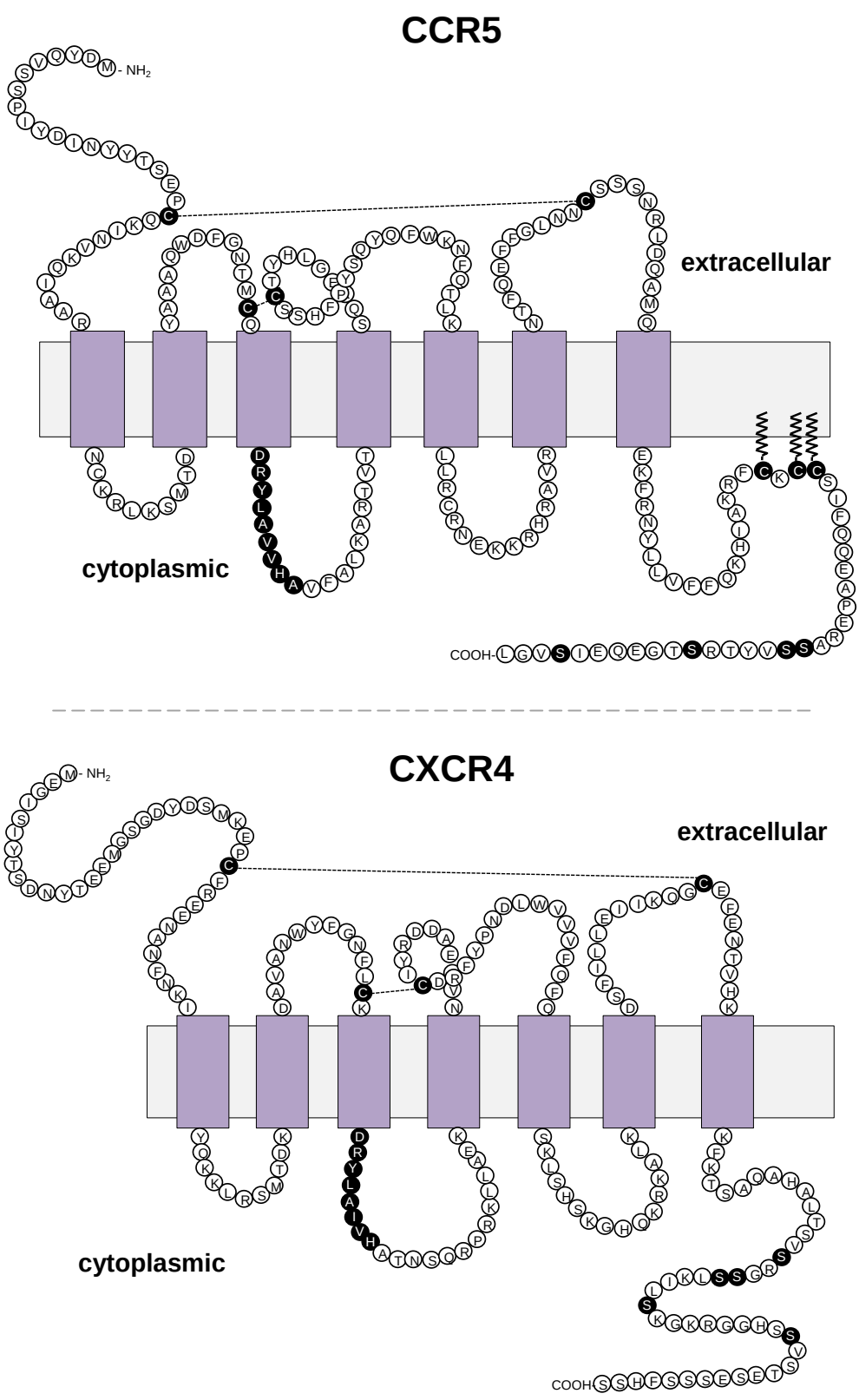

Figure 1.1: Schematic of major features of CCR5 and CXCR4. The diagram shows the single letter protein codes for the loops as well as the N- and C- terminal segments. Transmembrane regions are represented by purple boxes. Palmitoylated cysteine resides are shown bound to the membrane with a wavy line. Disulphide bonds are represented by dotted lines. The DRY motif responsible for G protein binding is highlighted, as are serine residues that have previously been reported to be phosphorylated in the C terminal tails. Adapted and based on diagrams and data from previous studies (Alkhatib, 2009; Busillo et al., 2010; Jähnichen et al., 2010).

away from the endogenous chemokine binding site contributes to the range of conformational arrangements of the receptor (Langmead and Christopoulos, 2014). Indeed, G proteins themselves are archetypal allosteric modulators and have been shown to modulate the chemokine-binding affinity of CCR5 (Colin et al., 2013). Colin et al. (2013) showed a vastly lower affinity of CCR5 for CCL3 when coupled to G proteins locked in nucleotide-bound forms by using non-hydrolysable forms of guanosine triphosphate (GTP) or pertussis toxin (PTX). Thus within the range of conformational forms available for a given chemokine receptor, particular forms can display partiality to chemokine binding (**Fig. 1.2a**).

1.1.2.3 Initiating downstream responses

Chemokine-bound receptors become coupled to G proteins that consist of three different subunits, designated α, β and γ. The exceptions to this rule are the atypical chemokine receptors, which signal via G protein independent mechanisms (Bachelerie et al., 2013). Different isoforms of the α-subunits exist and heterotrimeric G proteins are identified by the form of Gα that they possess. Use of PTX, which specifically ribosylates the $G\alpha_i$ subunit, has led to the finding that chemokine receptors primarily couple to G_i proteins in haematopoietic cells (Berro et al., 2013; Thelen and Stein, 2008). Nevertheless coupling to G proteins other than G_i may be important in functions related to antigen presentation. Coupling of CCR5 to G_q or G_{11} proteins has been suggested to promote adhesion between T cells and antigen presenting cells (APCs) during antigen-dependent interactions (Molon et al., 2005). Additionally, G_{13} dependent trafficking may promote CXCR4 heterodimerisation with the T cell receptor (TCR) (Kumar et al., 2011). Aberrant G proteins also participate in determining the directionality of cell migration and are triggered by HIV binding in order to mediate viral entry and cell-cell fusion (Harmon and Ratner, 2008; Rot and von Andrian, 2004; Thelen and Stein, 2008). Thus although coupling to G_i may be the *de facto* standard for chemokine receptors, the availability of other types of G protein acts to diversify the signalling functions of these receptors.

Despite the nomenclature focus on the α-subunit, leukocyte migration induced through G_i is primarily mediated through the βγ subunits, which dissociate from the stimulus receptor and $G\alpha_i$ when the latter binds GTP (**Fig. 1.2a**). The βγ subunits mediate actin polymerisation at the leading edge by initiating a cascade involving phosphatidylinositol 3-kinase (PI3K), protein kinapse B (PKB) and Rac but also act to trigger calcium signalling via interaction with phospholipase C (PLC)-β (Oppermann, 2004; Rot and von Andrian, 2004). This list is by no means exhaustive and the prevalence of components involved in signalling pathways that lead to actin polymerisation is often activation-status or cell type dependent (Thelen and Stein, 2008). Ultimately the balance of chemokine-induced

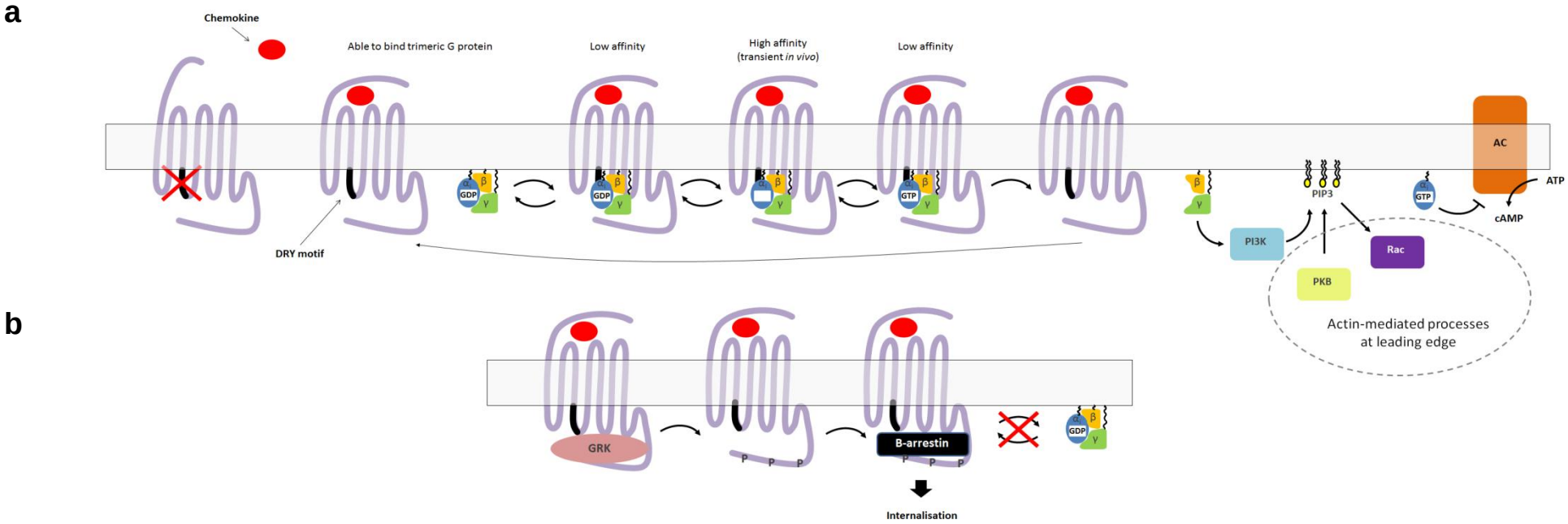

Figure 1.2: Turning signalling on or off in response to chemokine. (**a**) Signalling: Upon binding chemokines, chemokine receptors undergo conformational changes permitting heterotrimeric G protein binding. The GDP-bound Gα subunit binds to the DRY motif and coordinates the βγ subunits. It is important to realise that bound chemokine has both an on and off rate and in this state the receptor has a low affinity for bound chemokine. When GDP dissociates from the Gα subunit the receptor-G protein complex transits into a nucleotide-free state that has high affinity for the bound chemokine. GTP binding instigates a low affinity state that causes the Gα subunit, βγ subunits and receptor to dissociate (Chabre et al., 2009; Colin et al., 2013). The βγ subunits activate PI3Ks which generate PIP3. PIP3 acts as a docking site for PKB and activates members of the Rac family of small GTPases, both of which are involved in pathways nucleating actin polymerisation at pseudopodia (Rot and von Andrian, 2004). The GTP bound $G\alpha_i$ subunit acts to inhibit AC activity and the intrinsic GTPase activity of this subunit catalyses hydrolysis of GTP to GDP, in which form the Gα subunit re-associates with βγ subunits. (**b**) Desensitisation: Chemokine-bound receptor has a high affinity for GRK family members which phosphorylate the C-terminal tail of the receptor that causes steric inhibition of G protein activation. In turn, phosphorylated receptors have a high affinity for β-arrestin, which prevents further coupling to G proteins and act as a scaffold for receptor internalisation (Bennett et al., 2011; Rot and von Andrian, 2004). AC, Adenylate cyclase; GDP, guanosine diphosphate; GRK, G protein receptor kinase; GTP, guanosine triphosphate; PI3K, phosphatidylinositol 3-kinase; PIP3, phosphatidylinositol-3,4,5,-trisphosphate; PKB, protein kinase B.

signalling pathways acts to coordinate actin treadmilling at the leading edge, which is the primary physical mechanism behind leukocyte chemotaxis (Lammermann et al., 2008).

1.1.3 CCR5 regulation within the plasma membrane

Two regions of the C-terminal tail of CCR5 are required for CCR5 to reach the PM. The first is a string of basic residues (-KHIAKRF-) (Venkatesan et al., 2001), which are located N-terminally to the second key region consisting of three cysteine residues (-CKCC-) (Oppermann, 2004). These three cysteine residues have been shown to be palmitoylated and in the absence of this post-translational modification the expression of CCR5 at the PM is vastly reduced. This effect is mediated, in part, by increased receptor degradation as CCR5 demonstrates a much shorter half-life when palmitoylation is prevented (Percherancier et al., 2001). Furthermore palmitoylation plays a critical role in the mobility of CCR5 in the ER, which implies that this lipid modification may also be important in conferring lateral mobility of CCR5 at the PM (Blanpain et al., 2001).

Palmitoylation of integral membrane proteins has been reported to be necessary but not sufficient for association with lipid rafts (Levental et al., 2010). In fact, a previous study suggested that palmitoylation of CCR5 localises the receptor to lipid rafts (Venkatesan et al., 2003). Since certain families of G proteins have been proposed to be enriched in lipid rafts (Oh and Schnitzer, 2001), localisation to these dynamic domains may enhance the signalling function of CCR5. Indeed although palmitoylation deficient mutants continue to bind chemokine ligands with a high affinity and maintain the ability to signal, the duration of the functional response is reduced (Blanpain et al., 2001; Venkatesan et al., 2001). Perhaps the absence of palmitoylation, which is associated with decreased raft affinity (Levental et al., 2010), results in reduced stability of CCR5 clustering into raft signalling domains and thus a shortened functional response.

A parallel stream of evidence exists implicating cholesterol, which is enriched in lipid rafts, in CCR5 signalling. In contrast to the palmitoylation deficient CCR5, binding of CCL4 was found to be inhibited upon cholesterol extraction (Nguyen and Taub, 2002). This was thought to be due to a requirement of membrane cholesterol to enable conformations of CCR5 necessary for ligand binding (Signoret et al., 2005). As expected Nguyen and Taub (2002) found that calcium signalling after cholesterol extraction was negligible, however Cardaba et al (2008) employed a different cholesterol extracting agent and found that calcium signalling was reduced but not ablated. Moreover cholesterol extraction prevented ligand-induced G protein inhibition of adenylate cyclase (AC) and enabled calcium signalling to occur in the presence of PTX (Cardaba et al., 2008). This implies that the presence of membrane cholesterol may regulate the interactions of chemokine receptors

with G proteins and merits further investigations into the functions of rafts in CCR5 signalling.

Recently it has been proposed that the signalling-active conformation of CCR5 is associated with cholesterol whereas the signalling-inactive conformation is cholesterol independent (Berro et al., 2011). These forms have different affinities for an inhibitor of HIV, which is a property related to the G protein coupling ability of the receptors. Non-resistant strains of HIV preferentially bind the G protein- and cholesterol-independent form (Berro et al., 2011; Berro et al., 2013). This is consistent with the lack, or minor effect, of preventing palmitoylation on HIV entry and the notion that palmitoylation may promote raft coalescence.

1.1.4 Turning off signalling

In order to prevent inappropriate stimulation of leukocytes, chemokine-induced signalling is terminated by the process of chemokine receptor desensitization. When a particular receptor is acted upon directly by an agonist this is termed homologous desensitization (Kelly et al., 2008). The C-terminal region of chemokine receptors become phosphorylated by a member of the G protein receptor kinase (GRK) family within seconds to minutes of chemokine binding (Oppermann, 2004). CCR5 has four serine residues phosphorylated but only two are required for β-arrestin binding. Ser^{337} found to be specifically phosphorylated by protein kinase C (PKC), which may represent a negative feedback mechanism downstream of PLCβ activation, whilst phosphorylation of Ser^{349} is GRK specific (Oppermann, 2004). CXCR4 has more C-terminal serine phosphorylation sites than CCR5 (Busillo et al., 2010). Yet in similarity to CCR5 PKC is also employed to rapidly phosphorylate sites ($Ser^{324/5}$) on this receptor, although these sites may be targeted by the ubiquitination machinery their impact upon ligand-induced internalisation of CXCR4 is controversial (Busillo et al., 2010; Signoret et al., 1998). The phosphorylated form of the receptor has a high affinity for β-arrestin, which binds and targets chemokine receptors for internalisation (**Fig. 2.1b**) (Bennett et al., 2011). Ultimately this results in a decrease of the amount of chemokine receptor available at the cell surface for the chemokine to bind. Note however that GRK and β-arrestin binding to chemokine receptors also have other actions as differential usage has been shown to positively or negatively influence downstream signalling events (Busillo et al., 2010; Gurevich and Gurevich, 2008).

1.1.5 Staging a return: an inside job

Chemokine receptors internalise predominantly by clathrin or caveolin dependent mechanisms. Depending on the cell type and on the duration of stimulus, internalised receptors may follow a number of different trafficking pathways (Bennett et al., 2011).

Specifically, CCR5 undergoes clathrin-dependent internalisation in response to CCL5 stimulation and resides in recycling endosomes (REs) alongside transferrin receptor (TfR) before returning to the PM in a resensitised form (Mack et al., 1998; Signoret et al., 2005; Signoret et al., 2000). During trafficking CCR5 is dephosphorylated but can remain chemokine-bound (Signoret et al., 2000), meaning that the receptor may already be in a state able to engage G proteins or GRK once more at the PM (**Fig. 1.1**). Each CCR5 molecule may be desensitized/ internalised several times before the chemokine dissociates or is degraded (Oppermann, 2004; Signoret et al., 2000). However, the trafficking pathway is altered upon prolonged treatment of CCL5 or stimulation with an N-terminally modified form of CCL5 (archaic name: regulated and normal T cell expressed and secreted (RANTES)) called Nα-(n-nonanoyl)-des-Ser1-[l-thioproline2, l-α-cyclohexyl-glycine3] (PSC)-RANTES, which interacts more durably with CCR5 than the native chemokine (Escola et al., 2010). Indeed, Escola et al. (2010) reported that CCR5 only transiently resides in transferrin-containing REs before continuing to the *trans*-Golgi network (TGN). Under conditions of sustained agonist stimulation return from the TGN to the PM is the rate limiting step forming a 'molecular bottleneck' for CCR5 (Escola et al., 2010).

Although chemokine receptor internalisation is generally considered to be agonist dependent, CXCR4 also undergoes constitutive internalisation in similarity to the atypical receptor ACKR2 (D6) (Borroni et al., 2010). Both ligand-stimulated and constitutive endocytosis are thought to occur through a clathrin-dependent route (Signoret et al., 1997; Tarasova et al., 1998). However unlike CCR5, which recycles at a high efficiency, less than a third of CXCR4 recycles back to the PM after chemokine stimulation. Instead the majority of CXCR4 traffics through endosomal compartments and is sentenced for lysosomal degradation mediated through an ubiquitin-dependent process (Borroni et al., 2010; Tarasova et al., 1998). Juxtaposing the trafficking systems of CCR5 and CXCR4 is useful to exemplify the great diversity of internalisation routes and mechanisms adopted by chemokine receptors to control expression at the cell surface.

1.1.6 CCR5 and CXCR4 expression on leukocytes

1.1.6.1 T cell expression of CCR5

Lymphocyte expression of CCR5 is often sensitive to antigen experience. For example CCR5 is not typically expressed on naïve T cells, which by definition have not experienced antigen, but is known to be expressed on effector and memory cells (Bleul et al., 1997; Bromley et al., 2008; Groot et al., 2006; Sallusto et al., 2004). Often the expression of CCR5 on CD4+ T cells is associated with the T helper (Th)-1 phenotype,

which is typified by interferon-γ (IFNγ) production and orchestrates a response to intracellular microorganisms (Bromley et al., 2008; Murphy et al., 2011). However CCR5 has also been found to be expressed alongside other chemokine receptors that are often associated with the Th2 phenotype (e.g. CCR4), which is typified by interleukin (IL)-4/ IL-13 secretion and is involved in immune responses to parasites and in allergy (Bromley et al., 2008). Moreover, Th17 cells have also been reported to coexpress CCR5 and CCR4 (Lim et al., 2008), which warns against identification of Th subsets based on chemokine receptor profiles alone.

For CD4+ T memory cells, CCR5 expression predominates on the effector memory (T_{EM}) cells, which migrate through peripheral tissues and are primed to exert effector function. In contrast, central memory (T_{CM}) CD4+ T cells do not express CCR5 and circulate through lymphoid tissue in a state that is primed to respond to antigen, after which they differentiate into effector cells (Sallusto et al., 2004). Thus CD4+ T cells expressing CCR5 can predominantly be found in the peripheral tissues. However evidence exists that the same is not necessarily the case for CD8+ T cells. In fact, naïve CD8+ T cells were found to upregulate CCR5 expression via a mechanism that did not involve triggering the TCR and were shown to traffic to lymph nodes (LNs) in a CCR5 dependent manner (Castellino et al., 2006). Yet Castellino et al. (2006) also noted the effects of TCR stimulation on CCR5 expression in CD4+ and CD8+ T cells, showing that CD4+ T cell CCR5 expression was dependent upon TCR engagement and that CCR5 expression levels on CD8+ T cells were enhanced in the presence of cognate antigen. Additionally, since CCR5 is expressed on both CD8+ T_{EM} and T_{CM} populations (Sallusto et al., 2004) it is likely that CD8+ T cells expressing CCR5 may be found in both peripheral and lymphoid sites. In general, T cells that express CCR5 have previously undergone antigen-specific activation involving TCR signalling.

One of the cytokines that promotes T cell growth and proliferation, and as such an activated phenotype, is IL-2. IL-2 has a reciprocal relationship with CCR5 as it has been shown to upregulate CD4+ T cell CCR5 expression *in vivo* (Bleul et al., 1997; Weissman et al., 2000). In turn CCR5 expression increases the production of IL-2 through a positive feedback loop (Camargo et al., 2009). This is not to say however that T cell CCR5 is expressed under all activation conditions, in fact CCR5 expression levels actually decrease upon activation with CD3/CD28 beads *in vitro* (Richardson et al., 2012). Part of this latter phenomenon is mediated by local T cell secretion of CC (β-) chemokines, for example CCL3/4/5, which are then able to act in an autocrine fashion to downmodulate CCR5 from the cell surface, as described in section 1.1.4. Considered together this evidences that CCR5 expression can be enhanced by soluble factors induced in response to antigen-dependent signalling (e.g. IL-2), and highlights that chemokine receptor

expression in general is tightly regulated by the presence of chemokines in the local microenvironment.

1.1.6.2 T cell expression of CXCR4

CXCR4 is critical to survival in mice as knockouts of the receptor or its sole ligand CXCL12 prove to be lethal (Bachelerie et al., 2013). This receptor has widespread functions in haematopoiesis and development, and is thought to be important for T cell maturation in the thymus (Murdoch, 2000). CXCR4 is widely expressed on naïve T cells (Bleul et al., 1997; Bromley et al., 2008) as well as antigen-experienced T cells such as memory, Th1, Th2 and Th17 subsets (Murdoch, 2000; Viola and Luster, 2008). Although entry into secondary lymphoid organs is primarily coordinated by CCR7 on naïve T cells, memory T cell extravasation into lymphoid organs may involve CXCR4 (Viola and Luster, 2008). Together this suggests that, in contrast to CCR5, T cells expressing CXCR4 are found in both lymphoid and peripheral sites. However, because of the CCR5 expression profile the most likely region of CD4+ T cell CXCR4 and CCR5 co-expression is in the periphery. Nonetheless, since naïve T cells generally express high levels of CXCR4 it is tempting to speculate that the CCR5+ naïve T cells observed by Castellino et al. (2006) may undergo antigen-specific engagement whilst co-expressing CCR5 and CXCR4. These chemokine receptors have previously been suggested to play a coordinated role in promoting adhesion between specific antigen dependent cell-cell junctions (Molon et al., 2005).

With regards to CXCR4 expression after TCR engagement, it has been reported that CXCR4 promoter usage increases after anti-CD3/CD28 ligation (Moriuchi et al., 1997). This corroborates results showing an increase in CXCR4 expression due to T cell activation by the mitogen phyohaemaggutinin (PHA) (Bleul et al., 1997). Yet somewhat paradoxically, another study found that T cell surface CXCR4 expression decreases rapidly upon stimulation with PHA, anti-CD3, or staphylococcal enterotoxin A (SEA) (Bermejo et al., 1998). These studies demonstrate that antigen stimulation clearly has the capacity to induce changes in CXCR4 expression. Perhaps the differential regulation of CXCR4 by mitogen stimulation observed could be explained by differences in cell density between the two studies, which may result in different levels of autocrine stimulation by cytokines such as IL-2. Indeed, the levels of CXCR4 expression can be regulated by increased exposure to cytokines such IL-2, IL-4 and IL-10 and decreased by inflammatory cytokines such as IFNγ (Busillo and Benovic, 2007). However this roundup of the differential effects of groups of cytokines on CXCR4 may be an oversimplification. As an example, IL-10 was reported to increase CXCR4 expression on MDMs (Wang et al., 2001), but was previously observed to decrease CXCR4 expression on CD4+ T cells

(Jinquan et al., 2000). Thus cell-type dependent differences are likely to be of importance in determining how CXCR4 expression is regulated by cytokines.

1.1.6.3 CCR5 and CXCR4 expression on macrophages

In human tissue, macrophages that are present in numerous different anatomical locations, including vaginal macrophages, alveolar macrophages and microglial cells have been shown to express CCR5 and CXCR4 (Albright et al., 1999; Opalek et al., 2007; Shen et al., 2009). In contrast, very little CCR5 or CXCR4 expression occurs on intestinal macrophages, indicating that the expression of CCR5 on macrophages can be regulated by the tissue environment (Shen et al., 2009). In support of this idea, when MDMs during differentiation, but not after, were exposed to media conditioned by intestinal stromal cells the levels of CCR5 were dramatically reduced (Shen et al., 2011).

With regard to *in vitro* culture, differentiation of MDMs in the presence of macrophage colony-stimulating factor (M-CSF) or granulocyte-macrophage colony stimulating factor (GM-CSF) has been reported to increase CCR5 cell surface expression. However, the increase is far greater in the presence of M-CSF (Herbein and Varin, 2010; Lee et al., 1999b). In contrast, culture of MDMs in the presence of GM-CSF has been found to reduce CXCR4 levels via an arrestin-dependent mechanism (Lee et al., 1999b; Wang et al., 2001). Other factors that can be used for polarisation of MDMs to an M1 or M2 phenotype have also been demonstrated to have effects on CCR5 and CXCR4 expression. Treatment of MDMs with lipopolysaccharide (LPS) can induce CCR5 downmodulation via a chemokine-independent mechanism (Franchin et al., 2000). Additionally, whilst IL-10 can increase MDM CXCR4 expression (Wang et al., 2001), it has also been reported to decouple CCR5 from signalling on monocytes and dendritic cells (DCs), creating a functional decoy receptor of CCR5 in the presence of inflammatory stimuli (D'Amico et al., 2000). Altogether current evidence suggests that CCR5 and CXCR4 expression on MDMs is also observed on macrophages *in vivo* and the levels may be modulated by soluble factors encountered in pro- and anti-inflammatory environments.

1.1.7 Intracellular accumulation of CCR5

The sustained presence of chemokines can lead to appearance of intracellular accumulations of CCR5 in trafficking compartments (Escola et al., 2010). Corroborating this, the relative abundance of the intracellular fraction of CCR5 in peripheral blood CD4+ T cells was suggested to be partly dependent upon the presence of cognate chemokines in their environment. Despite controversy regarding the presence of an intracellular pool of CCR5 in CD4+ T cells and a monocytic cell line (Achour et al., 2009; Guglielmi et al.,

2011; Pilch-Cooper et al., 2011; Shirvani et al., 2011), this could provide a mechanism to rapidly replenish desensitized or degraded receptors at the PM to enable a continued response. Thrombin receptors are an example of a GPCR that employs this mechanism; the receptors internalised from the PM are replaced with a pool resident in the Golgi (Achour et al., 2008).

The results of Achour et al., (2009) suggest that intracellular pools of CCR5 are located within the endoplasmic reticulum (ER) and that interactions with CD4 promote the PM expression of CCR5. The potential interaction of CCR5 and CD4 is considered in section 1.1.10, however it is appropriate here to consider the percentage of cells that Achour et al. (2009) found to be CCR5+, and the ensuing debate by several groups. Nearly all (95%) CD4+ T cells were suggested to contain internal CCR5 (Achour et al., 2009), which exceeds the percentage of cell surface CCR5 in any CD4+ T cell subsets in peripheral blood (Lee et al., 1999b). Additionally, increased cell surface expression reported by Achour et al. (2009) upon activation with CD3/CD28 beads directly contrasts results of Richardson et al. (2012) who demonstrate a decrease in CCR5 using the same method. Ultimately, the CCR5 observed by Achour et al., (2009) was proposed to be non-specific as the majority of peripheral blood CD4+ T cells did not express CCR5 on either the protein or mRNA level (Pilch-Cooper et al., 2011). Thus CD4+ T cells lacking cell surface CCR5 do not appear have intracellular pools of CCR5. However for the minority peripheral blood CD4+ T cell population expressing surface CCR5, intracellular accumulations of CCR5 may contribute a substantial amount to the total cellular CCR5 (Guglielmi et al., 2011; Pilch-Cooper et al., 2011). Speculatively, including intracellular CCR5 when immunolabelling would give higher fluorescence levels of the CCR5+ population and better resolution of the positive population in one-colour flow cytometry assays. This may explain why Guglielmi et al. (2011) find an increase in the percentage of the CCR5+ population upon permeabilisation. As CCR5 was found to recycle rapidly back to the PM, 50-90% within an hour after removal of chemokine depending on cell-type (Mack et al., 1998; Signoret et al., 2000), ligand-induced intracellular accumulations may only occur upon sustained chemokine stimulation. Alternatively more stable pools may exist or could be formed by tethering in the biosynthetic pathway as has been observed for other GPCRs (Achour et al., 2008). Overall, intracellular accumulations of CCR5 may occur in a subset of CD4+ T cells but considering the specificity issues encountered by Achour et al. (2009) the subcellular localisation of any accumulations would need to be readdressed.

1.1.8 Generation and maintenance of a chemokine gradient

The notion that chemokines primarily exist in sustained soluble gradients that directly bind to cognate receptors on incoming cells is an archaic view that is probably far from reality,

especially *in vivo*. Structurally heterogeneous carbohydrate chains known as glycosaminoglycans (GAGs) are ubiquitously expressed by mammalian cells (Allen et al., 2007). GAGs play a critical role in the formation of chemokine gradients that enable directional mobility of cells and recruitment of leukocytes into inflamed tissue. Through binding to GAGs, chemokines secreted by a particular cell become locally restricted so that an increasing chemokine concentration is apparent in the direction of the source. Chemokines bind with a low-affinity to GAGs via electrostatic attraction, and possibly other more specific mechanisms (Viola and Luster, 2008). Different chemokines favour GAG binding, exemplified by one of the six splice variants of CXCL12 showing preferential GAG binding (Bachelerie et al., 2013). In general, chemokines show preferential binding to longer GAG sequences. The expression of different families and sulfation patterns of GAGs, which influence chemokine binding, are cell-type specific (Allen et al., 2007). Moreover, GAGs, which often demonstrate preferential binding of chemokine oligomers, may also regulate the balance of chemokine dimers or monomers in different tissues. Although chemokine receptors are thought to directly bind chemokine monomers to induce migration, both monomers and oligomers of chemokines mediate important roles in migration *in vivo*. (Allen et al., 2007; Bachelerie et al., 2013). Despite a large body of *in vitro* evidence suggesting how chemokine gradients might be formed, their existence has only recently been demonstrated *in vivo* (Weber et al., 2013).

1.1.9 The purpose of chemokine receptor oligomerisation

The functional ability of chemokine receptors can be modulated depending on the pool of other receptors that are also expressed on the same leukocyte. Hetero- or homo-multimerisation is able to rapidly modulate the activity, signalling and/or localisation of a chemokine receptor in an allosteric manner (Bennett et al., 2011; Chabre et al., 2009). Chemokine receptor oligomers may form in the biosynthetic pathway prior to cell surface expression where subsequent chemokine binding can act to stabilise or reorganise the receptor oligomers that are constitutively formed (Bennett et al., 2011). For example, a bioluminescence resonance energy transfer (BRET) study found that CCR5 oligomers exist in the ER in human embryonic kidney (HEK)-293 cells transfected with C-terminal CCR5-luciferase/CCR5-YFP (Issafras et al., 2002). Notably, neither CCL4 nor CCL5 were found to induce higher order oligomerisation of pre-existing CCR5 oligomers, suggesting that the pre-formed oligomers are the functional units of CCR5 (Issafras et al., 2002). In other situations chemokine binding to CCR5 can be modified as a result of heteromerisation with other chemokine receptors. Indeed, CCL4 was found to reduce the binding of CCL2 in human CD4+ T blasts co-expressing CCR5 and CCR2b (El-Asmar et al., 2005). This effect was proposed to be due to negative binding co-operativity induced

by CCR5:CCR2b heterodimer formation, which was shown to occur at equal efficiency to homodimer formation in transfected Chinese hamster ovary (CHO) cells (El-Asmar et al., 2005). Numerous other studies, many involving CXCR4 or CCR5, also show oligomerisation of chemokine receptors (reviewed by Bennett et al., 2011), with the overarching message that the diversity of chemokine receptor responses are vastly increased by the process of oligomerisation. In the next section, the focus is placed on those few studies that report the occurrence of chemokine receptor heteromerisation in situations of antigen-receptor engagement or in combination with receptors implicated in antigen dependent signalling.

1.1.10 Oligomerisation in APC-T cell interactions

In Jurkat T cells CXCR4 and green fluorescent protein (GFP) tagged-CCR5 were found to heterodimerise, as judged by co-immunoprecipitation (co-IP) and BRET, when stimulated by sAg-pulsed B cells. Furthermore in both primary human CD4+ T cells and Jurkat cells, the recruitment of CXCR4 to the interface of T cell-B cell conjugates formed in the presence of sAg was shown to be dependent upon the expression of GFP-CCR5 (Contento et al., 2008). Accumulation of either receptor to the Jurkat-B cell interface was inhibited by antagonism of the other receptor, leading Contento et al. (2008) to conclude that the receptors act co-dependently. The CXCR4:CCR5 heterodimer was suggested to have a role in enabling CXCL12-mediated TCR costimulation (Contento et al., 2008), a role typically performed by the costimulatory molecule CD28. Since CXCR4 and CCR5 are primarily expressed on antigen experienced cells in peripheral tissues, one may speculate that the formation of a heterodimer acts to lower the threshold for costimulation, enabling rapid re-priming and effector responses in inflamed sites. In support of this the chemokines CCL3 and CCL5 (inflammatory), but not CXCL12 (homeostatic), were found to stabilise constitutively forming CXCR4:CCR5 heterodimers (Isik et al., 2008).

Additional factors involved in antigen presentation may also play a potential role in stabilising CXCR4:CCR5 heterodimers. For example, although CXCR4 and CCR5 showed colocalisation by microscopy in a fibroblast cell line, the receptors were only found to co-IP in the presence of CD4 (Wang et al., 2004). Intriguingly, Achour et al. (2009) also suggest that CD4 is able to associate with CCR5 in the ER of transfected CHO cells and that this acts to promote CCR5 cell surface expression in a concentration-dependent manner. Given the role of CD4 in localising lymphocyte-specific protein tyrosine kinase (Lck) to the cell-cell interface when TCR is engaged, perhaps CD4 also recruits CXCR4:CCR5 in the same platform. Yet CD4 is typically involved at the cell-cell interface (Dustin et al., 2010), whilst CCR5 accumulation is not always present at the interface of antigen-dependent conjugates (Contento et al., 2008). Thus if CD4 is

associated with CCR5, the interaction must be tightly regulated so that CD4 is able to mediate its function at the interface without CCR5. A similar argument also applies for CXCR4, which has been suggested to heterodimerise with the TCR upon binding CXCL12 (Kumar et al., 2006). Overall, studies using different cell lines and techniques have mounted a body of evidence in support of the formation of combinatorial heterodimers between CCR5, CXCR4, CD4 or TCR. Such processes may dictate the switch to $G_{11/q}$ signalling, costimulatory capacity, and spatial regulation of these chemokine receptors on T cells during antigen-receptor engagement (Molon et al., 2005).

1.1.11 Chemokine and integrin directed leukocyte migration

1.1.11.1 Chemokine receptors can influence cell-cell adhesion

Inside-out signalling from chemokine receptors or TCR can cause integrins, which exist in a largely inactive form, to undergo cytoskeletal tethering and concomitant conformational changes (Hogg et al., 2011). Evidence suggests that ligand-bound chemokine receptors induce integrin extension and ultimately T cell arrest during the process of leukocyte extravasation (Shamri et al., 2005). In addition, Bromley and Dustin (2002) showed increased T cell-DC conjugate formation in presence of CXCL12, even though high cell-cell adhesion occurred with or without chemokine in a mechanism insensitive to PTX (Bromley and Dustin, 2002). Nevertheless this suggests that chemokines can promote cell-cell adhesion but that this effect may be subservient to TCR signalling. Environmental factors can also change the cellular interpretation of chemokine receptor-influenced adhesion. In particular, a previous report showed that resting T cells rapidly migrate on surfaces coated with bound CCL21 via a mechanism independent of integrin interactions (Woolf et al., 2007). Yet when Woolf et al. (2007) repeated the same assay under conditions of shear flow CCL21 drastically enhanced intercellular adhesion molecule-1 (ICAM1) dependent adhesion. This supports reports of the integrin-independence of mobility observed for leukocytes in LNs but integrin-dependence during extravasation (Lammermann et al., 2008). Thus the chemokine receptor interplay with integrins in the process of cell-cell interactions cannot simply be extrapolated from the mechanism of extravasation and must be studied individually.

In light of the observations of integrin independent adhesion in tissues, how can the chemokine-dependent increase in adhesion reported by Bromley and Dustin (2002) be rationalized? The answer comes from looking at the methodology used. Although sheer-flow was not employed during imaging, conjugates were only imaged after the cells had been subjected to sheer-flow wash steps. This may explain why CXCL12 was observed to

stabilise interactions but raises questions as to whether the results are physiologically relevant to the majority of T cell-DC interactions, which occur in the tissues.

1.1.11.2 Chemokine-directed movement within tissues

Irrespective of whether integrins are involved in adhesion in interstitial tissue, chemokines still act to influence leukocyte mobility. CCR7 plays the dominant role in directing T cell mobility in the LN in response to its ligands, which are secreted by stromal cells (Cahalan and Parker, 2008). A lack of CCR7 reduces the speed but not the 'random walk' pattern of naïve T cell movement in the LN (Mrass et al., 2010). Since the T cells also exhibit a slow random walk on glass coverslips this may be a cell-autonomous pattern of behavior (Cahalan and Parker, 2008). Thus CCR7 may be important for increased speed of antigen sampling that in turn increases the likelihood of recognition of strong agonist peptide-bound to the major histocompatibility complex (pMHC). Despite the fact that CXCL12 is also secreted by stromal cells of the LN, primarily in the medulla, CXCR4 was not found to play a role in mediating the mobility of naïve T cells within this site (Asperti-Boursin et al., 2007). Nonetheless, secretion of other chemokines in the LN may influence T cell mobility and show directional migration. In evidence of this, T cell directional bias in the LN has been demonstrated in an inflammatory setting, in which CCR5 directs naïve CD8+ T cells to DCs that have engaged in antigen-specific interactions with CD4+ T cells (Castellino et al., 2006). Thus T cell directionality within interstitial tissue can occur but may be primarily instigated by subsets of chemokines expressed in response to infection or inflammation.

1.2 The Immunological Synapse (IS)

1.2.1 What is an immunological synapse?

An immunological synapse (IS) is defined as the specialized junction that occurs when a cell of the immune system adheres to another cell, becomes polarised and participates in a stable interaction that enables a functional outcome (Dustin, 2009b; Grakoui et al., 1999). Signalling components, cell surface proteins and lipids become rearranged into micrometer scale three-dimensional domains that accumulate to the cell-cell interface (**Fig. 1.3**) (Burack et al., 2002; Dustin, 2009b; Fooksman et al., 2009; Monks et al., 1998). Although this definition encompasses many different cell types that can form ISs, the present study focuses on interactions between T cells and APCs. Indeed, this group shows variation enough in IS formation as there are many different subsets and combinations of T cells and APCs, and both cell types contribute to the diversity of molecular arrangements at the IS (Dustin et al., 2006; Friedl et al., 2005).

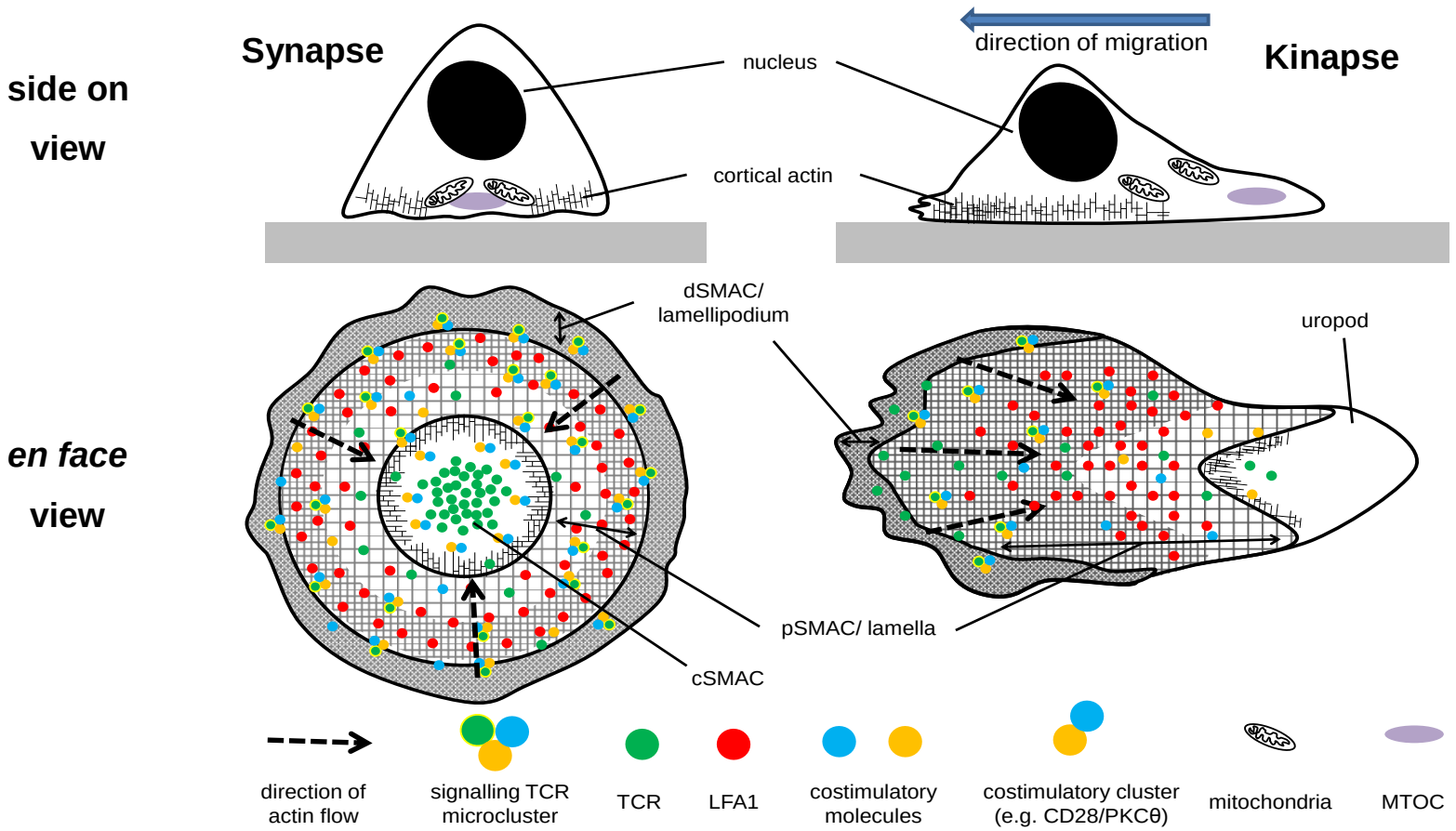

Figure 1.3: Organisation of the immunological synapse and kinapse. The diagram shows the dSMAC, pSMAC and cSMAC concentric circles of the IS and indicates regions that are similar in the kinapse. The degree of crosshatching indicates the amount of organized actin in each region. The dSMAC is the major region where monomeric actin is directed by hydrostatic pressure contributing to the vast actin filament extension in this region that causes the retrograde flow and microclusters of TCR that are formed there to be directed inwards towards the cSMAC or uropod. Note the cSMAC is not necessarily equivalent to the uropod, which shows enriched myosin II that drives contraction of this region in migrating cells. This diagram is based upon previously reported models (Beemiller and Krummel, 2013; Dustin (2008); Dustin, 2009b; Kummerow et al., 2009; Yokosuka et al., 2008).

The first observations of the IS were made by Kupfer and colleagues using deconvolution microscopy to study the interface of fixed murine B–T cell conjugates after 30 min co-incubation. Cell surface and signalling proteins involved in antigen presentation were found to organize into concentric circles, designated supramolecular activation clusters (SMACs), at the interface in an antigen-dependent manner (Monks et al., 1998). The integrin lymphocyte function-associated antigen (LFA1) occupies the peripheral SMAC (pSMAC) around an accumulation of the TCR complex and PKCθ (a T cell specific isoform of PKC) in the central SMAC (cSMAC) (**Fig. 1.3**) (Monks et al., 1998). Soon after, Dustin's group used live T cells and supported planar bilayers to show that the process of IS formation is highly dynamic. Initially, LFA1 bound ICAM1 is spread across the T cell-bilayer interface and TCR-pMHC molecules reside in an outer circle at the closely-apposed edges of the T cell- bilayer contact. However, within three minutes the T cell organises TCR-pMHC into the centre of the interface whilst LFA1-ICAM1 clusters outside, correlating with the cSMAC and pSMAC organisation, respectively, as reported by Monks et al. (1998) (Grakoui et al., 1999). Later, the region outside the pSMAC containing the bulky phosphatase CD45 became known as the distal SMAC (dSMAC) (Beemiller and Krummel, 2013). Rather than simply being a bin for bulky membrane proteins the dSMAC is now appreciated as an area of continuous membrane movement associated with rapid extension of actin filaments (Dustin et al., 2010). At this point it is prudent to highlight that the SMACs are not apparent in all types of IS and their frequency of occurrence *in vivo* is unknown (Dustin et al., 2010; Schubert et al., 2012). Nevertheless the LFA1-ICAM1 adhesion step was proposed to form a stable anchor-point around which cytoskeletal rearrangements occur that drive the central accumulation of TCR-pMHC (Grakoui et al., 1999). In support of this hypothesis stable APC-T cell engagement is promoted by LFA1 activation through inside-out signalling after TCR engagement. Also LFA1 or ICAM1 knockout mice demonstrate compromised CD4+ T cell priming and CD8+ T cell effector function and lose the ability to form stable DC- CD8+ T cell conjugates (Hogg et al., 2011; Scholer et al., 2008). Thus adhesion is a critical step in IS formation.

1.2.2 Signalling at the IS

Antigen recognition is central to IS formation. T cells recognize cognate antigen though TCR binding to pMHC, which triggers the T cell signalling cascade detailed below. The steps leading to calcium influx across the PM are focused on due to the dependence of many activation-induced genes on this process, and as calcium is used as a readout for TCR-triggering in later chapters (Kummerow et al., 2009).

1.2.2.1 Calcium signalling following antigen receptor engagement

Each TCR is associated with a total of six CD3 chains (two ε, two ζ, one δ, one γ) that contain signalling motifs known as immunoreceptor tyrosine-based activation motifs (ITAMs), which together form the TCR complex (Murphy et al., 2011). Upon TCR engagement signal transduction is initiated by a currently unclear mechanism, which prompts the phosphorylation of the ITAMs by the SRC-family kinases Lck and Fyn (Acuto et al., 2008; Kummerow et al., 2009). Constitutive phosphorylation of CD3 ITAMs in unstimulated T cells and recognition of self-pMHC resulting in partial CD3ζ ITAM phosphorylation both evidence the high native sensitivity of the TCR and overt regulation of signal triggering required to score the quality of antigen encountered (Acuto et al., 2008). This concept is supported by recent *in vivo* evidence, which clearly demonstrates that the T cell elicits a different type of functional behavior in response to high or low affinity TCR ligands (Moreau et al., 2012).

Binding of CD4 to a non-polymorphic region of MHC class II is independent of TCR binding and functions to concentrate associated Lck to regions of, rather than to stabilise, the TCR-pMHC interaction (Huppa et al., 2010). Through spatially concentrating Lck, CD4 strengthens signalling and enables downstream calcium mobilisation (Huppa et al., 2010). Phosphorylated ITAMs recruit ZAP-70 (ζ-chain-associated protein kinase of 70 kDa), which is activated by Lck and subsequently phosphorylates the PM-associated adaptor protein linker for activation of T cells (LAT). Phosphorylated-LAT recruits PLCγ, which hydrolyses phosphatidylinositol-4,5-bisphosphate (PIP2) into diacylglycerol (DAG) and inositol-1,4,5-triphosphate (IP3), the latter of which activates calcium release from ER-stores (Acuto et al., 2008). The other product, DAG, is thought to be important for the recruitment of PKCθ and the microtubule-organising centre (MTOC) to this IS (Griffiths et al., 2010; Yokosuka et al., 2008). This entire cascade occurs very quickly as the time taken between TCR-pMHC engagement and release of free calcium into the cytosol is less than 10 s (Acuto et al., 2008).

1.2.2.2 Sustained calcium signalling at the cell-cell interface

IP3 binds to the IP3-receptor in the ER-membrane, which begins to release calcium contained within the ER lumen. Note that other signalling molecules also stimulate calcium release and these can act in coordination with IP3 to enable sustained calcium signalling upon persistent TCR engagement. The decrease in ER-luminal calcium is sensed by the cytoplasmic domain of the ER-membrane protein stromal interaction molecule 1 (STIM1), which oligomerises and translocates to PM-proximal regions (Hogan et al., 2010). PM-proximal STIM1 oligomers recruit the calcium release activated channel

(CRAC) ORAI1 and bind directly to stimulate calcium influx over the PM through a tetrameric ORAI1 channel (Hogan et al., 2010). Moreover, ORAI1 and STIM1 were shown to be rapidly recruited to the human T cell–DC IS making this structure the main site of sustained calcium influx (Lioudyno et al., 2008). Indeed, intracellular calcium concentrations are higher just beneath the plane of the IS (Lioudyno et al., 2008), but because this is buffered by mitochondria translocated to the interface in an LFA-dependent manner CRAC channels remain open and thus calcium influx is sustained (Contento et al., 2010).

1.2.3 Microclusters as the signalling components of the IS

In the IS, actin is symmetrically organized and undergoes retrograde flow, which directs centripetal movement of TCR-pMHC or LFA1-ICAM1 microclusters newly formed in the dSMAC of the IS (Dustin et al., 2010; Varma et al., 2006; Yokosuka et al., 2005). The cSMAC was originally assumed to be the signalling module, as it is the region in which TCR accumulates (Grakoui et al., 1999; Monks et al., 1998). Yet in response to strong stimuli, phosphorylated proteins were not detected at the cSMAC but instead in peripheral microclusters (Yokosuka et al., 2005). Additionally, through inhibiting TCR triggering with antibodies against pMHC Varma et al. (2006) showed that calcium signalling is rapidly inhibited, even though cSMAC formation was not disrupted. Thus the TCR-pMHC microclusters in the periphery were implicated as the signalling components of the IS since their formation was found to be disrupted using this approach (Varma et al., 2006). The current view is that recognition of cognate pMHC causes preformed nanoclusters of TCR, and other TCR signalling components such as LAT, to aggregate into microclusters (Beemiller and Krummel, 2013). The costimulatory protein CD28 associates with TCR in the microclusters and recruits PKCθ (Yokosuka et al., 2008). Signalling components, such as LAT, ZAP-70 and Lck interact with TCR microclusters in a transient fashion, which may be sufficient for TCR to remain triggered. These interactions may be promoted by a localised increased density of cortical actin surrounding TCRs and involvement of lipid rafts with actin filaments (Kusumi et al., 2005). The microclusters at the periphery of the IS are loosely coupled to a conveyor belt of actin, which alongside association with microtubules via dynein, drives them towards cSMAC (Beemiller and Krummel, 2013; Dustin et al., 2010; Hashimoto-Tane et al., 2011). Corralled within the cSMAC TCR-pMHC microclusters may be divided into clusters of CD28-PKC, which function in a costimulatory signalling complex, exclusive from TCR-CD3 clusters, which terminate signalling and are targeted for degradation via ubiquitylation (Varma et al., 2006; Yokosuka et al., 2008). The relative contributions of these opposing functions have been postulated to enable negative regulation of TCR signalling in response to strong stimuli but support weak stimuli by

costimulation (Dustin et al., 2010; Yokosuka et al., 2008). Overall, microclusters can be imagined as the coloured dots that can form pointillist concentric circles (the SMAC modules) and their dynamics contribute to the changing picture of the IS at the cell–cell interface over time.

1.2.4 Functions of the IS

1.2.4.1 Antigen recognition and sustained signalling

The IS has been proposed to function as a molecular machine that is able to overcome 'barriers' to sustained TCR engagement (Grakoui et al., 1999). The organization of the IS promotes close apposition of the membrane in TCR-pMHC microclusters, which causes steric hindrance to larger glycoprotein phosphatases would otherwise inhibit signalling (Grakoui et al., 1999; Tybulewicz, 2002). This kinetic segregation model was supported by a study in which the extracellular domains of pMHC were elongated, which caused reduced signalling efficacy but maintained TCR-pMHC binding affinity (Choudhuri et al., 2005). In addition the vast reorganization of cortical actin at the IS, with tightly woven compartments in the periphery and relatively little in the centre, means that signalling molecules recruited to the interface may become corralled in nanoscale regions proximal to TCR (Beemiller and Krummel, 2013; Kusumi et al., 2005). Recruitment and coalescence of signalling components may also be supported by large-scale stabilisation of lipid rafts at the IS (Pike, 2006). Together these structural components of the IS may considerably promote the chances of molecular interaction in order to achieve sustained signalling. Although other organisations of the IS have been demonstrated (Friedl et al., 2005), the IS shown on planar bilayers can be viewed as the format that T cell aspires to in order to facilitate a high level of sustained signalling. For example the closer proximity of mitochondria to the cell-cell interface at the IS promotes sustained calcium influx, whereas in mobile antigen-dependent junctions the mitochondria primarily lie at the uropod and so calcium influx is less tenable (Kummerow et al., 2009). Thus in this capacity the IS functions to organize subcellular components to facilitate high level, sustained antigen-dependent signalling.

1.2.4.2 A vehicle for directed secretion

One of the proposed functions of the IS is as a vehicle for directed endo- and exocytosis (Griffiths et al., 2010). Cytotoxic T lymphocytes (CTLs) perform perhaps the most famed example of this function, as only minutes after TCR stimulation they commit the 'kiss of death' mediated by directed secretion of lytic granules into the IS (Huse et al., 2008). The annular pSMAC forms a seal that increases the efficiency of killing the target cell and is

thought to help prevent off-target effects on nearby cells (Dustin et al., 2010). The CTL-target synapse also exhibits a specialized organization, having a secretory domain alongside the cSMAC, both of which are surrounded by the pSMAC (Griffiths et al., 2010). This type of IS is a good example of how different cell-types can mould the IS organization to benefit their function.

Investigations have previously been made into whether chemokine ligands of CCR5 might be directionally secreted by CD4+ or CD8+ T cells (Catalfamo et al., 2004; Huse et al., 2006). Catalfalmo et al. (2004) found CCL5 present in vesicles of memory and effector human CD8 + T cells. Upon interaction with CD3/CD28 beads, vesicles containing CCL5 were found to localise to the bead–CD8+ T cell interface and were rapidly secreted (> 50% fluorescence decrease in 30 min) (Catalfamo et al., 2004). In contrast, another study observed multidirectional CCL5 and CCL3 secretion from murine CD4+ T cells engaged with B cells (Huse et al., 2006). This result did not appear to be due to any technical inability to detect directed secretion as Huse et al. (2006) showed directional secretion of cytokines such as IL-2, IFNγ and IL-10. The differences may be due to analysis of preexistent vesicles containing CCL5 in the CD8+ T cells compared to *de novo* CCL5 in the CD4+ T cells being synthesized in response to TCR engagement (Huse et al., 2006). In addition differences between the cell types utilised, including the nature of the APC, B cell vs. bead, may contribute to the differences in the directionality of chemokine secretion observed. Thus the IS may enable targeted action of cytokines or chemokines upon specific cells as a result of antigen recognition, e.g. macrophage activation and suppression by IFNγ or IL-10 secreted by Th1 or Th2 cells, respectively (Huse et al., 2008). Perhaps the IS has evolved as a single machine able to fit numerous different cell types and integrate both of the functions considered here, which can be mutually beneficial for an appropriate response upon encountering antigen.

1.2.5 Moving targets: stable and kinetic synapses

By definition the IS is stable and in support of its existence *in vivo*, stable DC-T cell interactions have been observed to exist in LNs (Dustin et al., 2010). However relatively soon after the original description of the IS, T cells were shown to be cumulatively activated in an antigen-dependent manner through multiple, dynamic interactions with APCs (Underhill et al., 1999). This type of dynamic interaction was also found to be relevant *in vivo* which led to the description of three phases involved in T cell antigen recognition: (i) contact initiation, prolonged but discontinuous interactions with multiple DCs; (ii) stable interaction, IS formation maintained for hours; (iii) release and swarming (Krummel and Cahalan, 2010). The fast integrin-independent mode of leukocyte migration through tissues discussed above may predominate *in vitro* at steady state, but in an

inflammatory environment, a slow or stationary integrin-dependent surface contact mode might exist (Krummel and Cahalan, 2010). When contact is formed the T-APC conjugate can transition between stable (<1 μm/min), slowly mobile (1-2 μm/min), and dynamically mobile (1-10 μm/min) junctions in order to cycle through the three possible phases of antigen recognition (Friedl et al., 2005). Depending on the quantity of antigen, T cells often initiate interactions with APCs in a mobile mode where pMHC is scanned and calcium signals are induced upon cognate antigen recognition (Dustin, 2009b; Krummel and Cahalan, 2010). This type of mobile contact is referred to as a kinapse (kinetic synapse) in order to distinguish it from the stable IS and exhibits a different modular arrangement (Dustin, 2009b) (**Fig. 1.3**).

Transition between mobile and stable phases implies interchangeability between IS and kinapse formations. Mechanically, this has been proposed to be mediated by cytoskeletal rearrangements in which the symmetrical ring of actin flowing to the centre of the IS becomes destabilised and polarises to one side of the cell (i.e. asymmetric) (Dustin, 2009b). In the asymmetric state actin flow pushes an edge of the cell forwards, causing movement. Yet, TCR microclusters still form at this edge and flow towards F-actin poor regions or 'sinks' (Beemiller et al., 2012). This indicates that the rules of flow imparted by structural features such as actin and lipid rafts may be maintained even when the overall arrangement of the IS is skewed or multicentric. After studying the transition between IS and kinapse using naïve T cells and planar bilayers Dustin's group proposed a model in which PKCθ disrupts actin assembly causing gaps in the pSMAC actin ring, whereas Wiskott-Aldrich syndrome protein (WASp) promotes actin nucleation and reinstates symmetry (Dustin, 2009b). Thus differential regulation of signalling molecules such as PKC and WASp may be a method by which T cells switch between mobile forms. Notably the synapse-to-kinapse decision may also be influenced by signals from chemokines in the local microenvironment, which have a hierarchical interplay with TCR engagement (Bromley et al., 2000), as discussed in section 1.2.7.

The initial decision of a cell to engage in stable or mobile interactions may be predetermined. For example T cell interaction stability with DCs is inversely correlated to activation status but directly correlated with the density of agonist pMHC (Friedl et al., 2005). Alternatively the decision may relate to the required effector function, for instance stable symmetric IS formation may facilitate directional cytokine secretion between B-T cells when the T cell secretes cytokines into the tight, enclosed junction (Beemiller and Krummel, 2013). Whilst the architecture of the kinapse promotes motility and thus efficient scanning and recognition of small numbers of agonist pMHC, it is not efficient for polarised secretion, unlike the IS (Dustin, 2009b). Intriguingly, WASp plays a critical role in directed secretion of IFNγ by CD4+ T cells, but not multidirectional secretion of

chemokines (Morales-Tirado et al., 2004). Considering the role of WASp in promoting stable IS formation it is possible that IFNγ may only be able to be secreted when cytoskeletal symmetry is achieved.

In addition to the factors discussed above, whether a synapse or kinapse is formed appears to depend, in part, upon the type of APC T cells interact with. In evidence of this, the same activated T cell population has been shown to engage in mobile interactions with DCs (kinapses) but show stable synapses with B cells (Azar et al., 2010). This is consistent with the notion that less stable interactions occur with APCs that have complex morphologies and have high cytoskeletal activity (Friedl et al., 2005). Finally, it is important to stress that both synapses and kinapses have been shown to evoke antigen-dependent T cell calcium signals *in vivo* and only the highest calcium signals result in consistently reduced mobility *in vitro* (Moreau et al., 2012) (Beemiller et al., 2012). In general, the synapse and kinapse are interchangeable structures and the decision to exist as either form is dependent upon a combination of cell type, activation status, antigen density, regulation of signalling and environmental cues. Both should be considered as active and physiologically relevant forms of antigen-dependent information exchange.

1.2.6 Role of APCs in the IS

Although different APCs are known to influence the formation of the IS (Azar et al., 2010; Friedl et al., 2005), the majority of interest in IS formation has been at the T cell side. In fact, only a small number of molecular components have been shown to localise to the APC side of the IS. One study showed that PIP2 becomes concentrated on the APC side of the IS and suggested that this lipid has a role in enabling CTL-mediated lysis (Fooksman et al., 2009). Another study found that spinophilin is expressed both in neuronal dendrites and DCs and subsequently showed that spinophilin is localised to the IS and acts to optimize T cell activation (Bloom et al., 2008). Additionally, by truncating the CD80 cytoplasmic domain, the APC was found to be able to modulate the localisation of CD80 and the strength of costimulation (Tseng et al., 2005). Such studies highlight that the APC is not simply passive with regard to IS formation. Despite recognition that the APC cytoskeletal complexity and activation status may also modify the structure of the IS (Friedl et al., 2005), very little is known about how APCs may contribute to events at the IS.

1.2.7 The hierarchy of chemokine receptors and TCR signalling

Certain soluble chemokines (CCL21, CCL19, CXCL10) have been proposed to be able to override the ‘stop’ signal that can be issued by TCR engagement and induce T cell mobility, an effect which does not occur through stimulation with other chemokines (CCL3,

CXCL12) (Bromley et al., 2000). Furthermore, the 'go' signal issued by CCL21 is most efficient at low concentrations and thus even small differences in the chemokine microenvironment may have a significant impact on the stability of IS formation (Dustin, 2004). Small differences can also be elicited by the differential susceptibility of chemokine receptors to desensitisation by bound ligand (Woolf et al., 2007). Additionally, results from our lab indicate that different forms of the same chemokine receptor can be preferentially downmodulated. Together, environmental and cell-autonomous mechanisms may collectively influence whether a 'stop' or 'go' signal dominates.

The intensity of antigen-dependent signalling may also be deterministic to 'stop' or 'go' theory. Intriguingly, CXCL10 signalling via CXCR3 has been demonstrated to result in phosphorylation of several signalling components downstream of TCR (LAT, ZAP-70, PLCγ) (Dar and Knechtle, 2007). Dar and colleagues observed quite the opposite effect of the override of TCR 'stop' signals by CXCL10 that was reported by Bromley et al. (2000), in that TCR ligation was found to attenuate CXCR3 signalling and chemotaxis (Dar and Knechtle, 2007). However, the two studies used different methods of TCR stimulation, one involving antibody-induced CD3-crosslinking (Dar and Knechtle, 2007) and the other ICAM and pMHC (Bromley et al., 2000). Thus it is possible that CXCL10 signalling was not able to overcome the effect of stronger antibody-mediated TCR engagement, which is several orders of magnitude greater than that of pMHC (Corse et al., 2011). This suggests interplay between the potency of TCR signals alongside a hierarchy of chemokines signals.

1.2.8 Chemokine receptors at the IS: the distraction hypothesis

GFP-tagged versions of CCR5 and CXCR4 have been shown to localise to the CD4+ T cell side of synapses formed with an immortalized B cell line or human monocyte-derived DCs (Contento et al., 2008; Molon et al., 2005). The recruitment of transfected GFP-CCR5 to the interface was inhibited by blocking chemokine binding using anti-CCR5 (clone: 45531), treatment with a functional antagonist, or blocking secretion from the B cells using Monensin A. The recruitment of CXCR4-GFP was blocked by treating with the antagonist AMD3100 (Molon et al., 2005). Additionally, T cell migration towards CXCL12 was reduced in the presence of sAg-pulsed B cells compared to Monensin A treated sAg-pulsed B cells, indicating that T cells engaged in the IS were less able to migrate towards CXCL12 gradients. These results, along with observations that CCR7 did not accumulate at the IS and the report by Bromley et al. (2000), led Viola and colleagues to propose the distraction hypothesis; certain chemokine receptors (CCR5 and CXCR4) may be recruited to the IS in order to prevent distraction from chemokine sources other than the engaged APC. This hypothesis appears to explain why CCL3/5 or CXCL12 did not result in a 'go'

signal in the study by Bromley et al. (2000). However it is important to note that no chemokine could be secreted by the APC in the study by Bromley et al. (2000), as the 'APC' was in fact surface-bound ICAM and pMHC. Nevertheless, it is possible that upon establishing a CCL3, CCL5 or CXCL12 gradient the Transwell set-up used meant that the solid surface mimicked an APC secreting cognate chemokine, thus supporting the distraction hypothesis. Despite this *in vitro* evidence, currently no *in vivo* evidence exists that CD4+ T cells co-expressing CCR5 and CXCR4 recruit these chemokine receptors upon synapse formation in the LNs or peripheral tissue sites.

Another study shows that chemokine receptors may also be involved in IS formation in a different type of cell-cell interaction *in vitro*. CD8+ tumour-infiltrating lymphocyte (TILs) clones forming an IS with a lung carcinoma cell line were found to recruit CCR5 to the interface (Franciszkiewicz et al., 2009). Accumulation of CCR5 to the IS, but not conjugate formation itself, was dependent upon the interaction between TIL integrin CD103 and E-cadherin expressed on the tumour cell. In the TIL-tumour IS the CD103-E-cadherin interaction is comparable to and augments the LFA1-ICAM1 function in adhesion, promoting efficient tumour cell lysis and TIL cytokine release (Franciszkiewicz et al., 2013). In support of the distraction hypothesis, knockdown of E-cadherin resulted in enhanced migration of tumour-engaged TILs towards CCL5 in a Transwell assay (Franciszkiewicz et al., 2009). Since the tumour cell line also secretes CCL3/4/5 it is tempting to speculate that if the authors had also inhibited secretion by tumour cells lacking E-cadherin they may have noticed a further enhancement of migration, comparable to the results of Molon et al. (2005). Note that, in contrast to a previous study in which CXCR4 recruitment to the Jurkat-B cell IS was co-dependently recruited with CCR5, TILs despite expressing both CXCR4 and CCR5 showed no accumulation of CXCR4 to the TIL-tumour interface (Franciszkiewicz et al., 2009). This suggests that chemokine receptor recruitment to the IS may be differentially regulated in different cell types. Nevertheless, common to all these studies are indications that CCR5 can play a role in promoting cell-cell adhesion at the IS and that this seems to be mediated by recruitment of CCR5 to the cell-cell interface. Overall IS formation alone does not appear to be sufficient for chemokine receptor recruitment to the cell-cell interface, but additional cues from chemokines, integrins or receptor heterodimerisation promote accumulation to the IS (Contento et al., 2008; Franciszkiewicz et al., 2009; Molon et al., 2005).

1.3 Macrophages and the IS

1.3.1 Macrophage origins and function

Macrophages are a highly diverse group of mononuclear phagocytes widely expressed throughout the body in different tissue environments. The function of macrophages is specialized to, and by, the tissue in which they are expressed e.g. phagocytosis and antigen presentation in the dermis, elimination of pathogens in the liver, tolerance in the intestine, to name a few (Murray and Wynn, 2011). In these environments macrophages exist in two major forms, as tissue-resident macrophages and MDMs. Until recently it was believed that both forms were replenished by blood monocytes, which begin to differentiate to macrophages upon extravasation (Murray and Wynn, 2011). However recent evidence in mice has shown that, in contrast to haematopoietic stem cell-derived MDMs, tissue-resident macrophages are long-lived, self-renewing cells that are derived from the yolk sac with minor contributions from foetal liver monocytes (Schulz et al., 2012). These tissue-resident macrophages were demonstrated to occupy numerous sites, in particular the liver (Kupffer cells) and the brain (microglia) (Schulz et al., 2012). In sites of inflammation or injury, blood monocytes become rapidly recruited and differentiate to MDMs, which transiently contribute to the tissue macrophage compartment (Zigmond and Jung, 2013). As an exception to this rule, monocytes are constitutively recruited to maintain a consistent population of CX_3CR1^+ macrophages in the gut, although this is potentially caused by tonic inflammation in response to the environment (Zigmond and Jung, 2013).

Monocyte recruitment occurs early on after tissue inflammation and is followed by differentiation and activation of macrophages, then conversion to suppressor cells and finally restoration homeostasis in the tissue (Murray and Wynn, 2011). The monocytes that give rise to both CX_3CR1^+ gut macrophages and MDMs can be identified based on the expression of myeloid marker of the lymphocyte antigen 6C ($Ly6C^+$) (Zigmond and Jung, 2013). Typically, high expression of Ly6C is indicative of the 'inflammatory monocyte' subset, which in humans is designated by the $CD14^{hi}CD16^-$ monocyte phenotype (Gordon and Taylor, 2005; Murray and Wynn, 2011). Both human and murine inflammatory monocytes express CCR2, which plays a key role in directing monocytes to inflammatory sites (Gordon and Taylor, 2005). Although there are phenotypic similarities, the lack of Ly6C in humans highlights a general problem; a number of the identifiers of monocyte or macrophage subsets in mice are absent or differentially expressed in humans cells (e.g. Ly6C, F4/80, *Ym1*, *Fizz1*) (Murray and Wynn, 2011). Nevertheless, the origins of different macrophage compartments and the principals of recruitment during

inflammation are likely to apply to humans. However the findings of Geissmann and colleagues imply that macrophages generated from monocytes or bone marrow *in vitro* may never be able to completely recapitulate the phenotype of tissue-resident macrophages present at steady state *in vivo* (Schulz et al., 2012).

1.3.2 Macrophages: plastic fantastic

Macrophages demonstrate a high degree of plasticity and integrate many different signals that define their position within a vast possible spectrum of immunosuppressive to pro-inflammatory functional phenotypes (Sica and Mantovani, 2012). It is unclear whether the differential macrophage phenotypes that promote inflammation and subsequent resolution result from newly recruited macrophages or repolarisation of macrophages *in situ*. Either way, macrophages become educated by the tissue environment, sensing tissue damage or the presence of pathogens and interacting with T cells, both directly and via reciprocal cytokine secretion (Biswas and Mantovani, 2010; Sica and Mantovani, 2012).

Macrophages are broadly classified into two groups according to their activation state, namely classically activated (M1) and alternatively activated (M2) (Biswas and Mantovani, 2010). Macrophages become polarised towards an M1 phenotype upon recognition of bacterial stimuli such as LPS, subsequent recruitment and activation of Th1 cells, which in turn secrete IFNγ and elicit full macrophage activation (**Fig. 1.4**). Typically M1 macrophages have been associated with expression of inflammatory cytokines, enhanced production of reactive oxygen species, efficient antigen presentation and upregulation of the costimulatory molecules CD80/86 (Biswas and Mantovani, 2010; Sica and Mantovani, 2012). M1 macrophages play a role in containing intracellular bacteria, protozoa (such as *Leishmania major* at the site of infection) and mediating anti-tumoural responses (Murray and Wynn, 2011).

Macrophages polarised towards an M2 phenotype promote Th2 responses, become immunoregulatory, exhibit changes in metabolic substrate preference, demonstrate an enhanced phagocytic capability and an increased expression of scavenger receptors (Biswas and Mantovani, 2010). Three subdivisions of M2 cells have been specified, namely M2a, M2b and M2c, which are defined according to the cytokines and complexes they are exposed to during differentiation *in vitro* (**Fig. 1.4**). Note that macrophages polarised towards M2b and M2c cells are sometimes collectively referred to as ‘M2-like’ cells (Biswas and Mantovani, 2010). M2a macrophages are polarised by the Th2 cytokines IL-4 and/or IL-13 and like M2b macrophages, which are differentiated in the presence of immune complexes and LPS, promote Th2 activation and responses (Mantovani et al., 2004). In contrast, M2c macrophages have a deactivated phenotype,

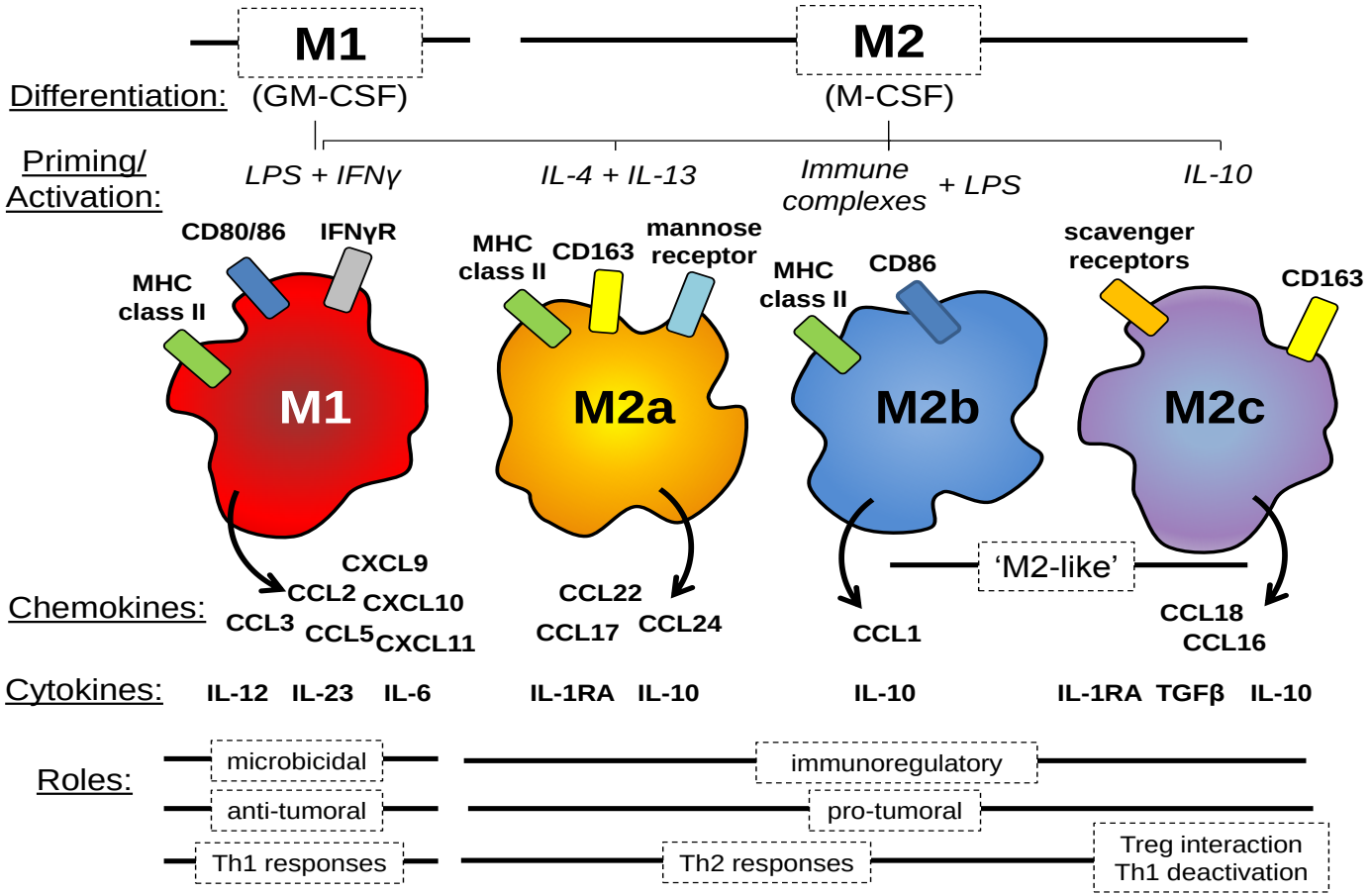

Figure 1.4: Macrophage polarisation and chemokine profiles. The diagram shows the factors that are used to influence the differentiation and activation of macrophages *in vitro*. The four types of polarised macrophage demonstrate chemokine and cytokine expression patterns that dictate their roles in directing different arms of the immune response. This figure is based on previous reports (Biswas and Mantovani, 2010; Gordon, 2003; Mantovani et al., 2004; Rey-Giraud et al., 2012). GM-CSF, granulocyte-macrophage colony stimulating factor; IFNγ, interferon-γ; LPS, lipopolysaccharide; M-CSF, macrophage-colony stimulating factor.

are primarily involved in immunosuppression and tissue remodeling and extensively downregulate MHC class II (Mantovani et al., 2004). Thus, M2c macrophages would not be expected to interact with CD4+ T cells in an antigen-specific manner that would lead to IS formation. M1 and M2 polarised macrophages have different chemokine expression repertoires (Mantovani et al., 2004), which not only promote the recruitment of different lymphocytes but may also potentially influence their antigen-specific interactions in the tissue. According to the two-signal activation model, recent lymphocyte immigrants would engage pMHC present on the APC (macrophage or DC) and in turn receive a cytokine signal from that APC that induces T cell activation (Martinez et al., 2009). This notion is consistent with the systems view of the immune system, in which T cells that have undergone previous antigen-recognition and expansion in the LN can be restimulated by APCs resident in the target tissue (Gerard et al., 2013). As an example of this type of activation, IFNγ secretion by Th1 cells may be induced following antigen-specific engagement with M1 macrophages secreting IL-12 (Martinez et al., 2009). Speculatively, the M1 macrophage secretion of CCL3/4/5 may enhance macrophage-Th1 cell adhesion according to the distraction hypothesis or even substitute as a costimlatory signal, as previously observed in IS formation between T-B cells (Contento et al., 2008; Molon et al., 2005). The notion of enhanced adhesion is particularly appealing considering IFNγ can be directionally secreted by T cells and that the IS may act as a vehicle for directed secretion (Huse et al., 2006). Yet in spite of this, current *in vitro* and *in vivo* data suggest that CD4+ T cell interactions with macrophages *in vivo* are often dynamic, see section 1.3.4. Nevertheless, this highlights that the M1 or M2 polarisation and the resulting chemokine and cytokine profile may affect the stability or occurrence of a macrophage-T cell IS.

1.3.3 Practicalities of generating human MDMs

There is a general lack of consensus as to the method by which human MDMs are generated. Serum, or the lack of, has been shown to affect the functional activity of MDMs (Rey-Giraud et al., 2012). In addition, foetal calf serum (FCS) is thought to contain numerous undefined factors that can activate signalling pathways able to initiate changes in cell morphology and adhesion (Rey-Giraud et al., 2012). The presence of these factors can be batch-dependent. Typically, M-CSF or GM-CSF are often used to polarise macrophages to M2 or M1 phenotypes *in vitro*, respectively, alongside the aforementioned cytokines (e.g. IL-4, IL-13 and IFNγ) and bacterial products such as LPS (Foucher et al., 2013; Jaguin et al., 2013; Martinez et al., 2006; Rey-Giraud et al., 2012). M-CSF in particular is often added to promote survival, although its addition can be rationalized by evidence that M-CSF is constitutively expressed *in vivo* (Hamilton and Achuthan, 2013). Use of different combinations of these factors may be a source of disparity between M1 and M2 polarised MDMs prepared in different studies.

1.3.4 Evidence for macrophage-CD4+ T cell interactions *in vivo*

IS formation is thought to occur between effector CD4+ T cells and macrophages in the tissue environment (Dustin et al., 2001b). *In vitro*, synapse or kinapse formed between murine macrophages and CD4+ T cells have been shown to be highly dynamic (Underhill et al., 1999). However direct visualization of this type of IS and whether typical markers accumulate to the cell-cell interface has not yet been demonstrated in human cells or *in vivo*. Nevertheless, a recent study in mice has indicated that macrophages and DCs are implicated in the local restimulation of primed CD4+ T cells in atherosclerotic lesions (Koltsova et al., 2012). In turn, the CD4+ T cells secrete proinflammatory cytokines enhancing lipid uptake (Koltsova et al., 2012), which amongst other T cell responses drives atherosclerotic plaque formation and disease progression (Libby et al., 2013). In humans, approximately two-thirds of T cells present in atherosclerotic plaques are CD4+ with the majority possessing an activated effector-memory phenotype (Libby et al., 2013). Despite the accumulation of CD4+ T cells into a macrophage-rich pathological location and indication that the direct interactions of these cell types has a functional outcome for disease progression, little is known about antigen-dependent macrophage–CD4+ T cell interactions in peripheral tissues.

CD4+ Th1 cells also play a key role in interacting with macrophages infected with mycobacteria in order to contain the infection (Murphy et al., 2011). However the level of mycobacterial-antigen presentation in granulomas (collections of macrophages) is only able to induce arrest and directed cytokine secretion in a small fraction of the total antigen-specific CD4+ T cells infiltrating the tissue (Egen et al., 2011). The authors suggest functional limitation of antigen presentation within the granuloma and generalise that there is insufficient antigen at sites of infection to support effector T cell responses in this region (Egen et al., 2011).

Antigen presentation to CD4+ T cells by macrophages infected with *L. major* in peripheral tissue (cutaneous) sites was shown to have a highly diverse nature (Filipe-Santos et al., 2009). Some CD4+ T cells exhibited transient, short-lived contacts whilst only a subset were shown to form longer lived (≥ 30 min), stable interactions with infected cells. It is notable that for the majority of stable interactions only one CD4+ T cell formed a conjugate with each infected macrophage (Filipe-Santos et al., 2009). This contrasts, the multiple CD4+ T cells to one macrophage previously observed *in vitro* (Underhill et al., 1999). In similarity to Egen et al. (2011) spatial heterogeneity in the efficiency of antigen presentation was observed in which a small number of T cell were observed to arrest at particular ‘hotspots’ in the infection site. Interestingly both antigen-specific and activated polyclonal CD4+ T cells were able to enter the site of infection with the same efficiency, although only the former were observed to pattern to areas of infected macrophages

within the cutaneous lesion (Filipe-Santos et al., 2009). In general the *in vivo* data tends to support the *in vitro* concept that the macrophage–CD4+ T cell interaction in tissues involves kinapse-type interactions and that synapses can occur but are limited by antigen availability.

The details and dynamics of the IS were developed through examining the interactions between T cells and planar bilayers, B cells or DCs. These interactions have been investigated using both murine and human cells *in vitro* and *in vivo*. Murine systems have previously been used to study the formation and dynamics of the macrophage-CD4+ T cell IS, yet very little, if any, work has been done in human cells. With regards to CCR5, this chemokine receptor has been implicated in IS formation between a number of cell types however its role in the macrophage–CD4+ T cell IS has not yet been established. This study examines the formation of a macrophage–CD4+ T cell IS *in vitro* using human cells and investigates the role of CCR5 with particular focus on the macrophage side of this interaction.

1.4 Research aims

- To develop an *in vitro* system using primary human MDMs and CD4+ T cells to characterise the formation of productive MDM-CD4+ T cell interactions leading to IS formation

- To determine whether endogenously expressed CCR5 and CXCR4 are recruited to the MDM-CD4+ T cell IS

- To explore factors that may impact the lateral mobility of endogenous CCR5 on the MDM membrane

Chapter 2: Methods

2.1 Isolation of primary human cells

2.1.1 Isolation of monocytes by adherence

Prior to commencing isolation, all media and solutions were equilibrated to room temperature (RT) for a minimum of 2 h and, for each donor, five 14.5 cm dishes (Greiner bio-one, Kremsmuenster, Austria) were coated with gelatin (Sigma Aldrich, Gillingham, UK) and left to dry during this period. Details of the composition of solutions used in this study can be found in **Table 2.1**. Single donor leukocyte aphaeresis cones (NHS Blood and Transport Service, UK) were drained into a tube containing 10 ml phosphate buffered saline (PBS) before residual cells were washed from the cone using 35 ml PBS. The volume was made up to 50 ml with PBS after removing two aliquots: 11 ml for CD4+ T cell isolation and 200 µl for comparison of the purity of CD4+ T cell isolation. The remaining volume of PBS diluted blood was distributed into three tubes containing 14 ml of Lymphoprep (Axis Shield, Oslo, Norway) by gently layering over the top of the density separation media. Tubes were centrifuged at 2000 rpm for 34 min (swing-out rotor, acceleration "5" and no brake). The peripheral blood mononuclear cell (PBMC) layer was removed using a Pasteur pipette and dispensed into a single 50 ml tube containing 10 ml PBS. PBMCs were washed twice in 35 ml PBS at 1050 rpm, then 2 – 4 times in 35 ml HBSS without Ca^{2+} or Mg^{2+} at 1100 rpm, both steps using gentle acceleration ("7") and braking ("6") during centrifugation. PBMCs were resuspended in 35 ml of RPMI without serum (nsRPMI), a cell-count taken using a haemocytometer (a mean of $6.5 \times 10^8 \pm 3.5 \times 10^8$ PBMCs), then washed into 25 ml 5% (v/v) FCS-RPMI and dispensed over the gelatin-coated plates before adding 10 ml 5% (v/v) FCS-RPMI v/v to each plate. Cells were incubated for 2 h at 37 °C, 5% CO_2 before non-adherent cells were removed and each plate washed vigorously a minimum of 4 times with 7 ml 5% (v/v) FCS-RPMI. Adherent cells were detached in 10% (v/v) FCS-RPMI using a cell scraper (Sarstedt, Nümbrecht, Germany), washed once, counted (on average $5.3 \times 10^7 \pm 2.5 \times 10^7$ monocytes) and aliquoted into 10 cm plates (TPP, Trasadingen, Switzerland), 7 ml/plate at a density of 0.7 – 1.0×10^6 monocytes/ml.

2.1.2 Isolation of CD4+ T cells

CD4+ T cells were isolated from total blood using the RosetteSep human CD4+ T cell enrichment cocktail (Stemcell Technologies, Grenoble, France) according to the manufacturer's instructions. Briefly, 0.5 ml RosetteSep human CD4+ T cell enrichment

Name	Composition
Cell Culture	
nsRPMI (RPMI without serum)	500 ml RPMI 1640 (without L-glutamine), 2 mM L-glutamine, 100 U/ml Penicillin, 100 µg/ml Streptomycin, 12.5 mM 4-(2-hydroxyethyl)-1-piperazineethanesulfonic acid (HEPES).
5% (v/v) FCS-RPMI	As for nsRPMI, plus 25 ml PAA gold FCS (PAA Laboratories GmbH)
10% (v/v) FCS-RPMI	As for nsRPMI, plus 50 ml PAA gold FCS (PAA Laboratories GmbH) Note: HyClone™ FCS (Thermo Fisher Scientific Inc.) was used for cells lines e.g. CHO-K1
5% (v/v) huAB-RPMI	As for nsRPMI, plus 25 ml human AB serum (PAA Laboratories GmbH)
10% (v/v) MEM eagle	500 ml Minimal essential media (MEM) eagle, alpha modification (Sigma-Aldrich), 2 mM L-glutamine, 100 U/ml Penicillin, 100 µg/ml Streptomycin, 12.5 mM HEPES, 50 ml Hyclone™ FCS.
MC5 Hybridoma media	DMEM with 4.5 g/L glucose, 2 mM L-glutamine, 1 x HT supplements, 1 mM sodium pyruvate, 100 U/ml Penicillin, 100 µg/ml Streptomycin
PBS	500 ml ddH_20, PBS tablet (Life Technologies Ltd.). Autoclaved
Immunolabeling Solutions	
Binding Media (BM)	10 ml 10x RPMI 1640 without carbonate or glutamine (Sigma-Aldrich), 90 ml ddH_20, 0.2% (w/v) BSA, 10 mM HEPES.
FACS buffer	PBS, 1% (v/v) FCS, 0.05% (w/v) Sodium Azide
Quench solution (NH_4Cl)	50 mM NH_4Cl in FACS buffer
Other Solutions	
Binding Buffer	20 mM Sodium Phosphate, pH 7.0
Elution Buffer	0.1 M Sodium Citrate, pH 3.0

Table 2.1: Composition and abbreviations of solutions used. All reagents are from Gibco® Life Technologies unless stated otherwise. Before use all FCS was decomplemented by heating at 56 °C for 30 min.

cocktail was added to 11 ml of blood, mixed and incubated for 20 min at RT. The sample was diluted 1:1 with 2% (v/v) FCS-PBS then gently layered over 15 ml Lymphoprep and centrifuged for 20 min at 1200 x g with no brake. CD4+ T cells were removed from the interface as described for the buffy coat in section 2.1.1, washed twice in 35 ml 2% (v/v) FCS-PBS, counted using a haemocytometer (on average 4.6 x 10^7 ± 2.5 x 10^7 CD4+ T cells), washed once with 35 ml 10% (v/v) FCS-RPMI and finally resuspended in 10% (v/v) FCS-RPMI at 2 x 10^6 cells/ml. A summary cartoon of separation and differentiation is shown in **Fig. 2.1a**.

2.2 Cell culture and differentiation conditions

2.2.1 Generating monocyte-derived macrophages

From the day of isolation (day 0), monocytes were cultured in 10% (v/v) FCS-RPMI for 48 h before media was replaced with 10% (v/v) FCS-RPMI supplemented with 50 ng/ml M-CSF (Peprotek, NJ, USA). During differentiation to MDMs, media was changed every 2 – 3 d as indicated (**Fig. 2.1b**). M1-polarised MDMs were also cultured in 10% (v/v) FCS-RPMI but instead of adding M-CSF, GM-CSF (R&D Systems, Abingdon, UK) was added on day 1 then 50 ng/ml IFNγ (Sigma-Aldrich) and 10 ng/ml LPS (Sigma-Aldrich) were added from day 5 onwards (**Fig. 2.1b**). All MDMs were harvested using cell scrapers.

2.2.2 Culture of CD4+ T cells

CD4+ T cells were cultured overnight in 10% (v/v) FCS-RPMI before adding 5 µg/ml phytohaemagglutinin-M (PHA; Sigma-Aldrich) for 3 d. After stimulation, cells were cultured in 10% (v/v) FCS-RPMI supplemented with 10 U/ml IL-2 (Peprotek) in T75 flasks for the remaining duration of the culture, replenishing media every 2 – 3 d (**Fig. 2.1b**). Alternatively, after overnight culture CD4+ T cells were adjusted to a density of 1 x 10^6 cells/ml, transferred to 24-well plates (Sigma-Aldrich) (1 ml/well), and to each well 25 µl of washed human T-activator CD3/CD28 Dynabeads® (Invitrogen, Paisley, UK) was added alongside 30 U/ml IL-2. These T cells were counted every 48 h using a haemocytometer and were split 1:1 when counts exceeded 2 x 10^6 cells/ml, after taking into account loss of media volume by weighing the 24-well plate. In all cases CD3/CD28 activated cells were magnetically separated before use according to the guidelines supplied from Invitrogen.

2.2.3 Culture of cell lines

DHFR-deficient CHO cells stably transfected with human CCR5 (CHO-CCR5) (Mack et al., 1998) were cultured in 10% (v/v) FCS-MEM eagle, α modification (Sigma-Aldrich) in 10 cm dishes (BD Biosciences) until 80-90% confluency, then detached with 10 mM

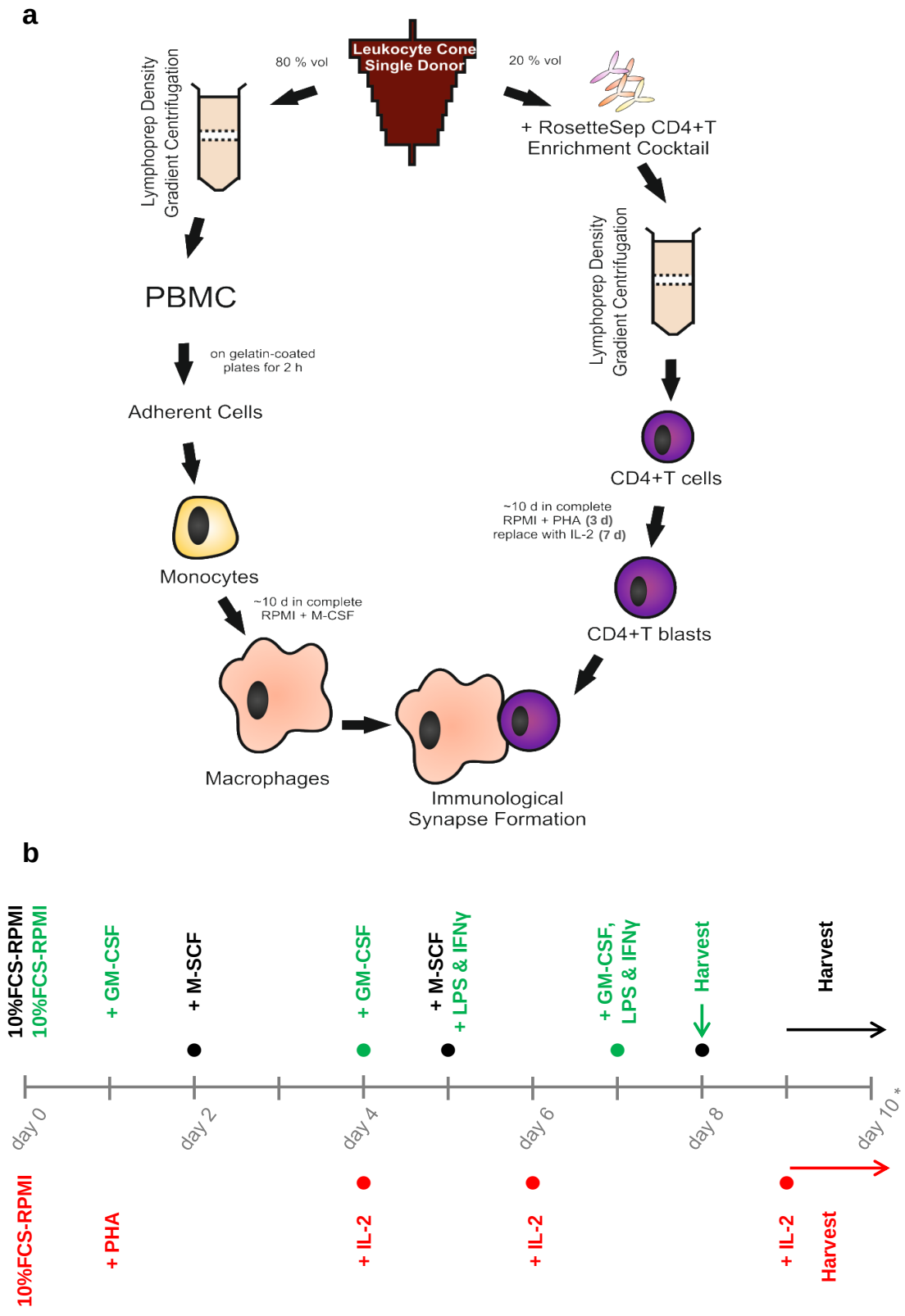

* After day 10, MDMs and CD4+ T cells were passaged on day 11 and 14.

Figure 2.1: Timeline for culture of primary cells. Monocytes isolated on day 0 are cultured to generate MDMs which are conditioned in **M-CSF** or **GM-CSF**. The timeline also shows the stages at which PHA and IL-2 are added in order to generate **PHA-activated CD4+ T cells**. The full circle (coloured accordingly) indicates the day on which media is replaced, which is not necessarily concomitant with the addition of growth factors or cytokines.

ethylenediamintetraacetic acid (EDTA) in PBS and split 1:30. CHO-K1 cells, kindly provided by Prof PM Kaye (University of York, York, UK), were cultured in an identical manner but using 10% (v/v) FCS-RPMI. Daudi cells, kindly provided by Dr G Doody (University of Leeds, Leeds, UK), were cultured in T75 flasks using 10% (v/v) FCS-RPMI and viability was assessed routinely by staining aliquots 1:1 v/v with 0.4% (w/v) trypan blue solution (Sigma-Aldrich). Daudi cells were maintained at 0.5 – 2.0 x 10^6 viable cells/ml and passaged by centrifuging for 5 min, 180 x g, resuspending in fresh media.

2.2.4 Cryopreservation of cells

Cells were centrifuged at 250 x g, 5 min then resuspended in PAA gold FCS (PAA Laboratories GmbH, Pasching, Austria), typically at a density of 2 x 10^7 cells/ml and aliquoted into Nunc™ cryovials (Thermo Fisher Scientific Inc.) before adding 20% (v/v) dimethyl sulphoxide (DMSO; Sigma-Aldrich) in FCS at a 1:1 ratio, inverting the vial to mix and transferring to a Mr. Frosty™ freezing container (Thermo Fisher Scientific Inc.) precooled to 4 °C. This was stored at -80 °C for 24 h before vials were transferred to liquid nitrogen for long-term storage. Note that PBMCs and any non-adherent cells (monocyte-depleted PBMCs) were cryo-preserved at higher final densities, ~5 x 10^7 and 1 x 10^8, respectively. Vials were thawed rapidly in a 37 °C water-bath until only a small crystal of ice remained before adding an equal volume of pre-warmed media dropwise to the vial over ~30 s. The entire contents of the vial were then transferred to a tube containing 20 ml media (at 37 °C) and cells were washed once more with media before incubation at 37 °C, 5% CO_2.

2.3 Purification and coupling of the anti-CCR5 mAb MC5

The monoclonal antibody (mAb) MC5 was produced by a hybridoma grown in MC5 hybridoma media (see **Table 2.1**) from which supernatant was collected by centrifugation at 300 x g, 5 min to remove cells, then frozen at -80°C. Once 500 ml of the hybridoma supernatant had been collected the volume was mixed 1:1 with Binding Buffer in a 1L sterile conical flask. A 1 ml HiTrap™ rProtein A FF column (GE Healthcare Life Sciences, Buckinghamshire, UK) was used to purify the antibody according to the manufacturers instructions. Briefly, the column was regenerated by running 15 ml Elution Buffer through, then equilibrated with 20 ml Binding Buffer before the supernatant:Binding Buffer solution was run through the column at 0.9 ml/min using a peristaltic pump. The column was washed with 15 ml Binding Buffer, then MC5 was eluted with Elution Buffer into 1 ml aliquots containing 100 µl 1M Tris-HCl (pH 9.0). Aliquots with A280 > 0.6 were combined and dialyzed into PBS using Snakeskin MWCO 3.5K (Pierce Biotechnology, IL, USA). The concentration was determined to be 5.4 mg/ml using the Bradford assay.

The MC5 antibody was fluorescently coupled using the DyLight^{488} kit or DyLight^{650} microscale kit (Pierce Biotechnology) according to the manufacturer's instructions (instruction sheet 1897.10; www.thermoscientific.com/pierce). For the DyLight^{488} kit a number of modifications were made in order to achieve a dye:protein (D:P) molar ratio of approx. 3. Specifically, 620 µl MC5 was mixed with 49.6 µl 0.67 M borate buffer and subsequently 600 µl (3 mg antibody) of this mixture was incubated with the vial of DyLight^{488}. Each spin column was packed with an increased amount of resin (300 µl) in order to accommodate the increased volume (300 µl) of MC5-DyLight^{488} solution that was loaded. The absorbance at 280 nm and 493 nm was measured using NanoDrop spectrophotometer (Thermo Fisher Scientific Inc.) in order to estimate the resulting concentration and D:P ratio.

2.4 Immunolabelling techniques for flow cytometry

Antibodies were acquired from the following sources as indicated in **Table 2.2.**

2.4.1 Standard flow cytometry immunolabelling method: characterisation of cells

On day 1 and day 9 of culture monocytes/MDMs, detached by scraping, and CD4+ T cells were counted and aliquoted into a Corning® U-bottomed 96-well plate (Thermo Fisher Scientific) at 1 x 10^5 cells/well. The plate was centrifuged at 300 x g, 3 min, 4 °C to pellet cells; centrifugation conditions were kept constant until cells were fixed, after which cells were centrifuged at 19 °C. Supernatant was flicked off and the cell pellets resuspended in 50 µl/well 30 µg/ml immunoglobulin G (IgG) human serum (huIgG; Sigma-Aldrich) made up in binding media (BM) and incubated for 30 min at 4 °C. Cells were centrifuged and the Fc-receptor (FcR) block discarded before resuspending pellets in 50 µl/well 5 µg/ml primary antibody solutions made up in BM and incubating for 90 min at 4 °C. Wells containing monocytes/MDMs were incubated with antibodies against CD3, CD4, CD11b, CD14, CD16, CD19, CD68, CD83, human leukocyte antigen-DR (HLA-DR) and CCR5 (MC5, CTC5, 2D7). T cells were incubated with antibodies directed against the underlined markers and additionally CD8, CD25 and CD45RO (**Table 2.2**). After incubation, cells were washed three times in 250 µl/well BM at 4 °C then resuspended in 200 µl/well cold 3% (w/v) paraformaldehyde (PFA: Polysciences Inc., PA, USA) made up in PBS and fixed for 20 min at RT. Fixative was removed and cells were washed and incubated for 20 min in quench solution, centrifuged then resuspended in 50 µl/well of 4 µg/ml goat anti-mouse (GAM)- R-phycoerythrin (PE) secondary antibody solution and incubated for 60 min. Cells were washed three times with 250 µl/well FACS buffer then analysed on a FACSArray^{TM}.

Primary Antibodies					
Specificity	**Clone**		**Isotype**	**Source**	**Catalogue Number**
CD3	UCHT1		IgG1	Biolegend	300402
CD3	OKT3		IgG2a	Biolegend	317304
CD4	RPA-T4		IgG1	Biolegend	300502
CD8	RPA-T8		IgG1	Biolegend	301002
CD11b	ICRF44		IgG1	eBioscience	14-0118-82
CD14	UCHM1		IgG2a	AbDSerotec	MCA596GA
CD16	eBioCB16		IgG1	eBioscience	14-0168-80
CD19	HIB19		IgG1	eBioscience	14-0199-82
CD25	BC29		IgG1	eBioscience	14-0259-82
CD45RO	UCHL1		IgG2a	eBioscience	14-0457-82
CD68	Y1-82A		IgG2b	BD Pharmingen	556059
CD80	2D10		IgG1	Biolegend	305201
CD83	HB15e		IgG1	BD Pharmingen	556854
CD163	GHI/61		IgG1	Biolegend	333602
GM130	35/GM130		IgG1	BD Biosciences	610822
HLA-DR	L243		IgG2a	Biolegend	307612
LPBA	6C4		IgG1	Echelon	Z-LBPA
TfR	H68.4		IgG1	Invitrogen	13-6890
TGN46*	TGOLN2		IgG	AbD Serotec	AHP500
Antibodies Against Chemokine Receptors					
CCR5	45531		IgG2b	R&D Systems	MAB182
CCR5	2D7		IgG2a	BD Pharmingen	555991
CCR5	CTC5		IgG1	R&D Systems	MAB1802
CCR5	MC5		IgG2a	Produced in-house	
pS^{349} CCR5	EII/19		IgG1	Biolegend	321602
CXCR4	12G5		IgG2a	Kind gift from Prof. Q Sattentau	
Isotype Control Antibodies					
IgG2a κ IsoControl^{488}	eBM2a		IgG2a	eBioscience	53-4724-80
IgG2a κ IsoControl	eBM2a		IgG2a	eBioscience	14-4724-85
IgG1 κ IsoControl	P3.6.2.8.1		IgG1	eBioscience	14-4714-85
Secondary Antibodies					
Specificity	**Name**	**Host**	**Fragment**	**Source**	**Catalogue Number**
Mouse IgG	GAM-Fab^{488}	Goat	Fab	Jackson ImmunoResearch	115-547-003
Mouse IgG	GAM^{488}	Goat	$F(ab')_2$	Invitrogen	A11017
Mouse IgG	GAM^{594}	Goat	$F(ab')_2$	Invitrogen	A11020
Mouse IgG	SAM^{PE}	Sheep	Whole IgG	Sigma-Aldrich	P8547
Sheep IgG	DAS^{488}	Donkey	Whole IgG	Invitrogen	A11015
Mouse IgG1	GAM-IgG1^{488}	Goat	Whole IgG	Invitrogen	A21121
Mouse IgG2a	GAM-IgG2a^{647}	Goat	Whole IgG	Invitrogen	A21241

Table 2.2: Details and sources of antibodies

Bioanalyser flow cytometer (BD Biosciences). All steps after fixation were carried out at RT and with shaking during incubations

2.4.2 Immunolabelling MDMs for CD80 and CD163 expression

MDMs generated by culture with GM-CSF or M-CSF (**Fig. 2.1b**) were harvested on day 8 of culture and aliquoted at 1 x 10^5 cells/well into U-bottomed 96-well plates. MDMs to be labelled with anti-CD163 were fixed immediately in 200 µl/well 3% (w/v) PFA (in PBS) for 20 min at RT. Cells were washed and incubated in 250µl/well quench solution for 20 min, FcR-blocked with 50 µl/well 30 µg/ml huIgG for 30 min, centrifuged, then resuspended in 50 µl/well 5 µg/ml anti-CD163 or IgG1 isotype control primary antibody solutions and incubated for 60 min. Cells were washed three times then resuspended in 50 µl/well 4 µg/ml GAM-IgG1^{488} secondary antibody solution, incubated for 60 min, then washed three more times. All antibody solutions prepared, and wash steps performed (250 µl/well) are in FACS buffer and all incubations involve shaking.

MDMs to be labelled with anti-CD80 were labelled live. Cells were FcR-blocked in 50 µl/well 30 µg/ml huIgG in BM for 25 min, centrifuged, and FcR-blocking solution discarded before the cell pellets were resuspended in 100 µl/well 5 µg/ml anti-CD80 or IgG1 isotype control made up in BM and incubated for 20 min. The cells were washed three times in 250 µl/well BM then resuspended in 100 µl/well 4 µg/ml GAM-IgG1^{488} made up in BM and incubated for 20 min. Subsequently, cells were washed twice with PBS before the cell pellets were resuspended in 200 µl/well violet live/dead fixable dye (Life Technologies Ltd., Paisley, UK) at 1:1000 in PBS (stock: 50 µl DMSO added to 1 vial of lyophilized dye) and incubated for 30 min. After washing cells twice in PBS, 200 µl/well ice-cold 3% (w/v) PFA was added to each well and cells were fixed at RT for 20 min. The plate was washed once with FACS buffer and samples were kept at 4 °C until analysis. All centrifugation was carried out at 300 x g, 3 min and cells were kept at 4 °C with shaking during incubations at all times, unless stated otherwise. All samples were analysed using a CyAn^{TM} ADP Analyser flow cytometer (Beckman Coulter Ltd., High Wycombe, UK).

2.4.3 Competition binding assay

MDMs (day 9) were treated in accordance with the method detailed in section 2.4.1, but with the following solutions in place of the primary antibody. To MDMs 50 µl/well of a solution of 15 µg/ml MC5^{488} alone or with 0.1, 1.0, 5.0 or 15.0 µg/ml MC5 was added. A control well containing 15 µg/ml IgG2a^{488} isotype control was also included. After fixation, cells were analysed using a CyAn^{TM} ADP Analyser flow cytometer. Background-corrected Median Fluorescence Intensity (MFI) values were calculated by subtracting the

fluorescence intensity of the isotype control, and results were expressed as a percentage of the MFI value at 15 µg/ml $MC5^{488}$ alone.

2.4.4 Titrations

MDMs (day 9-11 of culture) were detached by scraping, resuspended at 2 x 10^6 cells/ml in BM containing 30 µg/ml huIgG and incubated for 30 min, 4 °C. During this incubation a U-bottomed 96-well plate was prepared containing 12.5 µl/well MC5, CTC5, 2D7, IgG1 or IgG2a isotype controls in separate wells that had been double-diluted to cover a concentration range of 0.2-50 µg/ml. FcR-blocked MDMs (or CHO-CCR5 cells) were resuspended at 8 x 10^6 cells/ml in BM containing 10 µg/ml huIgG and aliquoted over the prepared 96-well plate at 12.5 µl/well, giving a final concentration range of 0.1-25 µg/ml. Cells were incubated for 90 min, 4 °C before 200 µl BM was added and cells were washed three times in 250 µl BM then fixed in 200 µl/well 3% PFA (w/v in PBS) for 20 min, RT. After washing and 20 min incubation in 200 µl/well quench solution, cells were resuspended in 50 µl/well 4 µg/ml GAM^{647} in FACS buffer and incubated for 60 min. Finally, cells were washed three times in FACS buffer and analysed by flow cytometry. After acquisition the concentration-matched isotype control MFI was subtracted from the MFI reading of each specific antibody.

A similar method was used for titration of $MC5^{488}$ (D:P ratio, 5.4) and MC5 followed by GAM-Fab^{488} but with the following amendments. $MC5^{488}$ and $IgG2a^{488}$ isotype control or MC5 and IgG2a isotype control were double diluted to give a final concentration range of 0.006-100 µg/ml after 1:1 v/v addition of 20 µl/well FcR-blocked MDMs (at 5 x 10^6 cells/ml). In line with the fluorescence recovery after photobleaching (FRAP) immunolabelling procedure $MC5^{488}$ and $IgG2a^{488}$ were incubated for 90 min, during which time MC5 and IgG2a were incubated for 60 min, washed then incubated with 50 µl/well 4 µg/ml GAM-Fab^{488} for 30 min. MDMs labelled using either method were then washed and analysed live on a CyAn ADP flow cytometer, adding 4',6-diamidino-2-phenylindole, dihydrochloride (DAPI; Invitrogen) at a final concentration of 5 µg/ml prior to analysis to enable live/dead exclusion. All steps were performed at 4 °C.

2.4.5 Testing MC5 dissociation

MDMs (day 8/9 of culture) were aliquoted (1x 10^5 cells/well) into U-bottomed 96-well plates, centrifuged at 300 x g for 3 min then resuspended in 25 µl/well 30 µg/ml huIgG in BM. Cells were incubated for 30 min before the addition of 25 µl/well 10 µg/ml MC5 or IgG2a isotype control in BM and a further incubation for 60 min. After washing three times with 250 µl/well BM, cells were resuspended in 100 µl/well 4 µg/ml GAM-Fab^{488} in BM and incubated for 30 min. Cells were washed as before and each well transferred into an

individual tube on ice. At this point half of the samples were fixed at 4 °C in 200 µl 3 % PFA (w/v in PBS) for 20 min, washed then incubated for 20 min in 200 µl quench solution. Note, all steps prior to this were carried out at 16 °C. The total volume was made up to 300 µl/tube with BM before samples were either incubated on ice or plunged into a 37 °C water bath for 0, 15 or 30 min. Immediately after incubation 700 µl ice-cold BM or 4.3% PFA (w/v in PBS) was added to samples that had, or had not, been fixed, respectively. Note that for one donor MDMs were not fixed at this point but were washed in BM and incubated once again with 100 µl 4 µg/ml GAM-Fab^{488} for 30 min, then washed and fixed. After 20 min incubation samples were washed into FACS buffer and kept on ice until analysis using a CyAn^{TM} ADP Analyser flow cytometer. The same procedure was carried out for CHO-CCR5 cells but without FcR-blocking steps.

General note: when immunolabelling primary cells all antibody solutions were supplemented with 5 µg/ml huIgG. All flow cytometry analysis was performed using FloJo (TreeStar, OR, USA).

2.5 Lymphocyte proliferation assay

2.5.1 CFDA-SE labelling PBMCs

PBMCs were thawed, as detailed in section 2.2.4, counted using a haemocytometer and the cell density adjusted to 1 x 10^7 PBMCs/ml. A solution of 1.68 µM Vybrant® carboxyfluorescein diacetate N-succinimidyl ester (CFDA-SE) (Life Technologies Ltd.) in PBS was made from a 10 mM CFDA-SE stock solution in DMSO and added 1:1 v/v to the PBMCs, mixed by pipetting and incubated at 37 °C, 5% CO_2 for 15 min. Labelled PBMCs were centrifuged at 400 x g, 5 min, the supernatant aspirated and the pellet resuspended in 2 ml 10% (v/v) FCS-RPMI, in which cells were incubated for a minimum of 30 min at 37 °C, 5% CO_2. Subsequently, cells were washed three times in 5% (v/v) huAB-RPMI to remove all traces of FCS then cultured overnight in a 10 cm dish (TPP). Labelled PBMCs were removed by scraping, counted, and the density adjusted to 2 x 10^6 cells/ml before pipetting 100 µl aliquots into a sterile Corning® U-bottomed 96-well plate (Thermo Fisher Scientific Inc.). 100 µl 5% (v/v) huAB-RPMI, alone or supplemented with stimulants, was added to triplicate wells of PBMCs in order to achieve final concentrations of 2.5 µg/ml PHA, 1:20000 Imject® Alum (Pierce Biotechnology) and 1:1000 Revaxis® (Sanofi-Pasteur MSD), a kind gift from Prof. C Lacey (University of York, York, UK). During CFDA-SE labelling all solutions had been pre-equilibrated to 37 °C. Finally the 96-well plate was incubated for 5 days at 37 °C, 5% CO_2.

2.5.2 Live/dead staining, fixation and immunolabelling of cells for flow cytometry

Post-incubation CFDA-SE labelled PBMCs were washed twice in PBS involving centrifugation at 300 x g, 3 min at RT (centrifugation and temperature are constant for all remaining steps), then cell pellets were resuspended in 200 µl/well violet live/dead fixable dye (Invitrogen) at 1:1000 in PBS and incubated for 30 min. After this, cells were washed twice with PBS then fixed in 250 µl/well 3.7% PFA (w/v in PBS) for 20 min, then immunolabelled with CD3 (OKT3) or IgG2a isotype control followed by GAM^{647} secondary antibody according to the method detailed for CD163 in section 2.4.2. Cells were analysed using a $CyAn^{TM}$ ADP Analyser flow cytometer.

2.6 Purification and transfection of CCR5-GFP DNA

2.6.1 Plasmid DNA: sources and purification

The N-terminal GFP-CCR5 plasmid (Gomez-Mouton et al., 2004) and the C-terminal CCR5-GFP sequence (Hüttenrauch et al., 2005) subcloned into pcDNA3.1(+) were kind gifts from Prof. M. Marsh. Plasmids were transformed by heat shock for 70 s, 42 °C into chemically competent DH5α and selected for by resistance to Ampicillin (100 µg/ml) or Kanamycin (50 µg/ml), as appropriate. Single colonies were picked and grown in Luria-Bertani broth overnight before being harvested for Midi or Maxi prep plasmid purification (QIAGEN Ltd., Manchester, UK) according to the manufacturer's instructions. The DNA concentration was assessed by Nanodrop A_{260} reading and adjusted to 1 µg/µl in Tris-EDTA buffer (QIAGEN Ltd.) before storage at -20 °C.

2.6.2 Transient transfection into MDMs and CHO-K1 cells

MDMs were transfected on day 8 using the Amaxa® Human Macrophage Nucleofector Kit (Lonza Group Ltd., Basel, Switzerland) according to the manufacturers protocol. Briefly, MDMs were detached using 2.2 ml/plate 0.25% (w/v) Trypsin-EDTA (Life Technologies Ltd.) for 25 min at RT, washed in 10% (v/v) FCS-RPMI, counted and adjusted to ~0.5 x 10^5 MDMs/tube. MDMs were then resuspended in Nucleofector solution and nucleofected on program Y-10 in the presence of 5 µg either CCR5-GFP or GFP-CCR5 plasmid DNA. Immediately, MDMs were transferred into 0.5 ml 10% (v/v) FCS-RPMI and split between two collagen-coated coverslip glass-bottomed dishes (MatTek Corporation, MA, USA) to adhere for 20 min at 37 °C, 5% CO_2 before adding 2 ml 10% (v/v) FCS RPMI supplemented with 50 ng/ml M-CSF to each dish and culturing for 48 h prior to FRAP. Notably, the transfection efficiency was very low as fewer than 20 CCR5-GFP+ cells were found on each dish.

CHO-K1 cells were transfected using a lipid-based reagent called GeneCellin™ (BioCellChallenge, Paris, France), according to the manufacturer's protocol. In short, 24 h prior to transfection CHO-K1 cells were seeded onto collagen-coated coverslip glass-bottomed dishes at 5 x 10^4 cells/dish in a volume of 2 ml 10% (v/v) FCS-RPMI. In a polypropylene tube, 2 µg GFP-CCR5 or CCR5-GFP was diluted in 200 µl nsRPMI before adding 8 µl GeneCellin™, vortexing and incubating for 15 min at RT. The solution was pipetted dropwise onto the CHO-K1 cells then incubated for 48 h at 37 °C, 5% CO_2 before FRAP was performed.

2.7 Coverslip coatings

To generate poly-D-lysine (PDL) coated coverslips a solution of 100 µg/ml PDL (70-150 kDa; from Poly-D-lysine hydrobromide (Sigma-Aldrich)) was pooled onto either 10 mm #1.5 coverslips (Agar Scientific, Stansted, UK) or the centre of 25 mm #1.0 coverslips (SLS, East Riding, UK), which had been washed with 100% ethanol and air-dried, and was incubated for 30 min, RT. Excess PDL solution was removed and coverslips were washed extensively with sterile water and air-dried before use.

35 mm uncoated, PDL or collagen coated coverglass-bottomed dishes (#1.5) were obtained from MatTek Corporation. For polyethylenimine (PEI) coating, uncoated dishes were washed in 100% ethanol then air-dried before pooling over 300 µl 1% (w/v) PEI solution and incubating for 10 min. Excess PEI was removed and dishes were washed with 95% ethanol, air-dried then incubated with 300 µl 0.1% (w/v) glutaraldehyde for 30 min. Dishes were washed extensively with sterile water and allowed to dry.

2.8 Immunolabelling for FRAP

2.8.1 Indirect immunolabelling procedure

MDMs were detached using cell scrapers on day 8, counted and seeded onto collagen-coated coverglass-bottomed dishes in 250 µl 10% (v/v) FCS-RPMI at 1.5 x 10^5 MDMs/dish. Cells were allowed to adhere to the glass for 20 min at 37 °C, 5% CO_2 before 2 ml 10% (v/v) FCS-RPMI, supplemented with 50 ng/ml M-CSF, was added to each dish and incubation at 37 °C, 5% CO_2 for 24 h followed. For experiments with CHO-CCR5 cells, cells were seeded at the same density 24 h prior to immunolablelling. On day 9, media was decanted and blotted away with filter paper then MDMs were FcR-blocked for 30 min with 100 µl 30 µg/ml Fc-fragment huIgG (Bethyl Laboratories Inc., TX, USA) made up in BM. After this, 100 µl MC5 at 10 µg/ml in BM was added to the MDMs, which were

then incubated for 60 min further. Antibody solutions were discarded and MDMs washed three times in 1 ml/dish BM, incubating for 2 min/wash. Excess BM was blotted away and MDMs were incubated for 30 min in 200 µl 4 µg/ml GAM-Fab^{488}, made up in BM supplemented with 5 µg/ml Fc-fragment huIgG, prior to washing three times as described previously. All immunolabelling steps were carried out at 16 °C and preceded addition of 2 ml pre-warmed phenol-red free RPMI and transfer to the 37 °C stage incubator on the confocal microscope. Samples were incubated on the stage for 20 min prior to commencing FRAP. The final imaging conditions are described in section 5.2.6 and accompanying figures. Under these conditions cells were imaged at 3 s intervals for 20 cycles, bleached, imaged for a further 20 cycles, then the interval switched to 10 s for the remaining 32 cycles.

2.8.2 Direct immunolabelling procedure

MDMs were seeded onto PEI, PDL or collagen-coated dishes, where indicated, and FcR blocked as described in section 2.8.1. Subsequently, FcR-block was removed and MDMs were incubated with 100 µl 20 µg/ml MC5^{488} (D:P ratio, 5.4) in BM containing 5 µg/ml huIgG for 90 min, 16 °C. Cells were washed three times with BM before addition of 2 ml pre-warmed 10% (v/v) FCS-RPMI, transfer to the 37 °C stage incubator and commencement of FRAP after a short period of incubation (~5 min) to equalize temperature inhomogeneity between the sample and the objective (Plan-Apochromat 63x/1.20 water immersion). For directly labelled MDMs, imaging conditions for PEI [Bleach: 100% laser power, 15 iterations, 8.70 x 3.43 µm region of interest (ROI). Acquisition: 1.7% laser power, 1.58 µs pixel dwell, 44.90 x 44.90 µm field of view, 51 µm pinhole,12 bit, no line average, 3 s interval, 121 cycles, bleach after 15 cycles] were similar to collagen/PDL/CyGel but with the following modifications [Bleach: 26% laser power, 20 iterations, 13.05 x 5.14 µm ROI. Acquisition: 2.55 µs pixel dwell, 67.34 x 67.34 µm field of view, bleach after 20 cycles].

All FRAP data was acquired using a Zeiss LSM 780 Axio Observer.Z1 invert confocal microscope (Carl Zeiss Ltd., Cambridge, UK) at 37 °C with a supply of 5% CO_2 mixed with atmospheric air to prevent acidification of the media. Zen 2010 software (Carl Zeiss Ltd.) was used for acquisition and export of the intensity data for each timepoint in the bleach, decay and background ROIs drawn.

2.8.3 Labelling with DiO

MDMs were seeded in dishes as described in section 2.8.1 and on day 9, media was removed and MDMs were washed with PBS. PBS was removed before 100 µl of a 5 µM Vybrant™ DiO Cell Labelling Solution (Life Technologies Ltd.) made up in PBS, was

pooled over the cells and incubated for 3 min at 37 °C. Excess dye was aspirated and MDMs were washed three times in 2 ml 10% (v/v) FCS-RPMI, 10 min incubation per wash, before phenol-red free RPMI was added and FRAP was performed. All solutions and incubation steps for this protocol were at 37 °C.

2.8.4 Mounting in CyGel

Imaging in CyGel^{TM} (BioStatus, Shepshed, UK) was performed on uncoated coverglass-bottomed dishes. CyGel^{TM} was prepared according to the manufacturer's instructions and 250 µl was pooled over the cells on the coverglass of the dish whilst on ice. Dishes were equilibrated to 37 °C for 20 min prior to FRAP.

2.9 Analytical techniques for FRAP

2.9.1 Single normalisation

FRAP bleach and decay ROIs were normalised using the FRAPcalc plugin developed by Dr. Kota Miura (EMBL, Heidelburg, Germany) for IGOR Pro (WaveMetrics Inc., OR, USA). Relevant equations from the FRAPcalc manual are presented below. For further information and definitions consult the online manual: http://cmci.embl.de/documents/frapmanu.

Each FRAP curve was loaded individually and a single exponential model was selected from the dropdown list in the 'FitPanel' window. The 'Back Multi' tickbox was checked before running the program. Using the data browser, single normalised decay ('bkgAvg_norm'; equation 1) and bleach ('FRAP_norm'; equation 2) values that had been calculated were exported into a table.

Equation 1: $I_{decay\text{-}norm}(t) = (I_{decay}(t) - I_{bkgd}(t)*(I_{bleach\text{-}pre}/ I_{decay\text{-}pre}))/ (I_{bleach\text{-}pre} - I_{bleach\ t=0})$

Equation 2: $I_{bleach\text{-}norm}(t) = (I_{bleach}(t) – I_{bleach\ t=0})/ (I_{bleach\text{-}pre} - I_{bleach\ t=0})$

$I_{decay\text{-}norm}(t)$ is the normalised decay value, $I_{decay}(t)$ is the intensity value of the decay ROI, $I_{bkgd}(t)$ is the intensity value of the background ROI, $I_{bleach\text{-}norm}(t)$ is the normalised bleach value, all at a particular timepoint (t). $I_{bleach\text{-}pre}$ is the mean value of all bleach ROI intensities, individually subtracted for background ROI intensities, which occur before the bleachpoint. $I_{decay\text{-}pre}$ is similar but is calculated using decay ROI intensities. $I_{bleach\ t=0}$ is the intensity of the bleach ROI at the bleachpoint (i.e. when t=0).

2.9.2 Double normalisation

The FRAPcalc plugin was run selecting the single exponential model from the dropdown list and the 'Phair' tickbox. The double normalised bleach curve (equation 3) was exported from the list in the data browser. Values were then spread over the full range (equation 4) in Microsoft Excel.

Equation 3: $I_{frap\text{-}norm}(t) = (I_{decay\text{-}pre}/ I_{decay}(t) – I_{bkgd}(t)) * (I_{bleach}(t) – I_{bkgd}(t)/ I_{bleach\text{-}pre})$

Equation 4: $I_{frap\text{-}spread}(t) = (I_{frap\text{-}norm}(t) - I_{frap\text{-}norm\ t=0})/ (I_{frap\text{-}norm\text{-}pre} - I_{frap\text{-}norm\ t=0})$

$I_{frap\text{-}norm}(t)$ is the double normalised decay value, $I_{frap\text{-}spread}(t)$ is the double normalised decay value spread over the full range (0 – 1), all at a particular timepoint (t). $I_{frap\text{-}norm\ t=0}$ is the double normalised intensity of the bleach ROI at t=0, $I_{frap\text{-}norm\text{-}pre}$ is the mean value of all double normalised bleach ROI values that occur before the bleachpoint.

2.9.3 Fitting normalised FRAP curves

Individual normalised bleach or decay curves for each donor were compiled and the mean ± standard deviation (SD) from the bleachpoint onwards was plotted. The single normalised decay curve for each donor was fitted with a single exponential decay (equation 5), whilst single and double normalised bleach curves were fitted with an exponential rise to maximum (equation 6). The regression curves (solid lines) for each donor are plotted, along with 95% prediction bands (dotted lines), and a plot of the mean residuals of the fit. The $t_{1/2}$ and mobile fraction values calculated alongside the regression of double normalised data were tabulated. For the mean single normalised curve and the mean 1-decay curve (generated by subtracting a value of 1 from all values comprising the decay curve) the area under each curve was calculated and tabulated. All these procedures were performed using GraphPad Prism 5 (GraphPad Softward Inc., CA, USA).

Equation 5: $I_{decay\text{-}fit}(t) = A_{decay}\, e^{\tau_{decay} t} + y_{0\ decay}$

Equation 6: $I_{frap}(t) = y_0 + Ae^{-\tau t}$

Where y_0 is the intensity value when time is zero, A is the difference between the plateau (intensity value at infinity time) and the y_0 value, τ is the time constant.

Additionally, FRAP curves were fitted individually using the FRAPcalc plugin, selecting the single exponential model from the dropdown list and the 'Phair' tickbox. This meant that each FRAP curve was double normalised (equation 3) then fitted with a single exponential rise to maximum (equation 6). Q-values for each fit were recorded. Mobile fraction and $t_{1/2}$ values from fits with residuals that passed D'Agostinos test for normality were plotted in GraphPad Prism 5.

2.9.4 Linear regression analysis of early post-bleach time-points

FRAP was performed on live or fixed MDMs that had been indirectly labelled with MC5 followed by Fab^{488}, as described in section 2.8.1. Intensity data from bleach and decay ROIs for the first 10 cycles (30 s) acquired immediately after the bleachpoint (t_0) were imported into MATLAB (Mathworks, MA, USA). Linear regression was performed by calling the *polyfit* function and the gradient of the fit, residuals, and the R^2 value were exported. The runs test was performed on the residuals and the gradients were plotted in GraphPad Prism 5.

2.10 Drug treatments

2.10.1 Disrupting cholesterol

On day 7, MDMs were seeded onto coverslip glass-bottomed dishes (1.5 x 10^5 MDMs/dish) or plated at 1.6 x 10^6 cells/well in 6 well plates then incubated for 24 h to allow the cells to adhere. Subsequently, MDMs were washed in nsRPMI then treated (at 37 °C, 5% CO_2) with the cholesterol-disrupting drugs methyl-β-cyclodextrin (MβCD), filipin III, and U18666A (all from Sigma-Aldrich) or with appropriate controls, as indicated in **Table 2.3**. MDMs in dishes were immunolabelled as described in section 2.8.1 then subjected to FRAP. MDMs treated in sterile Corning® 6-well plates (Themo Fisher Scientific Inc.) were detached by scraping, aliquoted across a U-bottomed 96-well plate and immunolabelled for CCR5 (mAbs: MC5, 2D7 and 45531) or respective isotype controls according to the method detailed in section 2.4.1.

Drug	**Stock Conc.**	**Final Conc.**	**Incubation**		**Control Dilution**
			Time (h)	**Media**	
MβCD	38 mM in ddH_20	10 mM	1	nsRPMI (+ 1:38 10x PBS)	5:19 PBS
Filipin III	1 mg/ml in Ethanol	5 µg/ml	0.25	nsRPMI	1:200 Ethanol
U18666A	10 mg/ml in ddH_20	1 µg/ml	16	10% (v/v) FCS-RPMI	1:1000 ddH_20

Table 2.3: Agents used to disrupt membrane cholesterol.

2.10.2 Downmodulation or antagonism of cell surface CCR5 on MDMs

MDMs (day 7/8) were seeded at 1 x 10^5/well into 24-well plates containing 10 mm coverslips and allowed to adhere for 24 h prior to treatment.

CCR5 downmodulation: MDMs adhered to coverslips were treated with 0.5 ml/well 100nM PSC-RANTES, a kind gift from Prof. O. Hartley (University of Geneva, Geneva, Switzerland), in 10% (v/v) FCS-RPMI for 16 h at 37 °C, 5% CO_2. After incubation, MDMs were washed three times with 10% (v/v) FCS-RPMI, coverslips were transferred to new wells then spiked or not with sAg for conjugate formation and immunolabelling as detailed in section 2.11.

CCR5 antagonism: MDMs adhered to coverslips were treated with sAg cocktail or left untreated, as described in section 2.11.1. For the final hour of sAg pulsing 0.5 ml/well 800nM TAK-779 (Ref #: ARP968: Centre of AIDS Reagents, NIBSC, Potters Bar, UK) in 10% (v/v) FCS-RPMI was added to give a final concentration of 400 nM TAK-779 in 1ml. After treatment, MDMs were washed three times in 10% (v/v) FCS-RPMI, transferred to new wells then resuspended in 250 µl 10% (v/v) FCS-RPMI before proceeding with to co-incubate MDMs with CD4+ T cells.

2.11 Imaging fixed MDM-CD4+ T cell conjugates

2.11.1 Conjugate formation

MDMs (day 7/8) were detached using cell scrapers, counted, then aliquoted at 2 x 10^5 MDMs/well into 24-well plates containing sterile 10 mm coverslips and allowed to adhere for a minimum of 24 h at 37 °C, 5% CO_2. On days 9-11 of culture media MDMs were pulsed with 0.5 ml/well sAg in 10% (v/v) FCS-RPMI for 2 h; either 1 µg/ml staphylococcal enterotoxin E (SEE) (Toxin Technology Inc., FL, USA) alone or a 1 µg/ml SEA, staphylococcal enterotoxin B (SEB) (Sigma-Aldrich) and SEE sAg cocktail, as indicated. Unpulsed controls were treated with 0.5 ml/well 10% (v/v) FCS-RPMI alone for the same duration. After treatment, media was aspirated and MDMs were washed in 1 ml/well 10% (v/v) FCS-RPMI and resuspended in 250 µl 10% (v/v) FCS-RPMI. Autologous CD4+ T cells were adjusted to 1.6 x 10^6 cells/ml and added at 250 µL/well to the MDMs in the 24-well plate giving a T cell: MDM ratio of 2:1. The plate was centrifuged at 100 x g for 1 min then incubated for 30 min at 37 °C, 5% CO_2. Immediately after incubation, media was aspirated and 0.5 ml/well 3% PFA (w/v in PBS) was added. Cells were fixed for 20 min, washed, then incubated in quench solution for 20 min before proceeding to immunolabelling. Note that prior to fixation all solutions were used at 37 °C.

2.11.2 Immunolabelling fixed conjugates: intact

Fixed conjugates were FcR blocked with 250 µl/well 30 µg/ml huIgG in 1% (v/v) FCS-PBS for 30 min. The blocking solution was aspirated and 250 µl/well 5 µg/ml UCHT1 plus 5 µg/ml MC5 in 1% (v/v) FCS-PBS was added. An isotype control was always run in parallel, which was a solution of 5 µg/ml IgG1 plus 5 µg/ml IgG2a isotype control antibodies in 1% (v/v) FCS-PBS. Cells were incubated in primary antibody solutions for 60 min then washed three times in 1 ml/well 1% (v/v) FCS-PBS, incubating for 5 min/wash, before adding 250 µl/well 4 µg/ml GAM-IgG1^{488} with 4 µg/ml GAM-IgG2a^{647} in 1% (v/v) FCS-PBS. Cells were incubated for 60 min in the secondary antibody solution, washed three times and stained for 5 min with 0.5 ml/well 1 µg/ml DAPI in PBS. Coverslips were mounted in Mowiol on Superfrost® Plus glass slides (Thermo Fisher Scientific Inc.) and set by incubating overnight. Slides were stored at -20 °C or imaged the day after immunolabelling. Conjugates were imaged with a Zeiss LSM710 Axio Observer.Z1 invert confocal microscope running Zen 2009 software (Carl Zeiss Ltd.) set up with gains and laser powers that gave no signal in the isotype control samples. The specificity of isotype-specific secondary antibodies was routinely checked by using an IgG2a primary antibody (e.g. MC5 or OKT3) with the GAM-IgG1^{488} secondary and an IgG1 primary antibody (e.g. CTC5 or UCHT1) with the GAM-IgG2a^{647} secondary. Note that all primary and secondary antibody solutions were supplemented with 5 µg/ml huIgG. Immunolabelling steps were performed at RT and incubations involved slow side-to-side shaking at 50 rpm.

2.11.3 Immunolabelling fixed conjugates: permeabilised

MDM-CD4+ T cell conjugates were labelled and mounted as described in section 2.11.2 but all blocking, wash and antibody solutions also contained 0.05% (w/v) saponin, made up from a 5% (w/v) stock of Saponin from Quillaja bark (Sigma-Aldrich), until the final staining step with DAPI.

2.11.4 Image processing

Scale bars were added and image intensities were adjusted, in order to optimise visibility when printed, using Adobe Photoshop CS3. No fluorescence was visible in associated isotype control images after identical adjustments were made. Volocity v 6.0 (PerkinElmer, MA, USA) was used for all 3D reconstructions of z-stacks. All maximum intensity projections and orthogonal sections were created using ImageJ (NIH, MD, USA).

2.12 Analysing MDM-CD4+ T cell conjugate formation by flow cytometry

2.12.1 PKH26 labelling MDMs

MDMs (day 8 of culture) were detached using a cell scraper and washed twice in 15 ml nsRPMI, centrifuging at 400 x g for 5 min. Cells were counted and 5 x 10^5 MDMs were aliquoted into a well of a 6 well plate for unlabeled controls. After centrifugation all nsRPMI was aspirated according to the manufacturer's instructions and the MDM pellet was gently resuspended in Diluent C (Sigma-Aldrich) to give a density of 2.5 x 10^6 MDMs/ml, before dividing into polypropylene tubes in 1 ml aliquots. A 4 µM PKH26 (Sigma-Aldrich) solution was prepared in Diluent C, added 1:1 v/v to the aliquoted MDMs and immediately mixed. MDMs were incubated in the PKH26 solution for 5 min at RT, and mixed by inversion half way through the incubation. To each tube 2 ml of FCS was added to stop the labelling reaction, cells were incubated for 1 min then centrifuged for 10 min at 400 x g. The supernatant was aspirated, MDMs resuspended in 10% (v/v) FCS-RPMI, then transferred to a new tube and washed twice more in 10% (v/v) FCS-RPMI to ensure removal of any unbound dye. PKH26-labelled MDMs were counted then aliquoted across a 6-well plate at 0.5 – 1 x 10^6 cells/well in 10% (v/v)FCS-RPMI supplemented with 50 ng/ml M-CSF.

2.12.2 Labelling CD4+ T cells with DiD

A 50 µM dilution of Vybrant^{TM} DiD Cell Labelling Solution (Life technologies Ltd.) was prepared in ethanol in a glass vial. CD4+ T cells were resuspended at 1 x 10^6 cells/ml in nsRPMI at 37 °C. Note that a minimum of 2 x 10^6 cells were left in culture for unlabeled control samples. CD4+ T cells were labelled with 250 nM DiD, incubating in a 37°C water bath for 5 min. Labelled CD4+ T cells were centrifuged at 400 x g for 5 min, the supernatant was aspirated and the cells were washed three times in 10 ml 10% (v/v) FCS-RPMI. Cell density was adjusted to 4 x 10^5 cells/ml in 10% (v/v) FCS-RPMI and T cells were incubated for 10 min (minimum) at 37 °C, 5% CO_2 prior to loading with a calcium sensitive dye.

2.12.3 Labelling CD4+ T cells with fluo-$2_{leakres}$

From a stock solution of fluo-$2_{leakres}$/AM (TEFlabs Inc., TX, USA) at 3.8 mM in DMSO, a 3.0 µM solution was made in 10% (v/v) FCS-RPMI, which was used to label all T cells from a particular donor. For each ml of DiD-loaded CD4+ T cells, 110 µl of 3.0 µM fluo-$2_{leakres}$/AM was added and cells were subsequently incubated at 37 °C, 5% CO_2 for 30 min. After incubation cells were washed twice in 10% (v/v) FCS-RPMI and resuspended at the same density as the sAg-pulsed MDMs to give a 1:1 CD4+ T cell: MDM ratio. Note

also that CD4+ T cells at 4 x 10^5 cells/ml that had not been loaded with DiD were labelled with $fluo2_{leakres}$/AM as controls. In experiments using fluo-8/AM (AAT Bioquest Inc., CA, USA) the same procedure was followed, except that a stock solution of 5 mM was prepared in DMSO and 110 µl of a 1.7 µM stock was added per ml of T cells.

2.12.4 Superantigen pulsing and cell conjugation

PKH26-labelled MDMs (day 10) were detached from one well of the 6-well plate using a cell scraper. MDMs were counted to ascertain the density at which DiD+ fluo-2+ CD4+ T cells need to be resuspended, and divided evenly across five tubes compatible for use with a CyAn^{TM} ADP Analyser flow cytometer. In samples where MDMs were pulsed with SEE prior to co-incubation, SEE was added to these tubes at a final concentration of 1 µg/ml at 0.5 ml/tube. MDMs were incubated with SEE for 2 h at 37 °C with 5% CO_2, mixing every 30 min to limit attachment. All samples were washed in 10% (v/v) FCS-RPMI then resuspended in 225 µl/tube 10% (v/v)FCS-RPMI. Quickly, 225 µl of autologous DiD+fluo-2+ CD4+ T cells were added to each tube to give a 1:1 CD4+ T cell: MDM ratio and cells were centrifuged at 100 x g for 1 min to initiate attachment. Immediately afterwards (time zero, t_0), one of the tubes was briefly vortexed then analysed using the flow cytometer whilst the remaining four tubes were incubated in a water bath at 37 °C for 5, 15, 30 or 45 min then analysed. Before analysis, DAPI was added at a final concentration of 5 µg/ml so that dead cells could be excluded. Furthermore, all samples were analysed twice, the second time adding 30 µl of 10 µg/ml ionomycin (Sigma-Aldrich) to a 270 µl sample. Care was taken to maintain the temperature of solutions at 37 °C throughout. In certain samples, MDMs were not pulsed with SEE or, alternatively, 50 µl 10 µg/ml SEE solution was added at t_0 instead of pre-treating MDMs. 20000 $DAPI^-$ $PKH26^+$ events were acquired for each sample. Seven compensation controls of MDMs and CD4+ T cells, labelled as detailed in **Table 2.4**, were run for each donor and compensation was performed post-acquisition using FloJo (TreeStar). The parameter of 'conjugate formation (%)' was the frequency of PKH26+DiD+ events within the DAPI- (live) parent population. The 'calcium signal relative to ionomycin (%)' was calculated by expressing the fluorescence value of the DAPI-PKH26+PW^{100} (pulse width ≥ 100) DiD+ gate from the primary analysis of the sample as a percentage of the fluorescence in the same gate upon secondary analysis of the sample (i.e. after the addition of ionomycin).

	Compensation Control						
Dye	**A**	**B**	**C**	**D**	**E**	**F**	**G**
PKH26	×	×	×	✓	✓	✓	✓
DiD	×	×	✓	×	×	✓	✓
Fluo-2$_{leakres}$	×	✓	×	×	✓	×	✓

Table 2.4: Compensation controls for live calcium flow cytometry assay

2.13 Live calcium imaging of MDM-CD4+ T cell interaction

2.13.1 CFDA-SE labelling MDMs

MDMs (day 7/8) were detached using a cell scraper, washed twice in PBS at 37 °C, then adjusted to a density of 1 x 10^7 cells/ml and labelled with Vybrant® CFDA-SE (Life Technologies Ltd.) as described in section 2.5.1. After the wash steps MDMs were resuspended at 2 x 10^6 cells/ml and a 100 µl drop was pooled over the centre of a 25 mm glass coverslip that had been coated with PDL in the centre, as described in section 2.7. MDMs were allowed to adhere for 1 h at 37 °C, 5% CO_2, before adding 2 ml 10% (v/v) FCS-RPMI supplemented with 50 ng/ml M-CSF and returning to the incubator. Note that Daudi cells did not need to be CFDA-SE labelled due to changes in the microscope hardware enabling brightfield images to be acquired instead. Daudi cells were seeded at 2 x 10^5 cells/coverslip onto 25 mm glass coverslips with a PDL-coated centre for 1 h prior to sAg-pulsing. MDMs (day 9/10) or Daudi were pulsed with 2 ml/well 1 µg/ml sAg-cocktail or SEE in 10% (v/v) FCS-RPMI for 2 h at 37 °C, 5% CO_2. Unpulsed controls were treated with 2 ml/well 10% (v/v) FCS-RPMI alone. All coverslips were washed once before loading into the perfusion chamber.

2.13.2 Fura-2/AM loading of CD4+ T cells

CD4+ T cells were adjusted to a density of 2 x 10^7 cells/ml in 10% (v/v) FCS-RPMI. A 10 µM solution of fura-2/AM (Biotium Inc., CA, USA) in 10% (v/v) FCS-RPMI, prepared from a 5 mM stock in DMSO, was mixed 1:1 v/v with the T cells and incubated in a water bath at 37 °C for 30 min. Cells were washed twice with 10% (v/v) FCS-RPMI, centrifuging at 300 x g for 5 min, then resuspended at 1 x 10^6 cells/ml in phenol-red free RPMI and incubated at RT for 30 min until use.

2.13.3 Performing live calcium imaging

A Nikon Eclipse TE200 wide-field fluorescence microscope (Nikon Instruments Europe BV, Amsterdam, Netherlands) fitted with a mercury lamp, an OptiScan™ II filterwheel controller (Prior Scientific, Cambridge, UK) and a Rolera-XR Fast 1394 camera (Q-Imaging, BC, Canada) was preheated to 37 °C. High vacuum grease (Dow Corning, MI, USA) was applied as a thin film on both sides of an RC-21BRFS perfusion chamber (Warner Instruments, CT, USA). All input and output tubing was filled with phenol-red free RPMI and the ends of tube were stoppered using bulldog clips. Excess media was blotted away from the coverslip seeded with sAg-pulsed or unpulsed APCs. The area outside of the PDL-coated centre was dried with lint-free tissue. The coverslip was applied onto the perfusion chamber insert and pressed down to ensure a tight seal with the grease. Phenol red free media (240 µl) was pooled into the central reservation on top of the coverslip before another 25 mm coverslip was placed on top, again pressure was applied to ensure a tight seal with the grease. The perfusion chamber was loaded into the P-2 platform (Warner Instruments), which was screwed in place before securing it onto the microscope stage. The loaded perfusion chamber was left for 10 min to equilibrate to temperature. During this time 1 ml of fura-2 labelled T cells were loaded into a 1 ml syringe, which was attached to the input tubing leading to the perfusion chamber. The syringe was fitted into a custom-built syringe pump, which was built based on a design originally devised by Dr. G. Chistol (University of California, Berkeley), and equilibrated for 10 min. Finally, the output tubing from the syringe pump was connected to a peristaltic pump.

After focusing on a field of view of macrophages in the centre of the perfusion chamber, the fura-2 loaded T cells were injected into the chamber at ~ 33 µl/s. The peristaltic pump was run simultaneously so that excess media running through the perfusion chamber was removed. Immediately, imaging was initiated: every 10 s, for a total of 1200 s, the sample was excited with a mercury lamp passed sequentially through 340 nm, 380 nm and 485/20 nm filters. Images were acquired through a green emission filter using SimplePCI (Hamamatsu Corporation, PA, USA) imaging software. After setup of the technique, exposure times were kept constant when imaging cells from different donors.

2.13.4 Processing calcium image-sequences

ImageJ was used to process the calcium image-sequences. T cells were manually tracked using the MTrackJ plugin, selecting a circular point size of 20 pixels (px). The same tracks were applied over 340 nm and 380 nm image-sequences and measurements of intensity, time, and position for each track were exported into Excel. The 340 nm intensity values were divided by the corresponding 380 nm intensity values to give the 340:380 ratio for each time point making up the total track of a T cell. All tracks spanning < 300 s were

excluded from further analysis. A function was written in MATLAB to automatically generate panels of '340:380 ratio' vs. 'time' plots for every tracked T cell in an image-sequence. These plots were used for the visual classification of calcium profiles according to the criteria detailed in section 3.2.8.

The maximum 340:380 value for each tracked T cell was also calculated in Microsoft Excel. Since the original tracks were saved, each tracked T cell could be linked to its corresponding max. 340:380 value using the track ID. This enabled the track line on the image-sequence to be colour-coded according to the max. 340:380 value. Tracks with a max. 340:380 value < 0.5 were coloured green. Tracks with a max. 340:380 value ≥ 1.0 were coloured red. The remaining tracks were coloured white. For visual presentation the ratio image-sequence was generated by applying the 340 nm and 380 nm channel image-sequences to the RatioPlus plugin available for ImageJ. The brightness and contrast of the resulting image was set to span between 0.5 and 2.0 before applying a '16 colours' look-up table (LUT) to the image-sequence. Colour-coded tracks were overlaid onto this image.

2.13.5 Piecewise linear regression and principal component analysis

The track data table was formatted so each row represented a single track and each column contained the 340:380 ratios for each image frame of that track. A separate datasheet was formatted identically but containing the time information of the tracks. These datasheets were the input files used for a c-script 'plr2.c' (**Appendix 1**) written by Dr J. Wilson (University of York, York, UK). The script performs piecewise linear regression and exports a list of 18 parameters to describe the fit for each track. This process was repeated for all image-sequences acquired (+/sAg) for each donor to generate a large datasheet where rows represented individual tracks and columns the piecewise linear regression parameters. Only thirteen of the parameters were taken forward. The datasheet was imported into MATLAB and all parameters were standardised using the *zscore* function before performing principal component analysis using the *princomp* function. The eigenvalues of each principal component were plotted in a bar chart known as the scree plot. The proportion of variance for each component was calculated: eigenvalue of each principal component/ sum of eigenvalues for all principal components. Kaiser's criterion was used do decide the number of meaningful principal components. Scores plots of all of the principal components fulfilling this criterion were generated in order to identify separate clusters between samples in the presence or absence of sAg.

2.14 Correlative calcium imaging

CFDA-SE labelled MDMs (section 2.13.1) were seeded onto collagen-coated coverslip glass bottomed dishes as described earlier. On day 10, MDMs were pulsed with 2 ml 1 µg/ml SEA/SEB/SEE in 10% (v/v) FCS-RPMI for 2 h. The sAg cocktail was removed and dishes were marked with tape, so that the same field of view could be easily relocated. To each dish 0.5 ml phenol-red free media at 37 °C was added and cells were incubated for 10 min on the stage of the Nikon Eclipse TE200 wide-field fluorescence microscope, which had been equilibrated to 37 °C. Imaging was immediately initiated after pipetting in 0.5 ml of fura-2 labelled T cells, and performed as described in section 2.13.3 but for 1800 s. Subsequently, imaging media was aspirated and cells were fixed for 20 min in 2 ml of 3% PFA (w/v in PBS). The fixative was removed and cells were washed, incubated in quench solution for 20 min, then incubated overnight in FACS buffer at 4 °C. Cells were permeabilised and blocked in 1 ml/dish of 30 µg/ml huIgG for 30 min, then incubated for 60 min with 250 µl 5 µg/ml OKT3. Cells were washed three times, incubated for 45 min with 250 µl of 4 µg/ml GAM^{594}, then washed three more times. Samples were mounted using a drop of Mowiol and laying a 10 mm coverslip on top. All antibody solutions and washes were performed using 1% (v/v) FCS-PBS with 0.05% (w/v) saponin. The original field-of-view was located using the mark and z-stacks of all CD3+ T cells within the field were acquired on the LSM710 confocal microscope. The position of each z-stack was drawn on the final field-of-view image (t = 1800 s) that had been acquired before cells were fixed, creating a map correlating the calcium signal of a given T cell with its distribution of CD3.

2.15 Statistics

Paired or unpaired two tailed Students t-tests were performed after testing data for normality using D'Agostinos test. Data that did not pass the test for normality at first were log-transformed and, if this resulted in normal distribution of the data, were then compared using a t-test. Data that were not normally distributed were compared using Wilcoxon matched pairs (paired data) or Mann-Whitney U test (unpaired data). Unpaired t-tests were only performed after checking for equal variance using F test; if unequal variance was found but data was normally distributed an Unpaired t-test with Welch's correction was used. Where three or more samples were compared a one-way analysis of variance (ANOVA) was used, followed by Tukey's post-test to identify differences between samples. Fishers exact test was performed using the GraphPad online calculator (http://graphpad.com/quickcalcs/ contingency1/). Unless stated otherwise, all statistical

comparison was performed using GraphPad Prism 5. A $P<0.05$ was considered to be significant and values given in text are mean ± SD.

Chapter 3: Investigating the formation of antigen-dependent MDM-CD4+ T cell conjugates

3.1 Introduction

TCR recognition of cognate pMHC leads to a concentration of signalling components at the cell-cell interface that enables the T cell to increase the signalling kinetics of the antigen-dependent cell-cell contact formed (Krummel and Cahalan, 2010). The signalling components are recruited to this region, spatially organized and dynamically regulated as part of the IS or kinapse (see section 1.2).

The micro-scale organization of components of the IS can vary according to the type of antigen presenting cell (APC) or effector involved (Friedl et al., 2005). One example is that the classical concentric circle structure observed at the B cell- T cell IS can differ in DC- T cell conjugates, which instead show a multicentric pattern of TCR accumulation (Dustin et al., 2006). Furthermore, APC cytoskeletal complexity, antigen frequency and quality, and the structure of the environment (e.g. 2D vs. 3D) all impact on whether stable or more dynamic interactions are undertaken (Friedl et al., 2005). In particular, antigen-dependent interactions involving macrophages have often been shown to be highly dynamic.

3.1.1 Macrophage-CD4+ T cell interactions: occurrence and dynamics

Despite the fact that macrophages have a spectrum of activation and polarisation states, MHC class II expression is retained on the majority of these states enabling antigen to be scanned by infiltrating CD4+ T cells (Biswas and Mantovani, 2010). Antigen-dependent interactions of macrophages with CD4+ T cells forms an important aspect of cell-mediated immunity that can result in macrophage activation (Murphy et al., 2011). Macrophage activation is important for the control of phagosome-dwelling pathogens, such as *Mycobacterium tuberculosis* (Murray, 1999) and *L. major* (Meier et al., 2003), and plays a role in non-infectious diseases, such as atherosclerosis (Libby et al., 2013). Recent *in vivo* evidence, discussed in section 1.3.4, has demonstrated a role for antigen-dependent macrophage-CD4+ T cell interaction in the aforementioned diseases within peripheral tissues (Egen et al., 2011; Filipe-Santos et al., 2009; Koltsova et al., 2012). Together these studies have shown that CD4+ T cell arrest on macrophages can occur, albeit at low frequency, which suggests that IS formation can take place between these cell types *in vivo*.

Several *in vitro* studies have also examined the role of antigen-dependent signalling between macrophages and CD4+ T cells using murine cells. Using fixed cell imaging of ovalbumin peptide (OVA)-pulsed murine macrophages and CD4+ T cells, Meier et al. (2003) identified IS formation by reorganisation of the MTOC to the cell-cell interface. Reorganisation of the MTOC was not found to be dependent upon CD28 costimulatory signalling, which is consistent with the fact that, so far, no costimulatory role has been confirmed for CD28 in effector T cell function (Chen and Flies, 2013; Meier et al., 2003). A different study imaged live murine T cells with GFP, under the control of a promoter region responsive to nuclear factor of activated T cells (NFAT), stably incorporated into the chromosomal DNA (Underhill et al., 1999). In response to antigen recognition via TCR, which triggers a signalling cascade involving translocation of NFAT into the nucleus, GFP becomes expressed. Using this method, Underhill et al. (1999) showed that interactions between macrophages and CD4+ T cells were highly dynamic, which was not apparent in the study by Meier et al., (2003). In response to OVA-pulsed macrophages, CD4+ T cells were observed to have an initial stable interaction followed by crawling across the surface of the macrophages (Underhill et al., 1999). T cells hopped from one macrophage to another sequentially in order to become activated (GFP+) (Underhill et al., 1999). There is potential that the human macrophage-CD4+ T cell IS is equally dynamic and that antigen-dependent signalling is predominantly associated with a kinapse-type organization. Thus by simply looking for the concentric circles of TCR and ICAM that are only found in certain types of synapse, many of the antigen-dependent signalling events may be ignored. The chosen approach must be able to detect a shared signal in order to acknowledge all types of T cell response to antigen.

3.1.2 A readout for productive macrophage-CD4+ T cell signalling

3.1.2.1 Calcium reports on antigen-dependent signalling

Calcium is a ubiquitous second messenger. Increases in cytoplasmic calcium are triggered by a myriad of upstream receptors (e.g. GPCRs and FcR) and calcium, in turn, has the capability to interact with thousands of proteins downstream (Clapham, 2007). In T cells the degree of activation is closely linked to the level of cytosolic calcium (Wülfing and Davis, 1998) through a series of carefully characterised events (Hogan et al., 2010). For decades TCR recognition of cognate peptide antigen presented in the context of MHC class II has been known to induce a rapid rise in T cell intracellular calcium levels (Dustin, 2009a). Furthermore, the subtleties of T cell calcium signalling have been studied in relation to formation of the IS. Elevation in intracellular calcium occurs prior to cSMAC formation (Grakoui et al., 1999) and correlates with the lifetime of TCR microcluster formation and residency at the IS periphery prior to reaching the cSMAC (Varma et al.,

2006). Indeed, the events are so closely linked that intracellular calcium signalling has been utilised as an immediate indicator of IS formation (Revy et al., 2001). Moreover calcium signalling is one of the descriptors of similarity between immunological synapses and classical neural synapses, from which the IS was named (Dustin, 2009b; Krummel and Cahalan, 2010).

3.1.2.2 Calcium signalling may distinguish mobile and stable interactions

Calcium signalling is an appropriate readout of antigen-receptor engagement but evidence also exists that the quality of signalling may reflect different modes of APC-T cell interactions. In a signalling model suggested by Kummerow et al. (2009), low levels of calcium signalling, resulting from low levels of IP3 and partial store depletion, are associated with kinapse formation. On the other hand, high sustained calcium signals are linked with stable synapse formation (Kummerow et al., 2009). On the basis of this model one may speculate that the mobile interactions, described by Underhill et al. (1999), are associated with low, intermittent intracellular calcium rises in T cells. Indeed, this type of signalling is known to result in the selective activation of NFAT (Dolmetsch et al., 1997). Furthermore, a report by Moreau et al. (2012) showed that both kinapse- and synapse-type interactions exist *in vivo* and both exhibit calcium signalling. Although no direct comparison of the calcium profiles was performed, they showed that the strongest TCR signals gave rise to synapses, whilst lesser TCR signals indicated kinapse formation. Working alongside this is evidence that differential calcium profiles are observed in response to agonist or partial-agonist peptides (Wülfing et al., 1997) and that cSMAC formation is dependent upon agonist quality (Dustin et al., 2010). Considered together this suggests that certain signatures of calcium signalling initiated downstream of TCR binding to different quality agonists might have the potential to identify different types of synapse/kinapse formation. Indeed, in a departure from the classical view that TCR-triggered calcium signalling equates to arrest, a new school of thought is emerging that considers T cell mobility as inversely proportional to the level of calcium signalling (Beemiller and Krummel, 2013; Moreau et al., 2012).

Thus, the present study used reporters of T cell intracellular calcium as a readout of productive human MDM-CD4+ T cell conjugate formation. Encompassed within this readout is antigen-dependent signalling in the form of both synapses and kinapses, which is useful as the nature of antigen-dependent MDM-CD4+ T cell interactions is unknown.

3.1.3 Tools to analyse calcium signalling

A wide range of fluorescent indicators, which bind to calcium, exist to study changes in intracellular calcium levels (Takahashi et al., 1999). The present study used fura-2 and

fluo-2 in order to study calcium signalling by wide-field fluorescence microscopy and flow cytometry, respectively. Fura-2 undergoes a decrease in its absorption wavelength upon binding calcium (363 to 335 nm) (Takahashi et al., 1999); therefore sequential excitation at 340 and 380 nm in the absence of calcium results in greater emission (500 nm) for 380 nm compared to 340 nm, but vice versa in the presence of calcium. Fura-2 is classed as a ratiometric dye since the ratio of fluorescence for excitation at 340:380 nm can be calculated to give an accurate estimation of the increase/decrease in calcium. This acts to correct for total concentration, uneven loading and leakage of the dye, but also aquisitional photobleaching (Takahashi et al., 1999). This final correction is critical for a microscopy-based technique in which aquisitional photobleaching can be rife. In contrast, fluo-2 is a non-ratiometric indicator and, similarly to related indicators such as fluo-3, demonstrates vastly increased emission intensity upon binding calcium (Takahashi et al., 1999). Fluo-2 is an effective indicator for use in standard flow cytometry assays as it is excited at 488 nm. Although photobleaching is not a major concern in cytometry assays, fluo-2 loading or leakage has to be carefully monitored as these factors cannot be corrected for in the same way as they can for fura-2.

3.1.4 Forming an IS in primary human cells

3.1.4.1 Generating antigen-specific T cells

The first step in forming an MDM-CD4+ T cell interaction that has the potential for IS formation is to generate CD4+ T cells with TCRs specific to a particular antigen presented in the context of MHC class II on autologous APCs. Typically this would involve immunization of a subject with an antigen, which induces a primary immune response or recalls a previous immune response and, after a short period, cells can be harvested from tissue or peripheral blood (Murphy et al., 2011). Upon culturing harvested cells with the same antigen *in vitro*, proliferation of antigen-specific T cells will occur and can be measured using CFDA-SE dilution or incorporation of ^{3}H-thymidine (Mariotti and Nisini, 2009). Antigen is added to autologous MDMs and is processed and presented in the context of MHC. Pure populations of antigen-specific T cells, obtained by repeated expansion or cell-sorting, can then be co-incubated with MDMs presenting cognate antigen and IS formation can be monitored.

3.1.4.2 Use of superantigen

sAg acts to crosslink MHC class II to a subset of TCR-Vβ regions through a binding mechanism that also involves CD28 and occurs outside of the MHC class II peptide-binding groove (Krakauer, 2013). A key difference between sAg and peptide antigen is in the requirement for processing. Macrophages receiving particular endogenous or

exogenous signals can have reduced ability to process peptide antigen (Gordon, 2003). However only if the macrophage MHC class II cell surface expression is also changed would the sAg show any difference in the ability to crosslink to TCR. Another difference between peptide antigen and sAg is that a particular TCR is specific for peptide-MHC, whereas many different TCRs sharing the same Vβ family are bound by sAg-MHC. Furthermore, the majority of sAgs bind several different Vβ families (**Table 3.1**). The result is that each sAg is able to stimulate 2-20% of all T cells, a much greater frequency than the number of antigen specific T cells in the same population (Murphy et al., 2011). Note that the sAg, staphylococcal enterotoxin E (SEE), recognizes many of the Vβ families commonly found in human peripheral blood lymphocyte (PBLs), from which the T cells in the present study were derived (**Table 3.1**). Overall, sAg facilitates *in vitro* studies of IS formation by effectively overcoming the requirement to generate large numbers of antigen-specific CD4+ T cells.

This chapter focuses on forming productive MDM-CD4+ T cell conjugates. Cell surface markers reporting on the phenotype of MDMs and activation of CD4+ T cells are evaluated. Conjugate formation and calcium signalling are analysed by flow cytometry and microscopy techniques. A classification system has also been devised in order to assess the quality of the calcium signal.

	TCR Vβ region usage	**Reference**
sAgs (SEA/SEB/SEE)	**3, 3, 5.1, 6.1-3, 8, 11, 12, 14, 15, 17, 18, 20**	(Murphy et al., 2011)
Peripheral blood lymphocytes	**6.2 > 6.1 > 5.1 > 8 > 2 = 13.1 = 13.2 > 4 = 5.2 >7 = 17** (remaining <4 % relative distribution)	(Ochsenreither et al., 2008)
	4, 5, 6, 8, 13 (frequent); **1, 9, 15** (infrequent) (not all Vβs examined)	(Geursen et al., 1993)

Table 3.1: TCR-Vβ regions recognised by various superantigens (sAgs) and their prevalence in peripheral blood lymphocytes.

3.2 Results

3.2.1 Attempt to recall T cells with Revaxis

In the present study no medical history was supplied with the peripheral blood leukocyte cones received from the NHS. In addition, when using this source of cells, no opportunity was available to immunize patients prior to collecting blood. Therefore any attempt to expand antigen-specific CD4+ T cells from this source of cells required recall with an antigen that had previously been experienced by a large percentage of the UK population. As tetanus immunisations have occurred across the UK since 1961 (Adeboye and Sangowawa, 2002), this made tetanus toxoid (TT) a likely candidate for antigen recall. Thus, a vaccine for diptheria, tetanus and poliomyelitis (DTP), marketed as Revaxis (which amongst other antigens contains TT) was used at a 1 : 1000 dilution in culture with PBMCs to recall DTP-specific CD4+ T cells. Revaxis is alum-adsorbed and, therefore, alum at a concentration matched for the aluminum content of Revaxis was used as a negative control for proliferation.

The PBMCs were isolated as described in section 2.1.1, labelled with CFDA-SE then cultured with Revaxis, alum or PHA for 5 days as detailed in section 2.5.1. After incubation, cells were immunolabelled for CD3 (OKT3) and stained with a live/dead dye, before analysis by flow cytometry. The representative colour density dot-pots illustrate that only live cells were included within the analysis and that, within this population, the vast majority of the cells were CD3+ (**Fig. 3.1**). An additional gate was drawn to determine the percentage of divided cells (CFDA-SE low). Little or no division is visible in plots of PBMCs stimulated with either alum or Revaxis, compared to PHA in which the majority of cells have lower CFDA-SE associated fluorescence indicative of cell division (**Fig. 3.1**). The graph shows the percentage of divided cells obtained for all donors tested, with no significant difference in division between alum and Revaxis indicating that this method is inefficient in the recall of DTP-specific T cells from the general UK blood donor population.

Despite the fact that T cell lines can be made with only one or two antigen-specific T cells, this process requires a ready source of feeder cells, which would necessitate generation of an autologous Epstein-Bar virus (EBV)-B cell line or the addition of autologous PBMCs every 20–30 days (Mariotti and Nisini, 2009). Unfortunately, both processes use valuable autologous PBMCs from which MDMs are isolated and would, therefore, vastly limit the number of assays that could be performed before a new line would have to be generated. As an alternative approach, sAg was chosen to study the formation of MDM–CD4+ T cell conjugates.

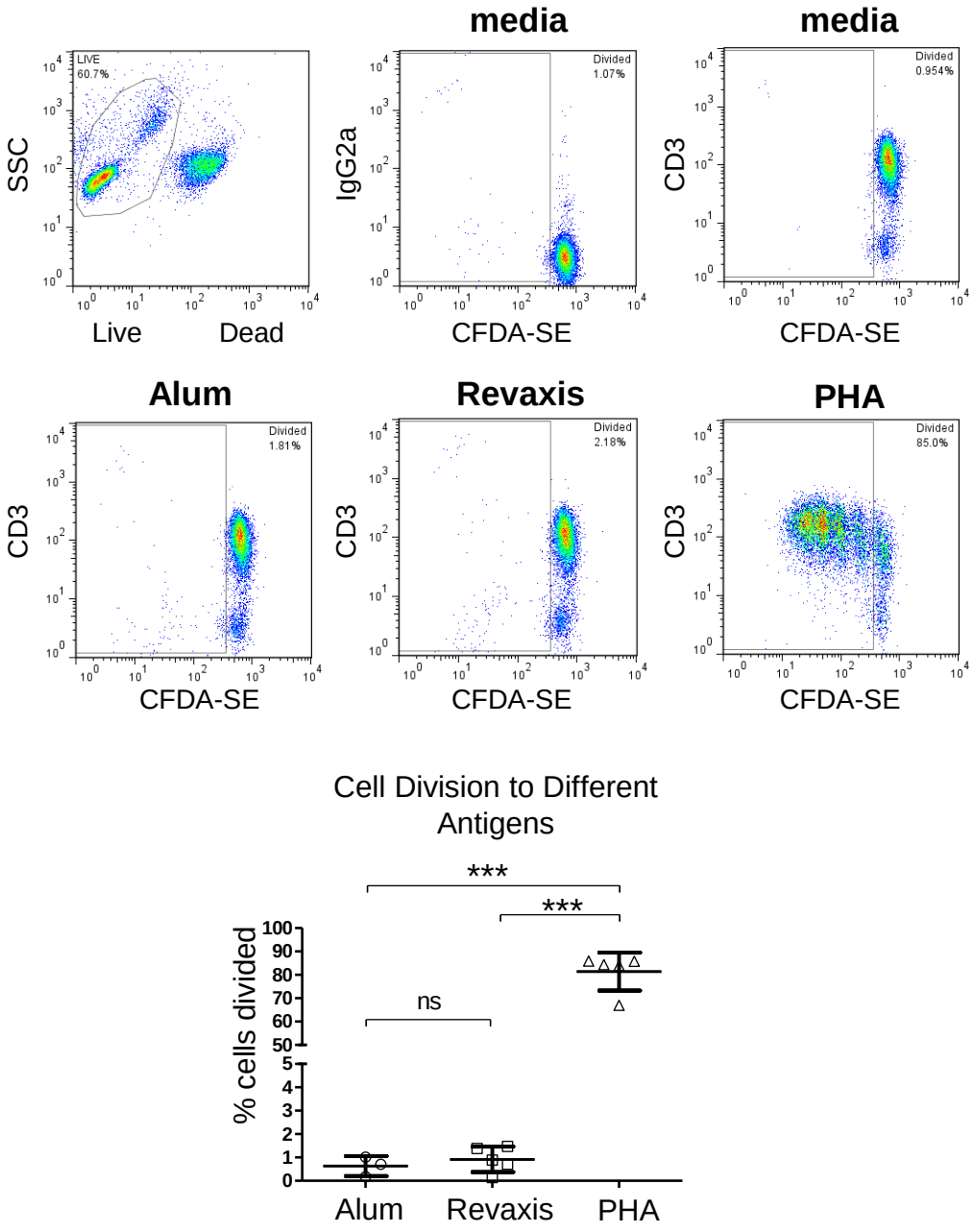

Figure 3.1: Recall of human antigen-specific T cells using Revaxis. PBMCs (n=5) were thawed and labelled with 0.84 µM CFDA-SE at a density of 1 x 10^7 cells/mL according to the protocol described in section 2.5.1. After 24 h incubation at 37°C, 5% CO_2, labelled PBMCs were transferred to a 96-well plate at 2 x 10^5 cells/well in 200 µL medium and 1:20000 Imject Alum, 1:1000 Revaxis or 2.5 µg/mL PHA was added. Cells were incubated for 5 days before FcR-blocking, immunolabelling live with CD3 (OKT3) or IgG2a isotype control, followed by a fixable live/dead dye. PBMCs were then fixed, quenched and labelled with GAM-647 secondary antibody. Representative colour density plots are shown to illustrate gating strategy and cell division. The graph shows the percentage of divided cells for each donor and the difference between stimulation agents was compared using ANOVA followed by Tukey's test. ns, not significant; ***, P < 0.001.

3.2.2 Monocyte and MDM cell surface markers

In order to indicate the phenotype and purity of cells isolated by adherence to gelatin, adherent cells were tested after overnight culture (monocytes; day 1) and again after differentiation to MDMs in M-CSF (MDMs; day 9). On either day the surface of live cells was stained with a panel of primary mAbs against CD3, CD4, CD11b, CD14, CD16, CD19, CD68, HLA-DR and CCR5 (three clones: 2D7, MC5 and CTC5) before fixation and labelling with GAM-PE secondary as detailed in section 2.4.1.

3.2.2.1 Markers of adherence isolated myeloid cells

CD11b is an integrin involved in cell–cell and cell–extracellular matrix (ECM) adhesion and is highly expressed on cells of myeloid lineage in humans (Dziennis et al., 1995). CD11b was expressed by the majority (82 ± 9%) of isolated adherent cells and MDMs differentiated from them (86 ± 9%), indicating that these cells are myeloid (**Fig. 3.2**). Additionally, the percentage of cells expressing CD68 at the cell surface increased upon differentiation to MDMs (**Fig. 3.2**), consistent with a previous report showing an increase in CD68 expression between monocytes and MDMs (Rey-Giraud et al., 2012). CD68 is a transmembrane glycoprotein, expressed in endosomal compartments and, to a lesser extent, at the PM. It is often used as a selective marker for monocytes and macrophages, although CD68 can be detected in other cell types (Gottfried et al., 2008). This provides supporting evidence of the monocyte/macrophage phenotype of adherence-isolated cells.

Another marker that predominates on monocytes and macrophages is CD14, which acts in concert with toll-like receptor-4 for pathogen recognition (Murphy et al., 2011). The percentage of CD14+ cells in the MDM population (81 ± 10%) was significantly higher than that of monocytes (66 ± 12%) (**Fig. 3.2**). Previously it has been reported that in healthy donors up to 25% of monocytes may be CD14- (Steinbach and Thiele, 1994), which may have contributed to the fraction of CD14- cells observed in the present study. This fraction may be also be populated by T cells (CD3+) or B cells (CD19+), although these were washed away over culture so that they represented only 2 ± 2% and 4 ± 2% after 9 days (**Fig. 3.2**). Additionally, the expression of CD83, a mature DC marker, remained low over the duration of culture (**Fig. 3.2**) evidencing that DCs were not isolated or expanded during differentiation. Together with the markers described above this indicated that, after 9 days of culture, the majority of cells were MDMs.

3.2.2.2 The polarisation of M-CSF conditioned MDMs

The percentage of cells expressing the IgG-specific FcγRIII receptor (CD16) was significantly increased upon differentiation of monocytes (17 ± 9%) to MDMs (71 ± 12%)

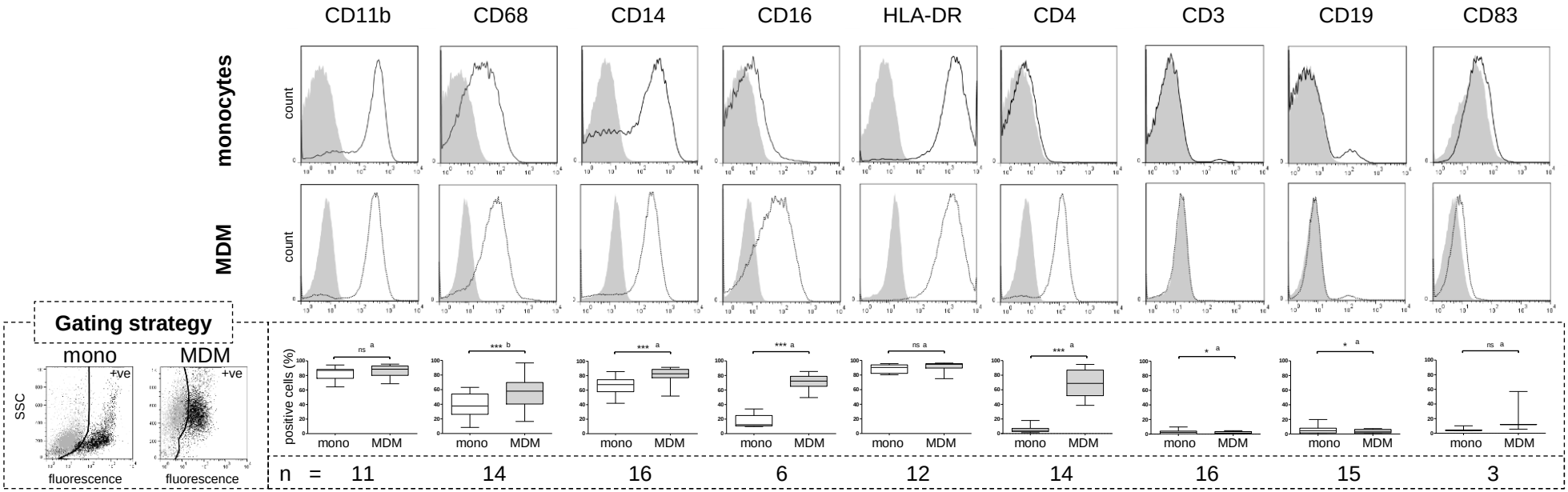

Figure 3.2: Cell surface markers of monocytes and MDMs isolated and differentiated from human peripheral blood. Samples of monocytes or MDMs were harvested and immunolabelled for the indicated marker and with the relevant isotype controls according to the method detailed in section 2.4.1 on day 1, prior to differentiation with M-CSF, and day 9, after differentiation. Representative histograms for monocytes and MDMs are shown overlaid on the relevant isotype control (shaded grey). Gates to estimate the percentage of positive cells were set using the relevant isotype control (grey) for each marker (black) according to side-scattered light (SSC) and fluorescence, as illustrated in the gating strategy. Bar charts show the percentage of positive cells on monocytes and MDMs of paired donors for each marker (mean ± SD). Statistical comparison was carried out as indicated: [a], Paired Student's t-test; [b], Wilcoxon matched-pairs test. ***, P<0.001; *, P<0.05; ns, non-significant.

(**Fig. 3.2**). Increased CD16 expression has been associated with both M1 and M2 phenotypes (Mantovani et al., 2004; Rey-Giraud et al., 2012). Importantly, HLA-DR expression levels were maintained over culture (**Fig. 3.2**), which was crucial for the MDMs to be able to form the IS but also excluded the M2c MDM phenotype, which does not express MHC class II. For further assessment of the degree of MDM polarisation, the expression levels of the CD80 and CD163 cell surface markers on the M-CSF conditioned MDMs were compared to those on the GM-CSF conditioned MDMs. MDMs were cultured with M-CSF or GM-CSF, as detailed in section 2.2.1, then immunolabelled live for CD80 and a fixable live/dead dye. Alternatively, MDMs were fixed and then immunolabelled for CD163 according to the method detailed in section 2.4.2**.** Cells were analysed by flow cytometry and M-CSF conditioned MDMs were found to express lower levels of the costimulatory ligand CD80 but higher levels of the scavenger receptor CD163 than GM-CSF conditioned MDMs (**Fig. 3.3**). Overall this suggests that the M-CSF conditioned MDMs were polarised towards an M2 phenotype.

3.2.2.3 Expression of CCR5 on MDMs

A subpopulation of monocytes was shown to express cell surface CCR5 when detected with mAbs directed against three different epitopes (MC5, 26 ± 15%; 2D7, 21 ± 15%; CTC5, 31 ± 28%). After differentiation the percentage of cells expressing CCR5 significantly increased (MC5, 67 ± 21%; 2D7, 52 ± 25%; CTC5, 68 ± 23%). Moreover, when gating only on CCR5+ cells the MFI for CTC5 was significantly higher on MDMs compared to monocytes; there was no significant difference on MDMs compared to monocytes for 2D7 and MC5 (**Fig. 3.4**). Note that comparison of the MFI of the entire population (ungated) also showed a significant increase in MC5 ($P = 0.0162$) and CTC5 ($P = 0.0012$) levels over differentiation (Wilcoxon matched pairs; data not shown) supporting previous work in our laboratory (Signoret lab, unpublished data). Furthermore, these results corroborate other reports which have shown increased CCR5 expression upon differentiation of monocytes to MDMs (Lee et al., 1999b; Naif et al., 1998). Overall this shows that, under the differentiation conditions of the present study, an increase in the *percentage* of CCR5+ cells has the greatest impact on the increase in CCR5 fluorescence.

Achour et al. (2009) suggested a relationship between CD4 and CCR5 expression at the PM, therefore the expression of CD4 on MDMs was also examined. A significant increase was apparent in the percentage of CD4+ cells in the MDM (69 ± 18%) population compared to monocytes (6 ± 5%) (**Fig. 3.2**). Notably, Lee et al. (1999b) also observed an increase in cell surface levels of CD4 and CCR5 after 6-7 days compared to 0–1 days of culture in M-CSF. Although both CD4 and CCR5 were significantly upregulated on MDMs,

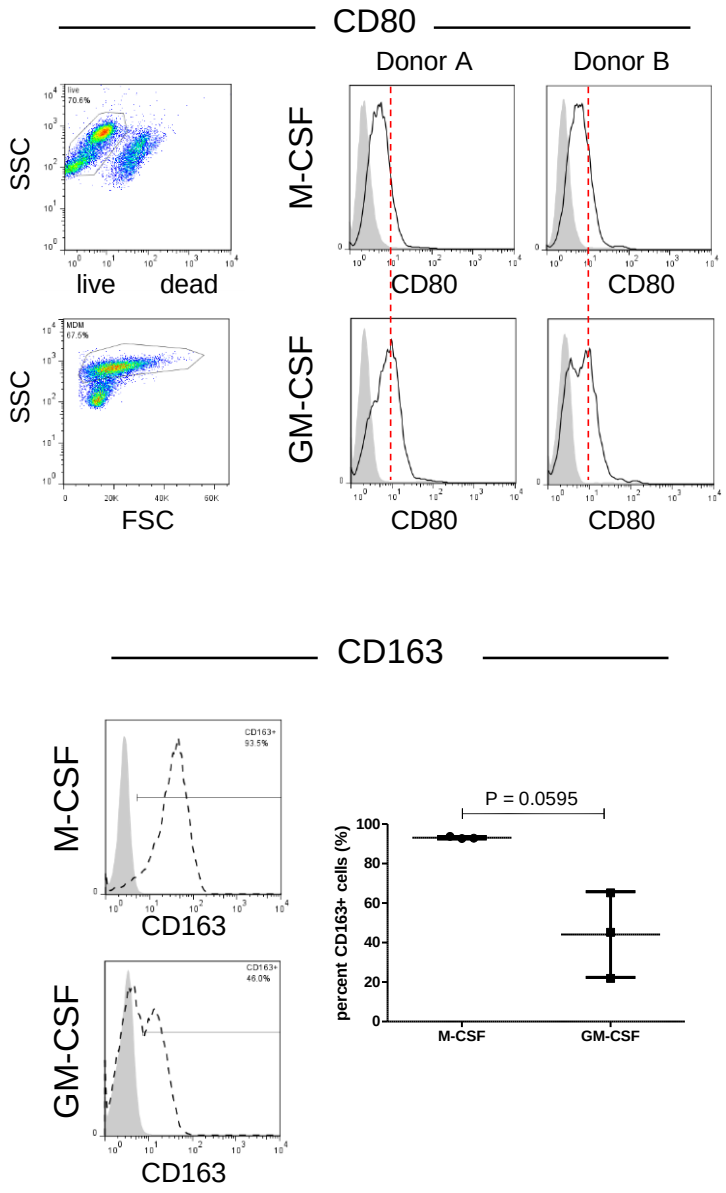

Figure 3.3: Expression of CD80 and CD163 by M-CSF vs. GM-CSF conditioned MDMs. MDMs were cultured in the presence of M-CSF or GM-CSF/IFNγ/LPS for 8 days. Cells were immunolabelled live for CD80 and also with a live/dead marker dye. Alternatively MDMs were fixed and immunolabelled for CD163, as detailed in section 2.4.2. For CD80, gates were set on live (fluorescence^{low}) FSC/SSC^{high} events as illustrated. Histograms show the expression levels of CD80 (n=2) or CD163 (n=3). The plot shows the percentage of cells in the positive gate (indicated on histograms) for CD163 for all donors.

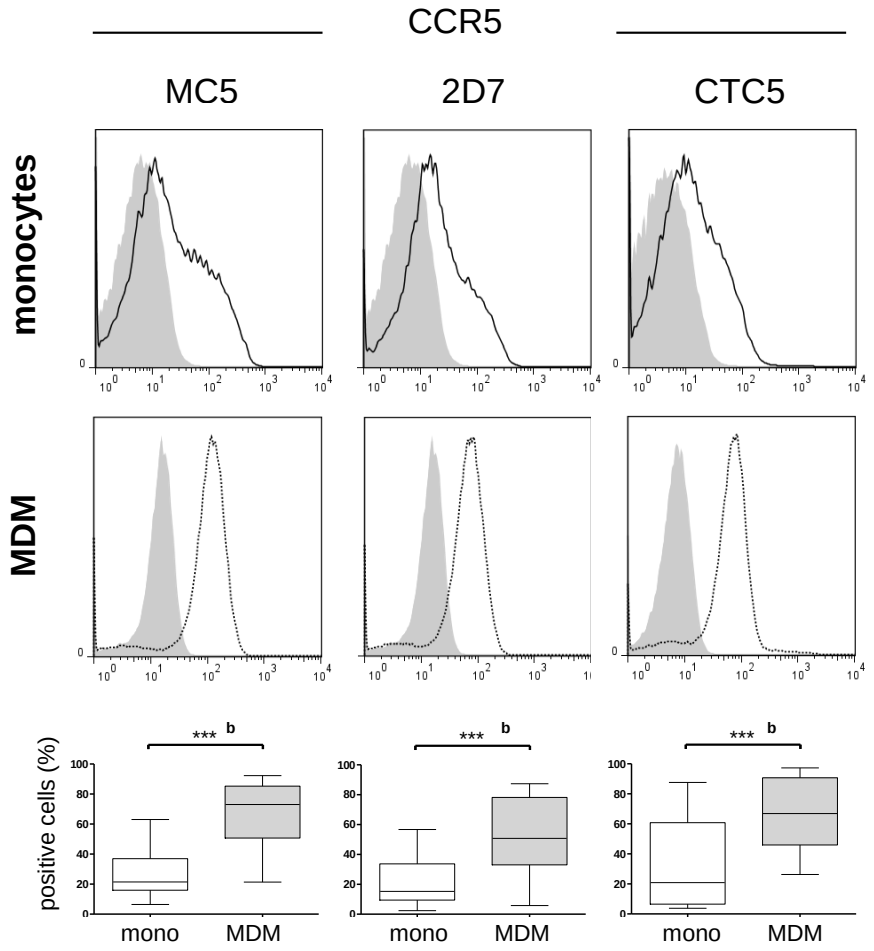

	MFI	P	MFI	P	MFI	P
Mono	39 ± 37	0.9902[a]	26 ± 24	0.2577[a]	25 ± 44	0.0018[b]
MDM	39 ± 56		19 ± 28		60 ± 78	
n	16		16		16	

Figure 3.4: CCR5 expression on monocytes and MDMs. Samples of monocytes or MDMs were harvested and immunolabelled with the indicated CCR5 mAb or the relevant isotype control, according to the method detailed in section 2.4.1, on day 1 prior to differentiation with M-CSF, and day 9 after differentiation. Representative histograms for monocytes and MDMs are shown overlaid on the relevant isotype control (shaded grey). Positive cells were gated as previously described (Fig. 3.2). Bar charts show the percentage of positive cells for each CCR5 epitope on monocytes and MDMs from matched donors. Table shows the number of donors and the median fluorescence intensity values (MFI) of cells within the positive gate. Statistical comparison was carried out as indicated: [a], Paired Student's t-test; [b], Wilcoxon matched-pairs test. ***, P<0.001.

investigation of any relationship between these proteins is beyond the scope of the present study.

3.2.3 Cell surface markers of differentially activated CD4+ T cells

Autologous CD4+ T cells were isolated alongside monocytes and activated by stimulation with PHA and recombinant IL-2 or CD3/CD28 beads according to the methods detailed in section 2.2.2. PHA is a non-specific mitogen that induces T cell activation by an unclear mechanism. CD3/CD28 beads directly engage antigen and costimulatory receptors, activating T cells in a mechanism more akin to physiological antigen presentation (Duarte et al., 2002). These different modes of activation were performed in order to investigate whether the frequency of MDM-CD4+ T cell IS formation could be increased by using T cells with differing activation statuses.

The CD4+ T cell purity was checked after every isolation by dual indirect immunolabelling for CD3 (OKT3) and CD4 (RPA-T4) co-expression and a mean purity of 96% CD3+CD4+ cells was determined (**Fig. 3.5**). Neither PHA/IL-2 nor CD3/CD28 activation resulted in a significant increase in the percentage of CD8+ or CD19+ cells, both of which remained minimal, nor was there a significant decrease in the percentage of CD4+ cells. Conversely, the percentage of CD14+ cells increased significantly using the CD3/CD28 activation method. Nevertheless, the majority of cells after activation remained CD3+CD4+.

Since T cell activation following antigen encounter induces expression of the IL-2α chain (CD25), which confers a higher affinity for IL-2 (Murphy et al., 2011), the expression of CD25 was assessed as a measure of activation. The proportion of isolated CD4+ T cells expressing CD25 (< 5%) was significantly increased by both the PHA/IL-2 and CD3/CD28 activation protocols, albeit to different extents (21 ± 6% and 84 ± 4%, respectively) (**Fig. 3.5**). Furthermore, CD3/CD28 activation, but not PHA/IL-2 activation, resulted in a significant increase in the percentage of cells expressing HLA-DR (**Fig. 3.5**), which is also upregulated upon T cell activation (Murphy et al., 2011). Both activation methods resulted in an increased percentage of cells expressing CD45RO (**Fig. 3.5**), which is the low molecular weight isoform of CD45 that becomes expressed after the T cell encounters antigen (Hamann et al., 1996). Although this increase was only significant for PHA/IL-2 stimulated cells, the CD3/CD28 activated cells showed an increase relative to unstimulated cells for every donor. Together these results show that both methods resulted in CD4+ T cell activation, but that using CD3/CD28 beads results in more pronounced activation.

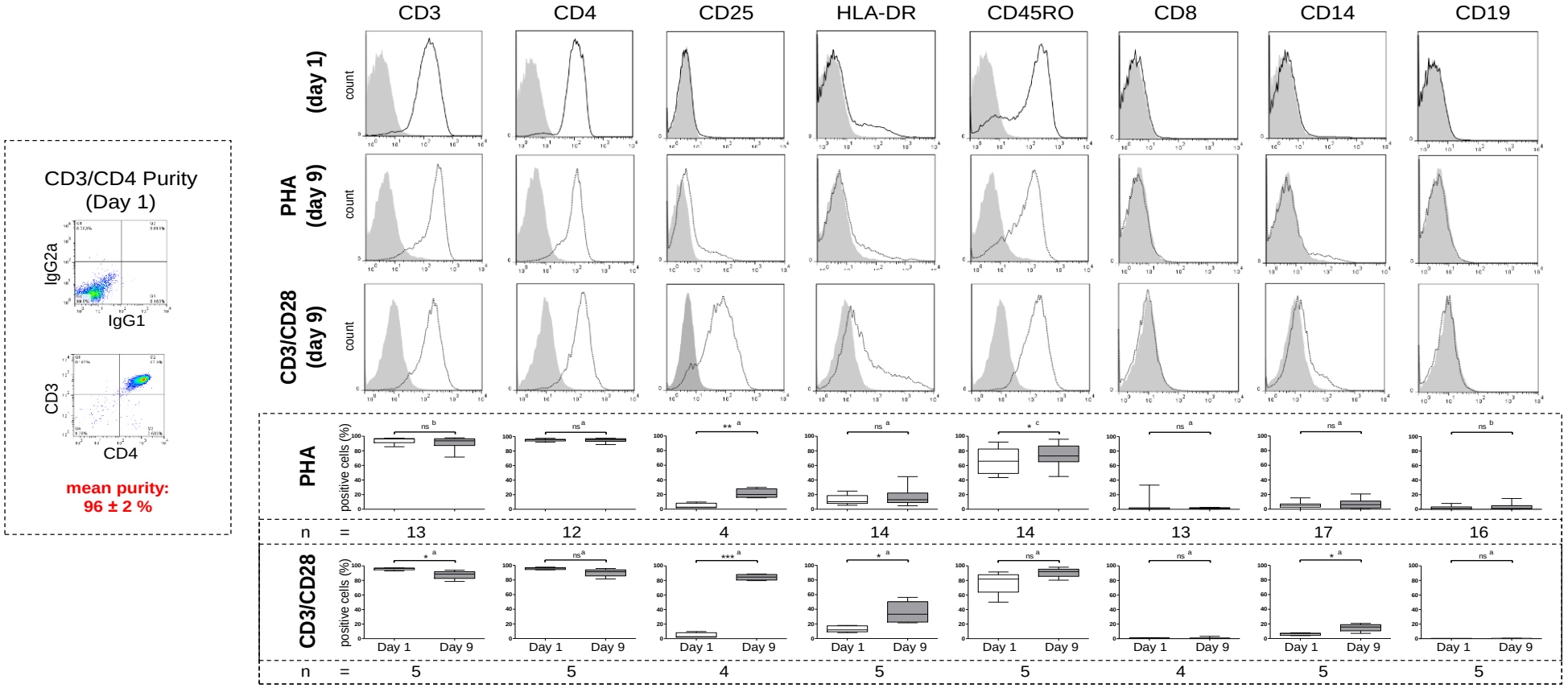

Figure 3.5: Cell surface markers of CD4+ T cells before and after stimulation with PHA/IL-2 or CD3/CD28 beads. The purity of CD4+ T cell isolations was assessed on day 1 by dual labelling with OKT3 and RPA-T4 or respective isotype controls. Samples of CD4+ T cells were harvested and immunolabelled with the indicated mAb directed against the indicated epitope or relevant isotype control, as detailed in section 2.4.1, on day 1 prior to activation in culture with PHA/IL-2 or CD3/CD28 beads, and on day 9 after activation. Representative histograms for days 1 and 9 are shown overlaid on the relevant isotype control (shaded grey). The percentage of positive cells for each marker was determined by setting gates above the isotype control as previously illustrated (Fig. 3.2). Bar charts show the percentage of positive cells for each marker on days 1 and 9 (mean ± SD). Statistical comparison was carried out as indicated:[a], Paired Student's t-test; [b], Wilcoxon matched-pairs test. ***, P<0.001; **, P<0.01; *, P<0.05; ns, non-significant.

3.2.4 CCR5 expression on activated T cells

CCR5 cell surface expression before and after CD3/CD28 or PHA/IL-2 activation was measured by flow cytometry using the mAbs MC5, 2D7 and CTC5. For both MC5 and 2D7, a decrease in the percentage of CCR5+ cells was apparent after activation by either method, although the effect was more pronounced after CD3/CD28 activation where the decrease showed significance (**Fig. 3.6a**). This result corroborates evidence from Richardson et al. (2012) who showed that CCR5 cell surface (and mRNA) levels were reduced to a greater extent by CD3/CD28 stimulation than PHA/IL-2 stimulation. Opposite to the reduction in CCR5 cell surface expression observed using MC5 and 2D7, the percentage of CTC5+ cells significantly increased on CD3/CD28 stimulated T cells and, within CTC5+ gates, the expression levels of CTC5 were increased after PHA/IL-2 or CD3/CD28 activation (**Fig. 3.6a**). To determine the cause of this, PHA/IL-2-activated T cells were dual labelled with a live/dead marker and either MC5 or CTC5 followed by GAM^{647}. The $CTC5^{hi}$ population was discovered to be composed of dead cells, which was not the case for MC5+ cells (**Fig. 3.6b**). This result indicates that the discrepancy between different mAbs in the level of cell surface staining after activation was due to the emergence of dead cells that label $CTC5^{hi}$, which are not present on day 1 (**Fig. 3.6a**, histograms). Thus, the $CTC5^{hi}$ population was excluded from analysis in flow cytometry experiments for the remainder of this study.

3.2.5 Flow cytometric analysis of MDM-CD4+ T cell conjugate formation

As well as being useful in determining the expression of markers in fixed cell populations, flow cytometry can be used to follow more transient events in live cells such as calcium signalling. The capacity of flow cytometry to rapidly analyse tens-of-thousands of cells labelled with several coloured dyes makes it particularly suitable for analysing heterogeneous MDM-CD4+ T cell co-culture samples. This, in turn, enables effective reporting of the frequency of stable conjugate formation and the calcium signalling that occurs within this subpopulation of conjugates (Burchiel et al., 2000).

3.2.5.1 Measuring conjugate frequency and calcium signalling

MDMs and CD4+ T cells were labelled with lipophilic membrane dyes PKH26 and DiD, respectively, according to the protocol detailed in section 2.12. This allowed clear identification of each separate population in co-culture and monitoring of the frequency of MDM-CD4+ T cell conjugates formed over the period of co-culture (**Fig. 3.7**). In addition, DiD+ CD4+ T cells were loaded with a calcium sensitive dye before being added to PKH26+ MDMs at 37 °C, immediately centrifuged to synchronize the initiation of MDM-

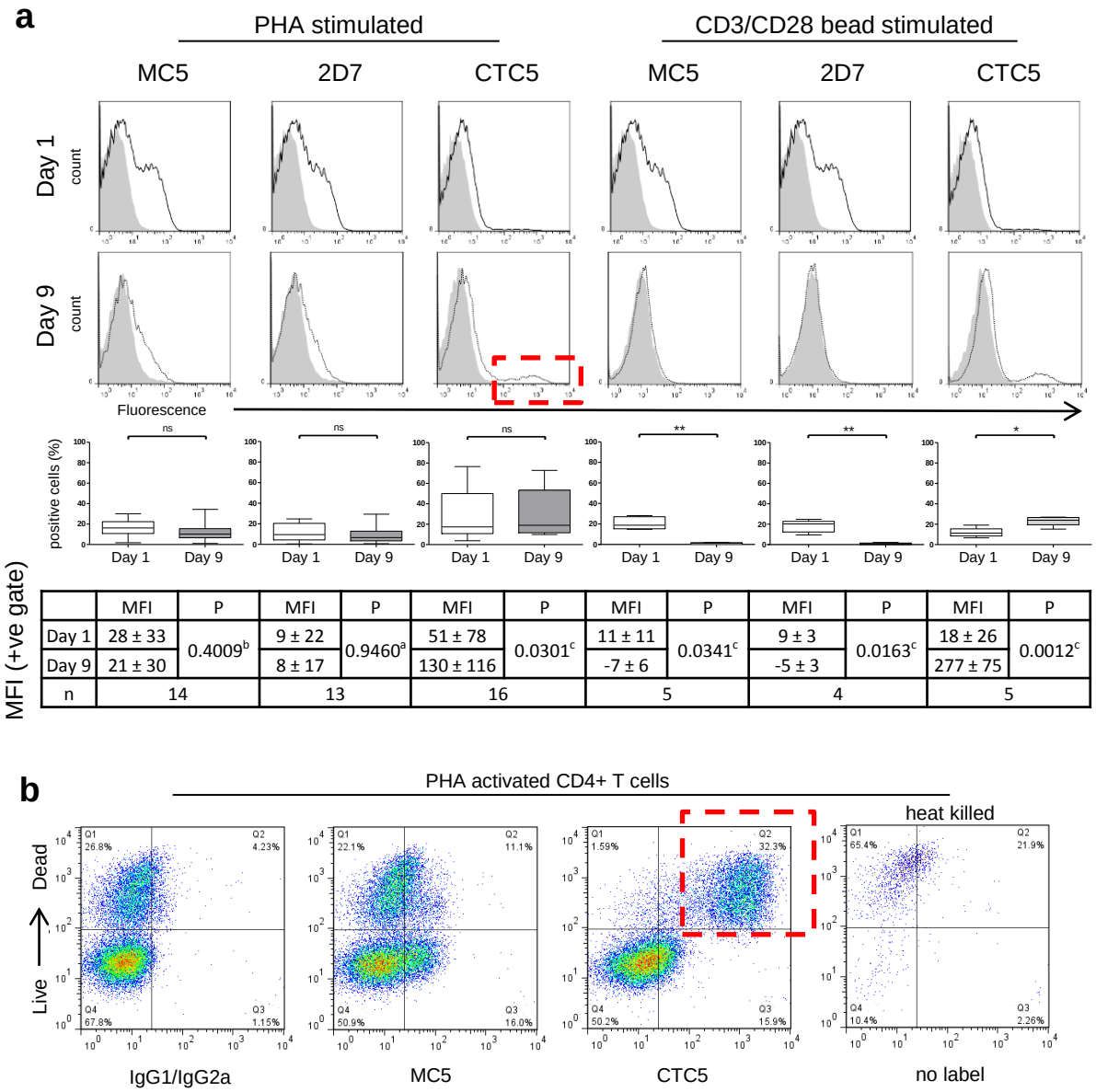

	MFI	P	MFI	P	MFI	P	MFI	P	MFI	P	MFI	P
Day 1	28 ± 33	0.4009[b]	9 ± 22	0.9460[a]	51 ± 78	0.0301[c]	11 ± 11	0.0341[c]	9 ± 3	0.0163[c]	18 ± 26	0.0012[c]
Day 9	21 ± 30		8 ± 17		130 ± 116		-7 ± 6		-5 ± 3		277 ± 75	
n	14		13		16		5		4		5	

Figure 3.6: Activation of human CD4+ T cells with CD3/CD28 beads results in a decrease in cell surface CCR5. (**a**) Samples of CD4+ T cells were harvested and immunolabelled with the indicated anti-CCR5 mAb or relevant isotype controls, as detailed in section 2.4.1, on day 1 prior to activation in culture with PHA/IL-2 or CD3/CD28 beads, and day 9 after activation. Representative graphs for days 1 and 9 are shown overlaid on the relevant isotype control (shaded grey). The box plots show the percentage of positive cells (+ve gate), as identified by gating all events above the isotype control, for days 1 and 9. Statistical comparison performed using a paired Student's t-test. **, P<0.01; *, P<0.05; ns, non-significant. Table shows the number of donors and the median fluorescence intensity (MFI) values of cells within the +ve gate. Statistical comparison was carried out as appropriate: [a], Wilcoxon matched-pairs test ;[b], Paired Student's t-test (after Log(Y) transform);[c], Paired Student's t-test. (**b**) Charts show PHA-activated CD4+ T cells that were FcR-blocked, labelled live with the indicated antibody and a fixable live/dead dye, fixed, quenched and labelled with a secondary GAM^{647} In one condition, CD4+ T cells were heat-killed by treating at 56°C 30 min prior to labelling. The red box indicates the CTC5^{hi} dead population.

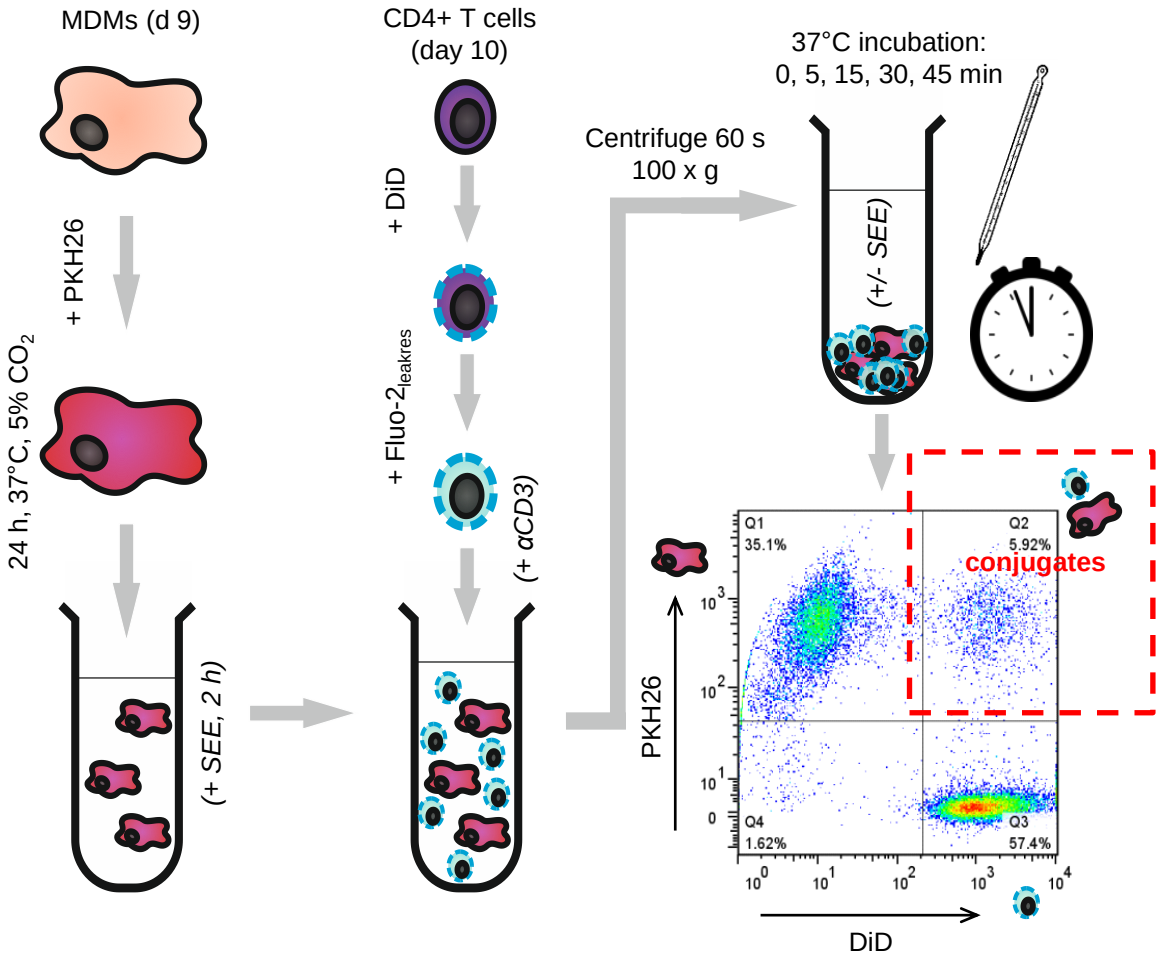

Figure 3.7: Diagram of flow cytometry method for measuring calcium signalling. Cartoon diagram summarising the method used to analyse formation of productive MDM-CD4+ T cell conjugates and the gate used to determine the percentage of conjugates formed, accompanying description in section 3.2.5.1.

CD4+ T cell interactions and then either analysed immediately (0 min) or after being maintained at 37 °C for various intervals (5, 15, 30, 45 min). At each interval DAPI was added to the co-culture sample immediately prior to analysis to identify live/dead cells; DAPI transits the membrane of dead cells more rapidly than live cells. After primary acquisition, ionomycin was added to the same sample before analysing it again (secondary acquisition). Further details of this protocol can be found in section 2.12.4. Compensation was performed post-acquisition before gating on live MDMs $DAPI^-$, $PKH26^+$, which were measured over a predefined event-width (pulse width ≥ 100 (PW^{100}); estimated MDM-CD4+ T cell width based on the pulse width of MDMs and CD4+ T cells alone) and were conjugated to CD4+ T cells (DiD+) (**Fig. 3.8a**). The fluorescence intensity of the calcium signal of events within the $DAPI^-PKH26^+PW^{100}DiD^+$ gate was exported and, for each interval, the MFI of the primary acquisition was expressed as a percentage of the MFI upon secondary acquisition, referred to herein as the 'calcium signal relative to ionomycin (%)'.

3.2.5.2 Calcium dye leakage impacts prolonged analysis

Previously, the calcium dye fluo-8 has been used in a flow cytometry method in our laboratory to study the calcium signalling of monocytes for up to 300 s in response to CCL2, CCL5 and lipoteichoic acid (Fox et al., 2011). On the basis of this assay fluo-8 was initially used to study calcium signalling in APC-CD4+ T cell conjugates at various intervals within a 45 min co-culture period at 37 °C. A higher intracellular calcium signal was detected in conjugates formed with SEE-pulsed MDMs at the 5 min time-point relative to conjugates formed in the absence of antigen. At 45 min the fluorescence levels of conjugates formed in SEE-pulsed and no antigen samples were remarkably similar, appearing to indicate that sAg-dependent calcium signalling had been abolished by this time. However, when ionomycin was added to the same sample no increase in fluorescence was observed (**Fig. 3.8b**) showing that it was, in fact, the ability to detect the calcium signal that had been abolished. This is consistent with the concept that different calcium indicators have different leakage propensities in different cell types (Takahashi et al., 1999). To combat leakage, cells can be treated with probenecid or, alternatively, a number of leak-resistant forms of calcium dyes exist which can be used in place of the traditional dyes (Takahashi et al., 1999). Therefore, a leak-resistant version of fluo-8 called fluo-$2_{leakres}$ (note: fluo-2 and fluo-8 are pseudonyms for the same indicator) was loaded alongside fluo-8 into CD4+ T cells from the same donor at final concentrations of 0.30 and 0.17 µM, respectively. The loss of fluorescence over time was compared directly over 45 min. In both the absence and presence of calcium released by ionomycin treatment, the MFI of fluo-$2_{leakres}$ showed far greater stability over time than that of fluo-8 (**Fig. 3.8b**). Moreover, when fluo-$2_{leakres}$ was used in the MDM-CD4+ T cell conjugate

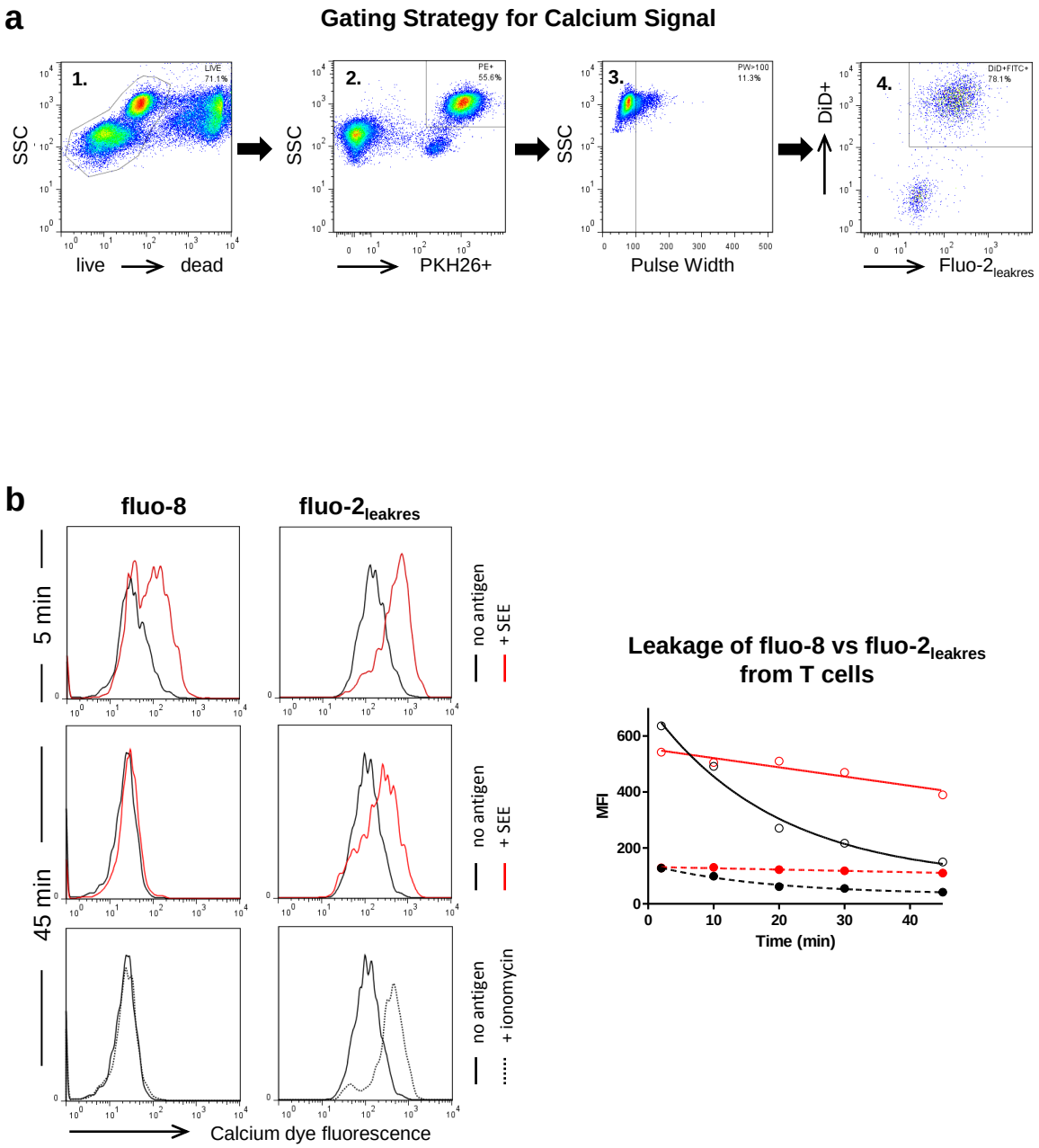

Figure 3.8: Leakage of calcium sensitive dyes. (**a**) Gating strategy employed to measure CD4+ T cell intracellular calcium level MFI when interacting with MDMs. (**b**) Leakage of fluo-8 compared to fluo-$2_{leakres}$ calcium dyes. Histograms of CD4+ T cells interacting with MDMs gated as indicated in (a) showing the ability of the different dyes to detect a change in fluorescence intensity (i.e. calcium signalling) after 5 or 45 min incubation at 37 °C in the presence of SEE or after addition of 1 µg/mL ionomycin. Graph shows leakage of fluo-8 (black lines/symbols) compared to fluo-$2_{leakres}$ (red lines/symbols) as a loss in MFI from CD4+ T cells of the same donor in the absence of MDMs in the presence (open circles) or absence (filled circles) of ionomycin.

assay, the conjugates formed in the presence of sAg showed higher fluorescence intensities than those formed in the absence of antigen at both 5 and 45 min (**Fig. 3.8b**).

3.2.5.3 Effect of sAg on MDM-CD4+ T cell conjugate frequency and signalling

Conjugates formed between PHA-activated CD4+ T cells and MDMs pulsed with SEE prior to co-incubation were of a similar frequency to those formed in the absence of antigen (45 min: 8 ± 2% and 8 ± 3%, respectively) (**Fig. 3.9**). No change in the frequency or kinetics of conjugate formation (45 min: 7 ± 1%) was observed when SEE was added to the MDM-CD4+ T cell co-cultures at the 0 min interval instead of pre-treating the MDMs. Similarly, the frequency of conjugates formed between CD3/CD28 activated CD4+ T cells and MDMs after adding SEE was not increased compared to conjugates formed in the absence of antigen (45 min: 9 ± 2% and 11 ± 0%, respectively). As a positive control for conjugate formation, CD4+ T cells were labelled/opsonized with whole IgG anti-CD3 (OKT3), which may be bound by MDMs expressing CD16 (see section 3.2.2). As expected anti-CD3 coated T cells showed a significant increase in the frequency of conjugates formed over time, evidenced by mean values at all time-intervals from 5 min onwards having mutually exclusive 95% confidence intervals (CI) compared to untreated controls. Overall, upon addition of SEE MDM-CD4+ T cell conjugate frequency remained low and was comparable to the frequency of conjugates formed in the absence of antigen. Certainly, the measure of conjugate frequency in this instance provided little evidence for the potential of stable IS formation occurring upon the addition of SEE.

To determine whether addition of sAg has any effect upon the potential of MDMs and CD4+ T cells to form synapses, the levels of intracellular calcium in T cells forming conjugates was studied. High calcium levels are an early indicator of the T cell response that is maintained over the course of antigen-dependent interactions between B- T cell conjugates (Huppa et al., 2003). The flow cytometry method was demonstrated to be able to detect the expected increase in intracellular CD4+ T cell calcium levels, which occurred due to Fc-crosslinking of anti-CD3 labelled T cells in MDM-CD4+ T cell conjugates. The intracellular calcium signal for CD4+ T cells forming conjugates with MDMs in the presence of SEE was high in comparison to the basal signal of conjugates formed in the absence of antigen (**Fig. 3.9**). For all conditions the intracellular calcium level peaked at the 5 min interval and did not return to the baseline level of conjugates formed in the absence of antigen over the time-course of analysis. When MDMs were pulsed with SEE or when CD4+ T cells were labelled with OKT3 prior to co-incubation, the calcium signal was relatively high at the initial 0 min time interval, compared to when SEE was added at the start of co-incubation. This shows that CD4+ T cell calcium influx upon TCR ligation or crosslinking through conjugate formation with MDMs occurs rapidly after conjugate

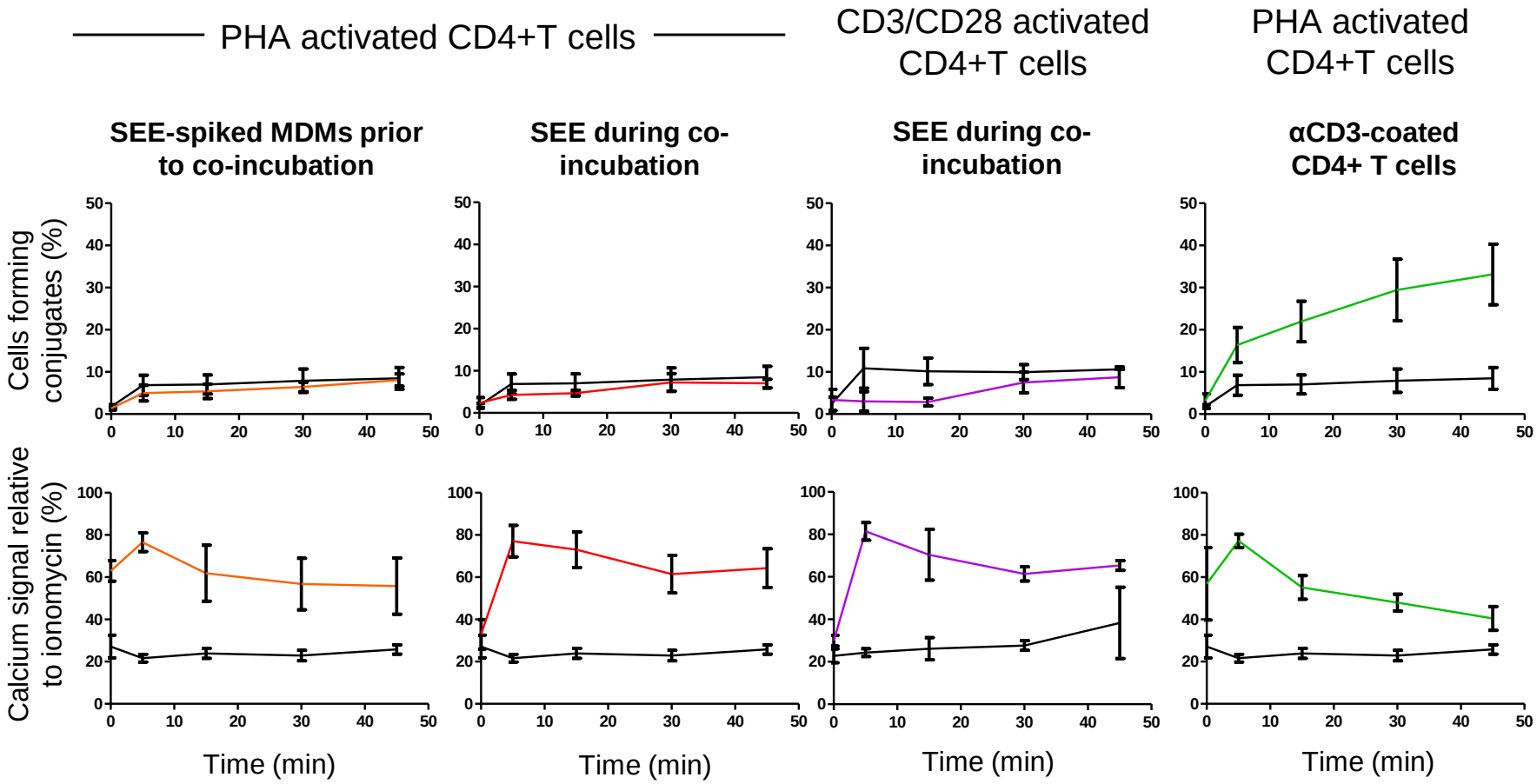

Figure 3.9: Analysing the formation of MDM-CD4+ T cell conjugates by flow cytometry. Upper graphs show the percentage of conjugates formed over time in the presence (coloured line) or absence (black line) of SEE. SEE was either incubated with MDMs for 2 h prior to co-incubation with CD4+ T cells or added at t = 0 (i.e. during co-incubation). The latter condition was completed for CD4+ T cells activated with PHA or with CD3/CD28 beads. As a positive control αCD3-coated CD4+ T cells were used to form conjugates with MDMs. Lower graphs show the intracellular calcium level in CD4+ T cells engaged in conjugates with MDMs as a fraction of the maximum calcium mobilisation by subsequent treatment of the same sample with 1 µg/mL ionomycin. Graphs show mean of donors (n=3); error bars, SD.

formation, faster than the time taken for centrifugation and initiation of sample acquisition (typically < 2 min). In comparison, the cases where SEE was added at 0 min showed a delayed rise in intracellular calcium, which can be explained by the time taken for the SEE to diffuse in solution and bind MHC class II and TCR (**Fig. 3.9**). Both the PHA/IL-2 and CD3/CD28 activated CD4+ T cells showed similar patterns of calcium signalling and, although they exhibited marginally different kinetics of conjugate formation relative to respective no antigen controls, neither showed greater than 10% conjugate formation. Therefore only the PHA/IL-2 activated CD4+ T cells were used for the remainder of the investigation into MDM-CD4+ T cell IS formation. Overall, sAg-dependent calcium signalling decreased marginally after the 5 min interval but then plateaued and was maintained above baseline levels for the duration of co-culture. In fact, the level of CD4+ T cell intracellular calcium signalling within MDM-CD4+ T cell conjugates was maintained to a greater extent with SEE than for conjugates formed with anti-CD3 coated CD4+ T cells. Thus, the addition of SEE enabled the MDM-CD4+ T cell conjugates to engage in sustained, sAg-dependent calcium signalling akin to that associated with IS formation (Huppa et al., 2003).

3.2.6 Live cell imaging of productive MDM-CD4+ T cell conjugates

Live cell microscopy of calcium signalling enables single cells to be followed over time, a parameter which is not possible using flow cytometry (Takahashi et al., 1999). In addition, in order to visualize IS markers and whether chemokine receptors accumulate at the interface of MDM-CD4+ T cell conjugates engaged in sAg-dependent signalling, an imaging-based approach must be adopted. Therefore a time-lapse fluorescence microscopy technique was developed to image intracellular CD4+ T cell calcium responses to sAg-pulsed or unpulsed MDMs (**Fig. 3.10**). Briefly, MDMs labelled with CFDA-SE were seeded onto PDL-coated coverslips, treated with SEE, a cocktail of SEA/SEB/SEE sAg or medium alone, then loaded into a perfusion chamber. Autologous CD4+ T cells (1 x 10^6 cells) that had been loaded with fura-2/AM were injected into the perfusion chamber containing adherent MDMs at a controlled rate. Imaging was initiated immediately after injection and images were acquired every 10 s for a total of 1200 s (20 min) (**Fig. 3.10a**). A similar procedure was also performed for Daudi-CD4+ T cell conjugates and further details of the protocol can be found in section 2.13. After CD4+ T cells were tracked, time-lapse images were processed as detailed in section 2.13.4. In these images CD4+ T cells with elevated intracellular calcium levels are represented by colour according to the intensity of the calcium rise. Tracks of the T cells are overlaid onto the image (**Fig. 3.10b**). An increased signal upon excitation at 340 nm compared to 380 nm (i.e. higher 340:380 ratio) indicates a rise in intracellular calcium levels.

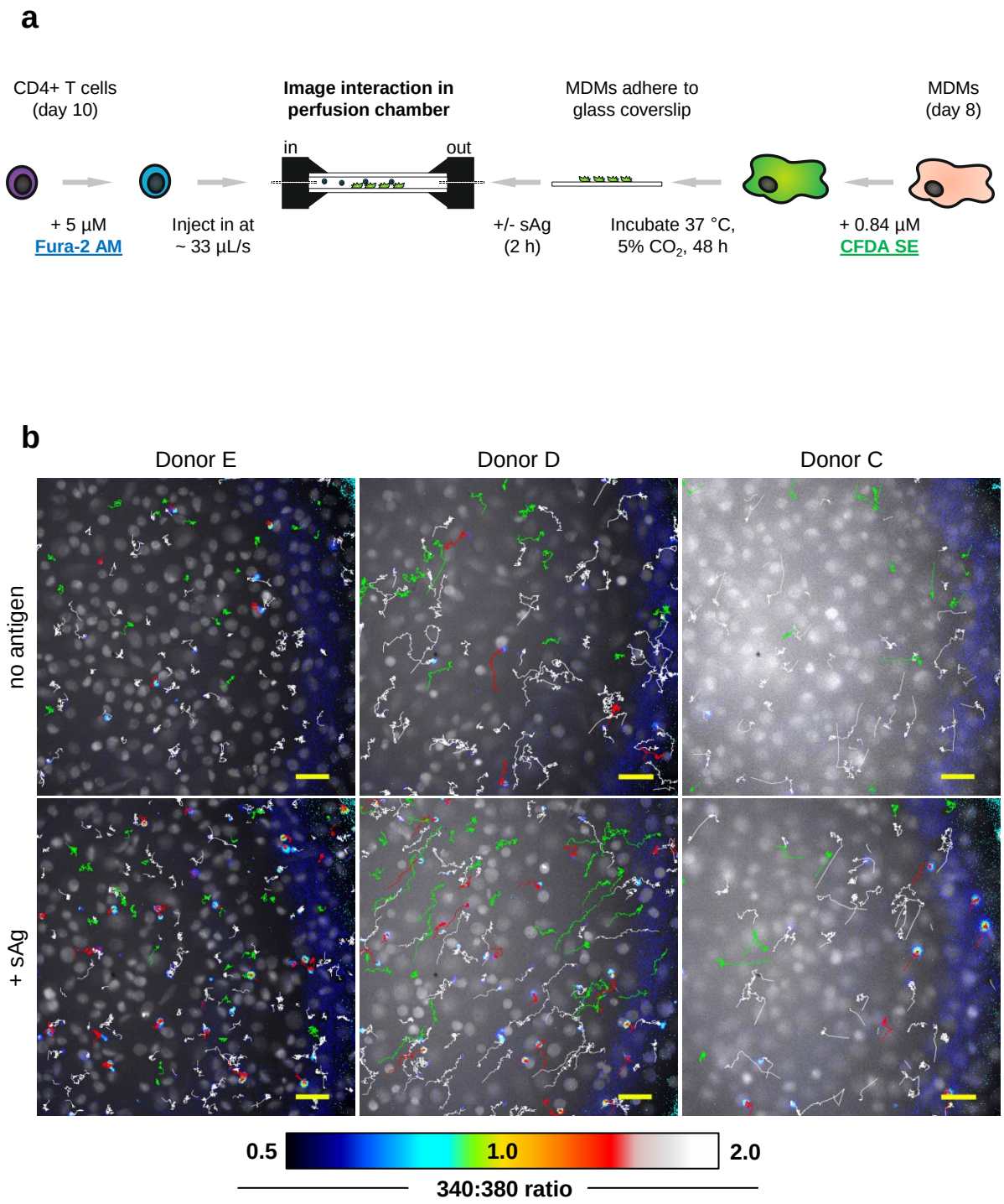

Figure 3.10: Live calcium imaging of MDM-CD4+ T cell interactions. **(a)** Cartoon diagram of the method used to image CD4+ T cell calcium signalling events when interacting with sAg-pulsed or unpulsed MDMs as described in section 3.2.6.(**b**) Final frame of the time sequence for each donor (n = 3) showing the entire field of view, representative of three time sequences. Images were processed to depict calcium flux of CD4+ T cells (coloured according to the intensity of calcium rise according to a 340:380 ratio using the indicated scale) interacting with MDMs (grey). CD4+ T cells were tracked using MTrackJ and tracks were colour coded according to the maximum 340:380 ratio experienced over time (**green tracks, <0.5**; **white tracks, ≥ 0.5 and < 1.0**; **red tracks, ≥1.0**). Scale bars, 50 µm.

Representative images of the final time-frame for each donor (n=3) illustrate that more CD4+ T cells with higher intracellular calcium intensities (cells coloured: yellow/red) were present in sAg-pulsed samples (+ sAg) compared to untreated controls (no antigen) (**Fig. 3.10b; supplemental movies 1-6**). The rise in intracellular calcium appeared to occur when CD4+ T cells were in close proximity to an MDM (i.e. forming signalling conjugates), supporting the results of the flow cytometry technique. Moreover, a greater number of tracked CD4+ T cells reached a high 340:380 ratio (≥ 1.0) over the duration of imaging (tracks colored red) in samples with sAg compared to no antigen controls (**Fig. 3.10b**). Note also that, compared to untreated controls, more CD4+ T cell tracks with a maximum 340:380 ratio < 0.5 (tracks coloured green) occurred in the presence of sAg (**Fig. 3.10b**). This effect is unlikely to be due to changes in CD4+ T cell number as this was kept constant. Rather, it may be related to sAg-treatment inducing flattened MDMs to become more rounded, so reducing the overall coverage of MDMs on the coverslip and opportunities for transient tethering.

During set-up and optimisation of the imaging protocol MDMs were pulsed with SEE alone before being exposed to T cells, in keeping with the flow cytometry protocol (**Fig. 3.11**). However, the two donors imaged with SEE-pulsed MDMs showed different results: 'Donor A' showed very few T cells with a higher calcium signal compared to no antigen controls and statistical significance of the population in the opposite direction than expected (i.e. higher maximum 340:380 ratio in the absence of antigen) (**Fig. 3.11**); 'Donor B' gave a number of T cells with higher calcium signal compared to no antigen controls and indicated a significant increase in the maximum 340:380 ratio upon sAg-treatment (**Fig. 3.11**). In an effort to try and improve the number of conjugates forming and consistency between donors, MDMs were pulsed with a cocktail of sAg (SEA/SEB/SEE) as used by Contento et al. (2008). SEE vs. sAg cocktail treatment was not directly compared in the same donors, therefore the benefit of SEA and SEB addition is unclear. Nevertheless, the three donors treated with the sAg cocktail gave consistently higher calcium responses when pulsed with sAg, which was not the case for one of the donors pulsed with SEE only (**Fig. 3.11**). Therefore the sAg cocktail was carried forward and used for the remainder of the study.

The difference observed in CD4+ T cell intracellular calcium levels between conjugates formed with sAg-treated and untreated MDMs was quantified by extracting the maximum 340:380 ratio for each tracked cell. For each donor, maximum 340:380 values were compiled from CD4+ T cells tracked in three separate movies when MDMs were treated, or not, with sAg. Two of the three donors tested showed significantly increased maximum calcium signal experienced by CD4+ T cells in the presence of sAg-treated MDM compared to untreated MDMs (**Fig. 3.11**; Mann-Whitney U test). Clearly, the number of

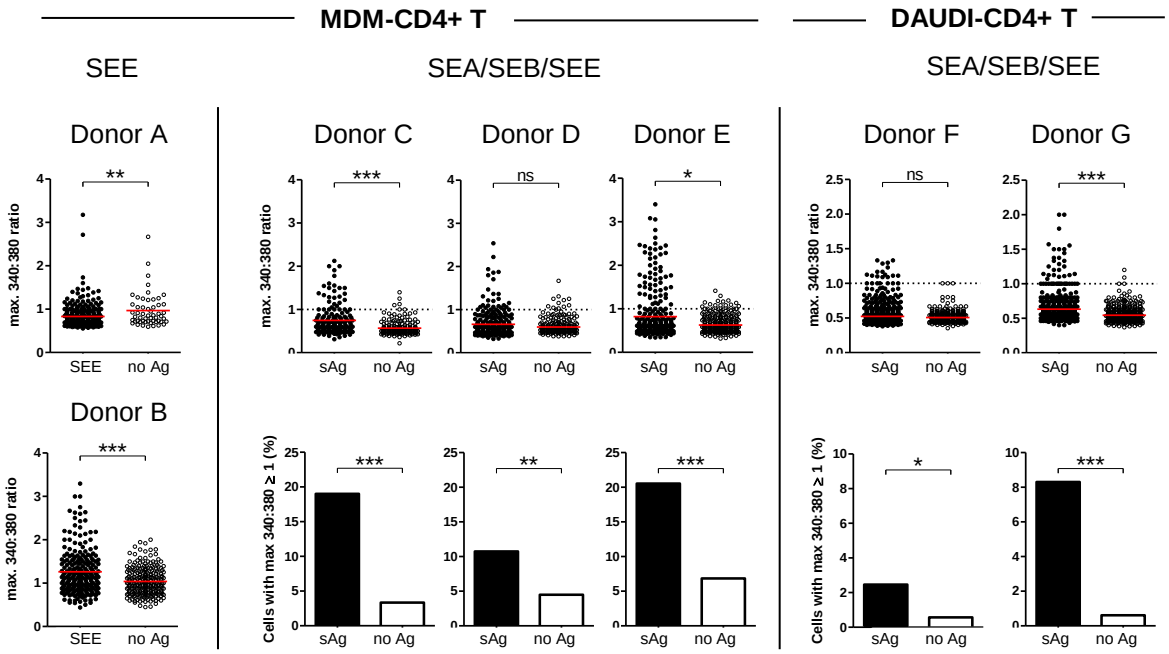

Figure 3.11: Analysis of MDM-CD4+ T cell conjugate formation by live microscopy. Fura-2 loaded CD4+ T cells were perfused over autologous MDMs or Daudi cells that were untreated (no Ag) or pulsed with sAg, specifically SEE alone or a cocktail of SEA/SEB/SEE at 1 µg/mL for 2 h. Intracellular calcium levels were imaged by fluorescence microscopy then CD4+ T cells were tracked and the maximum 340:380 ratio (calcium level) for each CD4+ T cell was calculated. For each of Donors A–G, the scatter graphs show the maximum 340:380 ratios in the presence and absence of sAg, with statistical comparison according to the Mann-Whitney U-test. For Donors C-G, which were imaged under identical conditions, the set of bar graphs show the percentage of cells above a cut-off value (maximum 340:380 ≥ 1.0) in the presence or absence of sAg and these proportions were statistically compared using Fisher's exact test.

responding cells and the level of intracellular calcium was highly variable between different donors. Nevertheless, for each donor a small population of CD4+ T cells showed a higher level of calcium signalling in the presence of sAg-pulsed MDMs compared to untreated MDMs. For this reason the effect of treating with sAg on the proportion of cells with a maximum 340:380 ratio ≥ 1.0 was compared using Fisher's Exact Test, as used by Kallikourdis et al. (2013). This analysis showed that the proportion of CD4+ T cells with higher calcium intensities (maximum 340:380 ratio ≥ 1.0) was significantly greater in the presence of sAg-treated compared to untreated MDMs (**Fig. 3.11, Donors C-E**).

To determine whether IS formation with MDMs was the cause of the limited frequency of T cells undergoing high calcium signals the present study also explored the T cell intracellular calcium response to B cells, which have been ubiquitously used in studies of IS formation. The frequency of CD4+ T cells that responded to sAg-pulsed B cells (Daudi cell line) by exhibiting a high rise in intracellular calcium was lower than that observed for MDMs pulsed with antigen. Despite this, the proportion of CD4+ T cells with maximum 340:380 ratios ≥ 1.0 was significantly greater in the presence of sAg-pulsed Daudi compared to no antigen controls (**Fig. 3.11**). Interestingly, in the absence of antigen Daudi-CD4+ T cell interactions appeared to result in a lower percentage of cells exhibiting intermediate calcium responses. Due to the smaller size of Daudi cells compared to MDMs this may simply reflect a reduced cell-cell surface area available for 'scanning'-associated calcium signals. Altogether these results show that a high intracellular calcium level is apparent in a small number of CD4+ T cells that engage MDMs. Although the frequency of these responses is low, this is also reflected through the previous observations in the flow cytometry based analysis, and the response frequency does not appear to be limited by the MDM cell type.

3.2.7 sAg changes the quality of calcium signalling in conjugates

Calcium signalling is not simply a digital on/off switch but rather an analogue system in which differences in amplitude and duration of the calcium signal result in differential cellular responses (Dolmetsch et al., 1997). Therefore it is important not only to consider the high-point of responses (e.g. maximum 340:380 ratio) but also the nature of the intracellular calcium signalling both before and after this point. To this end the levels of intracellular calcium for each individual CD4+ T cell in every time-sequence were plotted over time in an effort to identify patterns.

A sample of intracellular calcium profiles of CD4+ T cells that exhibited a maximum 340:380 ratio ≥ 1.0 in the presence of sAg-pulsed or unpulsed MDMs are shown alongside their corresponding cropped time-sequence images (**Fig. 3.12**). These images reiterate that high calcium signalling occurred when the CD4+ T cell was in close proximity

to MDMs (i.e forming conjugates) rather than occurring further afield whilst appended to other CD4+ T cells. Side-by-side inspection of each image time-sequence and calcium profile illustrates that high levels of intracellular calcium, even when transient, did not occur when the T cell was moving rapidly (**Fig. 3.12**; **supplemental movies 7-12**). The bottom 'no antigen' profile is an excellent example of this as nodules on the track that were formed when the cell was less mobile can be seen to coincide with transient rises in calcium (**Fig. 3.12**). A similar relationship is exemplified in the top 'plus sAg' profile in which the T cell was seen to crawl along the surface of the MDM, maintaining a low intracellular calcium signal prior to a sharp increase that coincided with arrest of movement. However, arrest of cell movement did not necessarily equate to an increase in intracellular calcium as tracks of T cells that did not show an increase in intracellular calcium (maximum 340:380 < 0.5) often migrated quickly at the start of imaging then arrested (green tracks: **Fig. 3.10b**). This was simply because T cells were injected at a controlled rate but the rate of flow was not maintained. Moreover, no significant difference in the meandering index (total straight-line displacement from the track origin (µm) / length of track (µm)) of tracks with a maximum 340:380 ratio ≥ 1.0 compared to tracks with a maximum 340:380 ratio < 0.5 was found within the sAg-pulsed time-sequence. Therefore, whilst a rise in intracellular calcium appeared to coincide with arrest of migration, in this experimental setting an arrest in migration did not necessarily identify a CD4+ T cell that was signalling.

CD4+ T cells that had been grouped into the category of 'maximum 340:380 ratio ≥ 1.0' and were interacting interacting with sAg-pulsed or unpulsed MDMs showed differently shaped intracellular calcium profiles with respect to each other. When interacting with sAg-pulsed MDMs a number of CD4+ T cells underwent a high-amplitude, sharp initial rise in intracellular calcium, which was maintained, often at a slightly lower level, over the imaging time-frame (**Fig. 3.12**). In contrast, CD4+ T cells interacting with unpulsed MDMs did not appear able to recapitulate this profile but, instead, followed sharp rises in intracellular calcium with a decrease to baseline levels (i.e. the 340:380 ratio for each track prior to the rise) over the time-frame of imaging (20 min) (**Fig. 3.12**). In general this suggests that the high calcium signals exhibited by CD4+ T cells in the absence of sAg were more transient than the high calcium signals in the presence of sAg.

3.2.8 Qualitative classification of CD4+ T cell calcium profiles

Visual comparison of all the calcium profiles with a maximum 340:380 ratio ≥ 1.0 demonstrates that, in the absence of antigen, none of the profiles showed the high amplitude and duration of calcium that were evident in a sizeable proportion of the profiles formed in the presence of sAg (**Fig. 3.13**). In order to assess whether the presence of sAg

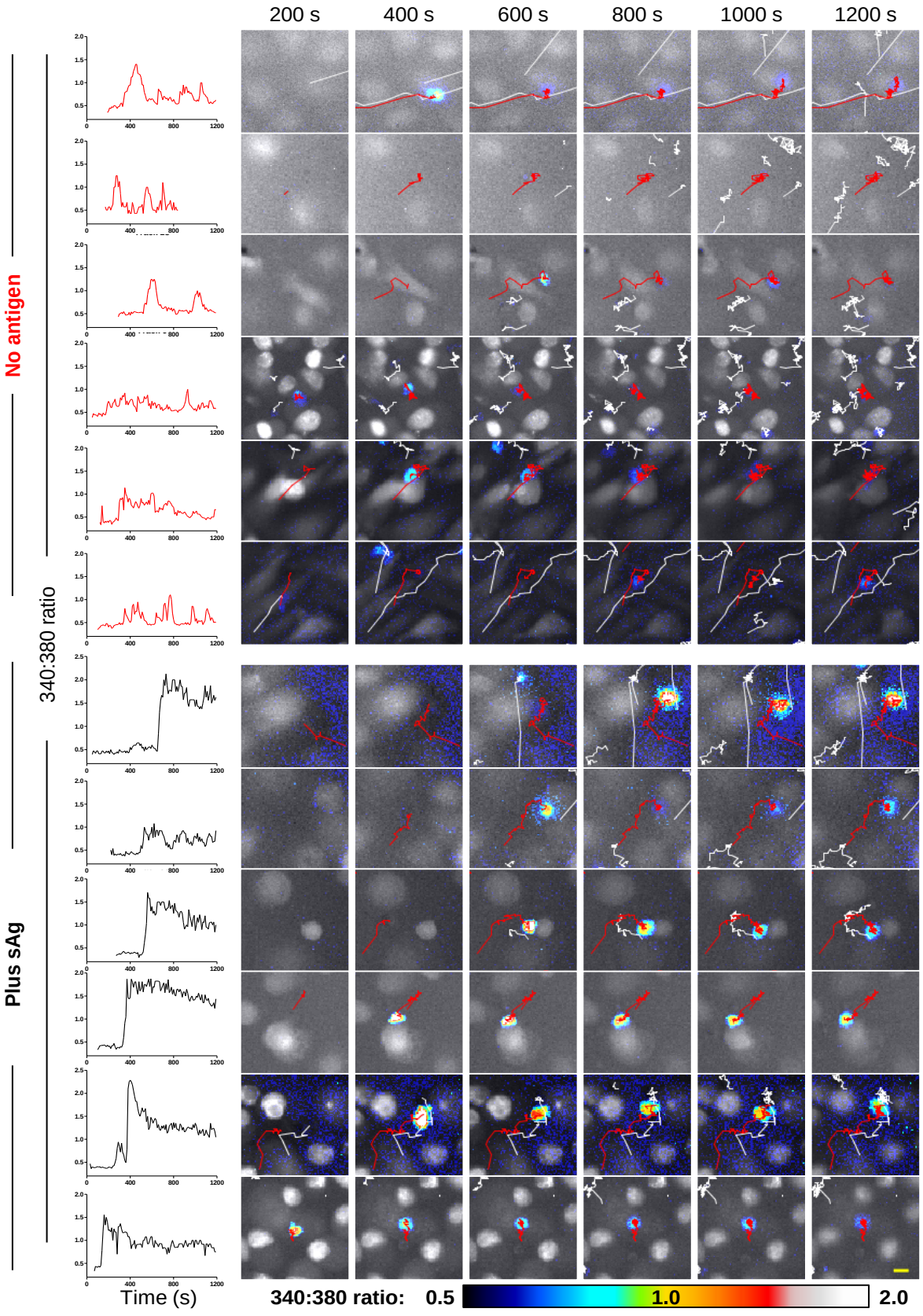

Figure 3.12: Arrest in CD4+ T cell mobility coincides with the onset of sustained calcium signalling. Example intracellular calcium profile of a CD4+ T cell identified to have a maximum 340:380 ratio ≥ 1.0 in the presence or absence of sAg. Corresponding image stills at regular intervals over the time-course are shown for each CD4+ T cell (colour coded to relate with intensity of the 340:380 ratio according to the indicated scale) interacting with MDMs (white cells). The track taken by the corresponding CD4+ T cell is highlighted in red. Scale bar, 10 µm.

Figure 3.13: Calcium profiles from cells reaching a maximum 340:380 ratio ≥ 1.0. Profiles were grouped into four categories: (i) flat, no rise or sharp spikes above baseline (not depicted in the figure as 340:380 < 1.0); (ii) transient, a rise in calcium followed by one or more returns to baseline over the course of analysis; (iii) low, a rise in calcium that did not return to baseline and did not fulfil the acceptance criteria of the high group; (iv) high, initial rise above a 340:380 ratio of 1.5 and sustained above a 340:380 ratio of 1.0 or alternatively an initial rise above 340:380 ratio of 2.0. **Black lines**, plus sAg. **Red lines**, no antigen.

also affected the proportions of transient or lower level calcium profiles occurring across the population, every calcium profile was qualitatively classified into one of four groups: (i) flat, no rise or sharp spikes above baseline; (ii) transient, a rise in calcium followed by one or more returns to baseline over the course of analysis; (iii) low, a rise in calcium that did not return to baseline and did not fulfil the acceptance criteria of the high group; (iv) high, initial rise above a 340:380 ratio of 1.5 and sustained above a 340:380 ratio of 1.0 or alternatively an initial rise above 340:380 ratio of 2.0 (**Fig. 3.14**). This classification method indicates that, even in the presence of sAg-pulsed MDMs, the majority of CD4+ T cells exhibited no change in intracellular calcium levels (group:'flat'). Nevertheless, a greater percentage of non-responders were present when MDMs were untreated (72 ± 14%) compared to sAg-pulsed MDMs (63 ± 11%). As noted above, the small percentage (5 ± 3%) of CD4+ T cells that responded with 'high' group profiles were exclusive to the sAg-treatment group. In addition, the proportion of CD4+ T cells undergoing sustained signalling at a low level more than doubled when interacting with sAg-pulsed MDMs (13 ± 5%) in comparison to unpulsed MDMs (5 ± 3%). This indicates that different subpopulations within the CD4+ T cell MDM milieu responded in distinct ways to the same sAg cocktail, resulting in different levels of calcium signalling. The percentage of CD4+ T cells with transient calcium profiles was relatively similar when interacting with sAg-pulsed (19 ± 7%) and untreated MDMs (23 ± 11%) (**Fig. 3.14**). The slightly reduced percentage of transient profiles in the presence of sAg together with the expansion of the 'high' and 'low' populations suggests that sAg acts to stabilise otherwise transient TCR-MHC scanning events.

3.2.9 Towards an automated classification strategy for calcium profiles

The qualitative classification procedure gave indications that an increased proportion of CD4+ T cells responded to sAg-pulsed MDMs with subtle rises in calcium compared to unpulsed MDMs. However, calcium profiles in both the 'high' and 'low' groups still showed substantial intragroup variation; some profiles having a sharp rise and others taking longer, some with high signals that decreased rapidly followed by a signal maintained at only a fraction of the initial rise, whilst others maintained the level of the initial rise or showed a gradual decrease. Further sub-grouping of like-by-like profiles (according to similarity of these features and delineation of the responses with or without sAg-treatment) by means of quantitative visual classification is extremely unlikely to yield meaningful or accurate comparisons. Thus, attempts were made to describe the curves in an automated fashion (i.e. without human-error of visual classification) using computational mathematics. One of these methods involved performing piecewise linear regression on each calcium profile to approximate/simplify each curve. A collaboration was initiated with

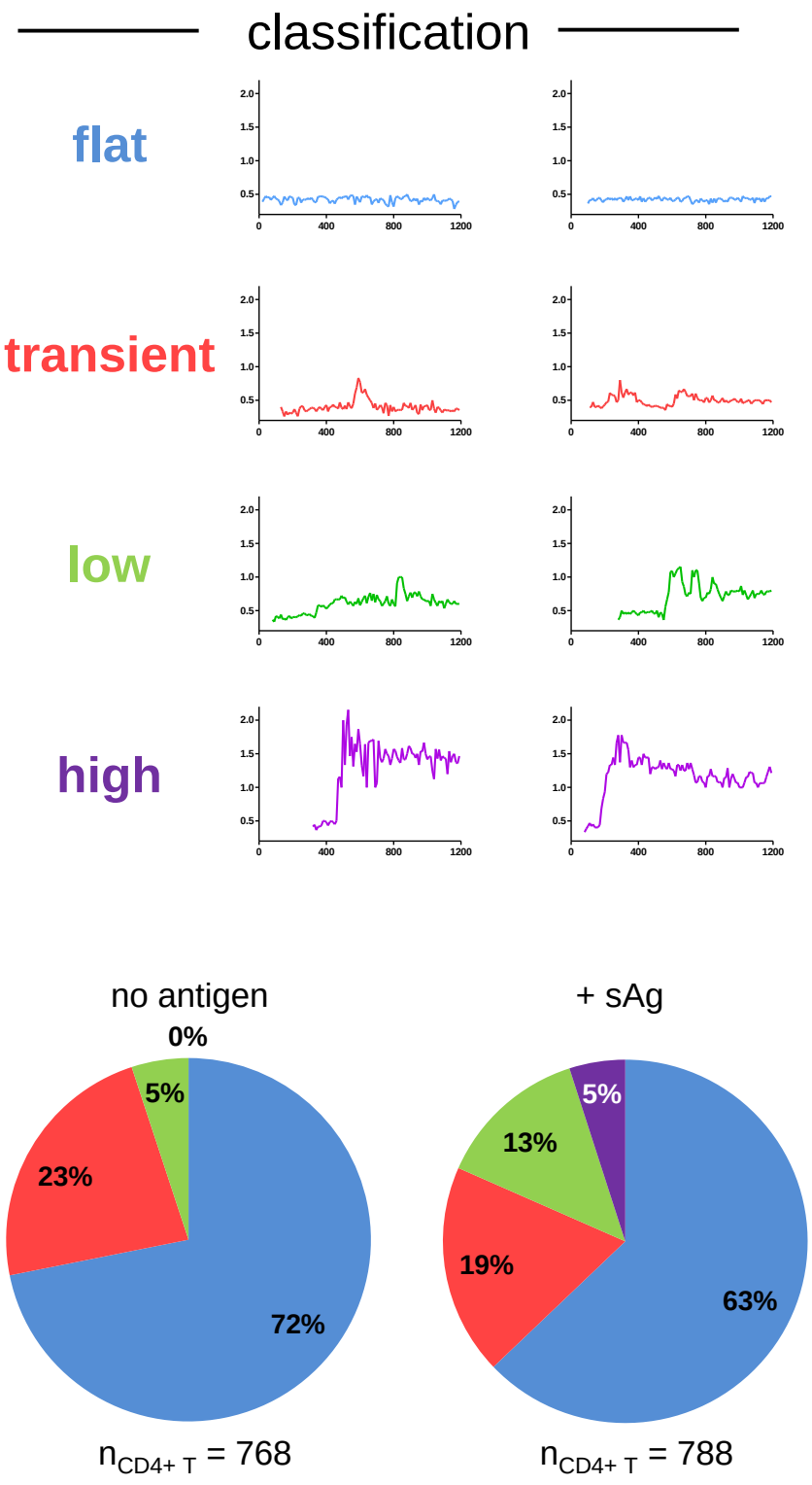

Figure 3.14: Qualitative classification of calcium profiles. Representative examples of calcium profiles visually classified into four groups (flat, transient, low or high) according to the criteria detailed in section 3.2.8. Pie charts showing the percentage of CD4+ T cell calcium profiles that fell into each group when interacting with unpulsed or sAg-pulsed MDMs.

Dr J. Wilson (University of York, York, UK) who wrote a c-script program (**Appendix 1**) that was able to fit each calcium profile with one to three linear segments. Segments were fitted in order to minimize the total R^2 value and eighteen parameters (**Fig. 3.15**) for each prolife were extracted to describe the fitted segments. Thus, calcium profiles could be analysed in a high-throughput manner and translated into a series of parameters that described the basic curve shape.

A function was written in MATLAB, which enabled parameters extracted using the linear piecewise regression curve to be reconstructed into linear segments and overlaid on the relevant raw calcium profiles in an array of individual subplots. Visual inspection of these revealed that the three segment linear regression appeared able to represent the major increases and decreases of the curves (**Fig. 3.15**). Indeed, this was reinforced by the R^2 values of the fitted profiles being similar to each other (0.79 ± 0.09). Thus, the segments fitted appeared to be reasonable approximations of the general shape of the calcium profiles.

Principal component analysis (PCA) was applied to the list of parameters, which had first been z-score normalised, in order to identify whether the combination of all of the parameters was able to discriminate between CD4+ T cell calcium profiles in the presence or absence of sAg. This type of analysis reduces the dimensionality of multiparametric data by finding the axes/directions within the data that give rise to the greatest variance (Jolliffe, 2002). The direction that describes the greatest variance is the first principal component, the direction describing the next greatest variance is the second principal component, and so on (Ringner, 2008). Only principal components with variance > 1 were considered. This cut-off was chosen according to Kaiser's rule, which stipulates that any principal component with variance ≤ 1 contains less information than the original parameters and, therefore, should be excluded (Jolliffe, 2002). Calcium profiles designated as 'flat' according to the visual classification of the data were removed prior to data analysis. Note also that five of the original parameters were not included in the analysis; the time-dependent parameters (iv, vii-x) are arbitrary because the time of cell-cell interactions was not synchronized. The scree plot shows that the first five principal components fulfilled Kaiser's criteria and together these components comprised 77% of the total variance of the data (**Fig. 3.15**). However, it can be argued that only the first two components will be useful as these occur prior to the elbow of the plot, which can be used as an alternative cut-off feature (Jolliffe, 2002). Nevertheless, scores for all combinations of the first five principal components were plotted against each other. Plots for the first three components are shown as examples. None of the plots showed separate clusters that corresponded to the CD4+ T cell calcium profiles interacting with either sAg-pulsed or unpulsed MDMs (**Fig. 3.15**). Therefore, using this method of analysis, even the low-onset

Calcium profiles fitted with piecewise linear regression:

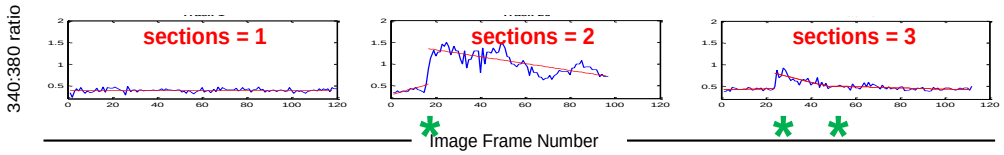

Parameters Extracted:

(i). First breakpoint
(ii). Second breakpoint
(iii). Distance between breakpoints
(iv). Length of time series
(v). Number of sections
(vi). R^2
(vii). Time of start
(viii). Time of first breakpoint
(ix). Time of second breakpoint
(x). Time of end
(xi). Slope of first section
(xii). Jump to second section
(xiii). Slope of second section
(xiv). Jump to third section
(xv). Slope of third section
(xvi). Intercept of line fitted to first section
(xvii). Intercept of line fitted to second section
(xviii). Intercept of line fitted to third section

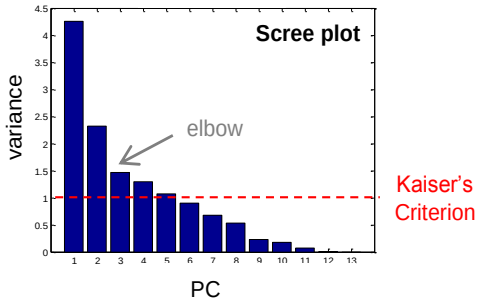

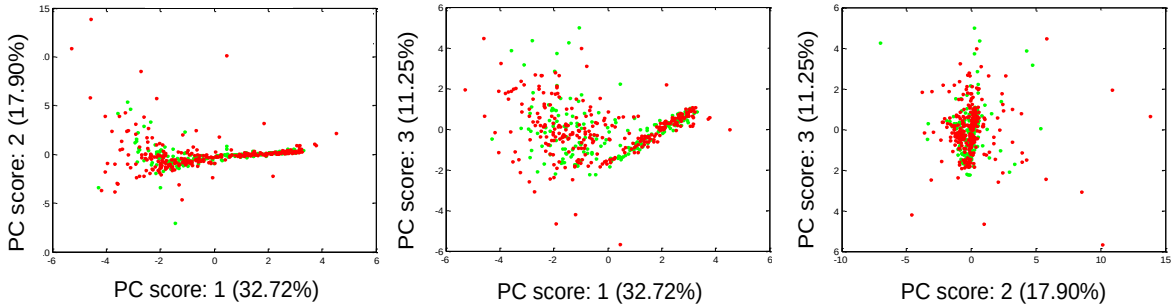

Figure 3.15: Quantitative classification using piecewise linear regression of calcium profiles. Examples of piecewise linear regression (red lines) overlaid onto calcium profiles (blue lines) where one, two or three linear sections are fitted. ✱ indicates the position of the breakpoints between fitted linear segments. Parameters extracted from the piecewise linear regression are stated; those in grey were excluded from further analysis. Principal component analysis was performed on the remaining 13 parameters and the relative contribution of all PCs is shown in the scree plot. PC scores plots of all combinations of the first three PCs illustrate that sAg (●) and no antigen (●) groups do not form separate clusters. PC, principal component.

intensity calcium profiles of the unpulsed cells could not be separated from the high-onset calcium profiles of the sAg-pulsed cells. Certainly, differences exist in the calcium profiles as evidenced by the visual classification system (**Fig. 3.13 & 3.14**), however these differences, or distinct groups of calcium profiles, are not evident using the above piecewise linear regression coupled with PCA.

3.3 Discussion

3.3.1 MDM cell surface markers and phenotype

The cell surface markers tested indicate that the population of cells, isolated by adherence and differentiated in M-CSF, were myeloid (CD11b+) and not populated by mature DCs (CD83+) or contaminated by large numbers of B cells (CD19+) or T cells (CD3+) (**Fig. 3.2**). Due to the absence of an adopted standard and the fact that subtle changes in culture conditions can alter MDM functional activity, the present study examined the expression of certain cell surface markers in order to determine the phenotype of the MDMs generated. A higher expression of CD14 has been shown to be associated with M2-polarised macrophages relative to M1 (Mantovani et al., 2002; Rey-Giraud et al., 2012). However the present study was concerned with comparing the expression of MDMs relative to monocytes at the start of culture. Under similar culture conditions Rey-Giraud et al. (2012) reported vastly increased CD14 fluorescence levels on M2 MDMs relative to monocytes, opposite to the decrease in fluorescence intensity observed in the present study (**Fig. 3.2; histograms**). Perhaps this difference stems from the analysis of monocytes after overnight culture in the present study, which has been reported to result in up- or down-regulation of other cell surface markers on monocytes. Indeed, the lack of CD4 observed on monocytes (**Fig. 3.2**) may be due to the transient cell surface downregulation of CD4 compared to freshly-isolated monocytes, which has been previously noted (Graziani-Bowering and Filion, 2000; Naif et al., 1998). Conversely, HLA-DR expression increases after overnight culture of monocytes (Andreesen et al., 1990; Graziani-Bowering and Filion, 2000). Evidently, placing monocytes into culture can rapidly alter their cell surface phenotype; thus attention should be paid to the time-point of immunophenotyping for comparison of expression between monocytes and MDMs.

In contrast to CD14, a large increase in CD16 expression levels was observed on MDMs (**Fig. 3.2; histograms**). However, the change in CD16 expression is controversial: a previous study associated it with M2 polarised MDMs (Rey-Giraud et al., 2012), and another with M1 (Mantovani et al., 2004). The expression of HLA-DR indicates that MDMs have the capability to bind and elicit the function of the sAg (Krakauer, 2013), but also

indicates that the MDMs do not adopt a deactivated (M2c) phenotype (Herbein and Varin, 2010). Based on CD14, CD16 and HLA-DR expression levels alone it is unclear whether the MDMs may be more M1 or M2 polarised. Therefore, CD80 and CD163 expression levels on M-CSF and GM-CSF differentiated MDMs were also compared (**Fig. 3.3**). The M-CSF MDM population had a higher percentage CD163 expression and a lower CD80 expression, consistent with the observations of other studies (Foucher et al., 2013; Rey-Giraud et al., 2012). Taken together these results indicate that our MDMs presented a more M2-polarised phenotype.

Culture in the presence of M-CSF is generally known to produce M2-polarised MDMs, although these can be skewed typically to secrete M1 inflammatory cytokines using LPS or M1 conditioned media (Rey-Giraud et al., 2012). This is a reminder that the M1 and M2 states represent extremes of a functional continuum (Mantovani et al., 2013) and, therefore, the ideal way to phenotype MDMs is to discern the functional state by assessing cell-associated markers, metabolic substrate preference and, most critically, cytokine secretion (Mantovani et al., 2002). Thus, the limited selection of cell-surface markers tested in the present study only give a simplistic view of which end of the continuum the MDMs generated may exist. More would need to be done to fully characterise the M1 or M2 phenotype.

3.3.2 CCR5 expression is dependent on cell type and activation

CCR5 is expressed on a significantly greater percentage of the MDMs compared to monocytes (**Fig. 3.4**). This observation is consistent with a report by Lee et al. (1999b) showing that the average number of 2D7 binding sites increases during differentiation of MDMs, and also with the suggestion that M-CSF increases CCR5 expression on MDMs to facilitate HIV entry (Herbein and Varin, 2010).

The CD3/CD28 activated CD4+ T cells clearly represent a more homogenously activated population than the PHA/IL-2 activated CD4+ T cells. However, the CD3/CD28 activation method is concomitant with CCR5 downregulation, which has been reported to be caused by increased β-chemokine production and loss of the quiescence-associated transcription factor, Kruppel like factor 2 (KLF-2) (Richardson et al., 2012). Despite differential CCR5 cell surface expression, a small population was consistently detected as CCR5+ when labelling with CTC5 after activation. This population was composed of late apoptotic/necrotic cells as it stained positive with a live/dead dye (**Fig. 3.6**). Since CTC5 recognizes the N-terminal region of CCR5 and is also able to recognize denatured CCR5 (Lee et al., 1999a), there is a case for CTC5 recognizing a form of CCR5 that is made accessible upon cell death. Although a subject of controversy (Pilch-Cooper et al., 2011),

CCR5 may exist in intracellular pools in some CD4+ T cells (Achour et al., 2009; Guglielmi et al., 2011). Whilst it is possible that necrotic degradation processes (lysosome rupture, protease activation, PM rupture) could result in denatured or incomplete intracellular CCR5 being released from the T cell that might be recognised by CTC5, MC5 is also able to recognise a very similar linear epitope on CCR5 (Blanpain et al., 2002). Thus because the $CCR5^{hi}$ population in question is only recognised by CTC5 and not MC5, the most likely explanation for this result is that the CTC5 mAb is demonstrating non-specific binding to the dead cells within the sample. In general, this demonstrates that live/dead exclusion can be useful in phenotyping cells for CCR5 using CTC5 and that care is required when drawing conclusions using a single mAb.

Unlike CD3/CD28 activation, a subpopulation of PHA/IL-2 activated cells express cell surface CCR5 after activation (**Fig. 3.6**). Considering that neither PHA/IL-2 nor the CD3/CD28 activated T cells showed higher frequencies of IS formation (**Fig. 3.9**), the PHA/IL-2 activated T cells are advantageous as the contribution of endogenous CCR5 on the T cell side of the IS can also be studied using this population. In future studies, considering the interplay between CCR5 and IL-2 (Camargo et al., 2009), it would be useful to determine the concentration of IL-2 that confers maximal CCR5 expression through the PHA/IL-2 activation method in order to increase the chance of imaging a CCR5+ T cell forming a synapse.

3.3.3 T cell recall using Revaxis: a problem of concentration

The inability to recall DTP-specific T cells from PBMCs using Revaxis (**Fig. 3.1**) may indicate a lack of recent immune challenge by DTP antigens in the donors tested. Furthermore, lack of proliferation to Revaxis was still observed when measured with ^{3}H-thymidine incorporation instead of CFDA-SE, which is known to be toxic at high concentrations and, thus, can lead to aberrant proliferative function (Parish et al., 2009). Additionally, no increase in proliferation was detected over a dilution range of Revaxis from 1:125 to 1:4000 that was tested for two donors. The optimal dilution of Revaxis (1:1000) had previously been determined by Dr. A. Itano (Tempero Pharmaceuticals, USA) and colleagues who were able to recall DTP-specific T cells successfully. However, if the donor cohort used in their study had recently received a booster vaccination then the chances of recalling antigen-specific T cells using this method would be much higher (Mariotti and Nisini, 2009). Another study used Revaxis (1:250 dilution) as a positive control for IL-17 production in response to a recall antigen, however an enzyme-linked immunospot assay was used and, therefore, this report did not directly examine whether any proliferative response actually occurred (Nogueira et al., 2010).

Even after immunization, the frequency of TT specific T cells that can be stimulated to proliferate is 1:10000 (Murphy et al., 2011). The success rate of isolating antigen-specific T cells from donors which have not been vaccinated in the past few years or have never received vaccination is low or near-zero (Mariotti and Nisini, 2009). Nevertheless, strong evidence exists that, even 10 years after vaccination, TT is able to induce a proliferative response in memory T cells *in vitro* (Sallusto et al., 1999). Perhaps influences of experimental procedures, such as the decrease in proliferative response to TT obtained when using PBMCs frozen in FCS compared to freshly-isolated PBMCs (Disis et al., 2006), may go some way to explaining the lack of proliferation in response to Revaxis in the present study. However, the main problem with using Revaxis may be that, even at 1:125 dilution, the quantity of TT is low (≥ 0.16 Lf U/ml TT) compared to a report showing that 13-52% of the PBMC population had undergone division after treatment with 2 Lf U/ml TT (Zaunders et al., 2009). The possibility still exists that a low dilution of Revaxis (e.g. 1:10) may be able to recall DTP-specific T cells in unprimed donors. However, the potential effects due to higher concentrations of alum and excipients, such as formaldehyde, would need to be carefully controlled.

3.3.4 Diverse potential of sAgs in CD4+ T cell stimulation

The use of sAg effectively overcomes the need to generate antigen-specific CD4+ T cells in order to form conjugates with MDMs in which the TCR and MHC class II molecules are engaged. There are, however, several important considerations when using sAg instead of conventional peptide antigen presented by MHC class II. The differences may bear relation to the frequency of conjugate formation (**Fig. 3.9**) and the spread of calcium profiles observed (**Fig. 3.14**). Yet sAgs bear some similarity (Omoe et al., 2010) to the way in which different peptide-MHC complexes give rise to different affinities for the same TCR which, in turn, has an effect on T cell function, calcium signalling and IS formation (Morris and Allen, 2012). This was evidenced by studies showing that the different binding affinity of SEA and SEA_{S206P} (SEA with a single point mutation) to TCR was the discriminating factor between preferential expansion of T cells expressing Vβ3 compared to Vβ11 and vice versa, respectively (Omoe et al., 2010). Working on this principle the level of different T cell responses measured by intracellular calcium levels across a polyclonal population stimulated by single sAgs would be expected to exhibit differences. The sAg-cocktail (SEA/SEB/SEE), however enables 11 (Murphy et al., 2011) of the 25 known functional TCR-Vβ families (Brewer and Ericson, 2005) to be engaged, with Vβ3 being bound by both SEA and SEB (**Table 3.1**). As each interaction has a potentially different affinity this effect may contribute, in part, to the variation in the range of calcium profiles seen in our experiments (**Fig. 3.13**).

The majority of CD4+ T cells do not form conjugates or exhibit any detectable elevation in intracellular calcium in either the presence or absence of sAg (**Fig. 3.9 & 3.11**). Several approaches were used to investigate the ability of the MDMs and CD4+ T cells to form productive conjugates: (i) pulsing with a sAg-cocktail instead of SEE only; (ii) substituting MDMs with B cells (Daudi) as APCs; (iii) using CD3/CD28-activated CD4+ T cells instead of PHA-activated CD4+ T cells.

More T cells in the samples pulsed with sAg-cocktail, as opposed to samples pulsed with SEE-only, showed a calcium increase above untreated controls (**Fig. 3.11**). Thus, using a number of sAgs together appeared to potentiate their effects. This indicates that a limiting factor for the number of conjugates responding may be the correspondence between Vβ profiles of the donors and the target Vβ families of the sAgs. TCR-Vβ usage in individuals is known to vary (Ochsenreither et al., 2008), reflected by the difference in the percentage of cells experiencing high calcium levels between each donor (**Fig. 3.11**). Despite this, existing literature suggests that, on average, the Vβ chains of highest frequency within the PBL population are those targeted by the sAg cocktail, in particular SEE (**Table 3.1**). This indicates that, in PBLs, the cumulative expression of Vβs that are recognized by the sAg-cocktail is unlikely to be the limiting factor for inducing conjugate formation or calcium signalling. However, as activation protocols can polarise Vβ expression profiles (Geursen et al., 1993), the profiles of PHA/IL-2 activated CD4+ T cells would need to be measured directly to determine whether relative Vβ expression changed substantially over the course of culture.

Conjugate number may also be affected by the ability of certain macrophages to present antigen. Certainly, macrophages are not as efficient as DCs in presenting antigen to naïve T cells (Zigmond and Jung, 2013). Yet naïve T cells were not in abundance at the time of conjugate formation in the present study. This was indicated by the upregulation of activation markers on both PHA and CD3/CD28 activated CD4+ T cell populations, along with the high percentage of cells expressing CD45RO, which is suggestive of an effector/memory cell phenotype. The ability of macrophages to be able to present antigen to effector CD4+ T cells has been demonstrated *in vivo* (Filipe-Santos et al., 2009; Koltsova et al., 2012; Morris et al., 2013). Nevertheless, under certain activation states macrophages are not efficient at antigen presentation and can suppress T cell function and proliferation (Hoves et al., 2006). However, in the present study when MDMs were substituted by B cells, the percentage of CD4+ T cells with a 340:380 ratio ≥ 1.0 did not increase (**Fig. 3.11**). Thus, the large percentage of non-responding CD4+ T cells in the presence of sAg did not appear to be due to the cell type engaged in the synapse nor the ability of MDMs to form productive conjugates with CD4+ T cells.

The flow cytometry method (**Fig. 3.9**) showed that, after 45 min, fewer than 10% of conjugates formed between MDMs and PHA/IL-2 activated CD4+ T cells. However, this population of PHA/IL-2 activated CD4+ T cells had a low activation status, indicated by the low percentage of cells expressing CD25 or HLA-DR and the reduced levels of CD45RO over culture (**Fig. 3.5**). Since a previous report showed that T cell activation status can impact on the dynamics of interactions with APCs (Azar et al., 2010), conjugate formation with CD3/CD28-activated CD4+ T cells was tested. Generally the CD3/CD28 activated T cells had a higher activation status, shown by a greater percentage of cells expressing CD25 or HLA-DR with respect to PHA/IL-2 activated CD4+ T cells. However, as with the PHA/IL-2 activated CD4+ T cells, MDM conjugate formation with CD3/CD28 activated CD4+ T cells did not exceed 10%. Therefore, the low number of conjugates formed was not limited by the low activation status of the PHA/IL-2 activated CD4+ T cell population. In addition, the low frequency of conjugates did not appear to be dictated by the APC type and was unlikely to be due to a lack of SEA/SEB/SEE-bound TCR-Vβ regions in the CD4+ T cell population.

3.3.5 Analysis of MDM-CD4+ T cell conjugates by flow cytometry

One other study (Rethi et al., 2002), has looked at T cell intracellular calcium signalling in conjugate formation over an extended time-course by flow cytometry. Rethi et al. (2002) examined calcium signalling at various time points over 180 min between co-cultured murine B cell and fluo-3 loaded T cell hybridomas. The results showed that intracellular calcium levels were increased in the presence of antigen-loaded B cells, with calcium levels peaking at ~40 min and then declining through to 180 min (Rethi et al., 2002). The fact that an increase in calcium was measured in the presence of antigen supports the results of the present study (**Fig. 3.9**). The differences in kinetics may be due to Rethi et al. (2002) using B cells instead of macrophages, gating on all fluo-3 loaded T cells rather than on conjugates only, or having no prior centrifugation step, which they suggest may “promote induction of the calcium signal” (Rethi et al., 2002). The present study used a much lower centrifugation speed than those tested by Rethi et al. (2002) (100 x g cf. 2000 x g) but, nevertheless, we accept that the calcium peak seen at ~5 min is more of a reflection of synchronized contact initiation in the presence of sAg, which becomes more asynchronous across the population over time. Thus, of all the aforementioned factors that may impact on the recorded kinetic, the difference is most likely due to the synchronized contact initiation employed compared to the asynchronous co-sedimentation utilised by Rethi et al. (2002). Nevertheless, the present study further supports the considerable evidence showing a rapid rise in intracellular calcium downstream of TCR ligation (Kummerow et al., 2009).

The method presented here has several beneficial aspects compared to the protocol used by Rethi et al. (2002). Only conjugates formed from the two separate populations were gated on, thus excluding any calcium signalling arising from events that may have occurred between calcium dye-loaded T cells only. Additionally, the fluo-$2_{leakres}$ was shown to have minimal leakage (**Fig. 3.8**), which has previously been reported as a problem when using fluo-3 in lymphocytes (Takahashi et al., 1999), therefore minimizing any artefactual reductions in the intracellular calcium levels measured over a long period that are simply due to dye leakage. Furthermore, pulse width gating helps to select for events involving two or more cells. For future optimization the protocol could make use of an intracellular dye instead of DiD, which may reduce the dye transfer that could occur by intercellular exchange of PM fragments (trogocytosis).

Overall the flow cytometry protocol showed that MDM-CD4+ T cell conjugates occurred at a similar frequency when pulsed with sAg compared to unpulsed conjugates. Importantly, a sharp rise in T cell intracellular calcium levels occurred for sAg-pulsed MDM-CD4+ T cell conjugates, but not for MDM-CD4+ T cell conjugates in the absence of sAg (**Fig. 3.9**). Moreover, live cell imaging studies supported observations of the cytometry protocol in illustrating that a small, but significantly greater, proportion of CD4+ T cells exhibited high levels of intracellular calcium upon interaction with MDMs pulsed with sAg compared to untreated MDMs (**Fig. 3.11**). This shows that productive MDM-CD4+ T conjugates were formed in the presence of sAg, which indicates that concurrent synapse and/or kinapse formation was likely to be occurring.

3.3.6 Apparent arrest of CD4+ T cells upon calcium onset

In the present study CD4+ T cells were found to arrest coincidentally with the onset of high intracellular calcium levels (340:380 ≥ 1) (**Fig. 3.10b & 3.12**). This appears to contrast with seminal work conducted by Underhill et al. (1999) who demonstrated that mobile murine T cells were able to be activated by macrophages. Critically, imaging was conducted over a much longer period of time (180 min) than in the present study (20 min). As cell-cell interactions can interconvert between immobile and crawling states (Friedl et al., 2005), it is possible that imaging for longer than 20 min may capture T cells in a mobile state that still maintains calcium signalling. Furthermore, Underhill et al. (1999) may have been looking more at kinapses than synapses as NFAT only requires a low level of intermittent calcium signalling in order to be selectively activated (Dolmetsch et al., 1997). In the present study, the sudden rise of calcium amongst T cells that exhibited 'high' profiles coincided with apparent arrest, which may classically reflect a synapse. Yet many other T cells exhibited 'low' calcium profiles, which if imaged for longer may be detected to be slowly-mobile and thus correlate with the observations of Underhill et al.

(1999). To identify such kinapses the imaging technique needs to be able to differentiate between stable (< 1 μm/min) and slowly-mobile (1-2 μm/min) states (Friedl et al., 2005). Thus, whilst the current low-resolution (0.92 μm/pixel) technique combined with manual tracking can report on larger-scale movements, such as dynamic crawling (1-10 μm/min) (Friedl et al., 2005), the difference between stable or slowly-mobile states would only be a change in a single pixel over a minute. In the future, imaging with the same hardware would require a higher magnification and automated cell tracking that uses shape to discern the T cell centroid. This set-up may be able to distinguish the differences between the stable and slowly-mobile states, though the compromise would be that the numbers of responders with 340:380 ≥ 1.0 per field would be very low.

3.3.7 Grouping calcium profiles to find a signature for IS formation

Most of the intracellular calcium profiles were flat but, where increases in calcium were apparent, the profiles were incredibly variable with regard to intensity and duration (**Fig. 3.13**). Using a reductionist system, different profiles and numbers of responding cells were previously observed to depend upon subtle differences in sequence and concentration of peptide that the APCs were pulsed with (Wülfing et al., 1997). This suggests, therefore, that using a variety of sAgs which preferentially bind different TCR-Vβ regions contributed to the variation in calcium profiles in the present study. Additionally, Wülfing et al. (1997) showed that low or high concentrations of agonist resulted in ~95% of T cells responding with a sustained singular onset signal. However, a similar percentage of cells responded to a partial agonist, which at a high concentration maintained the proliferative capacity, although the calcium profile was a singular onset signal that decreased slowly over time (Wülfing et al., 1997). Remarkably, in the present study the majority of calcium profiles with maximum 340:380 ≥ 1.0 in the presence of sAg showed a slowly decreasing signal after the initial onset. It is, therefore, tempting to speculate that the resulting response may also be associated with proliferative capacity, which is known to require calcium signalling to be sustained over a time-course of hours (Hogan et al., 2010). Certainly, the results of the flow cytometry study showed that calcium signalling in conjugates occurred for at least 45 min. This, combined with the observation that the percentage of cells classified as 'transient' did not increase upon addition of sAg, suggests that long-term calcium signalling may be taking place. However, although this may lead to effector function, the function is not necessarily proliferation but, perhaps, cytokine production, which also requires long-term calcium signalling (Hogan et al., 2010). Nonetheless, in the absence of sAg the majority of non-'flat' calcium profiles were 'transient' and expected to relate to the ubiquitous use of calcium downstream of numerous receptors, including GPCRs (Clapham, 2007). Indeed, our laboratory has previously demonstrated that transient rises

of a similar duration occur in monocytes in response to chemokine stimulation (Fox et al., 2011).

Classification of calcium profiles has the potential to enable identification of different types of synapse or kinapse. The first step in classification was to identify whether differences could be detected in the wide range of different calcium profiles apparent in the presence or absence of sAg (**Fig. 3.13**). The qualitative classification system indicated that only a small percentage of CD4+ T cells displayed some kind of sustained (i.e. classes: 'low' and 'high') response in the absence of sAg, whereas a larger proportion were engaged in sustained signalling in the presence of sAg (**Fig. 3.14**). This suggests that the addition of sAg enabled MDMs and CD4+ T cells to engage in productive conjugates with sustained calcium signalling downstream of TCR ligation. Since the sustained response was formed from a range of low to high amplitude calcium profiles, these may represent a mix of synapses and kinapses according to the model suggested by Kummerow et al. (2009). In particular, the high level signals were exclusive to interactions dependent upon sAg. These strong calcium signals may be associated with stable IS formation, supported by evidence of close CD4+ T cell apposition to MDMs and arrest coinciding with calcium onset of 'high' profiles (**Fig. 3.12**).

Unfortunately, the computational methods intended to further subgroup similar calcium profiles were unable to even resolve the difference between calcium profiles of CD4+ T cells with or without sAg. Visual inspection indicated this lack of difference was unlikely to originate from oversimplification of the data using the piecewise linear regression as the segments tended to reflect the general shape of the calcium profiles (**Fig. 3.15**). However, it may be that any differences in the 'jumps' between sections, which effectively report on the amplitude of the onset, only translate to a small degree of the overall variation when considered together with the other parameters. Thus, the principal components that dominate may not necessarily be those that were selected as dominant variables for the visual classification system (e.g. calcium onset amplitude). In several calcium profiles linear segments were observed to be fitted to the onset in order to minimize R^2, giving a steep positive gradient. Without modifying the c-script to restrict the fitting of sections with steep positive gradients it remains unclear whether these types of segment may give rise to systematic artefacts within the parameters. Systematic artefacts are known to contribute to variation and, thus, have the potential to dominate the principal components (Ringner, 2008). Nevertheless, the parameters extracted from the current piecewise linear regression analysis were unable to describe the evident visual differences between non-'flat' calcium profiles of CD4+ T cells in the presence or absence of sAg.

Recently, a method has been described where a high cell density tracking function was coupled to fluorescence signal processing and was subsequently presented as a heat map of cell number over time (Salles et al., 2013). Rather than grouping the highly variable calcium profiles to identify which profile types in antigen-pulsed samples also existed in unpulsed samples, Salles et al. (2013) used unstimulated cells as a background in order to set a threshold that identified peptide-specific activation. However, the threshold was set using fluorescence intensity parameters of the calcium profile which could lead to misrepresentation of the antigen-dependent response. For example this system would not detect whether the presence of antigen resulted in an increased frequency of a subset of calcium profiles lying just below the response threshold that are identical to a subset in the absence of antigen. Nevertheless, the one-look overview in the method presented by Salles et al. (2013) speeds up many of the time-consuming aspects of analysing APC-T cell calcium responses. Indeed, similar methods employing automated high-density tracking that are able to report on parameters, such as cell shape, will facilitate future work in the field and, perhaps, enable calcium profiles with similar features to be successfully grouped by automated approaches.

The results presented in this chapter demonstrate that a limited number of conjugates form between primary human CD4+ T cells and MDMs in the presence and absence of sAg. The low frequency of productive conjugates does not appear to be limited by the APC type nor was it increased by using differentially activated T cells. Imaging studies revealed that the calcium profiles of interacting T cells show a wide range of amplitudes and durations, which may reflect different mechanisms of antigen-dependent signalling. Crucially, T cells engaged in conjugates only exhibited high, sustained levels of intracellular calcium in the presence of sAg, which is suggestive of MDM-CD4+ T cell IS formation. Therefore, despite its limitations, we decided to use MDM-CD4+ T cell conjugates formed in the presence of sAg to assess the role of CCR5 at the IS.

Chapter 4: Chemokine receptors at the MDM-CD4+ T cell IS

4.1 Introduction

4.1.1 Chemokine receptors and IS formation

Chemokines play a role in priming cells into a signalling-ready state for antigen-receptor engagement (Contento et al., 2010). Indeed, in the presence of chemoattractants leukocytes adopt a polarised morphology where the uropod of the cell is largely pulled along by the protrusive flow of F-actin at the leading edge of the cell (Lammermann et al., 2008). This polarised morphology promotes TCR sensitization at the leading edge, possibly by enhancing the proximity of TCR to signalling components and/or through actin-flow mediated disruption of low affinity TCR-MHC interactions at the cell-cell interface (Beemiller and Krummel, 2010; Tybulewicz, 2002). Additionally, it has been proposed that T cell chemokine receptors crosstalk with the integrin LFA1 to direct mitochondrial translocation to the interface with an APC and through doing so set up the T cell in a signalling-ready state (Contento et al., 2010). Although integrins are not necessary for mobility within a tissue (Lammermann et al., 2008), such crosstalk interactions with chemokine receptors may reveal a more subtle role for integrins in regulating the dynamics of APC-T cell interactions. Generally, these mechanisms of chemokine-induced cell polarisation, which aid TCR signalling or cognate antigen recognition could lead to an enhanced frequency of IS formation.

4.1.2 Chemokine receptor distribution at the IS

Chemokine receptor signalling has been suggested to influence whether a T cell decides to ‘stop’ or ‘go’ in the context of TCR engagement (Bromley et al., 2000). One of the ways in which chemokine receptors may regulate this decision is according to the ‘distraction hypothesis’. Indeed, GFP-CCR5 and CXCR4-GFP, when overexpressed in T cells, have been shown to be recruited to the T cell side of the human B cell-CD4+ T cell or DC-CD4+ T cell IS (Contento et al., 2008; Molon et al., 2005). However since CCR7 did not become localised to the interface this is consistent with the proposed hierarchy of chemokine receptor and TCR signalling (Bromley et al., 2000; Molon et al., 2005). Furthermore, CXCR4 and CCR5 were found to be recruited to the IS in a co-dependent manner mediated by APC-secreted chemokines; this was suggested to involve CXCR4:CCR5 heterodimerisation. Hidden at the APC- T cell interface, these receptors were

hypothesised to prevent distraction and promote T cell adhesion rather than chemotaxis by signalling through $G_{q/11}$ (Contento et al., 2008; Molon et al., 2005). Notably, these studies did not consider chemokine receptor expression on the APC cell side nor did they show whether differences in localisation still occur with endogenously expressed receptors. Although CD8+ T cells expressing CCR5 have been suggested to be involved in IS formation at the LN and peripheral sites (Castellino et al., 2006; Franciszkiewicz et al., 2009), CD4+ T cells expressing CCR5 would be expected to predominate in peripheral sites, since they are primarily of activated or effector memory phenotype (Bleul et al., 1997; Sallusto et al., 2004). As macrophages are also present at peripheral sites and interact with CD4+ T cells in a number of diseases, discussed in section 1.3.4, it seems relevant to determine whether CCR5 and CXCR4 are also involved in the productive MDM-CD4+ T cell interaction demonstrated in chapter 3.

4.1.3 MDMs expressing cell surface CCR5

The results from chapter 3 show that MDMs generated in the present study express CCR5, in similarity to macrophages found in certain tissues *in vivo* (Shen et al., 2009). Thus these MDMs can be used as a model to investigate whether endogenous CCR5 may also localise on the APC side of the IS. In previous studies both GM-CSF and M-CSF conditioned MDMs have been shown to express CCR5 (Lee et al., 1999b). However their different polarisation towards M1 or M2 phenotypes, respectively (Rey-Giraud et al., 2012) can potentially have implications for IS formation. Indeed, M1 macrophages are often associated with more efficient antigen presentation and higher levels of costimulatory molecules than M2-polarised macrophages (Biswas and Mantovani, 2010). Consequently it is important to determine whether these factors translate to more frequent IS formation.

M-CSF and GM-CSF are cytokines that act to regulate myeloid cell number, survival and differentiation (Hamilton and Achuthan, 2013). Each binds to a different receptor and exhibits a different pattern of expression; M-CSF being ubiquitous and consistently expressed, in contrast to GM-CSF expression, which is normally upregulated in response to injury or infection (Hamilton and Achuthan, 2013). In general, M-CSF exclusively promotes macrophage differentiation and survival whereas GM-CSF is much more promiscuous, also acting on DCs, neutrophils and eosinophils (Hamilton and Achuthan, 2013). Together these findings constitute a reason for the addition of M-CSF to macrophage cultures *in vitro* in an effort to keep them in their ‘normal state’. Polarising macrophages with GM-CSF and M-CSF generates macrophages with similar but not identical features to M1 or M2 macrophages, which are polarised by exposure to LPS and IFNγ or IL-4 and IL-13, respectively (Gordon, 2003; Hamilton and Achuthan, 2013). In appreciation of this, the present study uses GM-CSF alongside LPS and IFNγ in order to

recreate as many of the inflammatory stimuli that may lead to M1 polarised MDMs as possible.

4.1.4 Visualising MDM-CD4+ T cell IS formation

CD4+ T cells form conjugates with sAg-pulsed MDMs, which in turn triggers a rise in T cell intracellular calcium levels, as demonstrated in chapter 3. One of the advantages of using calcium as a readout of productive MDM-CD4+ T cell conjugate formation was the ability to report on all types of antigen-dependent engagement. However productive conjugate formation does not necessarily equate to the accumulation of proteins at the MDM-CD4+ T cell interface. This is evidenced by the lack of large-scale molecular clustering in T cells forming kinapses compared to synapses (Azar et al., 2010). Thus a marker must be used to select for signalling MDM-CD4+ T cell conjugates that form an IS.

In the original description of the IS, antibodies directed against CD3, PKCθ, Lck and fyn, or talin and LFA1 were used to mark the cSMAC and pSMAC, respectively (Monks et al., 1998). In addition the MTOC or the Golgi, which is coordinated to the IS by the MTOC, become distributed to the APC- T cell interface upon IS formation (Griffiths et al., 2010). However although the MTOC can be used to identify IS formation, in 33% of conjugates it has been seen to localise within the third of the T cell proximal to the APC simply by chance (Meier et al., 2003). Considering the low frequency of MDM-CD4+ T cell conjugates undergoing high calcium signals, this high background level of MTOC alignment would not reliably report on IS formation. With regards to potential markers on the APC side, cognate ligands of antigen-presentation machinery such as MHC class II and ICAM1 have been shown to accumulate (Grakoui et al., 1999; Monks et al., 1998). Additionally the APC has been reported to coordinate the accumulation of spinophilin and PIP2 to the IS (Bloom et al., 2008; Fooksman et al., 2009).

The pSMAC of the IS is similar to the lamella observed in the kinapse, since both modules are enriched in actin, which undergoes continuous treadmilling (Dustin, 2009b). Furthermore both modules are enriched in LFA1 and talin, meaning that synapses and kinapses alike would show accumulations of these markers to the APC- T cell interface. However the LFA1/talin/actin would show different distributions at the synapse compared to the kinapse; a critical difference between these structures is that the pSMAC exhibits radial symmetry whilst the kinapse lamella does not (Dustin, 2009b). Note that Monks et al. (1998) observed a high percentage of total LFA1 accumulating to the IS, demonstrating that it is potentially a useful marker. Nevertheless the cSMAC has been proposed to be the most unique module of the IS with no equivalent in the kinapse (Dustin, 2009b). On this basis markers associated with the cSMAC are the most effective descriptors of IS

formation. Indeed, CD3 and markers against other components of the TCR complex as well as PKCθ have been widely used to mark IS formation and remain distributed at the IS for over 30 min, making them suitable candidates for the present study (Grakoui et al., 1999; Revy et al., 2001; Yokosuka et al., 2005).

This chapter investigates whether productive MDM-CD4+ T cell conjugates formed in the presence of sAg result in IS formation. Immunofluorescence microscopy is used to investigate the localisation of IS components and whether the frequency of IS formation changes with MDM polarisation. The contribution of cell surface CCR5 on the macrophage side of the MDM-CD4+ T cell IS is explored as well as the localisation of CCR5 and CXCR4 on the T cell side.

4.2 Results

4.2.1 CD3 capping marks MDM-CD4+ T cell IS formation

4.2.1.1 Relationship of CD3 capping with CD4+ T cell intracellular calcium

CD3 was selected from the potential markers to identify IS formation for several reasons: (i) other studies have used CD3 as a marker for IS formation, including the original description of the IS by Kupfer and colleagues; (ii) mAb clones of different isotopes are available enabling indirect immunolabelling with chemokine receptor mAbs using isotype-specific secondary antibodies; (iii) mAbs raised against CD3 are inexpensive. Another potential marker for the IS is PKCθ, yet despite attempting several different fixation and permeabilisation strategies no signal was obtained from immunolabelling MDM-CD4+ T cell conjugates using anti-PKCθ mAb C-18 (Santa Cruz Biotechnology, TX, USA). In contrast, CD3 accumulation was visible in a small percentage of sAg-pulsed MDM-CD4+ T cell conjugates, thus it was the preferred marker to identify IS formation in the present study.

Initially, T cells were labelled with an anti-CD3 Fab fragment digested from whole IgG OKT3 in an attempt to visualise accumulation of CD3 in live T cells loaded with the Fura-2/AM calcium indicator. Analytical gels confirmed that the CD3-Fab fragments generated were pure and of the correct size. However when T cells were indirectly labelled with CD3-Fab followed by Fab^{488}, a very low fluorescence signal above the levels of control T cells labelled with Fab^{488} secondary was identified by flow cytometry. Furthermore, no specific signal for these cells was able to be detected by wide-field fluorescence microscopy. Using whole IgG was not a viable alternative since T cells labelled with OKT3 and co-incubated with MDMs demonstrate enhanced conjugate formation and calcium

signalling (**Fig. 3.9**). In general, coating T cells with any whole IgG antibody would effectively opsonise them for interactions with the high affinity IgG receptor (CD16), which was previously shown to be upregulated on the MDMs used in the present study (**Fig. 3.2**).

As an alternative approach a correlative imaging technique was used to investigate the extent of CD3 accumulation in relation to CD4+ T cell calcium signalling. Glass-bottomed dishes were set up so that a central reference point could be easily relocated on different microscopes. Practically this meant that a small triangular piece of autoclave tape was fixed to the outside base of a glass-bottomed dish, which contained adherent MDMs that had been pulsed, or not, with sAg. The tape was positioned so that one of the corners of the triangle pointed to the centre of the dish. Dishes that had been marked in this way were placed on the microscope stage so that the triangle was located at three o'clock relative to the eyepiece. The field of view was then positioned so that the tip of the triangle corner was just visible on the middle right of an image acquired using the camera. Fura-2-loaded CD4+ T cells were pipetted onto the MDMs and conjugate formation was imaged live for 30 min. Cells were then immediately fixed, permeabilised, and immunolabelled for CD3 (OKT3). Guided by the mark, the original field of view was relocated on a confocal microscope and z-stacks of all remaining CD3+ T cells in this field were acquired. The position of each confocal z-stack was marked on the final field of view acquired during live calcium imaging. This process created a map linking each T cell labelled with CD3 to the calcium signalling that T cell had undergone prior to fixation.

Orthogonal views of the CD3 distribution on each T cell clearly show that CD3 can accumulate to the MDM-CD4+ T cell interface. Furthermore, the corresponding calcium profiles of each T cell indicate that the accumulation of CD3 appears to correlate to existence of a rise in intracellular calcium (**Fig. 4.1a**). The apparent relationship was tested by (i) visually classifying each CD4+ T cell calcium profile into 'high', 'low', 'transient' and 'flat' groups, according to the criteria described in section 3.2.8, and (ii) measuring the level of CD3 fluorescence at the interface compared with the rest of the CD4+ T cell. This measure was achieved by tracing the PM outline of the CD4+ T cell at the interface with the MDM in the appropriate orthogonal view in ImageJ (**Fig. 4.1b**). The position of the interface was determined using brightfield images acquired during the z-stack. The mean fluorescence across the trace at the interface was then divided by the mean fluorescence of the traced outline of the remaining PM (i.e. not at the interface). Results show that the ratio of CD3 at the interface is significantly higher for CD4+ T cells that have calcium profiles categorised as 'high' when compared to others (**Fig. 4.1b**). Further, the 'low' group also shows significantly more accumulation of CD3 compared with the 'flat' group. Notice however that many CD4+ T cells in the 'low' group show equal

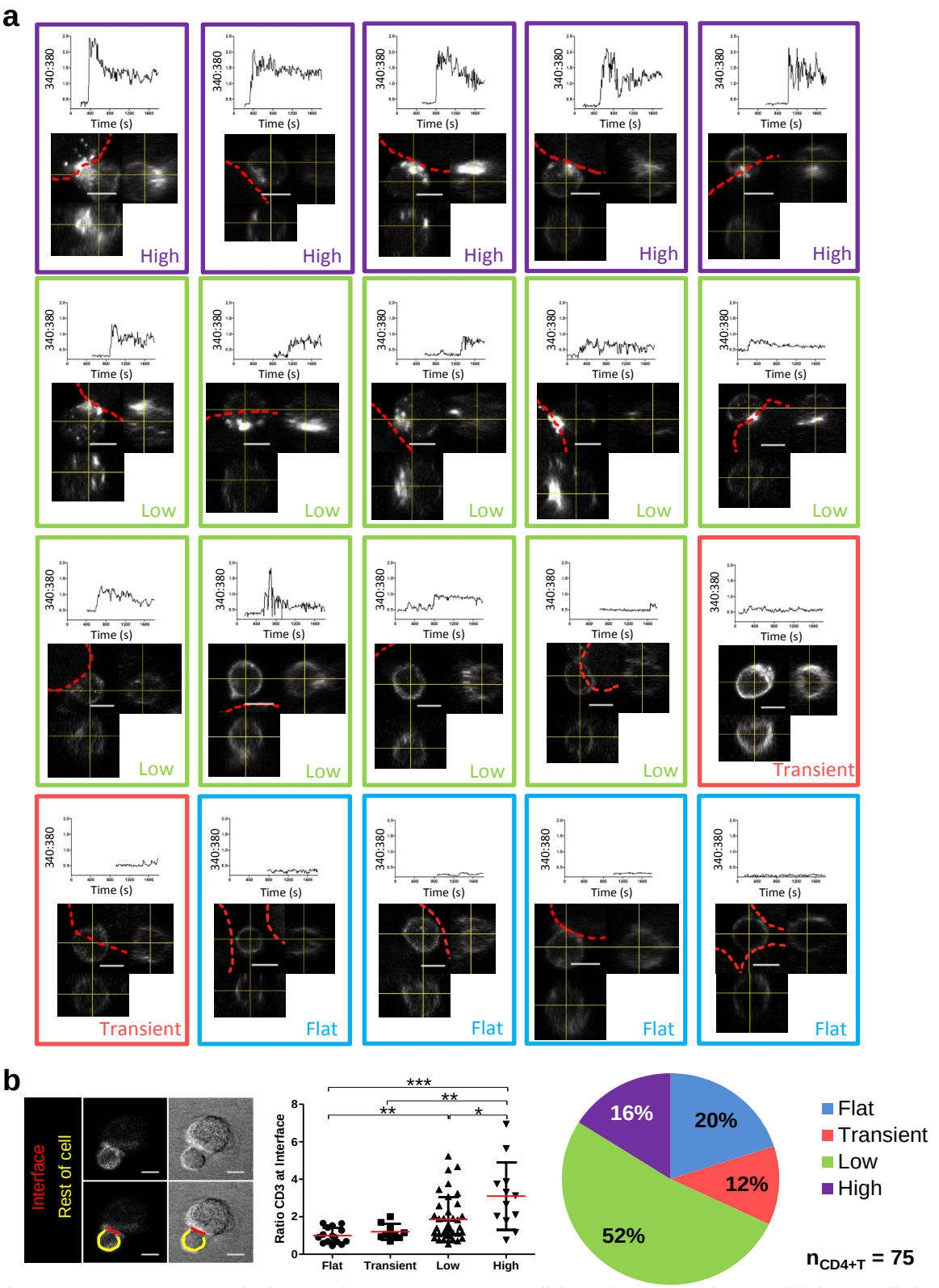

Figure 4.1: CD3 accumulation at the MDM-CD4+ T cell interface correlates with intracellular calcium rise. (**a**) The intracellular calcium rise in CD4+ T cells interacting with sAg-pulsed MDMs was imaged, cells were immediately fixed, permeabilised and immunolabelled for CD3 followed by GAM^{594}. Images show CD3 labelling on individual CD4+ T cells in orthogonal views and the correlating intracellular calcium profile. The dashed red line indicates the edge of the MDM in the brightfield image. (**b**) Quantification of CD3 capping (intensity of CD3 capping at the interface divided by CD3 intensity of the T cell membrane not at interface; line width, 10 px) from all T cells from 4 donors grouped according to visually classification of calcium profiles. Statistical comparison using ANOVA followed by Tukey post-test. Pie chart shows relative proportion calcium profile groups of CD3+ T cells in field of view after immunolabelling. Error bars, mean ± SD. *, $P < 0.05$; **, $P < 0.01$; ***, $P < 0.001$. Scale bars, 5 µm.

amounts of CD3 accumulation to the 'flat' or 'transient' group. It is possible that lack of CD3 accumulation alongside concomitant calcium signalling in these cells may indicate kinapse instead of synapse formation.

Overall this result shows that IS-formation and high calcium signalling are associated in CD4+ T cells engaged with sAg-pulsed MDMs. With regard to the T cells that remain on the coverslip after fixation and immunolabelling, a greater percentage were found to have 'high' or 'low' profiles compared to when the cells were imaged live (**Fig. 4.1b & Fig. 3.14**). This is most likely to be due to the wash steps performed during immunolabelling, which may have removed many of the T cells that were not strongly adhered to MDMs. T cells that are not adhered to MDMs cannot engage their TCRs with sAg-bound MHC and therefore may undergo lower levels of calcium signalling than adherent T cells. Thus the immunolabelling procedure enriches for the types of stable adhesion and high levels of calcium signalling that are associated with IS formation. In general, the correlative technique confirms the utility of CD3 as a marker and the occurrence of IS formation between sAg-pulsed MDM-CD4+ T cell conjugates.

4.2.1.2 CD3 accumulation with M-CSF vs. GM-CSF conditioned MDMs

The MDMs forming synapses in the present study showed indications of M2 polarisation; however, M1 macrophages are typically associated with more efficient antigen presentation (Biswas and Mantovani, 2010). Therefore investigations were made into whether CD3 capping, indicative of IS formation, may be limited by the MDM polarisation. MDMs were conditioned with M-CSF, or GM-CSF, LPS and IFNγ according to the method detailed in section 2.2.1 and seeded onto coverslips. Conjugates were formed between sAg-pulsed MDMs and autologous CD4+ T cells, then fixed and immunolabelled for CD3 (UCHT1). Using a wide-field fluorescence microscope the frequency of IS formation was counted via the eyepiece. Note that both DAPI and CD3 images were captured to provide a digital record of observations (images not shown). Results show that more CD3 capping was apparent in the presence of M-CSF compared with GM-CSF conditioned MDMs (**Fig. 4.2a**). Thus IS formation is not limited by the polarity of M-CSF conditioned MDMs that are used throughout the present study. Furthermore, MDM-CD4+ T cell conjugates were immunolabelled for the M2-marker CD163 alongside CD3, according to the method detailed in section 2.11.2. Images show that CD3 capping can occur in T cells engaged with CD163+ cells (**Fig. 4.2b**). This provides further evidence that IS formation is due to direct CD4+ T cell interaction with M2-polarised MDMs rather than with other cell types (e.g. contaminating B cells). Additionally, MDM-CD4+ T cell conjugates labelled for ICAM1 and CD3 (UCHT1) revealed that CD3 capping is concomitant with ICAM1 accumulation to the MDM-side of the interface (**Fig. 4.2c**). Generally, this demonstrates that hallmark IS

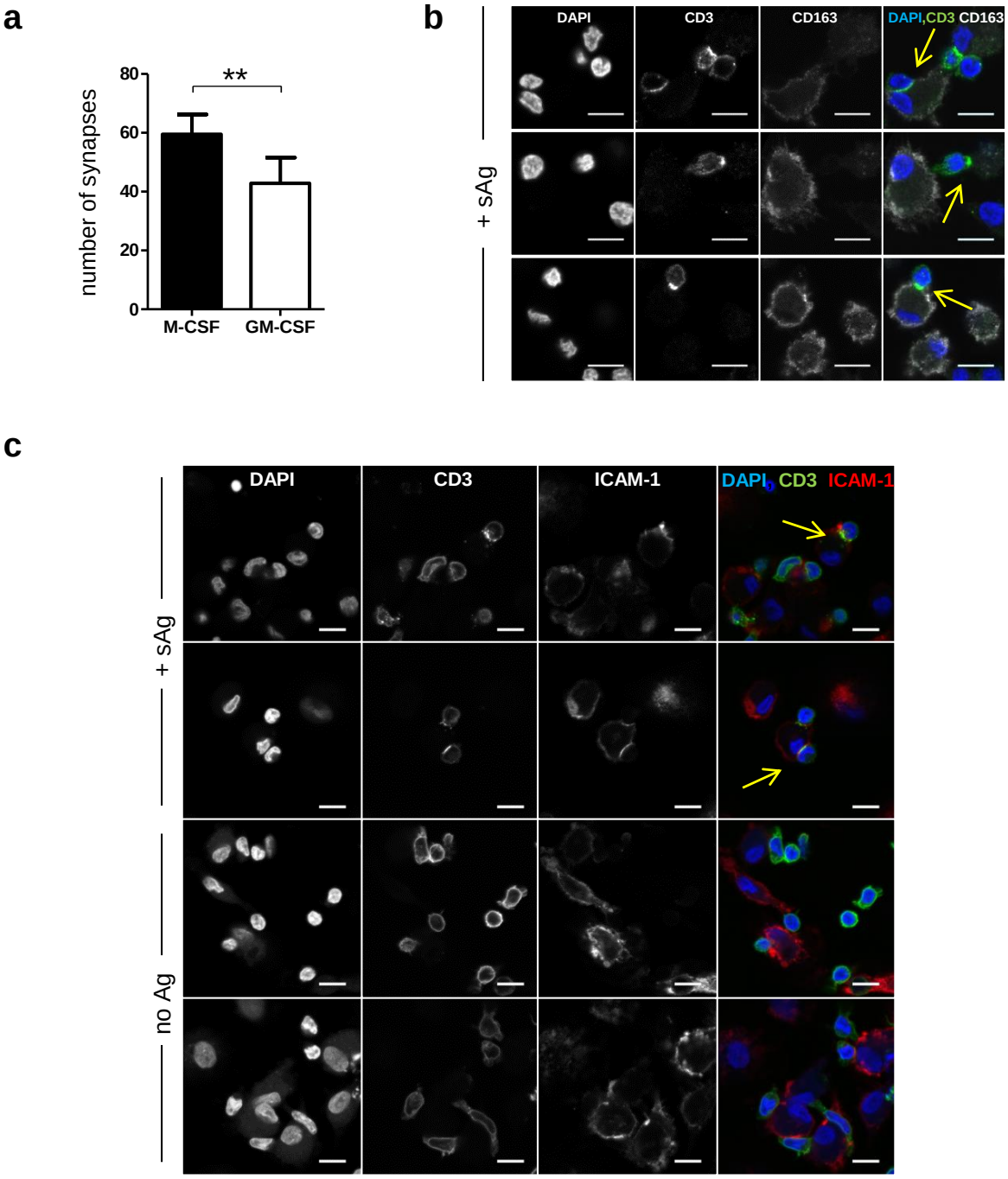

Figure 4.2: Hallmarks of IS formation between CD4+ T cells and M-CSF conditioned MDMs. (**a**) MDMs were cultured with M-CSF or GM-CSF/LPS/IFNγ as described in section 2.2.1 and seeded onto coverslips on day 7 at 2 x 10^5 cell/coverslip. After a further 72 h in culture MDMs pulsed with sAg cocktail for 2 h and coincubated with autologous CD4+ T cells for 30 min. Conjugates were immediately fixed and immunolabelled for CD3 (UCHT1) followed by GAM^{488} secondary antibody, stained with DAPI and imaged by fluorescence microscopy. Bar chart shows the number of synapses (according to CD3 capping), counted in 30 fields of view for six coverslips from two donors, formed between CD4+ T cells and either M-CSF or GM-CSF conditioned MDMs (mean ± SD). (**b**) Representative images (20 images, n = 2) of CD3-capping with CD163+ MDMs. Conjugates were formed between sAg pulsed M-CSF-cultured MDM and CD4+ T cells, fixed and immunolabelled for CD3 (OKT3) and CD163 followed by GAM-IgG1^{488} and GAM-IgG2a^{647} secondary antibodies. (**c**) Images showing sAg-pulsed or unpulsed MDM-CD4+ T cell immunolabelled for CD3 (UCHT1) and ICAM1 as described for (b). Yellow arrows indicates IS formation according to CD3 capping. Scale bars, 10 µm

markers such as CD3 and ICAM1 accumulate to the interface, in line with other types of synapse, and that synapse formation is not constrained by the M2 polarisation of MDMs.

4.2.2 MDM cell surface CCR5 distribution upon IS formation

To determine whether the distribution of endogenous CCR5 on the MDM PM changes upon IS formation, MDM-CD4+ T cell conjugates were formed, fixed and immunolabelled for CCR5 and CD3 according to the method detailed in section 2.11.2. No change in the cell-surface distribution of CCR5 (MC5) on MDMs was apparent upon IS-formation with CD4+ T cells when pulsed with sAg compared to unpulsed controls (**Fig. 4.3a**). The MDM membrane was traced to test whether a slight decrease, that is not detectable by eye, may occur in CCR5 levels at the IS (**Fig. 4.3b**). Using the trace, the median fluorescence value of CCR5 across the membrane was determined and then subtracted from every individual fluorescence intensity value in the trace. These values were plotted when the same trace detected regions of intensity in the CD3 channel, i.e. at the MDM-CD4+ T cell interface. Finally the distance across each MDM-CD4+ T cell interface was normalised to an arbitrary value of 100 to aid comparison. Still, no difference in the fluorescence intensity was detected at the interface between MDMs and CD4+ T cells either with or without sAg (**Fig. 4.3c**).

A recent study from our lab identified a functionally distinct pool of CCR5 on MDMs (Signoret lab, unpublished data). These receptors are specifically recognised by the mAb CTC5 and label discrete areas of the PM. We co-labelled MDM-CD4+ T cell conjugates with CTC5 and OKT3 and found that regions of CTC5 capping were not located opposite to CD3, but rather were apparent at the sides or opposite the position of IS formation (**Fig. 4.4**). Overall, the current evidence suggests that the distribution of CCR5 on the cell surface of MDMs is unaffected upon IS formation with CD4+ T cells.

4.2.3 Removal or inhibition of MDM cell surface CCR5 on IS formation

Despite the fact that MDM cell surface CCR5 is not accumulated to or excluded from the MDM-CD4+ T cell IS, we examined whether MDM cell surface CCR5 may play any other essential role in IS formation. Ligand-induced downmodulation is a well-characterised mechanism of chemokine receptor regulation, particularly with regard to CCR5 (Mack et al., 1998; Signoret et al., 2004; Signoret et al., 2005; Signoret et al., 2000; Signoret et al., 1998). The reduction in cell surface expression of CCR5 upon pulsing cells with native ligands, such as CCL5, is only transient. However synthetically modified forms of CCL5 induce a more robust and prolonged reduction in cell surface levels (Escola et al., 2010). Specifically, PSC-RANTES has a more durable association with CCR5 and treatment with this N-terminally modified form of CCL5 results in long-term sequestration in the TGN,

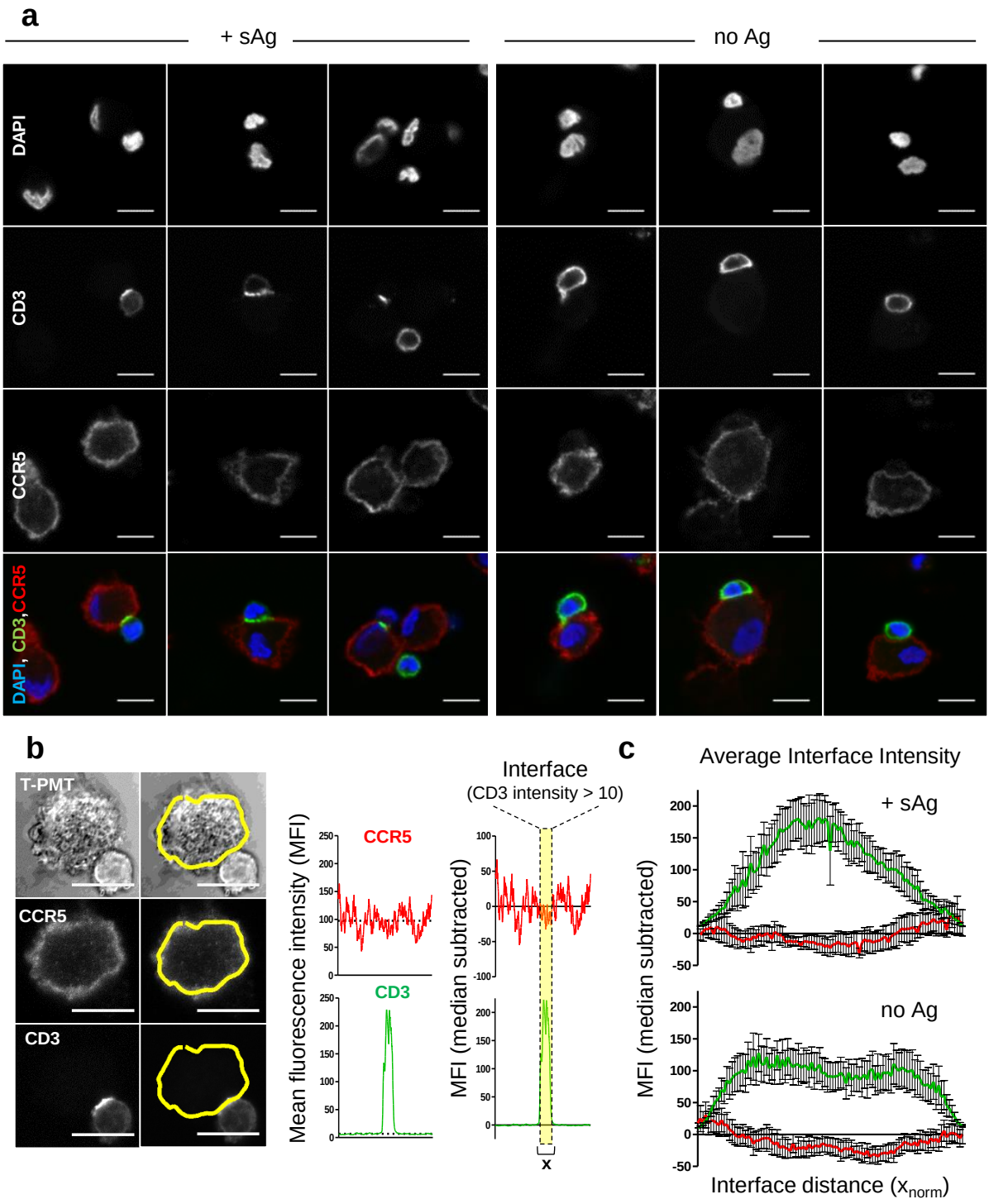

Figure 4.3: MDM CCR5 does not cap opposite CD3. (**a**) Representative images of MDMs pulsed +/- sAg and incubated with 1:2 with autologous CD4+ T cells (30 min), fixed then immunolabelled for **CCR5** (MC5) and **CD3** (UCHT1) followed by GAM-IgG1^{488} and GAM-IgG2a^{647}. (**b**) Diagram illustrating how MDM cell surface fluorescence at the is quantified at the interface. Yellow line shows an example of the 10 px wide line drawn around the MDM PM over which the fluorescence intensities of CD3 and CCR5 are measured (middle plots). The median value (black dotted line) for CD3 and CCR5 intensities is calculated and subtracted (right plots). The interface is designated as the intensity at which median-subtracted CD3 fluorescence exceeds 10 (yellow box). The original line distance spanned by this box (**x**) is normalised across a range of 0-100 and designated the interface distance (**c**) Average trace of CD3 and CCR5 intensity, subtracted for median MDM cell surface fluorescence value, at the MDM-CD4+ T cell interface (mean ± 95% CI for 15 conjugates) formed +/- sAg. Scale bars, 10 µm.

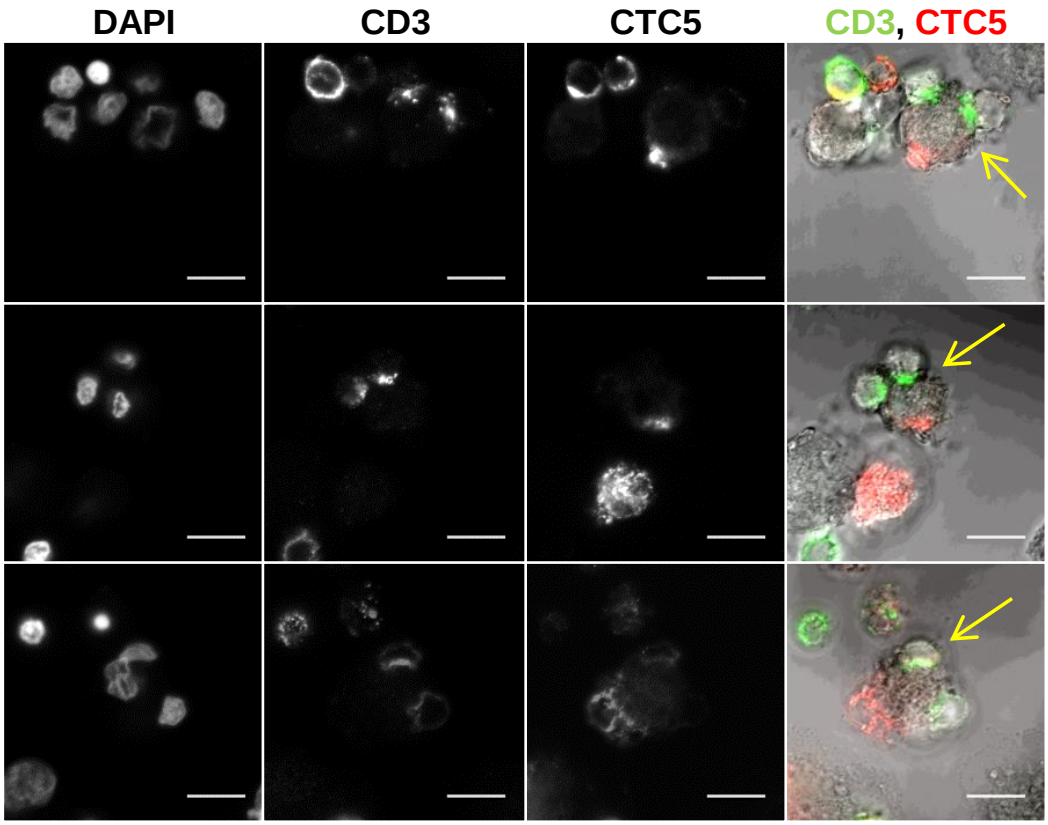

Figure 4.4: The CTC5-bound form of CCR5 does not localise to the MDM-CD4+ T cell IS. MDMs were pulsed with sAg then coincubated with autologous CD4+ T cells (30 min), fixed and immunolabelled for **CD3 (OKT3)** and **CCR5 (CTC5)** followed by GAM-IgG1^{488} and GAM-IgG2a^{647} secondary antibodies. Images are representative of 2 donors. Yellow arrow indicates IS formation. Scale bar, 10 µm

even after inhibition of PM CCR5 signalling (Escola et al., 2010). In addition, overnight-treatment of MDMs with PSC-RANTES was found to reduce cell surface CCR5 levels by more than 90% when labelling with MC5 (Signoret lab, unpublished data). Thus, MDMs on glass coverslips were treated with 100 nM PSC-RANTES or in media alone for 16 h. These MDMs were pulsed with sAg and then co-incubated with CD4+ T cells, fixed and immunofluorescently labelled for CCR5 (MC5) and CD3 (UCHT1), as detailed in section 4.2.2. MDMs on control coverslips, to which CD4+ T cells were not added, showed vastly-depleted CCR5 cell surface levels after treatment with PSC-RANTES compared to treatment with media alone (**Fig. 4.5a; left panels**). Note that PSC-RANTES was washed away 2.5 h prior to fixation, thus the continued absence of CCR5 at the cell surface corroborates evidence that downmodulation with PSC-RANTES results in long-term intracellular sequestration of CCR5 (Escola et al., 2010). Nevertheless, IS formation was observed despite CCR5 depletion from the MDM cell surface (**Fig. 4.5a**). This indicates that the presence of CCR5 on the MDM cell surface is not essential for MDM-CD4+ T cell IS formation.

In an alternative approach MDMs were treated with TAK-779, a small, non-peptide inhibitor of chemokine binding and downstream signalling of CCR5 (Baba et al., 1999). MDMs were incubated with 400 nM TAK-779 or media for 1 h in the course of pulsing with sAg. MDMs-CD4+ T cell conjugates were formed, fixed and immunolabelled as detailed for PSC-RANTES treated cells. Despite TAK-779 treatment CD4+ T cells demonstrated capping of CD3 to the MDM-CD4+T cell interface, indicative of IS formation (**Fig. 4.5b**). This indicates that signalling downstream of MDM cell surface CCR5 is not required for MDM-CD4+ T cell IS formation.

4.2.4 CXCR4 at the CD4+ T cell side of the IS

When overexpressed, CXCR4-GFP has been demonstrated to accumulate on the CD4+ T cell side of the B cell- CD4+ T cell IS (Contento et al., 2008). Since the majority of PHA/ IL-2 activated T cells express cell surface CXCR4 (Bleul et al., 1997), we decided to determine whether endogenous CXCR4 might localise to the T cell side of the MDM-CD4+ T cell IS. IS formation and immunolabelling of intact cells was performed as described in section 2.11.2, but using primary antibodies raised against CXCR4 (12G5) and CD3 (UCHT1). Representative images show that in sAg-pulsed MDM-CD4+ T cell conjugates forming the IS, endogenous CD4+ T cell CXCR4 can become enriched at the cell-cell interface (**Fig. 4.6a**). Furthermore, the images illustrate that little or no CXCR4 was detectable on any MDMs, therefore this enrichment is unlikely to be an artefact of fluorescence from the macrophage cell side of the IS.

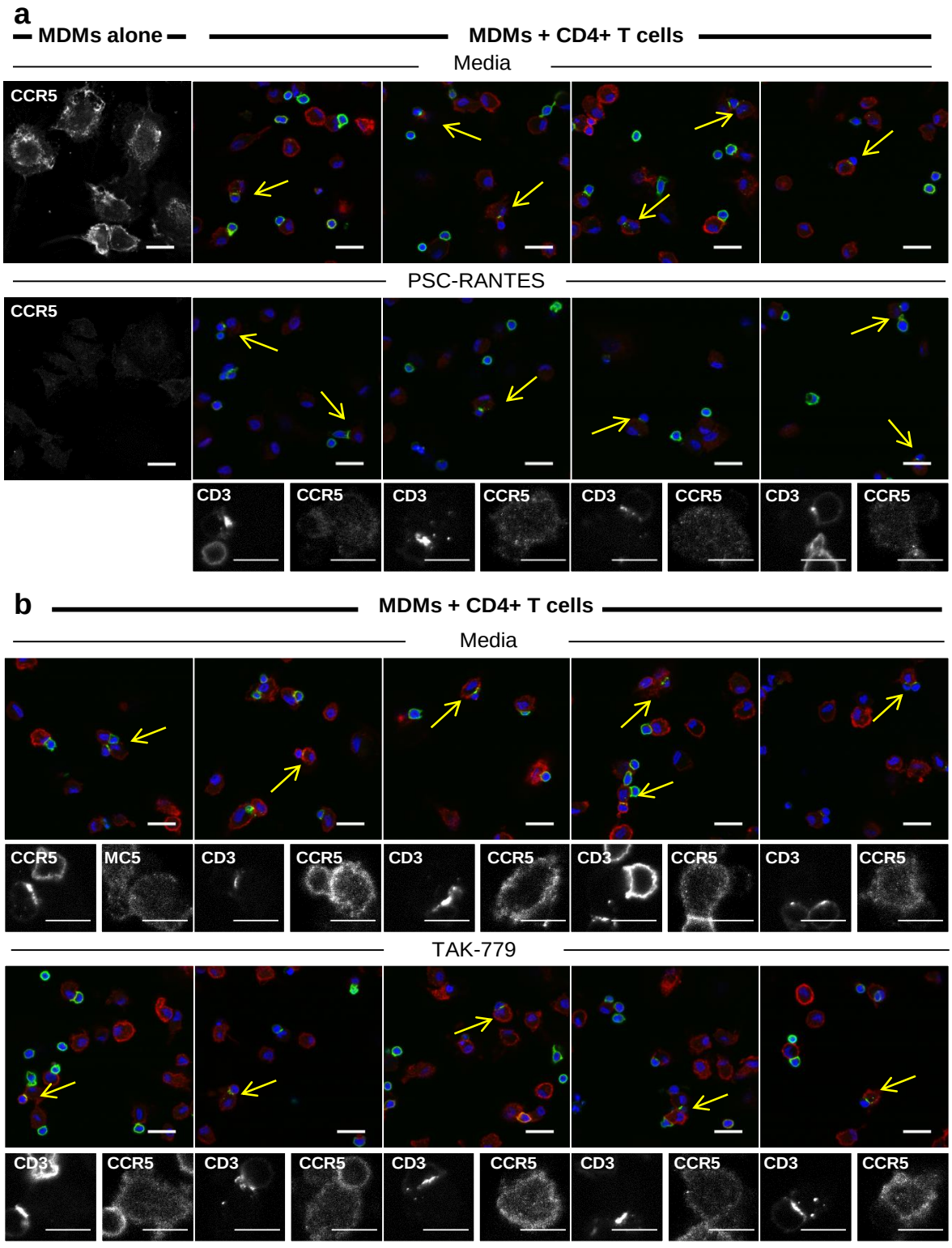

Figure 4.5: Decreasing or antagonising MDM cell surface CCR5 does not prevent IS formation. (**a**) MDMs were treated with 100nM PSC-RANTES or media alone for 16 h before pulsing with sAg and coincubating with autologous CD4+ T cells. During pulsing and coincubation MDMs only (left panels) were kept in media. All samples were immediately fixed and immunolabelled for CD3 (UCHT1) and CCR5 (MC5) according to the method detailed in section 2.11.2. (**b**) MDMs were pulsed with sAg and either 400 nM TAK-779 or media alone for the final 60 min of incubation. MDMs were coincubated with autologous CD4+ T cells, fixed and immunolabelled as described in (a). Coloured fields of view show merged CD3, CCR5 and DAPI fluorescence representative of two donors. Scale bar, 20 µm. Single channel images, zoomed on a region of IS formation in the merged image above, are also shown Scale bar, 10 µm. Yellow arrow indicates IS formation.

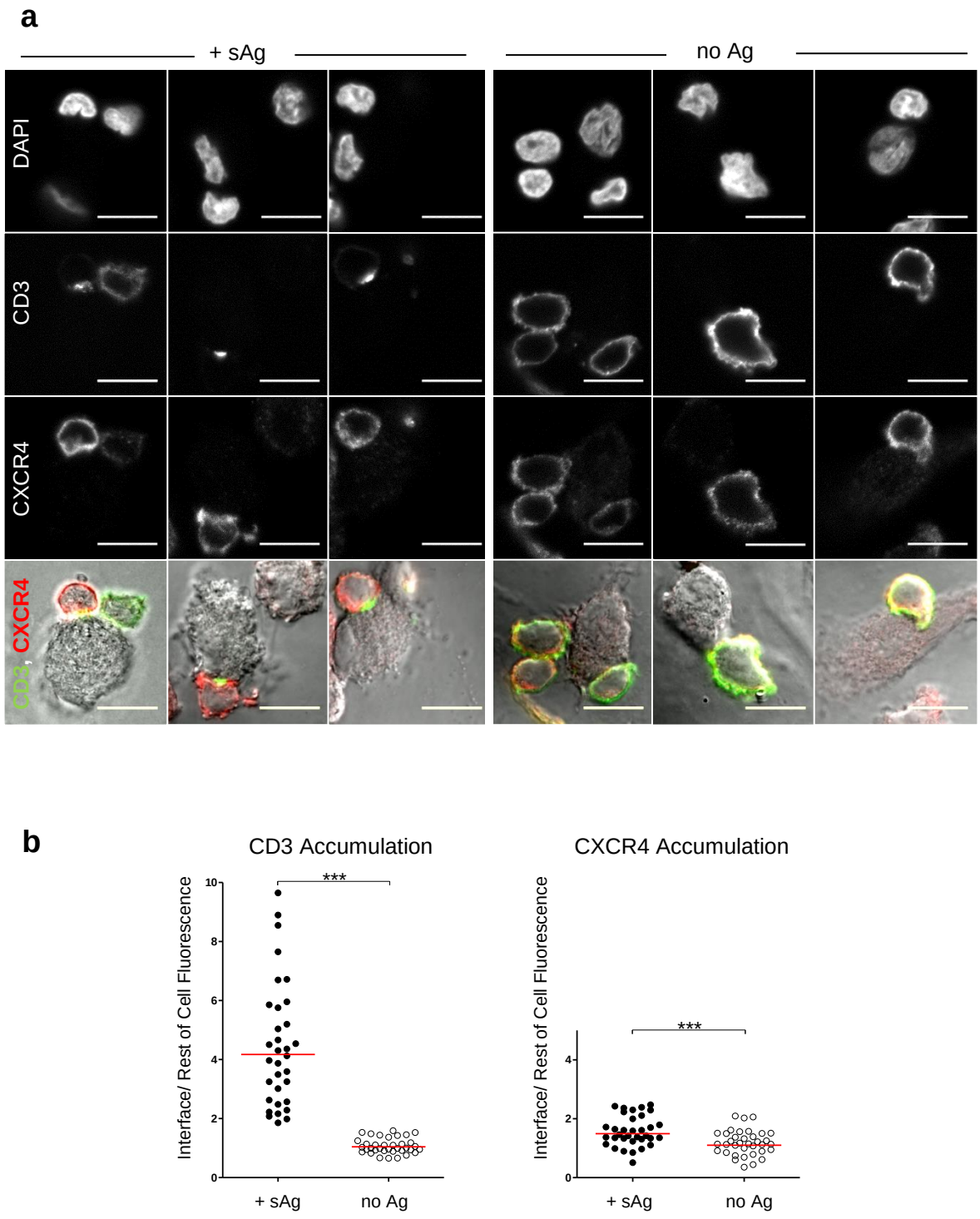

Figure 4.6: CXCR4 accumulation to the MDM-CD4+ T cell IS. (**a**) Conjugates were formed between CD4+ T cells and sAg-pulsed or unpulsed MDMs for 30 min, fixed and then immunolabelled for CXCR4 and CD3 followed by isotype specific secondary fluorophores. Representative images of CXCR4 accumulation at the interface between MDMs and T cells are presented. Scale bar, 10 µm. (**b**) Graphs show fluorescence quantification of the T cell membrane as described in section 4.2.1.1. Each symbol represents an individual T cell from a total of 2 donors when interacting with MDMs had been pulsed with (+sAg: 34 cells) or without sAg (no Ag: 36 cells). Red line geometric MFI. ***, P< 0.001 (Student's unpaired t-test). Cells with accumulation > 2 SD above the mean no Ag fluorescence value (2.02), sAg = 24%, noAg = 8%.

In order to compare the level of CXCR4 and CD3 accumulation at the IS relative to conjugates formed in the absence of antigen the ratio of fluorescence at the interface compared to the rest of the T cell was calculated, as described in section 4.2.1 (**Fig. 4.1b**). Results show that the mean accumulation of CD3 at the cell-cell interface is over four-fold greater in the presence of sAg-pulsed MDMs compared to unpulsed controls (4.8 ± 2.7 and 1.1 ± 0.3, respectively). In contrast, the mean enrichment of CXCR4 at the IS is less than two-fold of that observed in the absence of antigen (1.6 ± 0.5 and 1.2 ± 0.4, respectively) (**Fig. 4.6b**). Thus, although both CD3 and CXCR4 show significantly greater accumulation on CD4+ T cells upon IS formation compared to conjugates formed in the absence of antigen, the accumulation of CXCR4 to the interface is more modest (**Fig. 4.6a & b**). Additionally, the no antigen control interface ratio mean plus two SDs was used as a value to designate greater-than-normal accumulation of either CXCR4 or CD3 to the conjugate interface. Values calculated in this way are referred to as 'cut-off' values throughout the rest of this study.

The percentage of T cells showing CXCR4 accumulation above the cut-off value was 24% in the presence of sAg, compared to 8% of cells in the absence of antigen. In contrast, 100% of cells lie above the cut-off value for CD3. Thus only a quarter of T cells show levels of CXCR4 accumulation at the interface that are greater than those observed in conjugates forming in the absence of IS formation. Moreover, the level of CXCR4 that accumulates at the IS is only marginal in comparison to CD3.

4.2.5 CCR5 at the CD4+ T cell side of the IS

4.2.5.1 Accumulation of CD4+ T cell surface CCR5

Since CXCR4 accumulation has been reported to be directed by CCR5 on the CD4+ T cell side of the B cell-CD4+ T cell IS (Contento et al., 2008), we also investigated whether CCR5 may accumulate on the T cell side of the MDM-CD4+ T cell IS. In section 4.2.2, fixed MDM-CD4+ T cell conjugates were immunolabelled for CCR5 and CD3 to examine the MDM side of the IS; however, the role of CCR5 on the T cell side may have been overlooked. This is due to the low percentage T cells per coverslip that demonstrate CD3 capping combined with the fact that only 12 ± 9 % of PHA/IL-2 activated CD4+ T cells are CCR5+ (**Fig. 3.6**). Thus the chances of observing synapse formation involving a CCR5+ T cell are very low. Nevertheless, fixed MDM-CD4+ T cell conjugates were immunolabelled intact with CCR5 and CD3, as described in section 4.2.2. Conjugates involving CD4+ T cells expressing CCR5 were imaged by confocal microscopy. Representative images indicate that CD4+ T cell CCR5 accumulation can occur alongside CD3 capping at the IS,

although often very little, if any, enrichment of CCR5 at the MDM-CD4+ T cell interface is observed (**Fig. 4.7a**).

Even though MDMs express cell surface CCR5, no change in the levels of MDM CCR5 at the MDM-CD4+ T cell interface was detected compared to conjugates formed in the absence of antigen (**Fig. 4.2**). Based upon this evidence, any enrichment of CCR5 detected at synapses formed between MDMs and CCR5+ CD4+ T cells can be expected to be due to the T cell. Furthermore, by using the interface: rest of T cell ratio (as used for CXCR4 fluorescence quantification in section 4.2.4) contributions of MDM CCR5 can be controlled for by comparing accumulation at the IS to conjugates formed between CCR5+ CD4+ T cells and unpulsed MDMs. The ratio of CCR5 enrichment at the interface of MDM-CD4+ T cells forming synapses is significantly greater than that of conjugates formed in the absence of antigen (**Fig. 4.7b**). In similarity to CXCR4, the mean accumulation ratio of CD4+ T cell CCR5 in synapses is less than two-fold that of conjugates formed in the absence of antigen (1.7 ± 0.8 and 1.1 ± 0.3, respectively). Again, CCR5 accumulation is modest in comparison to CD3, which showed five-fold greater levels at the IS than in conjugates formed in the absence of antigen (5.2 ± 2.3 and 0.9 ± 0.3, respectively). Interestingly, 48% of CD4+ T cells engaged in synapses, versus 4% CD4+ T cells in conjugates formed in the absence of antigen, showed a level of CCR5 enrichment above the no antigen CCR5 cut-off value. Overall this shows that endogenous T cell CCR5 can be accumulated to the MDM-CD4+ T cell IS, corroborating GFP-CCR5 accumulation observed in other synapses (Contento et al., 2008; Molon et al., 2005). However as only half of the CCR5+ T cells showed CCR5 accumulation at the IS, there is an indication that certain synapses formed within the heterogeneous population of primary cells possess the features required for CCR5 accumulation, whilst others do not.

4.2.5.2 Localisation of CCR5 on permeabilised CD4+ T cells

To begin to determine whether cell surface CCR5 localisation at the IS may be regulated by internalisation at the interface, the presence and localisation of intracellular CCR5 in CD4+ T cells forming synapses was investigated. MDM-CD4+ T cell conjugates were fixed, permeabilised and immunolabelled for CD3 (UCHT1) and CCR5 (MC5) according to the method detailed in section 2.11.3. Images show accumulations of CCR5 on the CD4+ T cell side of the IS for conjugates formed with both sAg-pulsed and unpulsed MDMs (**Fig. 4.8a**). Thus CD4+ T cells appear to have intracellular accumulations of CCR5, only accessible upon permeabilisation, which localise to the cell-cell interface irrespective of IS formation. The interface ratio approach, used above to quantify CD3, CCR5 and CXCR4 accumulation to the IS, is not appropriate here as the 10 px lines drawn around the membrane will not include the intracellular fluorescence. For this reason an alternative

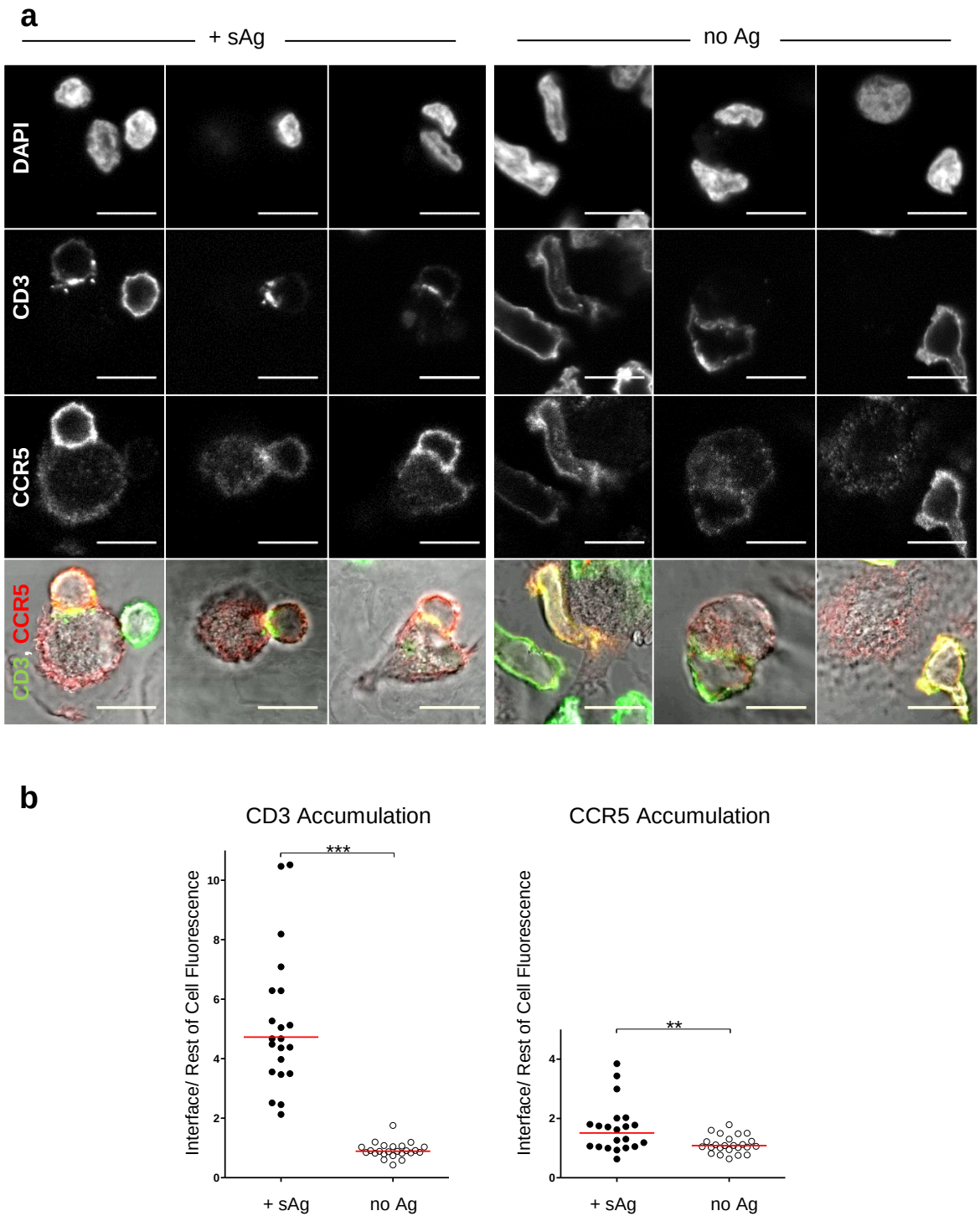

Figure 4.7: CCR5 accumulation to the MDM-CD4+ T cell IS for cells immunolabelled when intact. (**a**) Conjugates were formed between CD4+ T cells and sAg-pulsed or unpulsed MDMs for 30 min, fixed and then immunolabelled for CCR5 and CD3 followed by isotype specific secondary fluorophores as detailed in section 2.11.2. Representative images of CCR5 accumulation at the interface between MDMs and T cells are presented. Scale bar, 10 µm. (**b**) Graphs show fluorescence quantification of the T cell membrane, as described in section 4.2.1.1, of CCR5/CD3 labelled MDM-CD4+ T cell conjugates. Each symbol represents an individual T cell from a total of 2 donors when interacting with MDMs had been pulsed with (+sAg: 21 cells) or without sAg (no Ag: 24 cells). Red line shows geometric mean. **, P<0.01; ***, P<0.001 (Student's unpaired t-test). Cells with accumulation > 2 SD above the mean no Ag fluorescence value (1.70), sAg = 48%, noAg = 4%.

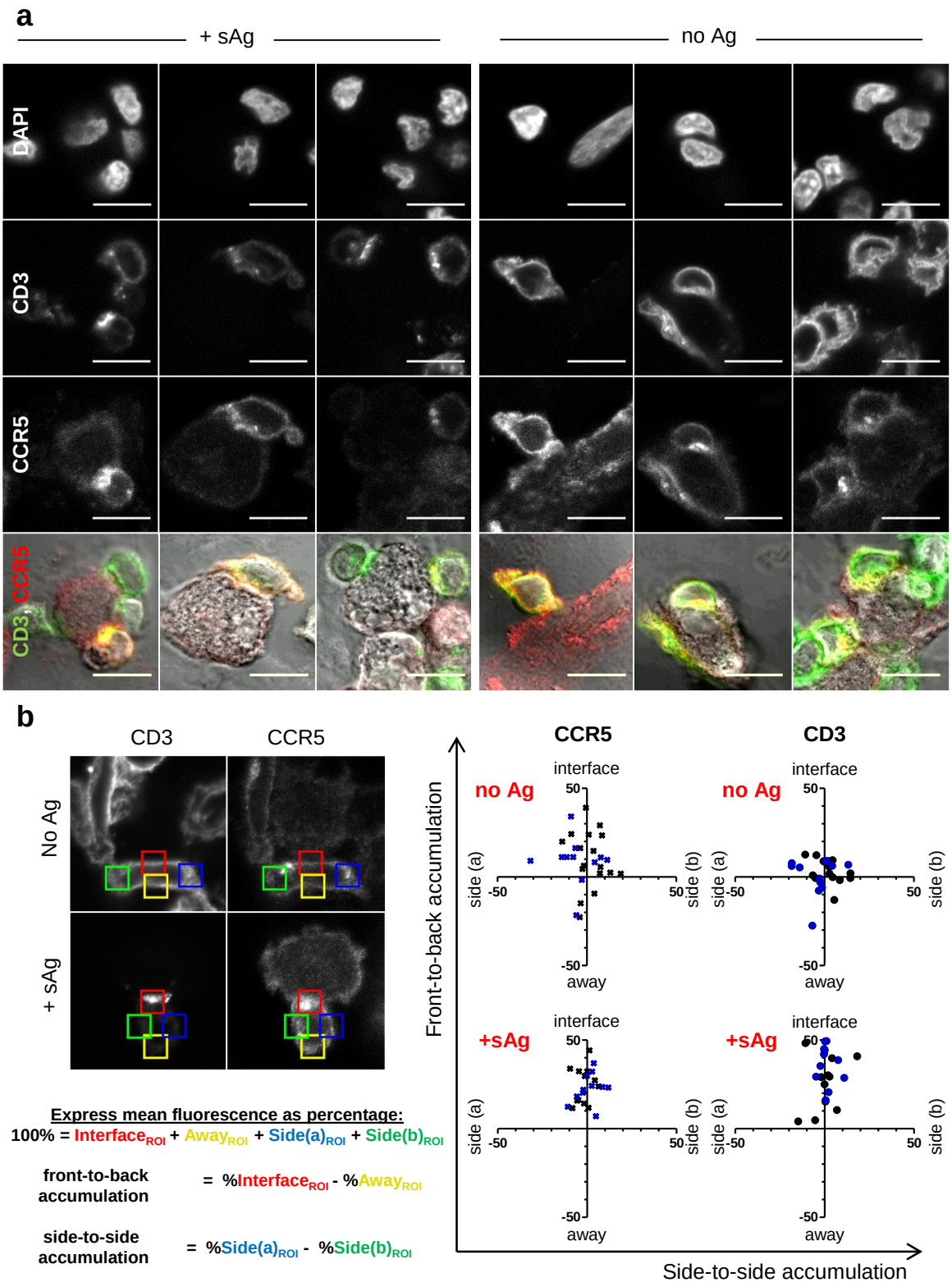

Figure 4.8: CCR5 accumulation to the MDM-CD4+ T cell IS for cells immunolabelled when permeablised. (**a**) Conjugates were formed between CD4+ T cells and sAg-pulsed or unpulsed MDMs for 30 min, fixed, permeabilised and then immunolabelled for CCR5 and CD3 followed by isotype specific secondary fluorophores as detailed in section 2.11.3. Representative images of CCR5 accumulation at the interface between MDMs and T cells from 2 donors. (**b**) Example of ROIs drawn and calculations involved in the quantification process, accompanying description in section 4.2.5.2. Graphs show the polarisation of CCR5 (crosses) or CD3 (filled circles) observed in each T cell analysed in conjugates formed with (n=23) or without (n=28) sAg from **D2013006** and **D2013007** using this fluorescence quantification method.

quantification method was adopted using four 50x50 px ROIs positioned on the T cell: one at the interface, one on the opposite side of the interface termed ‘away’, and one on either side of the interacting T cell termed ‘side (a)’ and ‘side (b)’ (**Fig. 4.8b**). The ROIs span some of the intracellular space enabling both internal and membrane fluorescence to be measured. Each ROI is expressed as a percentage of the total fluorescence of all four ROIs. Subsequently, by subtracting the percentage of fluorescence in the ‘away’ ROI from the ‘interface’ ROI a measure of front-to-back CCR5 polarity is obtained. Similarly, a measure of side-to-side CCR5 polarity is gained by subtracting the percentage of fluorescence of ‘side (b)’ from ‘side (a)’ (**Fig. 4.8b**). For each T cell the side-to-side and front-to-back polarity values can be plotted as x and y values giving a graphical representation of CCR5 distribution compiled for each cell measured. Such an approach is effective because in the absence of antigen, CD3 can be seen to be distributed about the axis intersection but upon addition of sAg the cells show polarity of CD3 towards the direction of the interface, as expected (**Fig. 4.8b**). The same CD4+ T cells also show increased CCR5 polarity towards the interface when engaged with sAg-pulsed compared to unpulsed MDMs. Indeed CCR5 front-to-back polarity for CD4+ T cells conjugated with sAg-pulsed MDMs was significantly greater compared to conjugates formed with unpulsed MDM ($P<0.001$; t-test with Welch’s correction). Further, after all plus or minus signs had been removed from the data (as designation of side (a) or (b) ROIs was arbitrary) CCR5 side-to-side polarity in CD4+ T cells engaged with sAg-pulsed MDMs was found to be significantly less than in conjugates formed with unpulsed MDMs ($P<0.05$; Mann-Whitney U-test). This demonstrates that CCR5 becomes more equally distributed across either side of the cell upon IS formation. Together these results indicate that CCR5, both intracellular and cell surface, accumulates towards the centre of the MDM-CD4+ T cell interface upon IS formation. Notice that the +sAg CCR5 graph indicates that in the presence of sAg-pulsed MDMs all measured cells show a degree of polarisation towards the interface. Yet this measure of polarity is partially due to fluorescence from the MDM, which is also labelled with CCR5. Additionally, not all CCR5 should be thought of as actively polarising to the interface upon IS formation. This is evident as in the absence of antigen a number of CD4+ T cells already show CCR5 polarised towards the interface rather than being more evenly distributed and surrounding the axis origin, as is the case for CD3 (**Fig. 4.8b**). In general, intracellular CCR5 can be observed at the cell-cell interface in the absence of IS formation, however far more cells demonstrate CCR5 polarisation to the cell-cell interface after IS formation. Thus the ability to visualise intracellular CCR5 can contribute to whether or not CCR5 accumulation is observed on the T cell side of the MDM-CD4+ T cell IS.

5.2.6 Colocalisation of intracellular CCR5 with TGN and TfR

It remains unclear whether accumulation of CCR5 is truly internal or whether cell surface epitopes, otherwise inaccessible to antibody, are revealed by permeabilisation. To investigate this, MDM-CD4+ T cell conjugates were colabelled with CCR5 (MC5) and a marker directed against an integral membrane protein of the TGN (TGN46), according to the method detailed in section 2.11.3. Z-stacks of sAg-pulsed or unpulsed conjugates were acquired. Confocal sections zoomed on the region of CD4+ T cell TGN staining showed that TGN46 partially colocalised with CCR5 in conjugates formed in both the presence and absence of sAg (**Fig. 4.9.1a**). This suggests that the CCR5 revealed by permeabilisation is at least partly intracellular.

In an effort to investigate whether the increased CCR5 accumulation at the MDM-CD4+ T cell interface formed with sAg-pulsed MDMs may be caused by alterations in trafficking of CCR5 conjugates were immunolabelled for TfR and CCR5. TfR is a marker for clathrin mediated endocytosis and the RE route that is followed by CCR5 during ligand-induced internalisation (Signoret et al., 2005). Speculatively, CCR5 may show a higher level of overlap with TfR if the rate of internalisation is increased at the IS. Yet, no change in the colocalisation of CCR5 with TfR was evident in conjugates formed in the presence of sAg (**Fig. 4.9.1b**). CCR5 colocalisation with TfR appeared to be less widespread than with the TGN. Overall, this suggests that the increase in CCR5 fluorescence at the IS when permeabilised is not caused by increased trafficking to the RE compartment. Thus it remains unclear as to whether the localisation of CCR5 in permeabilised cells at the IS is due to active internalisation of CCR5 at the IS or passive redistribution of intracellular pools of CCR5. In relation to the latter point, immunolabelling of sAg-pulsed and unpulsed MDM-CD4+ T cell conjugates for both GM130 and CD3 was carried out and z-stacks were acquired. Whilst no global change in the distribution of the MDM Golgi was observed, the T cell Golgi accumulated to the cell-cell interface preferentially in IS-forming conjugates (**Fig. 4.9.2**). Localisation of T cell Golgi to the IS is well-documented and results from association of the Golgi with the MTOC via motor protein attachments (Griffiths et al., 2010). Since a fraction of internal CCR5 appears to be colocalised with the TGN in both the presence and absence of sAg, Golgi polarisation to the IS is likely to contribute to CCR5 enrichment at the IS.

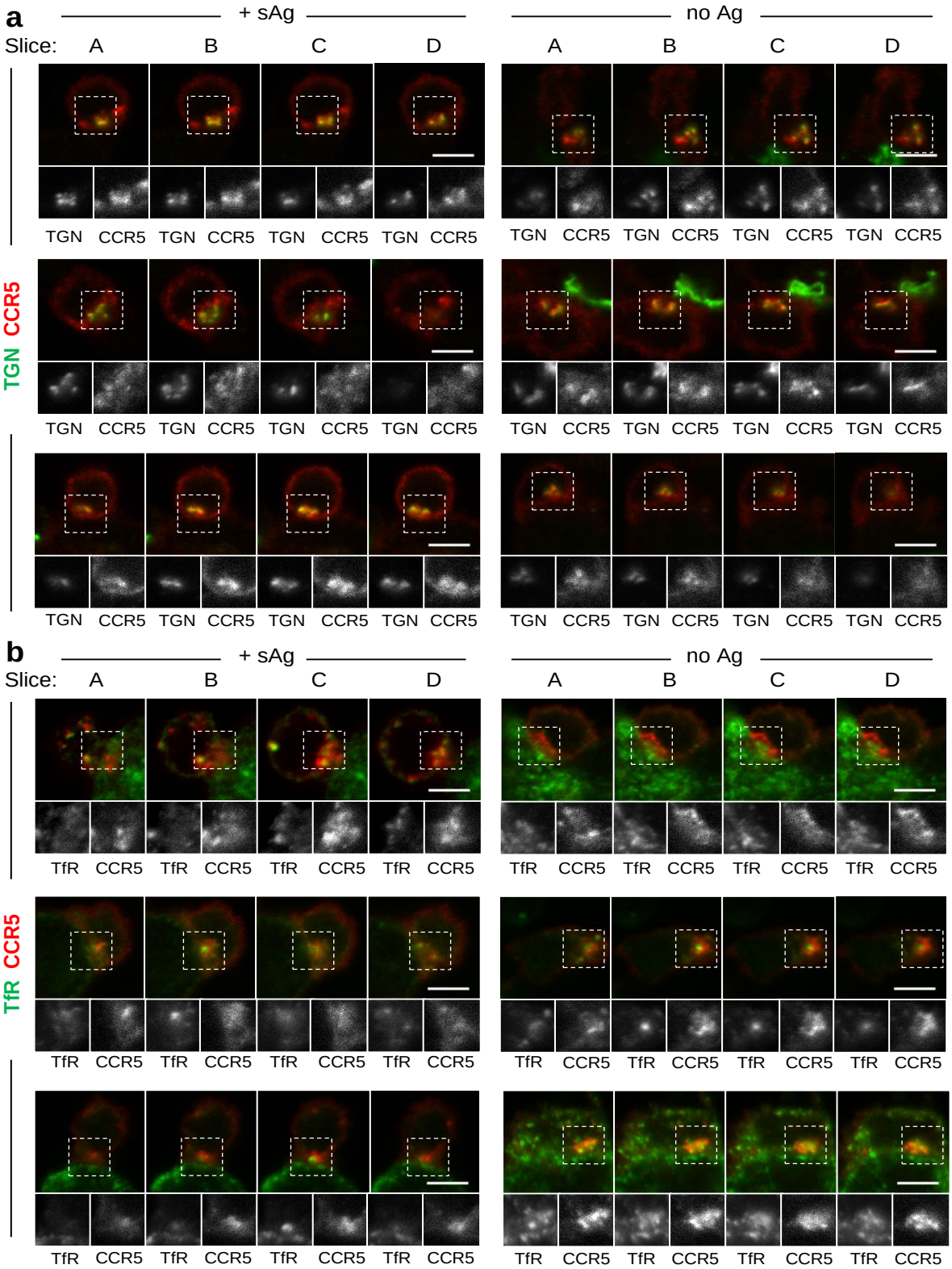

Figure 4.9.1: Colocalisation of TGN or TfR with CCR5. MDM-CD4+ T cell conjugates were formed, fixed and immunolablelled for (**a**) TGN and CCR5 followed by anti-sheep^{488} and GAM-IgG2a^{647} or (**b**) TfR and CCR5 followed by GAM-IgG1^{488} and GAM-IgG2a^{647} secondary antibodies according to the method detailed in section 2.11.3. Three examples of CCR5+ conjugates formed +/- sAg are shown, which are representative of z-stacks acquired from two or three donors. For each example individual slices of the z-stack are shown over the region of CCR5 intracellular accumulation at the MDM-CD4+ T cell interface. Within these slices the dotted box indicates the region where TGN or TfR and CCR5 are shown as separate greyscale images. Scale bar, 5 µm.

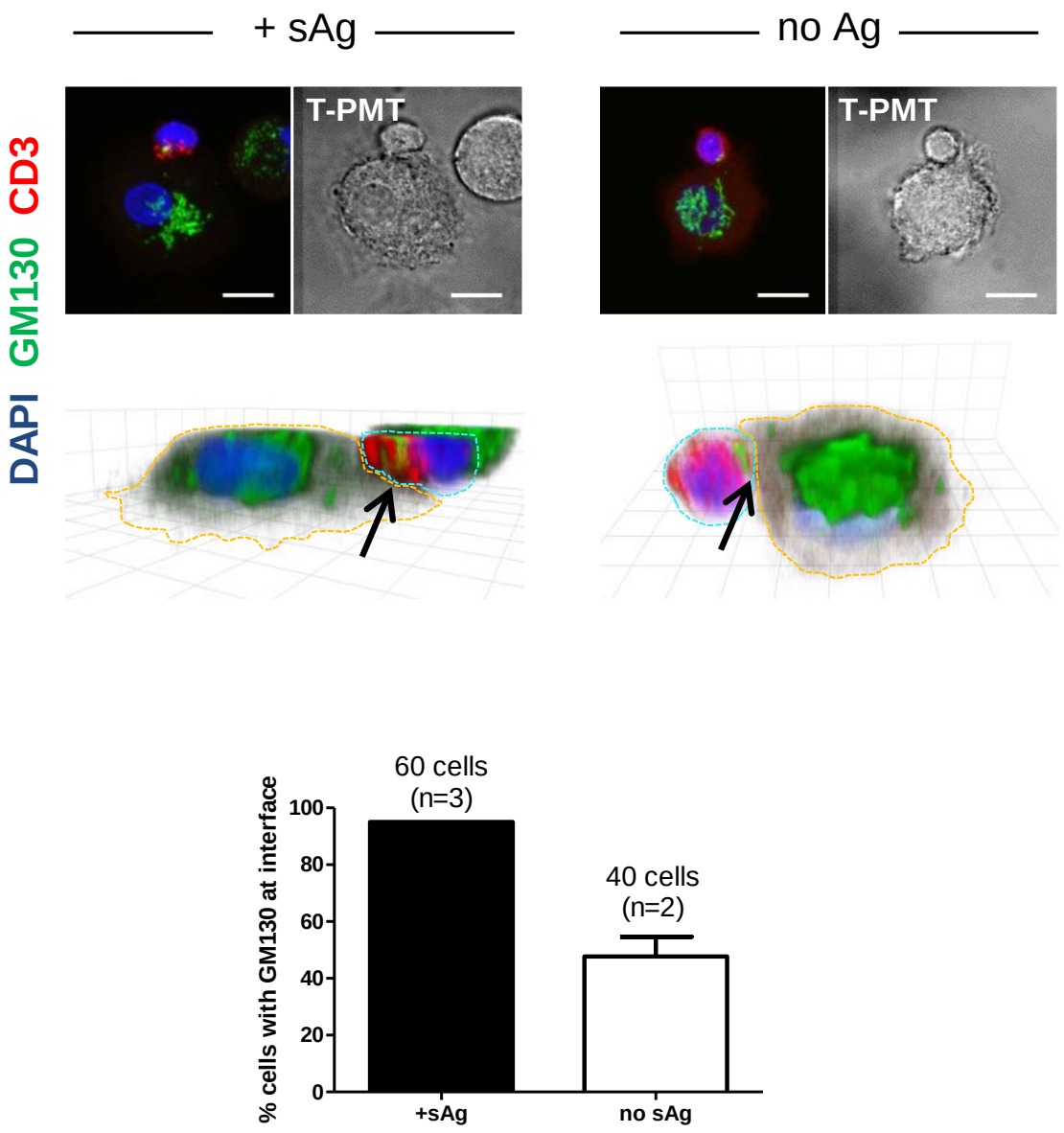

Figure 4.9.2: The Golgi redistributes to the T cell side of the MDM-CD4+ T cell IS. Conjugates were formed between CD4+ T cells and sAg-pulsed or unpulsed MDMs for 30 min prior to fixation and indirect immunolabelling for Golgi (GM130) and CD3 (OKT3) followed by GAM-IgG1^{488} and GAM-IgG2a^{647} according to the method described in section 2.11.3. Confocal Z-stacks were acquired to judge the position of the Golgi at the cell-cell interface. Images show max. intensity projections and a brightfield slice from the stack. 3D reconstructions were used to determine the region of cell-cell contact. Yellow and cyan dotted outline indicate the extent of MDM and T cell volumes, respectively. Black arrow indicates the position of the interface. The bar chart indicates the percentage of MDM-CD4+ T cell conjugates to which the Golgi localises to the cell-cell interface in the presence or absence of sAg (mean ± SD). Scale bar, 10 µm.

4.3 Discussion

4.3.1 Implications of defining IS formation by CD3 capping

CD3 accumulation to the interface was found to be significantly greater when calcium signalling was high (**Fig. 4.1**). This corroborates the concept that the higher, more sustained calcium profiles of CD4+ T cells engaging sAg-pulsed compared to unpulsed MDMs (section 3) are associated with spatial reorganization of TCR-CD3 to the cell-cell interface, a hallmark of IS formation (Monks et al., 1998). Yet observe that some of the 'low' calcium profiles also accumulate CD3 (IS formation) whilst others do not, which may indicate kinapse formation. This highlights that in using CD3 capping as a selection criterion, certain other antigen-dependent conjugates become excluded from the analysis.

The link between CD3 capping and calcium signalling was expected, due to the link between calcium signalling regulation and IS formation (Kummerow et al., 2009) In addition, correlation between CD3-capping and calcium flux has previously been used to demonstrate IS formation (Revy et al., 2001). In the present study, the correlative assay confirmed that capping of CD3 to the cell-cell interface is an appropriate marker to identify fixed MDM-CD4+ T cell conjugates forming synapses. This was an essential step in order to be able to select for the rare events of IS formation within the plethora of cell-cell interactions, so that the localisation of chemokine receptors and other proteins could be investigated. Moreover, bilayer studies have demonstrated that the central accumulation of CD3 at the IS interface begins only several minutes after initial calcium flux and remains present for 30-60 min (Yokosuka et al., 2005). Thus, although the duration of cell-cell contact may differ in the present study, selecting synapses by the presence of CD3 at the interface encompasses both nascent and longstanding synapses. However this may have implications for the frequency of cells in which CCR5 or CXCR4 are found to be present at the IS opposite to CD3, as CCR5 and CXCR4 may be recruited to IS for a shorter duration than CD3. Such transient localisation has been observed for PKCα (Gharbi et al., 2013) and for CD4, which initially accumulates to the cSMAC but shortly becomes redistributed to the pSMAC (Krummel et al., 2000). Note, however that Molon et al. (2005) reported that in synapses formed between Jurkat cells and B cells or DCs, GFP-CCR5 remained localised at the interface for at least 30 min.

4.3.2 IS formation with M1/M2 polarised MDMs

In order to determine whether the capacity to form an IS is affected by polarising MDMs towards an M1 or M2 phenotype, synapses were formed with MDMs, which had been cultured in GM-CSF/LPS/IFNγ or M-CSF, respectively. A greater number of synapses

were formed with M2 compared to M1 polarised MDMs (**Fig. 4.2**). Initially, this result appears paradoxical as M1-polarised MDMs are associated with more efficient antigen presentation, as judged by apparently higher levels of CD80 in comparison to M2 MDMs, shown in section 3.2.2.2 (Biswas and Mantovani, 2010; Martinez et al., 2009). However, this difference may not affect the ability to form an IS. The absence of functional CD80 is neither essential for, nor reduces the frequency of synapse formation and would only affect the area and density of TCR-MHC accumulated to the interface (Choi and Schwartz, 2011; Wetzel et al., 2002). Additionally the difference in synapse number is not likely to be caused by an inability of sAg to bind to either M1 or M2 MDMs. This is because the M2 cells used here still express CD80, albeit at lower levels than the M1 cells, as well as MHC class II and so fulfil the requirements of sAgs in order to contact the full range of Vβ regions (Lando et al., 1996). Instead, perhaps the differences are caused by the relative abundance of different T cell phenotypes (e.g. Th1 and Th2 cells) within the population of PHA/IL-2 cells. M2 MDMs are known to preferentially secrete Th2-linked chemokines so a greater number of synapses may be formed if more T cells in the population express cognate chemokine receptors. However, apart from CCR5 the chemokine receptor expression profile of the CD4+ T cell population is unknown, as is the chemokine secretion pattern of the MDMs that are utilised in the present study.

4.3.3 Differential CCR5 accumulation to the IS

The MDM side of the IS is relatively unexplored in comparison to the T cell side. The accumulation of several APC markers to the IS is coordinated by their cognate receptors on the T cell, as evidenced by studies with planar bilayers (Grakoui et al., 1999). For this reason the accumulation of ICAM1 on the MDM side of the IS (**Fig. 4.2**) observed in the present study is thought to be nucleated by the engaged CD4+ T cell. Nevertheless this does not mean that the APC is passive in the synapse, as demonstrated by the fact that CD80 and the APC cytoskeleton may modulate the organisation of the IS (Friedl et al., 2005; Tseng et al., 2005). Moreover, some components that are localised to one side of the synapse are not necessarily reflected on the other. An example of this is the evidence presented in this chapter showing that CCR5 does not accumulate to the MDM side of the MDM-CD4+ T cell synapse (**Fig. 4.3**) but can accumulate to the T cell side (**Fig. 4.7**).

Previous research suggests that IS formation alone is not sufficient to prompt CCR5 accumulation to the interface, but another trigger is required (Contento et al., 2008; Franciszkiewicz et al., 2009; Molon et al., 2005). For CD4+ T cells engaged in synapses with DCs or B cells, this trigger has been suggested to exist in the form of cognate chemokines secreted by the APC (Molon et al., 2005). If CD4+ T cell CCR5 in the present study is indeed brought to the IS via a mechanism dependent upon APC secretion of

cognate chemokines, why is MDM CCR5 not also recruited to the interface? Two theories are evident: (i) MDMs secrete CCL3/4/5 uniformly so autocrine signalling does not induce CCR5 polarisation; (ii) CCR5 is not coupled to the same regulatory machinery on MDMs as in T cells.

The first theory is perhaps the simplest explanation. Although directional secretion of chemokine across the IS by T cells can occur (Catalfamo et al., 2004), directionality is often cell-type or activation-status specific (Huse et al., 2008). Multi-directional distribution of chemokine would aid recruitment of relevant T cells in a given microenvironment (Huse et al., 2008) and therefore may speculatively be the dominant secretion pattern for APCs. This means that MDM CCR5 would be exposed to an equal level of autocrine chemokine all around the cell. In contrast, the T cell would sense a gradient and migrate towards the APC, a mechanism which has been shown to polarise the cellular CCR5 distribution in other situations such as chemotaxis (Gomez-Mouton et al., 2004).

Regarding the latter theory, the susceptibility of distinct conformational forms of CCR5 to undergo ligand induced down-modulation has demonstrated the differential regulation of CCR5 between monocytes/MDMs and T cells (Signoret lab, unpublished data). Additionally, Moore and colleagues have identified conformations of CCR5 that are dependent upon the availability of cholesterol in order to signal (Berro et al., 2011). Also, CCR5 signalling via G proteins in specific microdomains is known to be stabilised by the presence of membrane cholesterol (Cardaba et al., 2008), which may be present at different quantities/distributions in T cells compared to MDMs. Indeed, differences are apparent even within the same cell type, evidenced by the fact that lipid rafts become enlarged and associate with more signalling components in activated compared to resting T cells (Tuosto et al., 2001). Taken together with the evidence that T cell CCR5 redistribution towards anti-CD4 coated beads is cholesterol dependent (Nguyen et al., 2005), accumulation of MDM CCR5 to the IS may be limited to a particular conformational form. However, no evidence was found to support the recruitment of an alternative form of CCR5 to the IS on the MDM side since neither MC5 nor CTC5 mAbs, which identify different pools of CCR5 that are susceptible or not to ligand induced down-modulation, demonstrated any accumulation towards the IS (**Fig. 4.3 & 4.4**). Nevertheless the different components of the cellular background, such as the absence of Lck and the reduced levels of CD4 on MDMs (Lee et al., 1999b; Pelchen-Matthews et al., 1998), may contribute to why accumulation of CCR5 is observed on the T cell side but not the MDM side of the IS. This variation may be due to differences in chemokine receptor cross-talk pathways between cell-types (Bennett et al., 2011).

Notably, one study found evidence for crosstalk between MHC class II and β-chemokine receptors. Specifically, sAg-treatment of monocytes resulted in rapid down-modulation of the receptors for CCL3 and CCL4 as well as the inhibition of calcium mobilisation in response to these chemokines (Rahimpour et al., 1999). Thus sAg-pulsing of MDMs may induce CCR5 unresponsiveness, which in turn could influence recruitment of CCR5 to the IS. Despite this, no decrease in CCR5 expression on sAg-treated MDMs was evident by immunofluorescence microscopy (**Fig. 4.3**) demonstrating that the observations of Rahimpour et al. (1999) may not apply to MDMs.

Efforts were made to determine whether CCR5 could be involved in a signalling capacity at the IS. Numerous attempts were made to detect phosphorylation of CCR5 on chemokine-treated MDMs by immunofluorescence using CCR5 antibodies that preferentially bind CCR5 phosphorylated at either Ser^{337} or Ser^{349}. CCR5 phosphorylation in response to exogenous CCL5 treatment was successfully detected using an anti-CCR5 phosho-Ser^{349} mAb (clone: E11/19) on CHO-CCR5 cells, confirming previous results on these cells and on monocytes (Fox et al., 2011; Signoret et al., 2004). However no increase in CCR5 phosphorylation was detected when MDMs were treated and immunolabelled in the same way. Interestingly, even after MDMs were treated overnight with amino-oxypentane RANTES (100 nM) and focal regions of internalised CCR5 were evident, no E11/19 staining could be detected. Altogether this indicates a lack of sensitivity of detection of E11/19 on MDMs, possibly as a result of MDM cell size; even though CCR5+ monocytes and MDMs express similar levels of CCR5 by flow cytometry (**Fig. 3.4**) the MDMs are much larger when adhered to coverslips and therefore the fluorescence signal per unit area is less.

Inhibition of cell surface CCR5 signalling (using TAK-779) or drastic reduction in cell surface CCR5 expression (by treatment with PSC-RANTES) did not prove to influence MDM-CD4+ T cell IS formation (**Fig. 4.5**). Whether the same is true when CCR5 functions are inhibited on CD4+ T cells is currently unknown. Although Contento et al. (2008) treated T cells with CCL5 or TAK-779, the authors did not assess whether there was an inhibitory effect on IS formation or conjugate number. Perhaps the effect of PSC-RANTES or TAK-779 treatment would be much more subtle. Indeed, rather than being essential or not for IS formation, CCR5 may affect the number or dynamics of synapses formed. Bearing in mind that previous reports have shown that the IS still forms on planar bilayers or with naïve T cells, which typically do not express CCR5 (Bromley and Dustin, 2002; Grakoui et al., 1999), the assessment of more subtle features of IS formation may be worthwhile considering in future investigations.

4.3.3.1 CCR5 at the CD4+ T cell side of the IS

The evidence presented here builds upon previous studies, which demonstrate that GFP-CCR5 accumulates to the B cell- CD4+ T cell or DC- Jurkat IS (Contento et al., 2008; Molon et al., 2005), by showing that primary MDM-CD4+ T cell synapses can also localise endogenous CCR5 on the T cell side (**Fig. 4.7**). However, this is not a complete localisation of CCR5 to the IS, in contrast to the depiction of GFP-CCR5 on CD4+ T cells in previous studies (Contento et al., 2008; Molon et al., 2005). This raises issues regarding the interpretation of why CCR5 may localise to the IS. A study examining the hierarchy of chemokine- and TCR-stimulated signalling showed that soluble CCL3 is not able to induce T cell migration when the TCR is engaged (Bromley et al., 2000). This gives rise to the distraction hypothesis, which might account for why certain chemokine receptors such as CCR5 can be localised at the IS (Molon et al., 2005). Yet in the present study the average accumulation ratio shows less than a two-fold increase in the levels of CCR5 at the synapse compared to the rest of the cell. This means that a substantial amount of receptor remains spread over the rest of the cell. In addition, the surface area of the cell-cell interface is typically less than the remainder of the cell, which implies that the amount of CCR5 spread over the rest of the cell is, if anything, underestimated by the accumulation ratio. Together, these factors indicate that a significant amount of CCR5 is still positioned across the rest of the T cell, which could bind 'distracting' chemokine ligands.

Less than half of the CCR5+ CD4+ T cells that engaged in synapses with MDMs showed a level of CCR5 accumulation above that typically expected in the absence of antigen (according to the cut-off ratio) (**Fig. 4.7**). Molon et al. (2005) previously showed that CCR5 accumulation to the Jurkat-B cell IS is dependent upon chemokine secretion by the B cell and the ability of T cell surface CCR5 to bind this chemokine. Based on this premise, the results of the present study might perhaps imply that only a subset of MDMs are secreting CCR5 ligands. Indeed this is not unprecedented, as M1 or M2 polarised MDMs are known to have different chemokine secretion profiles, with M1 macrophages preferentially secreting chemokines that are bound by CCR5 (Mantovani et al., 2004). Although the MDMs used in the present study are more M2 than M1, given the immense plasticity of macrophages the population used here may have features of both phenotypes or represent a heterogenous mix of these cells. Indeed evidence for the latter is apparent from images illustrating that a range of levels of the M2 marker, CD163, exist across the population (**Fig. 4.2 & Fig. 3.3**). Speculatively, the $CD163^{low}$ MDMs might demonstrate more secretion of M1-linked chemokines than the $CD163^{high}$ MDMs. Since synapses can be formed with both $CD163^{low}$ and $CD163^{high}$ MDMs (**Fig. 4.2**), the potential differences in

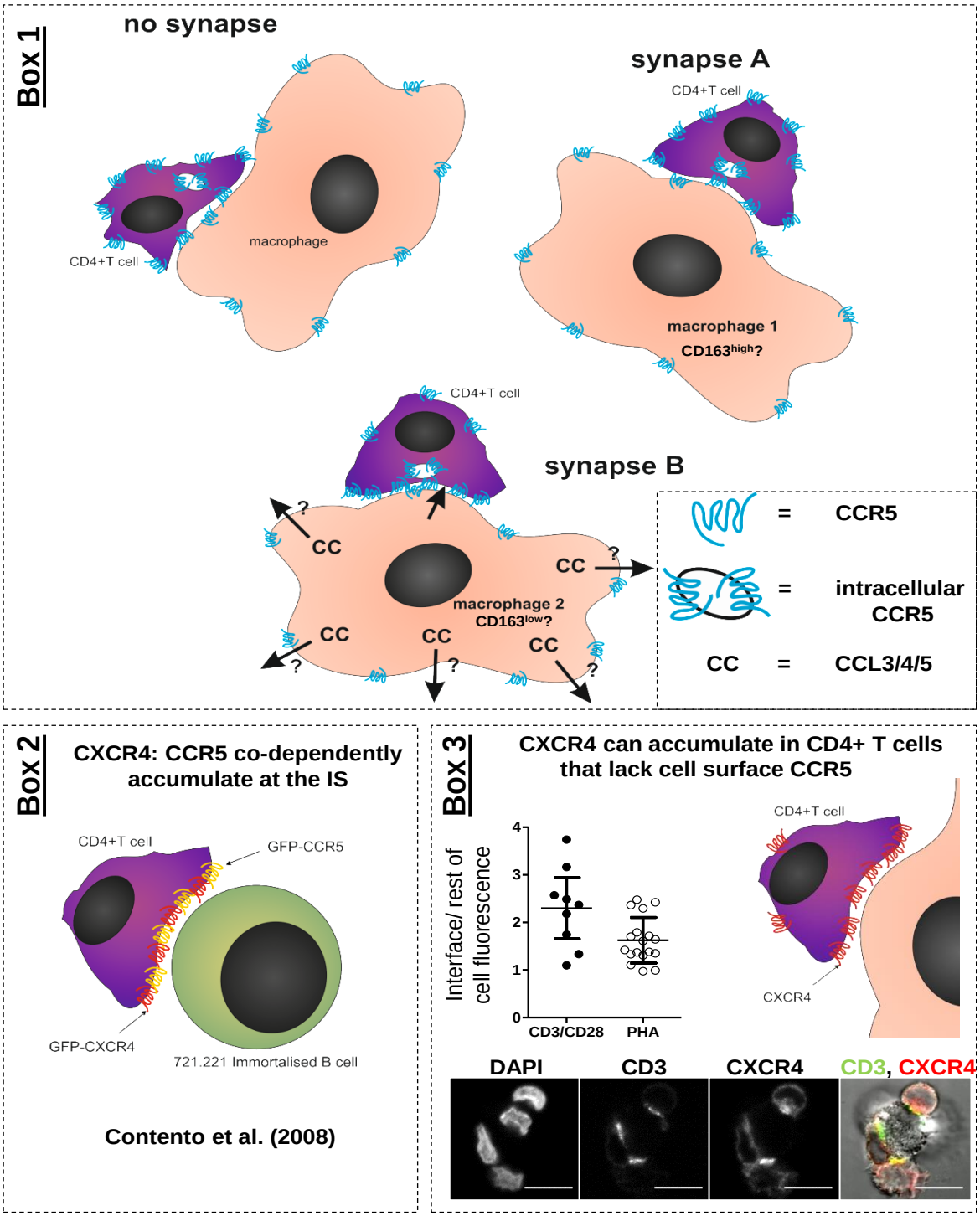

Figure 4.10: Summary of chemokine receptor recruitment to the IS. (**Box 1**) MDM cell surface CCR5 does not accumulate to the IS. On the CD4+ T cell no cell surface CCR5, but intracellular CCR5 can accumulate to the cell-cell interface in some T cells in the absence of IS formation. Upon IS formation intracellular CCR5 generally shows polarity to the cell-cell interface. Also, some T cells show cell surface CCR5 recruitment to the IS. One explanation may be multidirectional secretion of chemokine by some MDMs but not others in the heterogeneous MDM population. (**Box 2**) Diagram summary of previous work by Contento et al. (2008) showing CXCR4-CCR5 co dependently accumulate to the IS. (**Box 3**) Accumulation of CXCR4 to the MDM-CD4+T cell IS on T cells lacking cell surface CCR5. Conjugates formed between CD3/CD28 activated CD4+ T cells and sAg-pulsed MDMs (30 min), fixed and immunolabelled for CD3 (UCHT1) and CXCR4 (12G5) followed by GAM-IgG1^{488} and GAM-IgG2a^{647} secondary antibodies. Images representative of a single donor. Plot shows quantification of CXCR4 accumulation at the IS. Scale bar, 10 µm

secretion of CCR5 ligands by these subsets might explain whether or not CCR5 localises to the MDM-CD4+ T cell synapse (**Fig. 4.10**). Notably, different expression of E-cadherin, the ligand of CD103, is also apparent on M1 and M2 MDMs (Sica and Mantovani, 2012). Thus these differences may also be apparent if CD103 was found to trigger CCR5 to the MDM-CD4+ T cell IS, as it does in TIL-tumour synapses (Franciszkiewicz et al., 2009).

4.3.3.2 Intracellular T cell CCR5 redistributes to the cell-cell interface

Immunolabelling after permeabilisation reveals intracellular epitopes of endogenous CCR5 which polarise towards the IS. Moreover, intracellular CCR5 can also localise to the MDM-CD4+ T cell interface in the absence of sAg (**Fig. 4.8a**). This is reflected by the distribution of the CCR5-fluorescence quantification, which shows a skew towards the interface ROI even in the absence of sAg (**Fig. 4.8b**). Whilst the fluorescence of MDM CCR5 will also contribute to this interface-skewed baseline distribution, as measured by the fluorescence quantification method, images indicate that the level of CCR5 fluorescence associated with the T cell is generally dominant. Thus the quantification still primarily reflects the distribution of T cell CCR5 towards the interface. Despite these technical aspects, there is an increase in the levels of CCR5 polarisation towards the cell-cell interface upon the addition of antigen (**Fig. 4.8b**). Indeed the majority of conjugates demonstrate CCR5 polarisation to the IS, which is in contrast to the lower percentage of intact T cells showing cell surface CCR5 accumulation to the IS.

Permeabilisation enables detection of total cellular CCR5 meaning that this approach is most comparable to studies that have utilised CCR5 tagged with GFP, which identifies both cell surface and internal CCR5 (Contento et al., 2008; Molon et al., 2005). Even though the authors of these studies claimed to have omitted non-PM fluorescence from their analysis, they did not exclude the possibility that the GFP-CCR5 observed might reside in intracellular compartments that are tightly apposed to the PM. Indeed the Golgi is an example of such a compartment; the constituent stacks have previously been shown to contact the PM at the IS (Stinchcombe et al., 2006). Together with the results of the present study, which shows that CCR5 localisation to the IS is more apparent after permeabilisation (**Fig. 4.8**), this indicates that the localisation of cell-surface CCR5 to the synapse may have been overestimated in previous studies utilising GFP-CCR5 (Contento et al., 2008; Molon et al., 2005).

The present study indicates that both cell surface and intracellular CCR5 can accumulate to the MDM-CD4+ T cell IS on the T cell side. However, the mechanisms involved in recruiting CCR5 in these different cellular locations are likely to be different as APC-secreted chemokines cannot access any CCR5 resident inside the T cell. Perhaps an

alternative mechanism may involve the Golgi, which we found to preferentially localise to the cell-cell interface upon IS formation, consistent with previous reports (**Fig. 4.9.2**) (Griffiths et al., 2010; Stinchcombe et al., 2006). Since the intracellular CCR5 shows partial colocalisation with the TGN (**Fig. 4.9.1a**) it is possible that the intracellular pool of CCR5 becomes redistributed to the IS as a passenger in the Golgi.

Due to the partial colocalisation with the TGN, the internal CCR5 identified in the present study is not thought to be the same intracellular pool of CCR5 previously identified in the ER of T cells (Achour et al., 2009). CCR5 has been shown to accumulate in the TGN of primary human T cells in response to prolonged treatment with CCL5 (Escola et al., 2010), but also to TfR+ REs in CHO-CCR5 cells (Mueller et al., 2002; Signoret et al., 2000). However CCR5 colocalisation with TfR (**Fig. 4.9.1b**) appeared to occur to a lesser extent than the TGN, although perhaps this reflects previous observations that upon prolonged CCL5-treatment residence in the TfR+ compartment is transient (Escola et al., 2010). It is currently unknown whether this intracellular pool of CCR5 may be caused by internalisation of cell surface CCR5 or receptor in the biosynthetic pathway. However internalisation and recycling via REs and/or TGN trafficking compartments that have been implicated in the trafficking of CCR5 and are known to polarise to the IS, may represent a mechanism by which CCR5 becomes localised to the plane of the IS. This type of mechanism is not unheard of, as redirection of REs to the IS has been shown to contribute to TCR accumulation at the cell-cell interface (Das et al., 2004).

Finally, no change in CCR5 colocalisation with either the TGN or TfR was apparent in conjugates pulsed with sAg (**Fig. 4.9.1**), suggesting that CCR5 trafficking through these compartments is not influenced by the IS. However one major limitation of this observation is that these may not represent *bone fide* synapses, as identified using CD3 in all other sections of the present study. This is because conjugates forming 'synapses' were selected based on the localisation of RE and *trans*-Golgi markers to the interface, since these compartments are known to accumulate to the IS (Das et al., 2004; Griffiths et al., 2010). Yet accumulation of the Golgi to the cell-cell interface is also apparent in the absence of antigen, albeit to a lesser degree, thus the sAg-pulsed conjugates observed with organelle markers are purposefully not referred to as synapses (**Fig. 4.9.2**).

4.3.4 CXCR4 localisation and T cell activation

CXCR4 was also shown to be localised to the MDM-CD4+ T cell IS. In similarity to that observed for CCR5 the level of recruitment to the IS was marginal. Fewer T cells (24%) were found to express CXCR4 levels at the IS above the levels in conjugates in the absence of antigen. A previous report suggests that CXCR4 forms heterodimers with

CCR5, which accumulate at the B cell-T cell IS in a mechanism dependent upon the presence of CCR5 and cognate ligands secreted by the APC (Contento et al., 2008). However, when we formed the MDM-CD4+ T cell IS using T cells that had been activated with CD3/CD28 beads, expressing little or no cell surface CCR5 (**Fig. 3.6**), CXCR4 accumulated to the IS (**Fig. 4.10: Box 3**). Thus, in the absence of CCR5 there appears to be potential for CXCR4 to be brought to the IS via other processes. Indeed, CXCR4 has been suggested to heterodimerise with the TCR complex in order to mediate signalling functions via ITAM domains in response to CXCL12 (Kumar et al., 2006). Another study has also found CXCR4 transactivation of the TCR, although via more classical TCR-signalling mechanism involving ITAM phosphorylation mediated Lck linked via an adaptor protein (Patrussi et al., 2007). Yet it is unknown whether MDMs in the present study would represent a source of CXCL12. Nevertheless, a previous report found that CXCR4 capped in response to anti-CD4 beads via a mechanism dependent on Lck and lipid rafts (Nguyen et al., 2005) providing further evidence for CXCR4 redistribution with signalling components that are known to be recruited to the IS.

In summary, endogenous CCR5 was not seen to accumulate to the macrophage side of the MDM-CD4+ T cell IS. In contrast, endogenous CCR5 and CXCR4 were able to accumulate to the T cell side of this IS, as shown for other types of synapses (Contento et al., 2008; Franciszkiewicz et al., 2009; Molon et al., 2005). This may indicate differential exposure to chemokine gradients or receptor regulation on the T cells and MDMs. Furthermore the intracellular CCR5 in the T cells, which partially colocalised with the TGN, polarised to the MDM-CD4+ T cell interface upon IS formation. However the role of this intracellular CCR5 is unclear regarding its contribution to cell surface CCR5 at the IS.

Chapter 5: Investigating the mobility of plasma membrane CCR5 in MDMs

5.1 Introduction

5.1.1 Current working models of plasma membrane organisation

Study of the mobility of the transmembrane protein, CCR5, in the plasma membrane (PM) calls for an understanding of the environment within which such proteins exist. The PM is a bilayer organisation of phospholipids in which hydrophobic fatty acid tails are butted together and hidden from the aqueous environment by counterpart polar head groups (Cooper, 2000). There is a preferential association of different phospholipids with either leaflet of the PM, e.g. phosphatidylcholine and sphingomyelin with the outer leaflet, and phosphatidylethanolamine, phosphatidylserine, and phosphatidylinositol with the inner leaflet (Cooper, 2000). Embedded within this lipid bilayer are different types of membrane protein: (i) integral (e.g. transmembrane proteins such as CCR5), (ii) peripheral (e.g. PLC), (iii) lipid anchored (e.g. G proteins). These proteins are arranged in an amphipathic fashion within the lipid matrix; an organisation that was initially considered a two-dimensional arrangement of proteins within a viscous fluid, according to the 'fluid mosaic' model (Singer and Nicolson, 1972).

5.1.1.1 The inclusion and reinvention of lipid rafts

The 'fluid mosaic' model was soon found to be incomplete following the discovery that the lipid bilayer can undergo phase separation into both liquid-ordered and liquid-disordered domains (Pike, 2009; Simons and Vaz, 2004). Before the end of the 20th Century these domains had become termed lipid rafts and were described as detergent insoluble collections of laterally-associated sphingolipids packed with cholesterol and located within the PM. The 'lipid raft hypothesis' formally proposed and described the existence of the two domains and suggested that they might act to concentrate receptors, thereby promoting appropriate interactions and enhancing signalling efficiency (Simons and Ikonen, 1997). In the last decade, the traditional view of lipid rafts has been refashioned as many of the original techniques used to demonstrate their existence (e.g. detergent extraction, mechanical disruption, Shiga toxin or cholera toxin labelling) intrinsically disrupt their native organisation (Lingwood and Simons, 2010). The definition of lipid rafts as "small (10-200 nm) heterogeneous, highly dynamic, sterol- and sphingolipid-enriched domains that compartmentalise cellular processes" much more

accurately describes the nature of these lipid entities (Pike, 2006). Indeed, at steady state in unstimulated cells rafts are thought to exist as short-lived transiently-forming nanoscale sterol- and sphingolipid clusters (Lingwood and Simons, 2010). These lipid entities exist in an energy state that is on the tipping-point of stable raft formation (Kusumi et al., 2005) that can occur on coalescence by actin remodelling or receptor oligomerisation, such as occurs during IS formation (Lingwood and Simons, 2010).

Two partially related hypotheses, the protein islands theory and the picket-fence model, have supplemented the original lipid-based models by considering the influence of the cortical cytoskeleton upon membrane compartmentalisation. The protein islands theory suggests that membrane-associated proteins and cholesterol accumulate into cytoskeletal-rich regions, which are surrounded by a sea of protein-free PM (Lillemeier et al., 2006). Lillemeier et al. (2006) used protein chimeras, which are normally organised into mutually exclusive raft and non-raft regions, to show that after activation these proteins can become amalgamated. It was proposed that oligomerisation and other interactions of proteins and lipids from different islands occur as a result of hop diffusion (Lillemeier et al., 2006). Hop diffusion was shown to occur by single fluorescent molecule video imaging (SFVI) of fluorescent lipid and describes the event of a PM component (e.g. a protein) crossing over the boundary between two adjacent compartments of the PM, within which the component is temporarily corralled. It is a key concept of the picket-fence model (Kusumi et al., 2005).

5.1.1.2 A picket-fence model of the plasma membrane

The picket-fence model is based on observations from techniques such as single particle tracking (SPT) and SFVI as well as FRAP. SPT and SFVI enable analysis of the molecular dynamics of the PM in scales of less than 100 nm, whereas FRAP is designed to analyse dynamics over scales greater than several hundred nanometers (Kusumi et al., 2005). In the picket-fence model the cortical actin cytoskeleton compartmentalises the PM by forming a ‘fence’ that is anchored through both leaflets of the PM by transmembrane protein fence posts or ‘pickets’ (Kusumi et al., 2005). Proteins and lipids are thus temporarily corralled and experience hop diffusion at varying rates depending on the density of the cortical actin meshwork and number of transmembrane protein pickets linked to the actin fences at any given moment (Kusumi et al., 2005). The underlying meshwork has been visualised and the compartment sizes that have been observed support concomitant hop diffusion rates, thereby providing direct evidence to support the picket-fence model (Morone et al., 2006).

The complexities of the PM have meant that model systems are often employed to study particular aspects of membrane biology. Model bilayers, composed from just two or three lipid species rather than hundreds in a typical cell membrane, have demonstrated the existence of lipid-lipid immiscibility founding the underlying principle of raft formation (Simons and Vaz, 2004). Despite their usefulness, concatenation of different models can sometimes lead to misinterpretation due to a lack of understanding of the technical constraints of each system. A good example of this is the pocketed distribution of cholesterol shown by Lillemeier et al. (2006), which appears to contradict a later study suggesting that the majority of the PM exists in a liquid-ordered phase (Levental et al., 2009). However, whilst one study used EM to visualise ripped membrane sheets and the accompanying cortical cytoskeleton of T cells (Lillemeier et al., 2006), the other used giant PM vesicles, which are intrinsically devoid of a functional cortical cytoskeleton (Levental et al., 2009). The latter system lacks the machinery to limit or concentrate cholesterol to particular regions of the PM, which may account for the difference in results. Thus, although reductionist models have their use, it is important to consider the protein or lipid of interest in the context of its native membrane complete with an intact cytoskeleton.

5.1.2 GPCRs: flexible signal transducers within the plasma membrane

The organisation of the PM forms a complex type of chessboard on which thousands of transmembrane protein pieces play. Inherent to each piece are structural properties that influence the functional outcome, or type of move it is able to make. Whilst numerous growth factor and cytokine receptors require dimerization to switch on downstream signalling events, the 7TM structure of GPCRs enables receptors to act as conformational switches (Thelen, 2001). Indeed, the interactions between transmembrane helices of CCR5 are thought to contribute to a range of active conformations that may influence downstream signal transduction (Springael et al., 2007). Despite a seemingly intrinsic structural ability to signal as monomers, the capacity of CCR5, as well as GPCRs in general, to signal as monomers, dimers or oligomers has been a subject of intense debate (Gurevich and Gurevich, 2008; Hernanz-Falcón et al., 2005; Lemay et al., 2005). Application of advanced imaging techniques, such as SFVI, has recently provided visual evidence that the chemoattractant GPCR N-formyl peptide receptor exists in an equilibrium of rapid monomer-dimer formation and dissociation (Kasai et al., 2011). This supplements the idea that any given GPCR can exist in a number of oligomeric states (Gurevich and Gurevich, 2008). Indeed, CCR5 has been shown to form homodimers and heterodimers with C5aR (Hüttenrauch et al., 2005), CXCR4 (Contento et al., 2008) or CCR2b (El-Asmar et al., 2005). Evidently the process of receptor multimerisation requires that at least one of the receptors involved has a degree of mobility within the PM. FRAP is

one of the ways that this level of mobility can be analysed in an undisturbed state (Phair et al., 2004). Photometric data from the steady-state can then be compared to FRAP in the presence of drug/ligand treatment; these data can then be used to discern whether the receptor of interest is immobile in order to determine the nature of tethering or inform about the occurrence of multimerisation.

5.1.3 Principles of fluorescence recovery after photobleaching (FRAP)

FRAP is a technique that involves irreversible bleaching and the subsequent measurement of fluorescence in a small region of interest (ROI) over a period of time (Ishikawa-Ankerhold et al., 2012). This technique is used to determine the mean mobility of many individual molecules within that small ROI (Klein and Waharte, 2010). Repeat images of the same field of view are recorded using a low laser power at given intervals over a defined period of time. Within this field of view several regions are drawn from which intensity values are extracted that enable normalised curves to be calculated according to the equations detailed in section 2.9 (**Fig. 5.1**).

5.1.4 Presentation of FRAP curves and data

In the present study FRAP curves are shown as the mean (± SD) of all normalised curves from an individual donor at each time-point (t). These single and double normalised mean curves are fitted with an appropriate single exponential equation, as described in section 2.9.3. Mobile fraction and $t_{1/2}$ values derived from regression of double normalised curves are presented in tables below the FRAP graphs. To aid visual comparison an overall mean curve was generated from the mean double normalised FRAP curves for each donor acquired under identical experimental conditions, with ± SD values propagated according to $\sqrt{([var_1+var_2+\ldots+ var_n]/n)}$.

Each FRAP curve was also fitted individually with a single exponential rise to maximum after double normalisation. The $t_{1/2}$ and mobile fractions were derived only from the fitted curves that met the Gaussian assumptions of regression; curves were excluded on failure of residuals to pass D'Agostinos test for normality. Any $t_{1/2}$ values derived from extrapolated mobile fraction values were excluded. Mobile fractions >1.5 were also excluded on the basis that the original measurement of pre-bleach fluorescence was likely to be inaccurate in these instances. Upon fulfilment of these criteria $t_{1/2}$ and mobile fraction values derived from individual FRAP curves from different donors were pooled before being graphed and statistically compared with values from other treatment conditions.

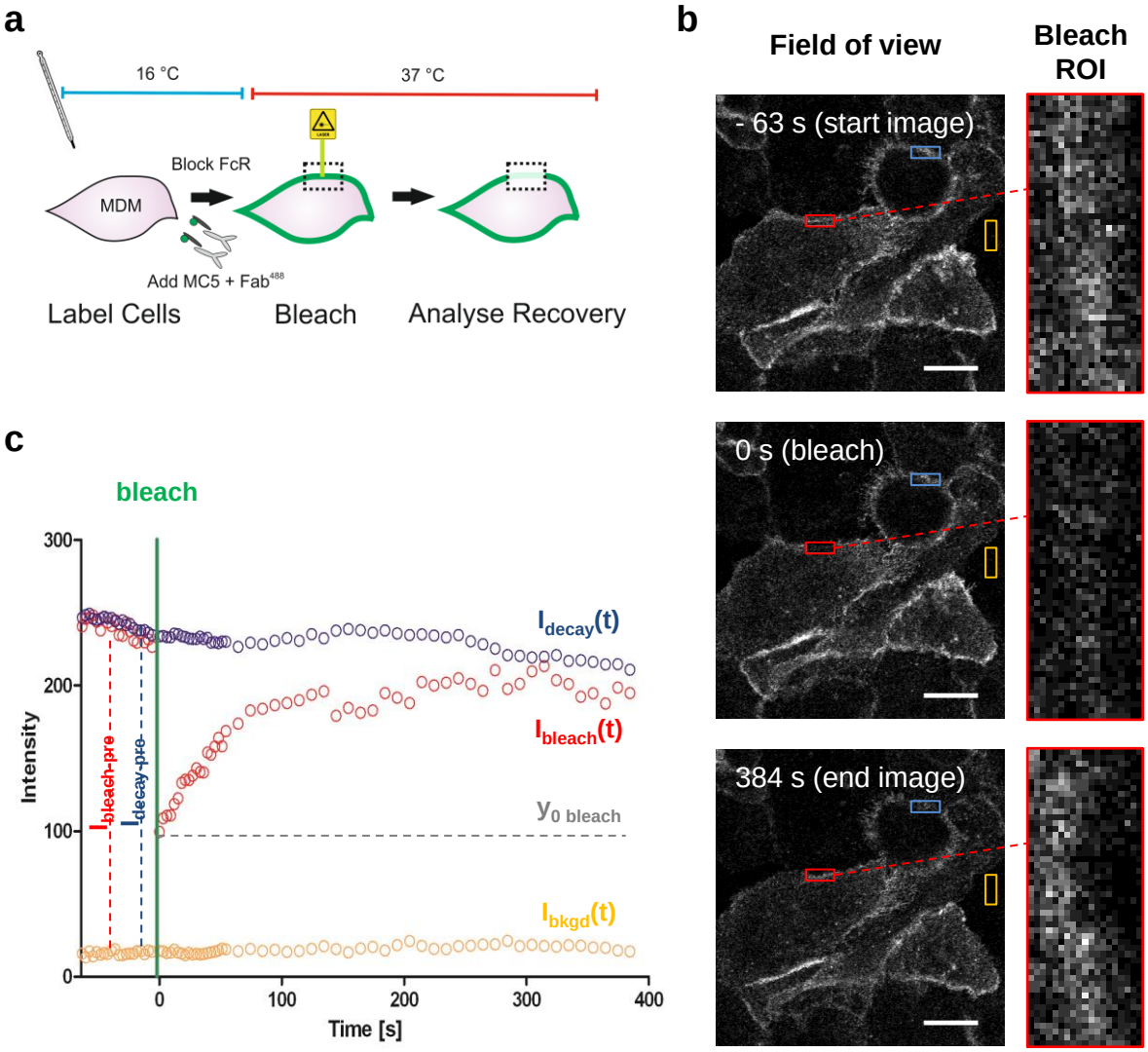

Figure 5.1: Summary of the performance of FRAP and extraction of photometric data. (**a**) CCR5 is immunofluorescently labelled according to the technique detailed in section 2.8.1. A small region of fluorescence is bleached with a high-powered laser pulse. Recovery of fluorescence into the bleached region is analysed over time. (**b**) Imaged fields of view showing the three regions of interest (ROIs) used to extract photometric data: (i) the **bleach** ($I_{bleach}(t)$) ROI is the region in which bleaching occurs at t = 0; (ii) the **decay** ($I_{decay}(t)$) ROI is drawn on another cell, where possible, and acts as a reference for loss of fluorescence during FRAP; (iii) the **background** ($I_{bkgd}(t)$) ROI is used to measure background non-cell-associated fluorescence. Note that as only a very small amount of the total cell intensity is bleached, no ROI was drawn to calculate the 'gap-ratio' which accounts for a significant drop in fluorescence in other studies (Phair et al., 2004) (**c**) Plot showing the fluorescence intensity at every time-point in each of the three ROIs. Notice that a number of images are taken prior to bleaching (-63 – 0 s: 20 cycles) to determine the mean level of fluorescence in **bleach** and **decay** ROIs, from which the $I_{bleach\text{-}pre}$ and $I_{decay\text{-}pre}$ values are derived, respectively. The intensity value measured immediately after bleaching ($y_{0\ bleach}$) is the final parameter required for the normalisation transformations detailed in section 2.9.

5.1.5 CCR5 in the plasma membrane

The mobility of CCR5 within the PM has been studied with particular interest because of its implications with regard to HIV infection. Receptor mobility of CCR5 and CD4 facilitates sequential interactions with HIV envelope proteins that are required for viral binding and entry (Rawat et al., 2008). CCR5 mobility has been studied by FRAP on several occasions in different cell lines but never at endogenous expression levels in primary cells. FRAP studies of HIV-fusion permissive and non-permissive cells indicate that, for both cell types, CCR5-GFP has a similar mobility and exists almost entirely as a mobile fraction in the PM (Rawat et al., 2008). CCR5-GFP was also reported to be highly mobile in the PM of transfected human osteosarcoma (HOS) cells, with 100% recovery seen within 90 s (Steffens and Hope, 2004). Recovery was dramatically reduced on cholesterol depletion, which the authors suggested may indicate a possible role for lipid rafts in mediating the membrane mobility of CCR5 (Steffens and Hope, 2004). Another FRAP study, using U373-MAGI cells transfected with CCR5-YFP, reported 84% recovery within 8 min (480 s) (Nakata et al., 2010). Although this study also noted the presence of a greater immobile fraction after cholesterol depletion, the speed of recovery in untreated cells was markedly slower than that reported by Steffens and Hope (2004). This disparity highlights the importance of performing FRAP on CCR5 in a more physiologically relevant cell type as the percentage and timeframe of recovery are likely to be different again.

In this chapter the mobility of endogenous CCR5 is investigated in primary human MDMs using FRAP. The recovery of CCR5 is compared to the steady-state mobility of CCR5 in stably transfected CHO-CCR5 cells and to MDMs transiently transfected with GFP-CCR5 constructs. The effect of cholesterol depletion on the mobility of endogenous CCR5 in MDMs is also examined and discussed.

5.2 Methodological Developments

5.2.1 Selecting a suitable antibody to study CCR5 mobility

The binding properties of three monoclonal antibodies (mAbs) that recognise distinct extracellular epitopes of CCR5 (MC5, 2D7 and CTC5) were tested by titration on MDMs and CHO-CCR5 cells (**Fig. 5.2a**). Comparison of the half maximal concentration ($½B_{max}$) shows that functional binding affinity of the three clones differs significantly on MDMs but not on CHO-CCR5 cells (**Fig. 5.2b**). On MDMs the binding affinity of CTC5 is much lower than that of MC5 and 2D7. This builds on the finding of a previous study reporting that CTC5 has a lower affinity than 2D7 when these mAbs were titrated across human CD4+ T cells and U87-CD4-CCR5 cells (Berro et al., 2011). In fact, the high $½B_{max}$ value, which

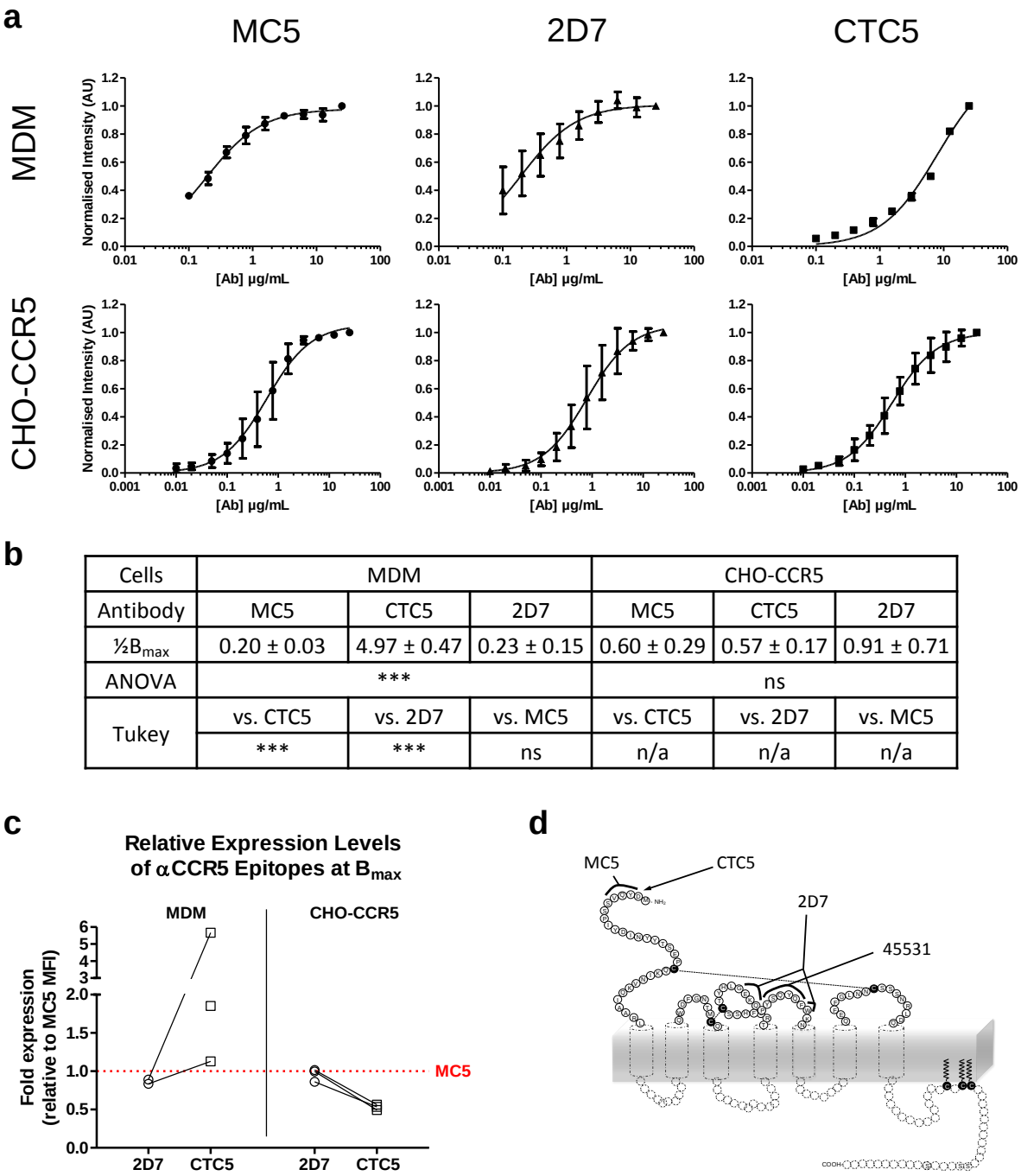

Cells	MDM			CHO-CCR5		
Antibody	MC5	CTC5	2D7	MC5	CTC5	2D7
½B_{max}	0.20 ± 0.03	4.97 ± 0.47	0.23 ± 0.15	0.60 ± 0.29	0.57 ± 0.17	0.91 ± 0.71
ANOVA	***			ns		
Tukey	vs. CTC5	vs. 2D7	vs. MC5	vs. CTC5	vs. 2D7	vs. MC5
	***	***	ns	n/a	n/a	n/a

Figure 5.2: Comparison of binding properties of three anti-CCR5 monoclonal antibodies to MDMs and CHO-CCR5 cells. (**a**) The anti-CCR5 clones MC5, 2D7, and CTC5 were titrated across MDMs and CHO-CCR5 cells and values were normalised to the maximal concentration (25 µg/mL). Graphs show mean ± SD of MDM (n=3) and CHO-CCR5 (n=4) titrations performed on separate days. (**b**) Table showing ½B_{max} values (µg/mL) calculated for each antibody clone from normalised titration data fitted with a one-site ligand binding regression ($Y=B_{max}*X/[Kd+X]$). One-way (MDM) or repeated-measures (CHO-CCR5) ANOVA tests were performed followed by Tukey post-test. (**c**) The mean expression level of 2D7 and CTC5 relative to MC5 (red line) at the maximum concentration titrated (25 µg/mL) is shown for both matched donor MDM and CHO-CCR5 cells. (**d**) Schematic representation of the extracellular epitopes of CCR5 bound by the mAbs MC5, CTC5, 2D7 and 45531.

indicates the low affinity of CTC5 binding, is likely underestimated in the present study as binding saturation was not achieved across the titrated concentration range.

At the highest concentration used for titration (25 µg/mL), the relative level of CTC5 bound was greater than that of MC5 and 2D7 on MDMs (CTC5>MC5>2D7; **Fig. 5.2c**). Although this indicates a greater epitope availability, the low affinity of CTC5 infers a lower binding stability rendering it inferior to MC5 and 2D7 as a tool to study CCR5 mobility by FRAP.

Berro et al. (2011) showed that, for human CD4+ T cells and U87-CD4-CCR5 cells, maximal CTC5 binding was greater than that of 2D7. In contrast to this and my previous results on MDMs, the present study found the relative binding level of CTC5 on CHO-CCR5 cells to be lower compared to MC5 and 2D7 (**Fig. 5.2c**). Taken together this suggests that the different CCR5 antigenic determinants may be influenced by the cell-type in which CCR5 is expressed (Signoret lab, unpublished data). As MC5 binds at a greater level and interferes less with the chemokine binding and signalling of CCR5 (Blanpain et al., 2002) it is a superior tool to analyse the native properties of CCR5 on live cells. The mAb clones tested here, as well as others used in this chapter, were previously mapped to epitopes on CCR5 (Blanpain et al., 2002) and their positions are illustrated in **Fig. 5.2d**.

5.2.2 Testing adherence of MDMs to different coverslip coatings

5.2.2.1 FRAP of MDMs on PEI-coated coverslips

MDMs that were seeded onto PEI-coated coverslips and labelled with $MC5^{488}$ were subjected to FRAP under initial imaging conditions, as described in section 2.8.2. Single normalised bleach curves for each donor (**Fig. 5.3.1a**) showed a similar mean recovery curve. This was despite vast differences in the individual FRAP curves recorded for each cell, which are reflected in wide standard deviation (SD) error bars even at time intervals close to the bleach point. In contrast, mean decay curves showed divergence between donors, with one donor having much greater decay than the other (**Fig. 5.3.1a**). Thus, since double normalisation calculations account for decay, the double normalised mean recovery profiles (**Fig. 5.3.1a**) for each donor diverged after this process. The regression curve of the double normalised data was associated with wide 95% prediction bands, the lower of which lay below a normalised fluorescence value of zero for both donors over the entire time series. This means that fluorescence intensity measurements may be less than the initial bleach value and indicates an immense degree of variation between individual FRAP curves. Nevertheless, the mean half-time ($t_{1/2}$) and mobile fraction values for cells from each donor can be estimated from the regression curve (**Fig. 5.3.1a**). On MDMs seeded on PEI-coated coverslips the mean $t_{1/2}$ was 77 s and was associated with similar

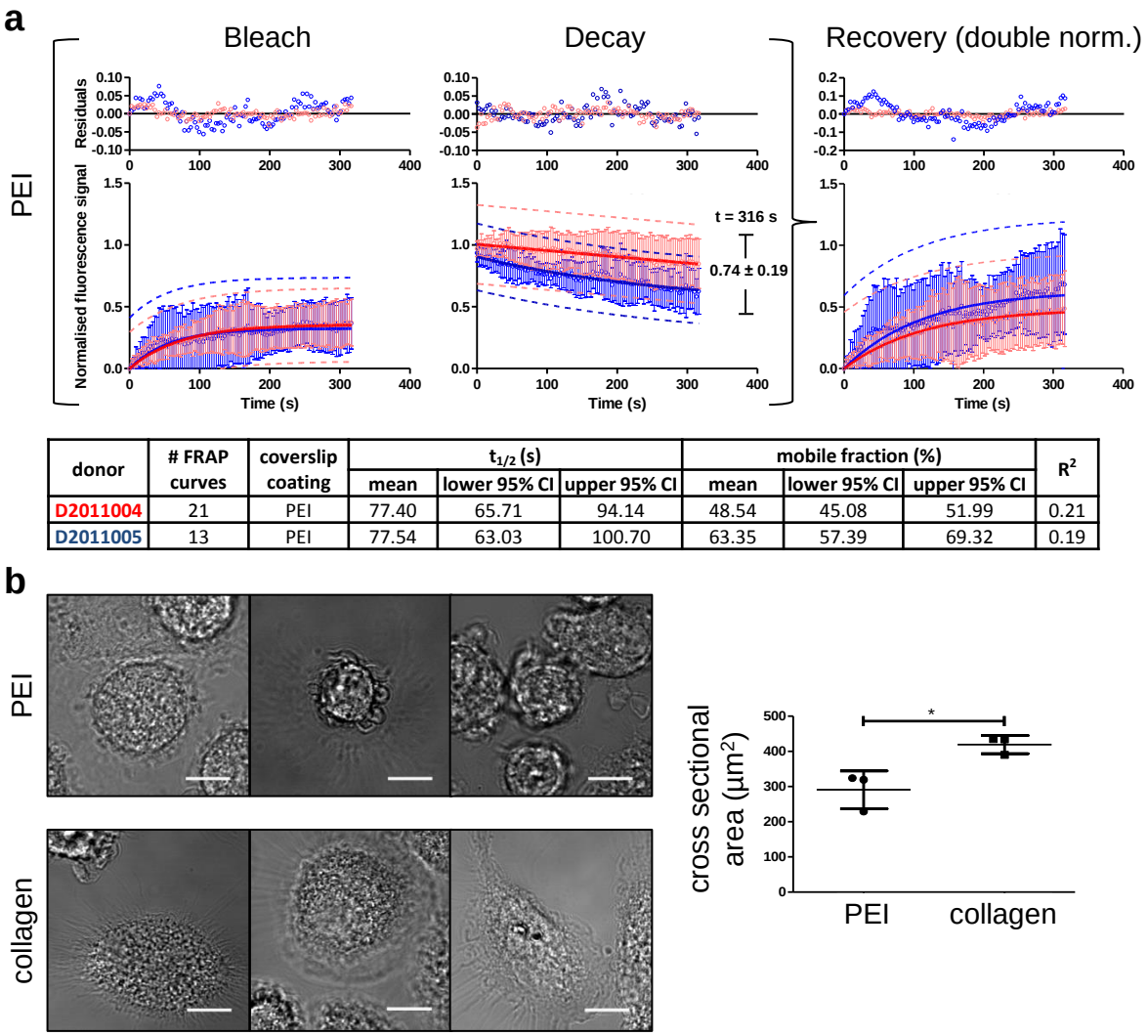

donor	# FRAP curves	coverslip coating	$t_{1/2}$ (s)			mobile fraction (%)			R^2
			mean	lower 95% CI	upper 95% CI	mean	lower 95% CI	upper 95% CI	
D2011004	21	PEI	77.40	65.71	94.14	48.54	45.08	51.99	0.21
D2011005	13	PEI	77.54	63.03	100.70	63.35	57.39	69.32	0.19

Figure 5.3.1: Investigating seeding MDMs on PEI- or collagen-coated coverslips to minimise cell movement. (**a**) Single normalised FRAP curves showing bleach and decay curves acquired for MDMs seeded on PEI-coated coverslips. Two donors (○ **D2011004**, ○ **D2011005**) were assayed under identical imaging conditions (see section 2.8.2). The normalised fluorescence value at the final time-frame is shown on the decay graph (mean ± SD). Decay was accounted for to yield double normalised FRAP curves as described in section 2.9.2. Data show the mean ± SD error bars for each donor overlaid with appropriate regression curves (solid lines) associated with 95% prediction bands (dotted lines) and mean residual values for each fit, which are plotted above. The table shows $t_{1/2}$, mobile fraction and R^2 values calculated from the double normalised regression curve. (**b**) Representative bright-field images of MDMs seeded on PEI- and collagen-coated coverslips. Using the first time-frame of FRAP the cross-sectional cell area (cell size) was estimated. Graph shows mean ± SD values from 10 cells for each donor (n=3) from MDMs seeded on PEI and collagen statistically compared using an unpaired Student's t-test. Scale bars, 10 µm. *, $p < 0.05$. CI, confidence interval.

CIs for both donors. However, the calculated mobile fraction was markedly different for each donor with recovery values of 49% and 63% lying within mutually exclusive 95% CIs. Together this indicates that a slow mobile fraction of CCR5 exists on the cell surface of MDMs. Considering the experimental error, more accurate description of the speed and level of CCR5 mobility was not appropriate. For this reason efforts were made to investigate and improve the experimental conditions.

5.2.2.2 The morphology of MDMs is influenced by PEI

The PEI-coating was originally used with the ideal view that this cationic polymer would promote adhesion and, therefore, reduce cell drift across the field of view. Global cell drift causes variation in the recovery curve as the cell membrane moves out of the bleach ROI. PEI has previously been described in promoting cell attachment of PC-12 and HEK-293 cells with an efficacy comparable to more classical coatings, such as collagen and PDL (Vancha et al., 2004). Although PEI has also been successfully used as an attachment factor in other culture systems (Khanam et al., 2007; Ruardij et al., 2003), in the present study it was noticed that the MDMs adhering to this cationic polymer exhibited aberrant morphologies. Bright-field images of bleached MDMs from each donor (n=3) are provided to visually represent the difference in morphology seen between cells seeded on PEI vs. collagen-coated coverslips (**Fig. 5.3.1b**). The cross-sectional areas of MDMs, seeded on PEI or collagen-coated coverslips and bleached during FRAP were compared and the MDMs adhered to PEI were found to be significantly smaller than when adhered to collagen **(Fig. 5.3.1b**). This indicated that MDMs seeded on PEI-coated coverslips did not spread and attach as well as those seeded on collagen, therefore the PEI protocol was discontinued.

5.2.2.3 FRAP of MDMs on collagen, PDL or in CyGel

FRAP was performed on cells from the same donor in order to investigate whether MDMs seeded on collagen- or PDL-coated coverslips, or when embedded in a thermoreversible hydrogel (marketed as CyGel), gave more reliable results than seen with PEI. FRAP of MDMs seeded on collagen or PDL yielded recovery curves of a similar profile to the original FRAP curves observed on PEI (**Fig. 5.3.2a**). For collagen the lower 95% prediction band lay above zero at later time-points (**Fig. 5.3.2a**), unlike for the double normalised recovery on PEI (**Fig. 5.3.1a**). This indicates that on collagen the recovery curves exhibited less variation than on PEI, perhaps due to the improved cell attachment on collagen as demonstrated above. The mobile fraction and/or $t_{1/2}$ values for collagen and PDL showed some difference to those for PEI; in several cases these differences were significant as determined by having mutually exclusive 95% CIs. Yet considering that

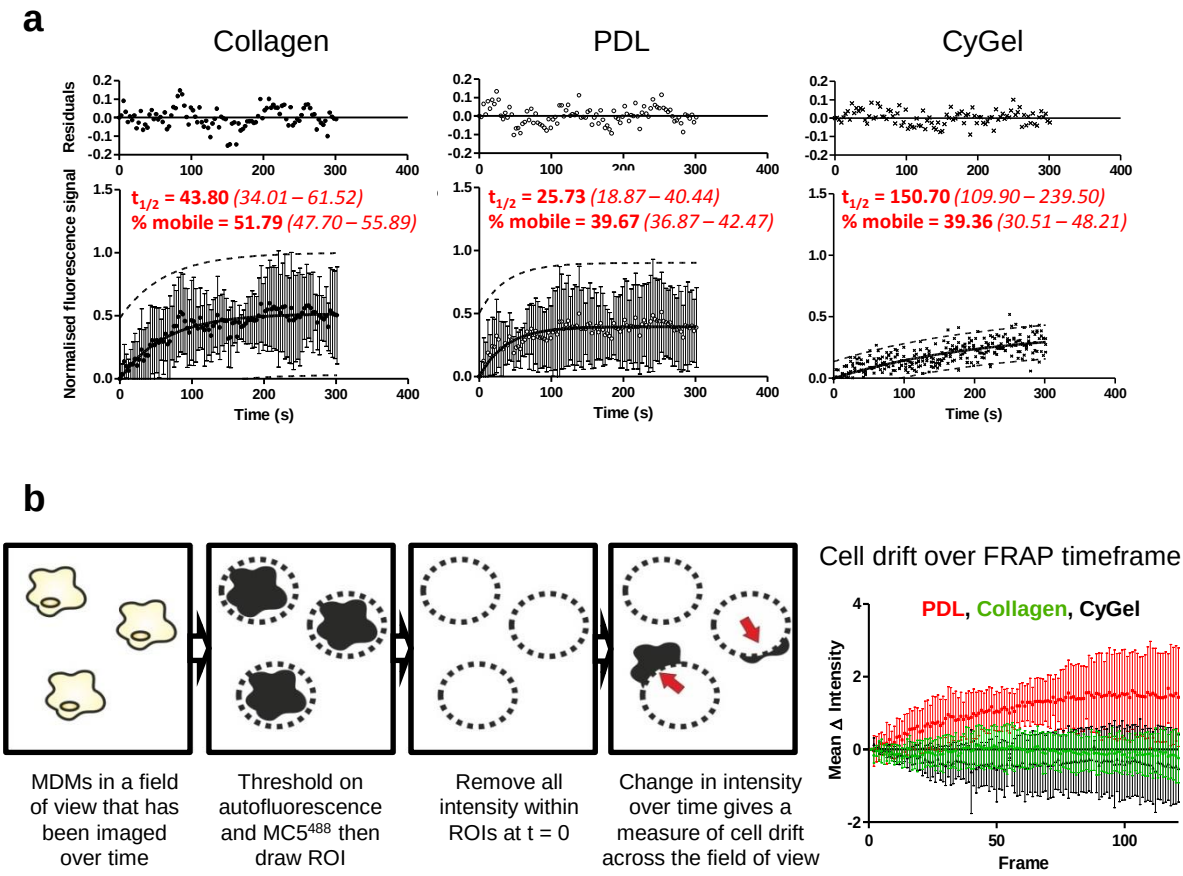

Figure 5.3.2: Investigating seeding MDMs on PDL- or collagen-coated coverslips or in CyGel to minimise cell movement. Double normalised FRAP curves for cells from the same donor seeded on collagen (filled circles), PDL (unfilled circles) or embedded in CyGel (crosses) and assayed under identical imaging conditions. For CyGel, where fewer than five traces were acquired, each replicate is shown, otherwise mean ± SD is plotted. A regression curve (solid line), 95% prediction bands (dotted line), and plot of mean residuals is shown. Mean $t_{1/2}$ and mobile fraction values (lower and upper 95% confidence intervals in parentheses) are indicated in red. (**b**) Cartoon of the process used to measure level of cell drift as a mean change in intensity. Briefly, FRAP time-sequences of $MC5^{488}$-labelled MDMs seeded on PDL, collagen or in CyGel were acquired. In ImageJ the time-sequence was thresholded so that $MC5^{488}$ and cellular autofluorescence highlighted the MDMs. In the first frame circular ROIs were drawn around the MDMs to occlude their signal. The same ROIs were applied across the entire time-sequence so that only if the MDM drifted from its original position would an increase in intensity be detected. Graph shows the mean ± SD change in intensity as a measure of drift of MDMs (n = 1) seeded on **collagen**, **PDL** or embedded in **CyGel** over the time-frame of FRAP (frame interval, 3 s).

FRAP curves from only a single donor were tested and minor changes in the imaging technique had been made, it was inappropriate to extrapolate these small differences into general patterns. When MDMs were embedded in CyGel, regression of the recovery was associated with much tighter prediction bands and a flatter profile compared to PEI, collagen or PDL (**Fig. 5.3.2a**). This may stem from the CyGel physically restricting the cell from any global movement (**supplemental movies 13 & 14**). Further, the effects of CyGel on the fluidity of the membrane and on the antibody used to label the MDMs were unclear. CyGel was, therefore, deemed not appropriate for use when analysing the recovery of antibody-labelled CCR5 on MDMs.

5.2.2.4 Choosing collagen for FRAP

Observation of MDMs in FRAP time-sequences led to the finding that some MDMs appeared to move across the plane of the coverslip. To determine whether MDMs seeded on collagen- or PDL-coated coverslips exhibit a lower level of cell drift, FRAP time-sequences were analysed using a method that enables any global cell movement to be identified as an increase in the mean intensity of the image (**Fig. 5.3.2b**). MDMs embedded in CyGel, which exhibit no movement, were used as negative controls. Results showed that MDMs seeded on PDL tended to migrate from their original position (i.e. a general increase in intensity per frame) whilst MDMs seeded on collagen were more stationary (i.e. intensity fluctuated around zero; **Fig. 5.3.2b**). Therefore, MDMs seeded on collagen had a lower cell drift than those seeded on PDL. Theoretically this means a more repeatable recovery will be obtained using collagen as fluctuations occurring due to movement of the PM out of the ROIs are reduced.

5.2.3 Enhancing image signal: noise

As the fluorescent signal from MDMs was relatively low compared to the background, a number of steps were taken to improve the signal:noise ratio. The DyLight and AlexaFluor dye series were selected as the fluorochromes of preference since they have suitable quantum yields and other properties that make them appropriate for FRAP studies (Ishikawa-Ankerhold et al., 2012). In addition, to ensure the LSM780 hardware was configured for maximal sensitivity, gallium arsenide phosphide (GaAsP) detectors were fitted to side-port (SP) and direct-coupled (DCo) positions sequentially and used to image the same field of $MC5^{488}$-labelled MDMs. When using the DCo configuration enhanced detection of the specific fluorescent signal was observed whilst keeping cellular autofluorescence low (**Fig. 5.4a**).

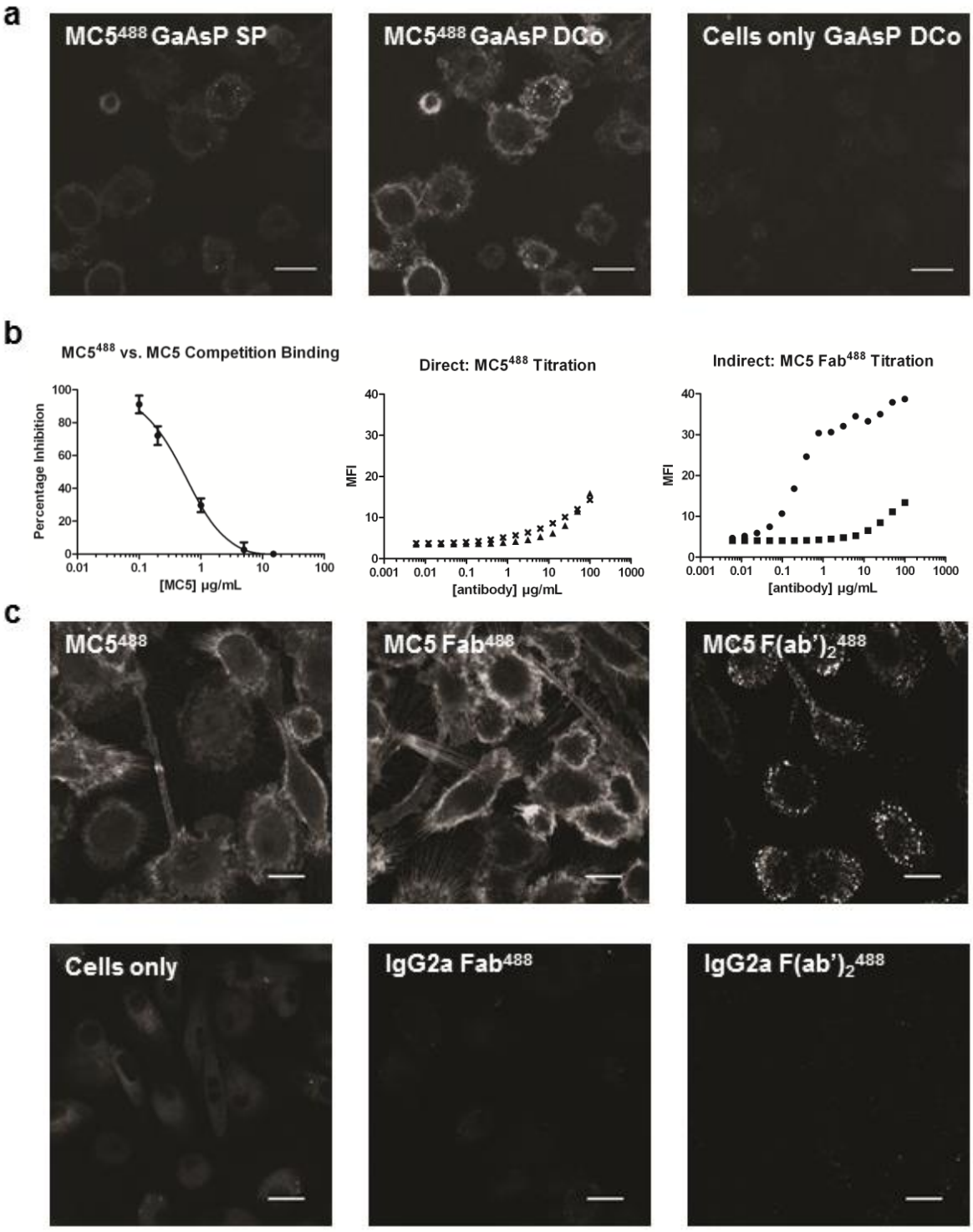

Figure 5.4: Enhancement of the signal:noise ratio during FRAP imaging. (**a**) A field of MDMs labelled with DyLight^{488}-coupled MC5 (MC5^{488}) was imaged with detectors in SP or DCo positions, as indicated. (**b**) A competition binding assay in which increasing concentrations of unlabelled MC5 were incubated with a constant concentration (15 µg/mL) of MC5^{488} on MDMs from three different donors. MDMs were titrated using direct (**x** MC5^{488} or ▲ Isotype-IgG2a^{488}) and indirect (● MC5 or ■ Isotype-IgG2a, all followed by Fab^{488}) labelling; graphs show data from one donor. (**c**) Images of MDMs labelled with: MC5^{488}; MC5 followed by Fab^{488}; MC5 followed by a divalent F(ab')$_2$^{488}; or matched isotype controls. GaAsP, gallium arsenide phosphide detector; SP, side-port; DCo, direct coupled; scale bars, 20 µm.

A binding competition assay showed that the binding affinity of MC5 is impaired by fluorescent coupling, as a low concentration of unlabelled MC5 can displace a high concentration of $MC5^{488}$ (**Fig. 5.4b**). Direct and indirect immunolabelling procedures ($MC5^{488}$ and MC5 followed by Fab^{488}, respectively) were compared in parallel by titration across MDMs from the same donor (**Fig. 5.4b**). The indirect immunolabelling procedure was clearly advantageous as it gave higher fluorescence intensity above the isotype control. In addition, use of the monovalent Fab fragment greatly increased the level of fluorescence detectable on MDMs by microscopy but did not alter the uniform staining pattern seen with $MC5^{488}$ (**Fig. 5.4c**). In contrast, labelling with a divalent $F(ab')_2^{488}$ secondary antibody resulted in a punctuate staining pattern on MDMs. This is important as it showed that CCR5 can be cross-linked and that, under these conditions, can be brought into close contact with other CCR5 molecules in the plane of the MDM membrane. However, in order to enhance the signal:noise ratio whilst maintaining the uniform distribution observed with $MC5^{488}$, the indirect immunolabelling procedure employing GAM-Fab^{488} is preferable.

5.2.4 Impact of temperature on fluorescence decay

Accounting for acquisitional photobleaching is an important factor in achieving accurate estimations of recovery by FRAP (Zheng et al., 2011). The decay (or reference) ROI exists to enumerate the degree of acquisitional photobleaching that occurs over the chosen time-course in order for it to be corrected for through the process of double normalisation. Ideally the level of decay should not be greater than 10% of the pre-bleach signal (Phair et al., 2004). To reduce the level of decay that occurs as a result of acquisitional photobleaching but still maintain the ability to resolve any fast recovery that occurs immediately post-bleach, all further FRAP was performed by changing the delay between image acquisitions from every 3 s to every 10 s at 1 min post-bleach.

From FRAP experiments with MDMs on PEI-coated coverslips it was clear that, despite identical FRAP conditions, different levels of decay were possible (**Fig. 5.3.1a**). To investigate whether the experimental design could introduce a decay variable other than acquisitional photobleaching, the fluorescence of cells that had been labelled for FRAP according to the indirect immunolabelling procedure and then incubated for 0, 15 or 30 min at either 4°C or 37°C, was measured by flow cytometry. At 4°C little or no loss of fluorescence occurred for either CHO-CCR5 or MDMs after 30 min of incubation, relative to the fluorescence at 0 min (**Fig. 5.5a)**. However, at 37°C CHO-CCR5 cells showed a mean loss of fluorescence of 22% after 30 min, whilst MDMs lost a mean of 78%

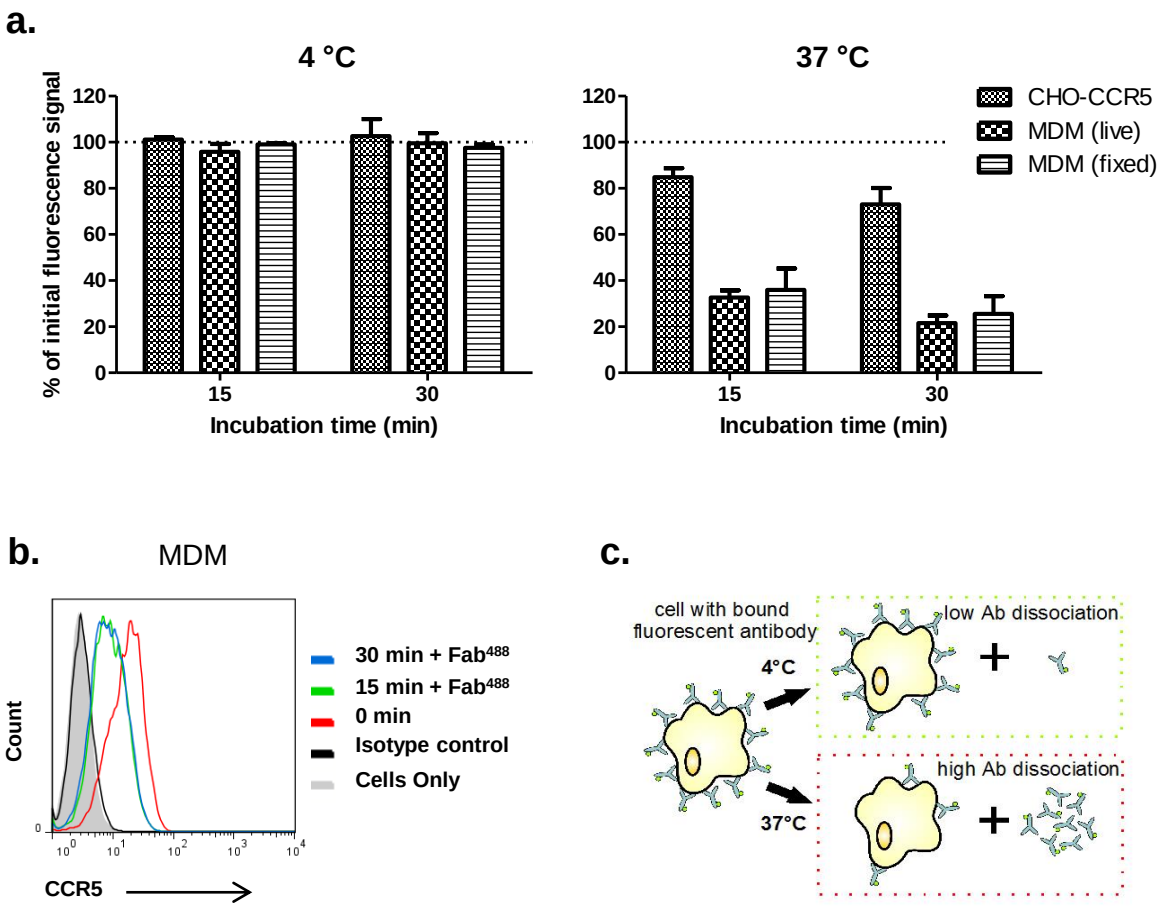

Figure 5.5: Temperature-dependent dissociation of MC5 contributes to decay. (**a**) CHO-CCR5 cells (n = 2), live MDMs (n = 3) or fixed MDMs (n = 2) were labelled with MC5 then Fab^{488}, according to section 2.4.5, before being incubated for 0, 15 or 30 min at either 4°C or 37°C and the level of fluorescence detected by flow cytometry. Fluorescence at 15 or 30 min is expressed as a percentage of the start signal (0 min; indicated by the dotted line). Mean ± SD. (**b**) The same assay was performed at 37°C but, after MDMs had been incubated for 15 or 30 min, they were transferred to ice and relabelled with Fab^{488} before analysing fluorescence by flow cytometry (n=1). (**c**) Cartoon depicting temperature-dependent dissociation of a fluorescent antibody bound to a cell. Transferring a cell labelled with a fluorescent antibody in a solution of medium at a higher temperature (e.g. 37 °C) increases the binding on and off rates leading to a more rapid loss of fluorescent antibody as the antibody moves towards equilibrium. The overall result is a faster loss of cell-associated fluorescence at a higher temperature.

fluorescence relative to the initial (0 min) signal (**Fig. 5.5a**). This showed that CHO-CCR5 cells retain the majority of their fluorescence after 30 min at 37°C, but the bulk of MDM fluorescence is rapidly lost (67% within 15 min). Therefore, photobleaching is not the only factor influencing the decay curve. Fixed MDMs were also subjected to the same treatment to investigate whether this process may actively involve CCR5 (e.g. multimerisation or endocytosis), but as the result was the same as that on live cells this hypothesis was rejected (**Fig. 5.5a**). The loss in fluorescence could be due to dissociation of the secondary Fab^{488} fragment from CCR5-bound MC5. To determine whether this was the case, the above assay was modified so that, after the 37°C incubation period, cells were re-labelled with Fab^{488} (**Fig. 5.5b**). As the loss in fluorescence was not rescued using this approach, it indicated that this phenomenon must be caused by the primary antibody (MC5) dissociating from MDM CCR5.

The most likely explanation for the observed decrease in fluorescence is the Arrhenius nature of antibody-epitope interactions, as first described by Svante Arrhenius over a century ago (Arrhenius, 1907). In general this is the principle that outlines how the binding kinetics of antibodies may be modified at different temperatures. More recently this phenomenon has been applied to describe the binding kinetics of different antibodies (Johnstone et al., 1990). As FRAP was performed on cells bound with a high number of antibody molecules in comparison to an absence in the surrounding imaging medium, an increased off-rate at 37°C combined with diffusion into the medium would explain the loss in fluorescence (**Fig. 5.5c**). The finding that Arrhenius dissociation of MC5 contributes to loss in fluorescence means that the decay is multifactorial. Within the first 15-30 min Arrhenius dissociation is likely to dominate the apparent decay curve, however, over time this factor will become subordinate to the impact of aquisitional photobleaching. Due to this result the imaging protocol was modified so that no FRAP curves were acquired for the first 20 min after cells had begun incubation at 37°C. Decay ROIs were also chosen to match the pre-bleach intensity as closely as possible. Theoretically this limited the contribution of Arrhenius dissociation to the bleach curve but still enabled the bleach ROI to account for the lower rate of dissociation alongside aquisitional photobleaching over the time-frame of FRAP.

5.2.5 Testing for depths and artefacts of bleaching

It is common to use FRAP on fixed cells in order to set the bleach depth to > 70% as no rapidly mobile fraction is able to lower the perceived bleach level detected in the first frame post-bleach (Phair et al., 2004). Different laser powers (4%, 8% and 26%), each kept at 50 iterations, were tested for bleach depth achieved on fixed MDMs. Mean ± SD

bleach depths of 30 ± 6%, 49 ± 5% and 66 ± 12% were calculated for the 4%, 8% and 26% laser powers, respectively. As the 26% laser power bleached to an appropriate depth, this was chosen as the preferred setting. In addition, FRAP curves on fixed MDMs bleached with 26% laser power showed a lower level of decay compared to FRAP with lower laser powers (**Fig. 5.6.1a**). Fixed cells would not be expected to have any true recovery as proteins are cross-linked thus FRAP of fixed cells enables the effect of decay upon the double normalised recovery to be clearly visualised. Single normalised plots show that FRAP with 4% and 8% laser power resulted in high levels of decay but bleach recovery values remained close to zero. However, after double normalisation apparent recovery of CCR5 occurs solely due to decay, from which mobile fractions of up to 34% are calculated from regression (**Fig. 5.6.1a**).

A value was calculated to indicate the level of decay. This value, termed '1-decay' was defined by calculating the area enclosed between the normalised regression decay curve and the fluorescence value of 1 (**Fig. 5.6.1b**). This area can be compared to the area under the mean single normalised recovery curve in order to obtain an idea of whether the double normalised recovery is dominated by the bleach, whether bleach is equal to the decay (i.e. 1-decay and bleach area values are within ± 10 units of each other), or is dominated by the decay. As no true recovery can occur in fixed cells this dataset is able to exemplify the utility of the 1-decay value as a confidence indicator for true recovery. A high 1-decay value (> 100) indicates that the double normalised recovery is likely to be an overestimate, whereas a small 1-decay value (e.g. < 60; such as is the case here for 26% laser power) is associated with only small errors introduced by the decay curve. For a 26% laser power any recovery with a calculated double normalised mobile fraction < 7% can effectively be considered as immobile.

To check that the selected bleach condition (26% laser power, 50 iterations) was not causing photoinduced cross-linking of proteins via the formation of free-radicals (Ishikawa-Ankerhold et al., 2012), the recovery rate was checked against FRAP performed with lower bleach intensity (8% laser power, 50 iterations). Double normalised recovery curves showed that, for each bleach condition, the level of recovery was similar between donors (n = 3) (**Fig. 5.6.1b**). Notice that for FRAP with the 26% laser power there are indications of much lower variation, such as smaller SD error bars and tighter 95% prediction bands, than FRAP with the 8% laser power or previous FRAP curves acquired under non-optimised conditions (e.g. PEI, $MC5^{488}$, etc.; **Fig. 5.3.1a & 5.3.2a**). The mean FRAP curve of all donors bleached at 26% laser power has been overlaid with the mean curve of those bleached at 8% in order to aid visual comparison (**Fig. 5.6.1b**). For the majority of the time-course the 8% curve mirrors the 26% curve, the exception being that the 8% curve

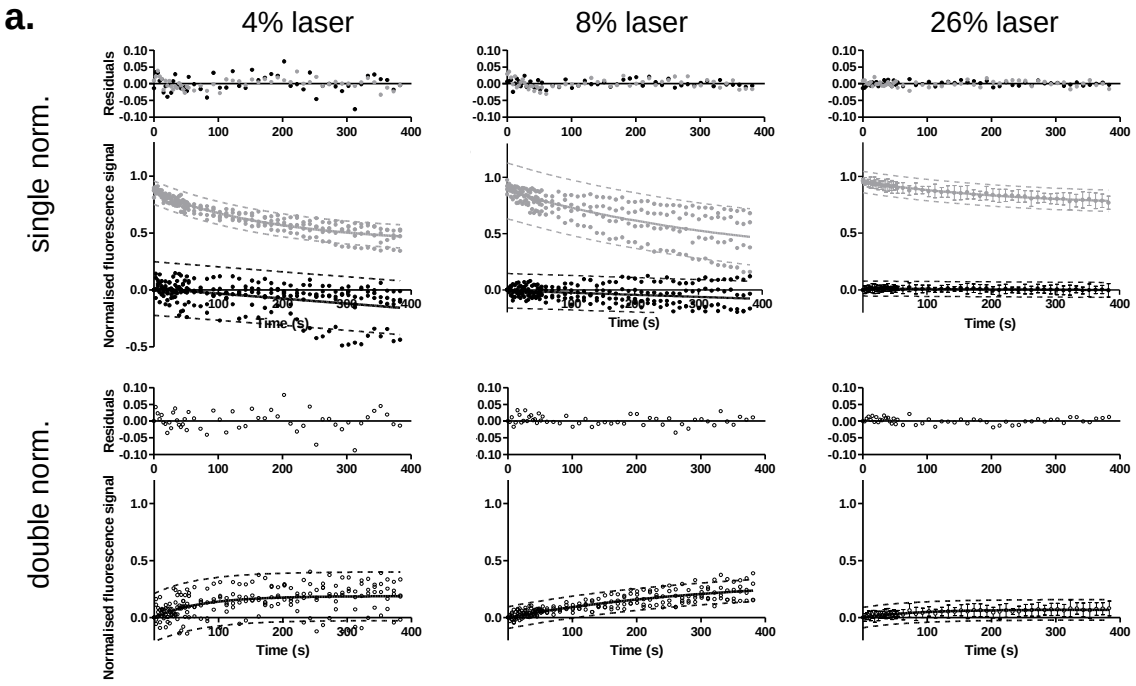

bleach power	bleach depth (% ± SD)	# FRAP curves	Area under mean curve			$t_{1/2}$ (s)			mobile fraction (%)			R^2
			1-decay	bleach	dominance	mean	lower 95% CI	upper 95% CI	mean	lower 95% CI	upper 95% CI	
4%	30 ± 6	4	151.10	0.46	decay	50.70	33.80	101.40	18.82	15.99	21.64	0.23
8%	48 ± 5	4	135.90	0.02	decay	219.90	149.10	418.20	33.90	23.48	44.32	0.71
26%	66 ± 12	10	58.45	3.01	decay	56.06	40.70	90.06	6.89	4.16	7.70	0.16

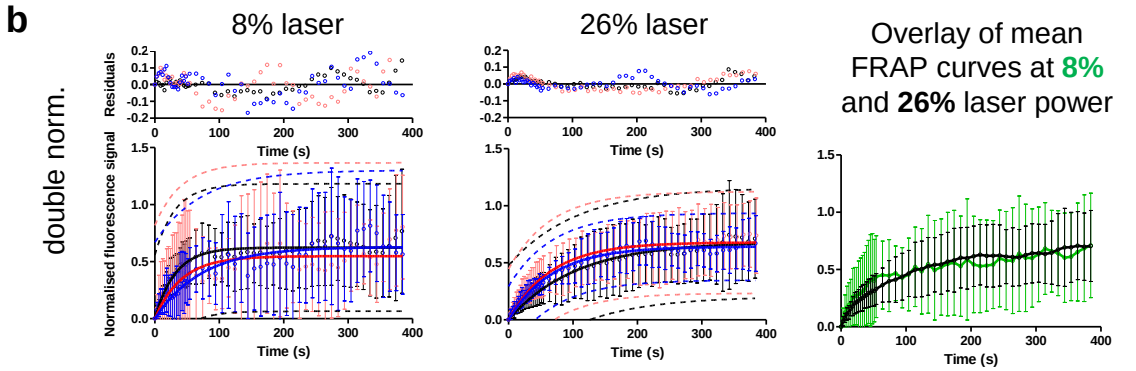

donor	marker	bleach power	Area under mean curve			$t_{1/2}$ (s)			mobile fraction (%)			R^2
			1-decay	bleach	dominance	mean	lower 95% CI	upper 95% CI	mean	lower 95% CI	upper 95% CI	
D2012004	CCR5 (MC5)	8%	101.20	137.90	bleach	21.82	17.69	28.46	62.31	58.98	65.64	0.26
D2013007			78.11 (lin)	127.70	bleach	28.53	19.97	49.88	54.75	48.93	60.56	0.10
D2013008			137.50	92.26	decay	50.37	38.19	73.99	62.94	38.19	73.99	0.22
D2012006	CCR5 (MC5)	26%	62.17 (lin)	142.90	bleach	72.52	62.87	85.67	68.25	64.48	72.03	0.43
D2013001			47.74 (lin)	180.10	bleach	46.06	40.20	53.93	67.87	65.03	70.72	0.44
D2013002			59.85	156.40	bleach	47.43	42.51	53.64	64.21	61.99	66.42	0.64

Figure 5.6.1: Controlling for bleaching artefacts: decay dominance and photo-induced cross-linking. (**a**) MDMs that had been labelled indirectly with MC5 then fixed were subjected to FRAP with bleach laser power at 4%, 8% and 26%. Plots of single normalised data show (●) decay ROI curves and (●) bleach ROI curves. The dominance of decay at lower laser power has the effect of causing apparent recovery in double normalised plots. FRAP was performed on MDMs from two (4%, 8% laser) or three (26% laser) donors but, where fewer than five traces were acquired, each replicate is shown, otherwise mean ± SD is plotted. (**b**) Double normalised recovery curves for FRAP on MDMs labelled indirectly with MC5 and bleached at 8% (**D2012004**, **D2013007**, **D2013008**) or 26% (**D2012006**, **D2013001**, **D2013002**) laser power. Regression curves (solid line), 95% prediction bands (dotted line) and a plot of the mean residuals of the fit for each donor (n = 3) are shown. A plot showing the overall mean curves of all donors at **8%** and **26%** laser power is shown for ease of comparison. All graphs show mean ± SD. Tables below the plots show the values derived from the single and double normalised FRAP curves for each condition. CI, confidence interval; lin, linear regression.

appears to show a slightly faster initial phase of recovery. This profile is reflected in the values calculated from regression: the mean $t_{1/2}$ values of the 8% curve are generally lower, although most of the 95% CIs overlap with those of the 26% curve; the mean mobile fractions of both the 8% and 26% laser powers are similar with the majority of associated CIs overlapping. In addition, FRAP curves were individually fitted as intra-donor variation was high (**Fig. 5.6.2a**). Comparison of $t_{1/2}$ and mobile fractions from individually fitted curves showed no evidence of a statistically significant difference between bleaching with the 8% or the 26% laser powers (**Fig. 5.6.2b**). Thus, there is no evidence that the preferred bleach conditions (26% laser power, 50 iterations) cause abnormalities in the recovery of CCR5.

5.2.6 Summary of FRAP technique development

Testing and minimising sources of error have been critical in being able to extract meaningful photometric data at the low fluorescence levels obtained through labelling endogenous CCR5 on live MDMs. Many steps have been involved in the development process (**Fig. 5.7a**). Cell drift was minimised through testing with PEI, PDL, collagen and CyGel which, ultimately, led to the decision to use collagen-coated coverslips. Microscope hardware was optimised and an indirect labelling technique was used to amplify the signal from CCR5. Intense ruffling and cell movement made attempts to position the bleach ROI on the top face of MDMs futile (**supplemental movie 15**); therefore the bleach ROI was positioned at the side of the cell just above the plane of the coverslip. Different laser powers were tested in live and fixed cells, the latter of which enabled appropriate bleaching conditions to be determined. Experiments with fixed MDMs also gave insight into how the extent of the decay curve can cause apparent recovery. The rapid Arrhenius dissociation of MC5 revealed that the decay curve is multifactorial and informed the start time of FRAP acquisition post-equilibration. As the final bleach conditions were compared to a lower laser power and shown not to cause artefacts in the recovery of CCR5, this final set-up (**Fig. 5.7b**) appears suitable to study the recovery of CCR5 in MDMs.

5.3 Results

5.3.1 Mobile and immobile fractions of CCR5 on the MDM membrane

The fluorescence signal from MDMs labelled indirectly with MC5 Fab^{488} does not recover to the pre-bleach value. Initial indications of this were apparent from the raw FRAP images in which fluorescence in the central region of the membrane in the bleach ROI after recovery appeared to be less than that of the same region at the start of FRAP

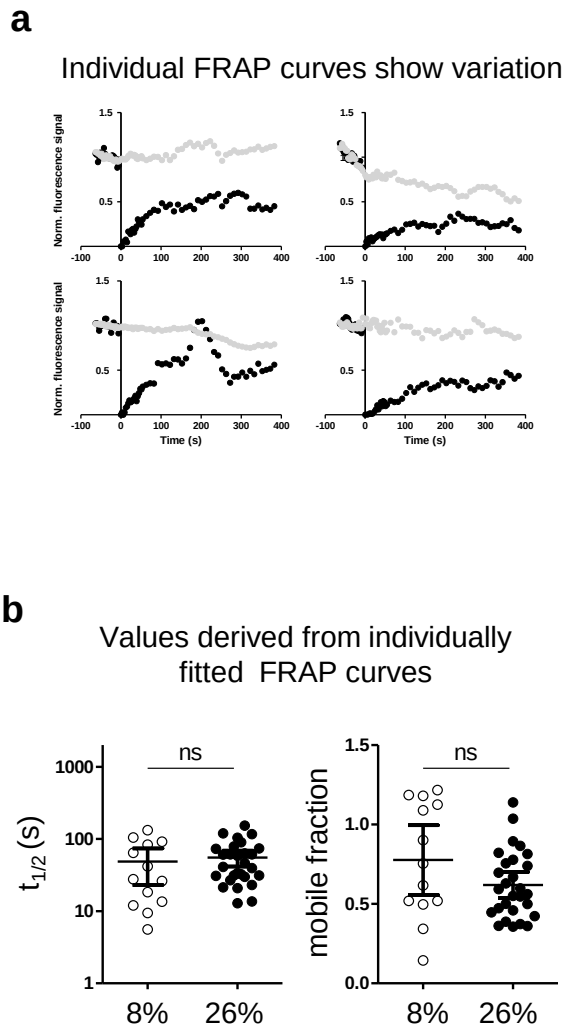

Figure 5.6.2: High level of intra-donor variation in FRAP curves necessitates fitting of individual FRAP curves. MDMs that had been labelled indirectly with MC5 were subjected to FRAP (**a**) Representative single normalised individual recovery curves of cells from a single donor show the variation in (●) decay and (●) bleach ROI curves. (**b**) FRAP was performed with bleach laser powers of 8% or 26%. Each point on the plot shows the $t_{1/2}$ or mobile fraction value derived from an individually fitted double normalised FRAP curve. FRAP curves from three donors were fitted and excluded/included according to the criteria detailed in section 5.1.4. Statistical comparison was performed using an unpaired Student's t-test with Welch's correction. Bars, mean ± 95% confidence interval; ns, not significant.

a

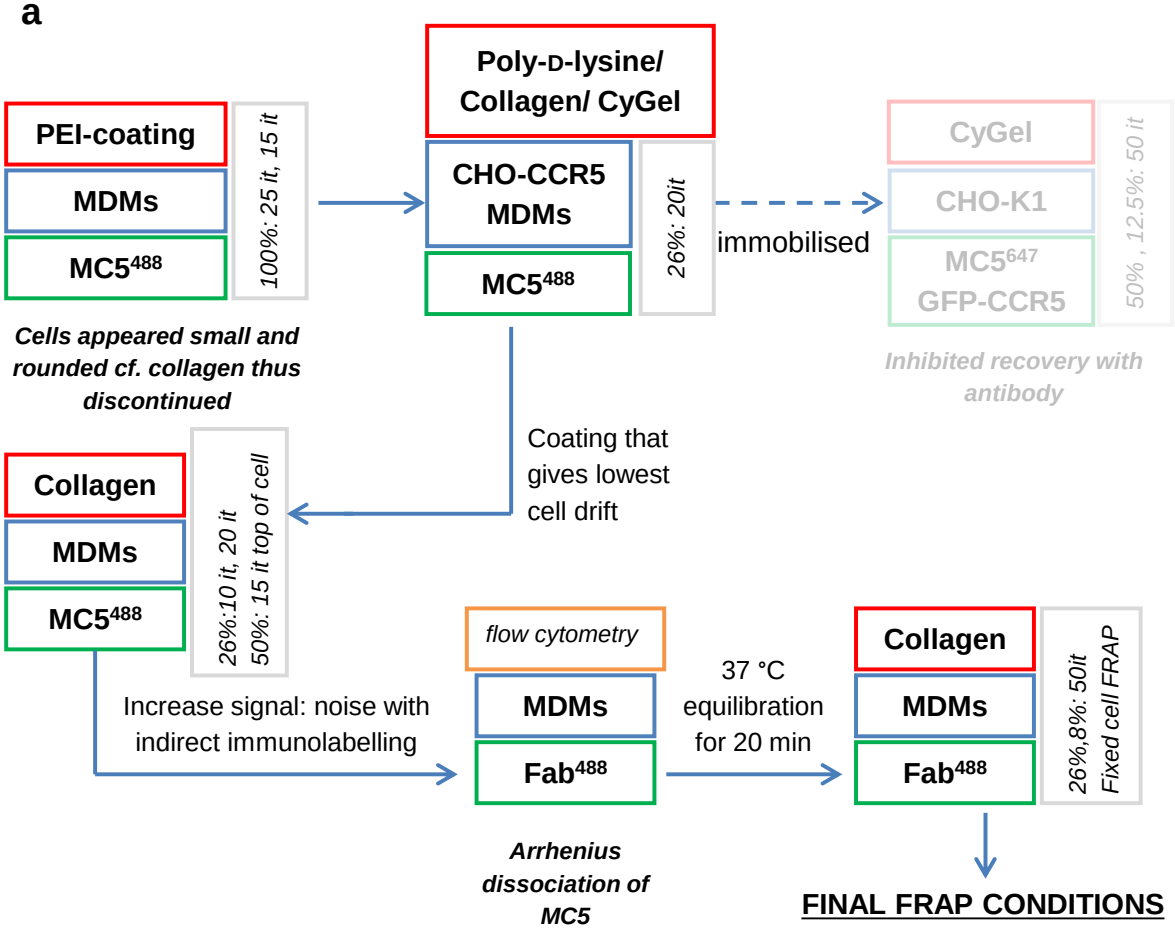

b **Final FRAP conditions:**

	objective	laser (nm)	laser power	iterations	dimensions (µm)
Acquisition	40x/1.1 (water)	488	1.80%	---	106.07 x 106.07
Bleaching			26%	50	10.17 x 3.94

	pinhole	bit depth	pixel dwell	line avg.	gain	offset	cycles	interval
Acquisition	67 µm	12	2.55	1	700	4	72	cycle 1-40: 3 s cycle 41-end: 10 s
Bleaching							after 20	

Figure 5.7: Summary of FRAP technique development leading to final FRAP conditions. (**a**) The flow chart illustrates investigations that have contributed to improvement of the FRAP technique. Developments include: efforts to minimise global cell movement whilst maintaining cell morphology and unperturbed CCR5 recovery; the effectiveness of different bleach positions and higher signal:noise with MC5 Fab^{488} labelling; determining the contributions of decay, the correct bleach depth and controlling for effects of photo-induced cross-linking. Key: coverslip coating, red boxes; cells used, blue boxes; immunolabelling technique, green boxes; bleach conditions explored, grey boxes; it, iterations. (**b**) Table detailing the final FRAP conditions used specifying properties of the total acquisition field and the bleach region.

(**Fig.5.8a; supplemental movie 16**). Indeed, the mean double normalised recovery curve of all donors (n = 5) which, unlike the raw images, takes into account the level of decay, showed that fluorescence intensity does not recover to the pre-bleach value (**Fig. 5.8a**). This indicated that a small proportion of CCR5 at the PM of MDMs was resident as an immobile fraction. Furthermore, even though the profile of recovery curves can vary between donors, no double normalised FRAP curves reached the pre-bleach intensity (**Fig. 5.8b**). This shows that the general conclusion of an immobile fraction of CCR5 is not drawn from an artefact of calculating the mean of curves that completely recover with those that show no recovery. The speed of CCR5 recovery, indicated by the $t_{1/2}$ values derived from regression of double normalised FRAP curves, was highly variant between donors (**Fig. 5.8b**). Even after the exclusion of values from D2012003, in which the decay curve was a dominant factor in recovery, MDMs still appeared to fall into two groups according to their $t_{1/2}$ means and CI overlaps (73 and 86 s vs. 46 and 47 s). Calculating the overall mean of these values would be meaningless as the different speeds of CCR5 recovery may reflect real differences in the regulation and genetic background between donors. In contrast, general trends in the extent of the mobile fraction can be seen, as all donors (bar D2012004) have overlapping CIs. The overall average mobile fraction is 73 ± 10% (mean ± SD) and, therefore, the immobile fraction is estimated to be in the region of 17 – 37%. The presence of an immobile fraction was also supported by tests on MDMs that involved double bleaching. After the initial recovery the original bleach region was bleached again; the second recovery curves often returned to ~100% (data not shown). In the presence of a true immobile fraction, recovery after the second bleach will always be complete or, at the very least, greater than the primary bleach.

Despite the alterations to the FRAP technique that reduced variation, widespread differences were still apparent in the recovery curves of individual cells from a particular donor (**Fig. 5.6.2a**). In order to confirm that some level of recovery of CCR5 occurs on MDMs, raw data points of the bleach and decay ROIs from the first 30 s post-bleach were analysed by linear regression, as detailed in section 2.9.4. The advantage of this method of analysis is that raw data can be used and fluorescence decay is minimal over this time-frame. The runs test was used to determine whether data from the bleach ROI significantly deviated from linearity over this time-frame; for MDMs, 93% of all FRAP curves fulfilled the assumption of linearity. If CCR5 was not mobile over this initial period of time, the gradient of the bleach slope would be expected to be similar to that of the decay or to that of the bleach gradients of fixed MDMs. Results showed that the gradients from the MDM bleach region were all positive (mean gradient, 1.2), whereas the fixed MDM gradients were close to zero and most decay gradients were slightly negative (**Fig. 5.8c**). Generally, this indicates an upward trend in fluorescence within the bleached ROI,

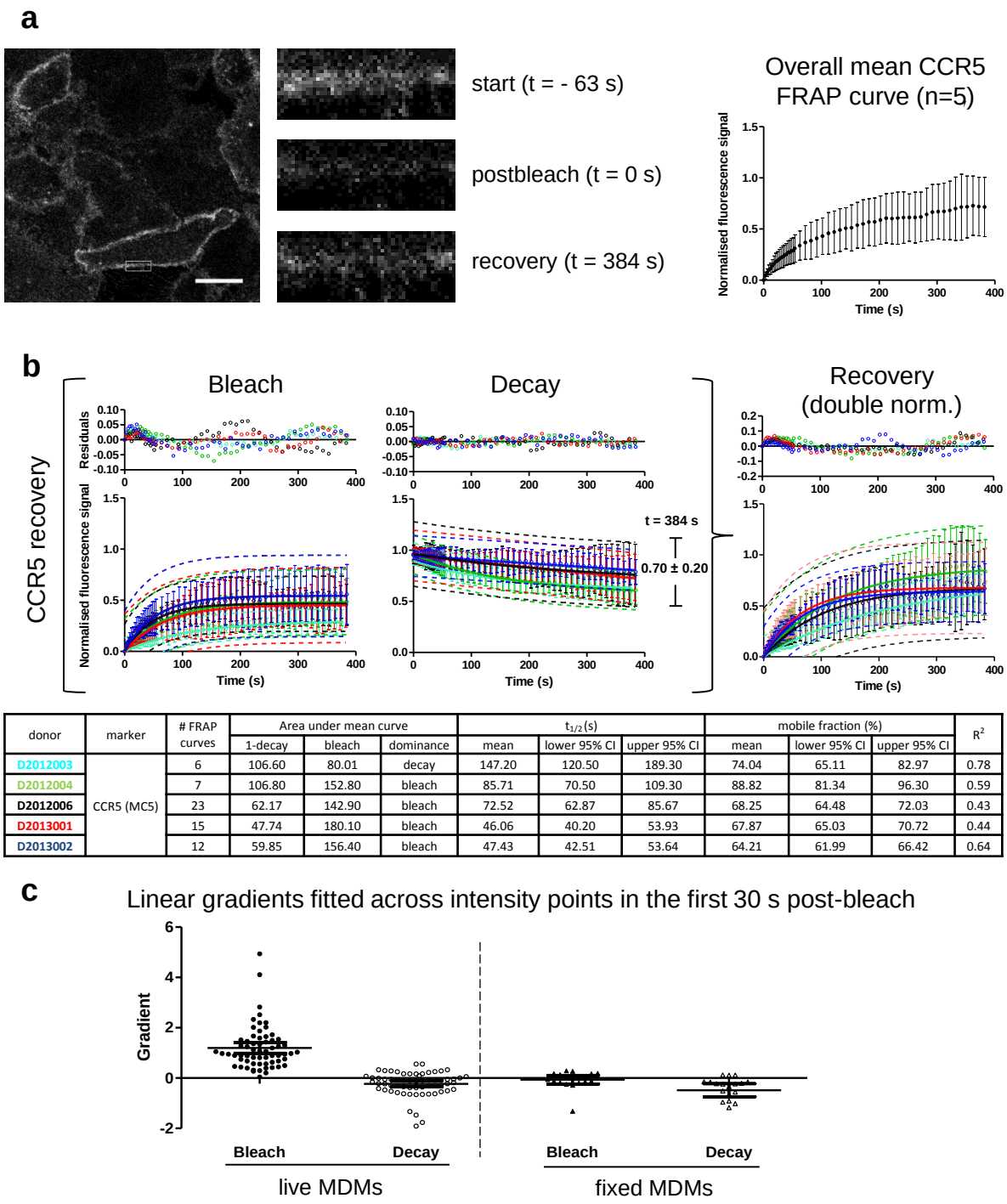

donor	marker	# FRAP curves	Area under mean curve			$t_{1/2}$ (s)			mobile fraction (%)			R^2
			1-decay	bleach	dominance	mean	lower 95% CI	upper 95% CI	mean	lower 95% CI	upper 95% CI	
D2012003	CCR5 (MC5)	6	106.60	80.01	decay	147.20	120.50	189.30	74.04	65.11	82.97	0.78
D2012004		7	106.80	152.80	bleach	85.71	70.50	109.30	88.82	81.34	96.30	0.59
D2012006		23	62.17	142.90	bleach	72.52	62.87	85.67	68.25	64.48	72.03	0.43
D2013001		15	47.74	180.10	bleach	46.06	40.20	53.93	67.87	65.03	70.72	0.44
D2013002		12	59.85	156.40	bleach	47.43	42.51	53.64	64.21	61.99	66.42	0.64

Figure 5.8: An immobile fraction of CCR5 exists on the cell surface of MDMs. MDMs from a total of five donors were labelled indirectly with MC5 followed by Fab^{488} and then subjected to FRAP under final conditions as detailed in **Fig. 5.7b**. (**a**) An example FRAP field and bleach ROI fluorescence at the indicated time-points illustrates that CCR5 recovery is not total. The overall mean FRAP curve was calculated from the mean of the double normalised recovery curves of all donors (n = 5). Graph shows mean ± SD. Scale bar, 20 µm (**b**) Single normalised bleach and decay curves, as well as double normalised recovery curves are presented as the means of all curves acquired each donor (2012003, 2012004, **2012006**, 2013001, 2013002). Regression curves (solid line), 95% prediction bands (dotted line) and a plot of the mean residuals of the fit for each donor are shown. Table of values derived from single (area under curve values) and double ($t_{1/2}$ and mobile fraction values) normalised FRAP curves. (**c**) Short time-frame analysis of ROI intensities acquired from FRAP of live or fixed MDMs labelled with CCR5 and Fab^{488}. Plots show the gradients, calculated by linear regression, of raw fluorescence intensity values from bleach and decay ROIs acquired over the first 30 s after bleaching, as detailed in section 2.9.4.

implying that CCR5 is mobile. Appropriate parametric or non-parametric tests could not be performed as the populations of gradients do not satisfy the assumptions of equal variance (Bartlett's test; P<0.0001). However, when re-analysed without the bleach region gradients, all other populations showed equal variance by the Bartlett's test. This indicates that the variance of the MDM bleach gradients is greater than the variance of the fixed and decay gradients, and highlights how variable the observed recovery is from cell to cell even within this short time-frame.

5.3.2 The recovery of CCR5 compared to DiO

FRAP was performed (using conditions detailed in **Fig. 5.7b**) on MDMs that had been uniformly labelled with the fluorescent lipid analogue DiO (**Fig. 5.9a**). The FRAP recovery curves illustrate that DiO recovered much faster than CCR5 (**Fig. 5.9b**). Means of the $t_{1/2}$ and mobile fractions extracted from regression (**Fig. 5.9b**) are 12 ± 3 s and 85 ± 8%, respectively. Comparing $t_{1/2}$ and mobile fraction values from individually fitted DiO FRAP curves with those from individually fitted CCR5 FRAP curves showed that DiO recovery on MDMs was significantly faster and was associated with a higher mobile fraction than CCR5 (**Fig. 5.9c**).

5.3.3 Effects of cholesterol depletion on MDM cell surface CCR5

5.3.3.1 Effects of MβCD, filipin and U18666A on CCR5 cell surface expression

MDMs were treated with chemical compounds that act to disrupt cholesterol, as detailed in section 2.10.1, and then labelled with antibodies to detect the level of cell surface CCR5. Histograms show that the level of MDM cell surface CCR5 was reduced by treatment with MβCD relative to the levels of CCR5 on control-treated cells (**Fig. 5.10.1a**). A similar decrease in cell surface CCR5 upon MβCD treatment has previously been described for mAb clone 45531 in human CD4+ T cells (Berro et al., 2011). In contrast, neither filipin nor U18666A treatment caused a decrease in cell surface CCR5 relative to respective control-treated samples. On U18666A treatment, a minor decrease in levels of the CCR5 epitope detected by mAb clone 45531 was observed for both donors however, unlike MβCD, the same decrease could not be detected with either MC5 or 2D7. As previously reported, intracellular accumulation of lysobisphosphatidic acid (LBPA) could be visualised by immunofluorescence microscopy in U18666A-treated, but not in control-treated samples (data not shown), thereby showing that treatment was effective (Kobayashi et al., 1999).

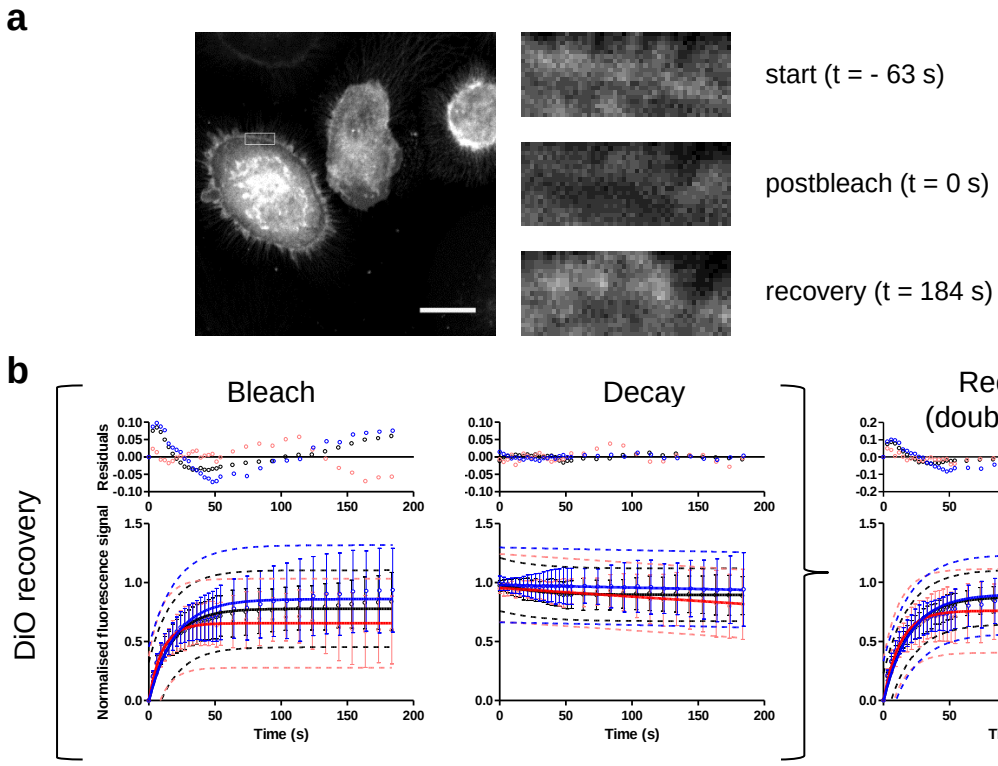

donor	marker	bleach power	Area under mean curve			$t_{1/2}$ (s)			mobile fraction (%)			R^2
			1-decay	bleach	dominance	mean	lower 95% CI	upper 95% CI	mean	lower 95% CI	upper 95% CI	
D2013005	lipid analogue (DiO)	26 %	16.55	130.80	bleach	13.13	12.18	14.25	87.75	85.99	89.52	0.78
D2013006			20.44 (lin)	114.00	bleach	8.67	7.37	10.52	75.95	73.25	78.65	0.50
D2013007			7.32 (lin)	143.30	bleach	13.99	12.44	15.98	90.10	87.11	93.09	0.63
D2012006	CCR5 (MC5)		62.17 (lin)	142.90	bleach	72.52	62.87	85.67	68.25	64.48	72.03	0.43
D2013001			47.74 (lin)	180.10	bleach	46.06	40.20	53.93	67.87	65.03	70.72	0.44
D2013002			59.85	156.40	bleach	47.43	42.51	53.64	64.21	61.99	66.42	0.64

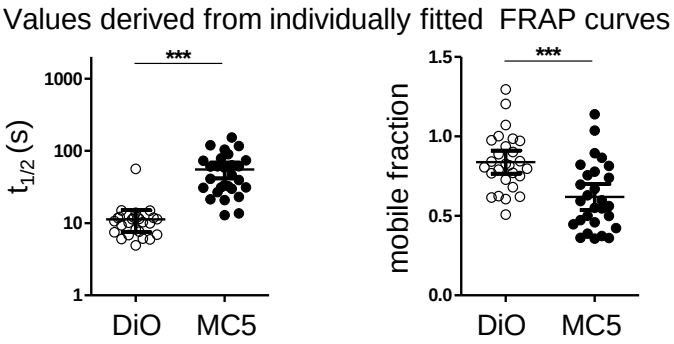

Figure 5.9: Recovery of DiO occurs much faster than CCR5. FRAP was performed on MDMs (n=3) labelled with DiO, as detailed in section 2.8.3. (**a**) Images showing an example FRAP field and bleach ROI fluorescence at the indicated time-points. Scale bar, 20 µm. (**b**) Single normalised bleach and decay curves, as well as double normalised recovery curves presented as the means of all curves acquired each donor (**2013005**, **2013006**, **2013007**). Regression curves (solid line), 95% prediction bands (dotted line) and a plot of the mean residuals of the fit for each donor are shown. Table of values derived from single (area under curve values) and double ($t_{1/2}$ and mobile fraction values) normalised FRAP curves of DiO-labelled MDMs. Comparative values from FRAP of MC5 Fab^{488}-labelled MDMs are also shown (**c**) Plots showing $t_{1/2}$ and mobile fraction values, calculated by individually fitting FRAP curves from three donors, from MC5 Fab^{488} and DiO-labelled MDMs acquired under identical conditions. $t_{1/2}$ values were compared using a Mann-Whitney U-test whilst mobile fraction values were compared using an unpaired Student's t-test. Bars, mean ± 95% confidence interval; ***, P < 0.001.

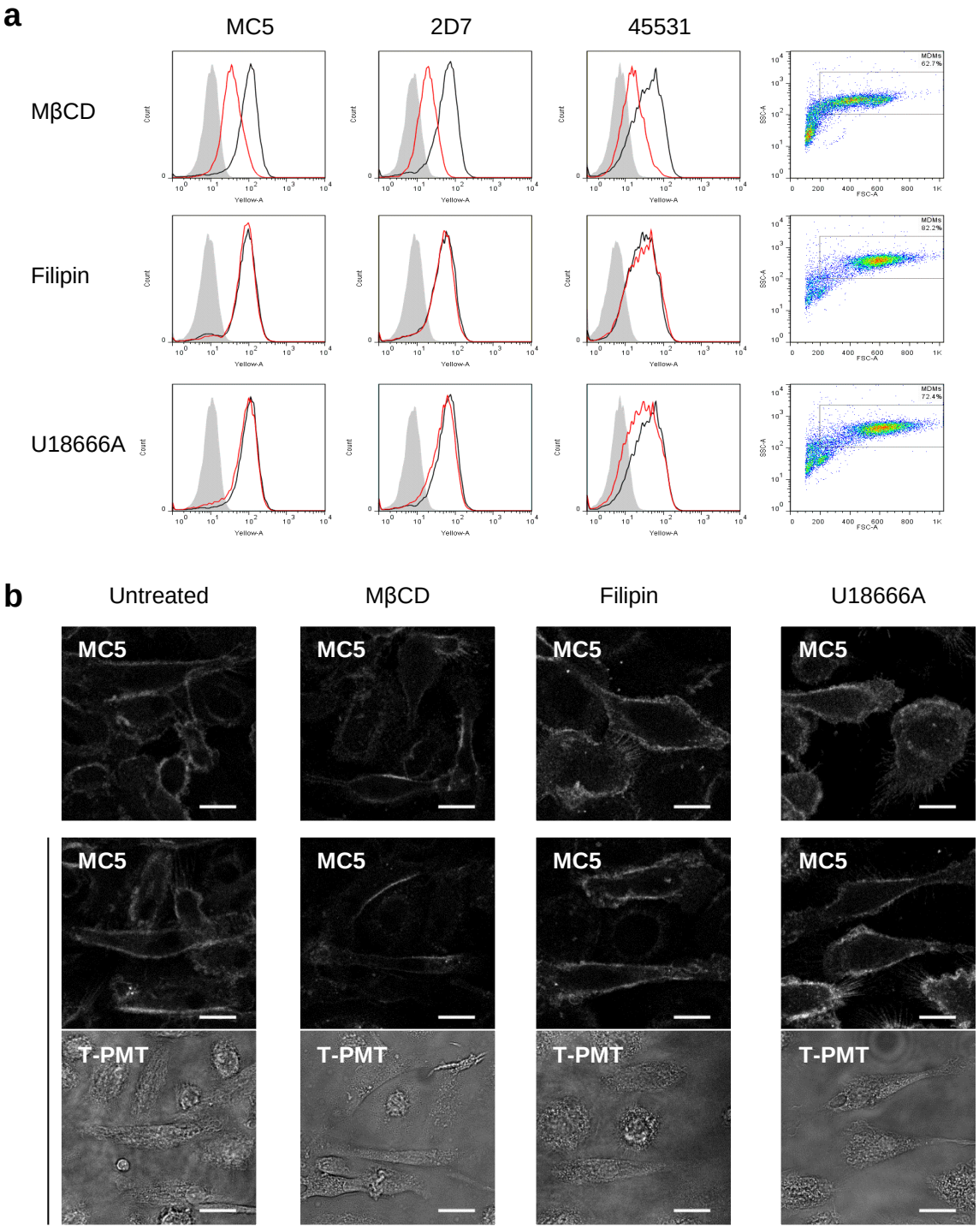

Figure 5.10.1: MβCD treatment decreases cell surface expression and alters the distribution of CCR5. (**a**) MDMs were treated with 10 mM MβCD, 5 µg/mL filipin, 1 µg/mL U18666A or diluent volume-matched controls (PBS, ethanol, and water, respectively). Cells were then labelled with MC5, 2D7, 45531 or isotype controls, fixed and then labelled with secondary GAM-PE. Histograms show the fluorescence of the cell population gated on in the FSC/SSC dot plot and are representative of two donors. Black line, **control-treated cells**; red line, **drug treated cells**; grey fill, relevant **isotype control**. (**b**) MDMs were left untreated or treated with MβCD, filipin, U18666A then labelled with MC5 Fab^{488} for FRAP as described in section 2.10.1. Two representative fluorescence images, one with the concomitant bright-field (T-PMT) image from a single donor are shown for each treatment type. Scale bars, 20 µm.

Even though MβCD caused a decrease in levels of CCR5, the fluorescence signal remained detectable above the isotype control. This lower level of fluorescence was still detectable by microscopy, although the distribution of CCR5 no longer appeared with the same uniformity seen in untreated MDMs (**Fig. 5.10.1b**). On many MDMs the majority of CCR5 staining appeared to be localised to one or two discrete regions of the PM. Thinner lines of fluorescence were also observed in MβCD-treated samples in comparison to untreated cells, which may be connected to the observation that wrinkling and ruffling of the PM seen in bright-field time-sequences were also reduced (**supplemental movies 17 & 18**). By comparison, the U18666A and filipin treated samples exhibited a generally even fluorescence labelling with MC5 (**Fig. 5.10.1b**), very similar to that of the untreated MDMs.

5.3.3.2 Cholesterol influences the mobile fraction of CCR5 on MDMs

Following treatment with MβCD, filipin or U18666A, MDMs were labelled with MC5 Fab^{488} and FRAP was performed under final conditions (**Fig. 5.7b**). Double normalised plots showed similar levels of recovery with untreated, filipin-treated and U18666A-treated cells (**Fig. 5.10.2**). In fact, despite all drugs affecting cholesterol, only MβCD-treatment appeared to have an effect on CCR5 recovery (**Fig. 5.10.2**). The same relationships between treatment and recovery were mirrored in the single normalised bleach recovery profiles. The decay curves for all conditions were remarkably similar; indeed, one-way ANOVA comparison of the 1-decay values for each treatment yielded no significant difference. In contrast the same test revealed a significant difference between areas under the bleach ROI curves that Tukey's post-test showed to be due to the MβCD-treated samples (data not shown). This reinforces that the differences in double-normalised recovery reflect a real increase observed in the intensity of the bleach ROI rather than artefacts that could be introduced from the decay curve.

Mean curves were calculated from all donors for each treatment group. Overlaying each curve with the untreated FRAP curve clearly illustrated the decreased recovery of CCR5 seen with MβCD-treated MDMs (**Fig. 5.10.3a**). By comparison the recovery curve of filipin-treated MDMs appeared to be only slightly lower (**Fig. 5.10.3a**) and the U18666A-treated MDMs gave a mean FRAP curve that was very similar to the untreated MDM FRAP curve (**Fig. 5.10.3a**). Individual FRAP curves from each donor for each treatment group were fitted and the associated $t_{1/2}$ and mobile fractions were compared between each treatment group. No significant difference was found in the speed ($t_{1/2}$) of CCR5 recovery, however the reduction in the overall mobile fraction as seen in the overlaid FRAP curves was found to be significant (**Fig. 5.10.3b**).

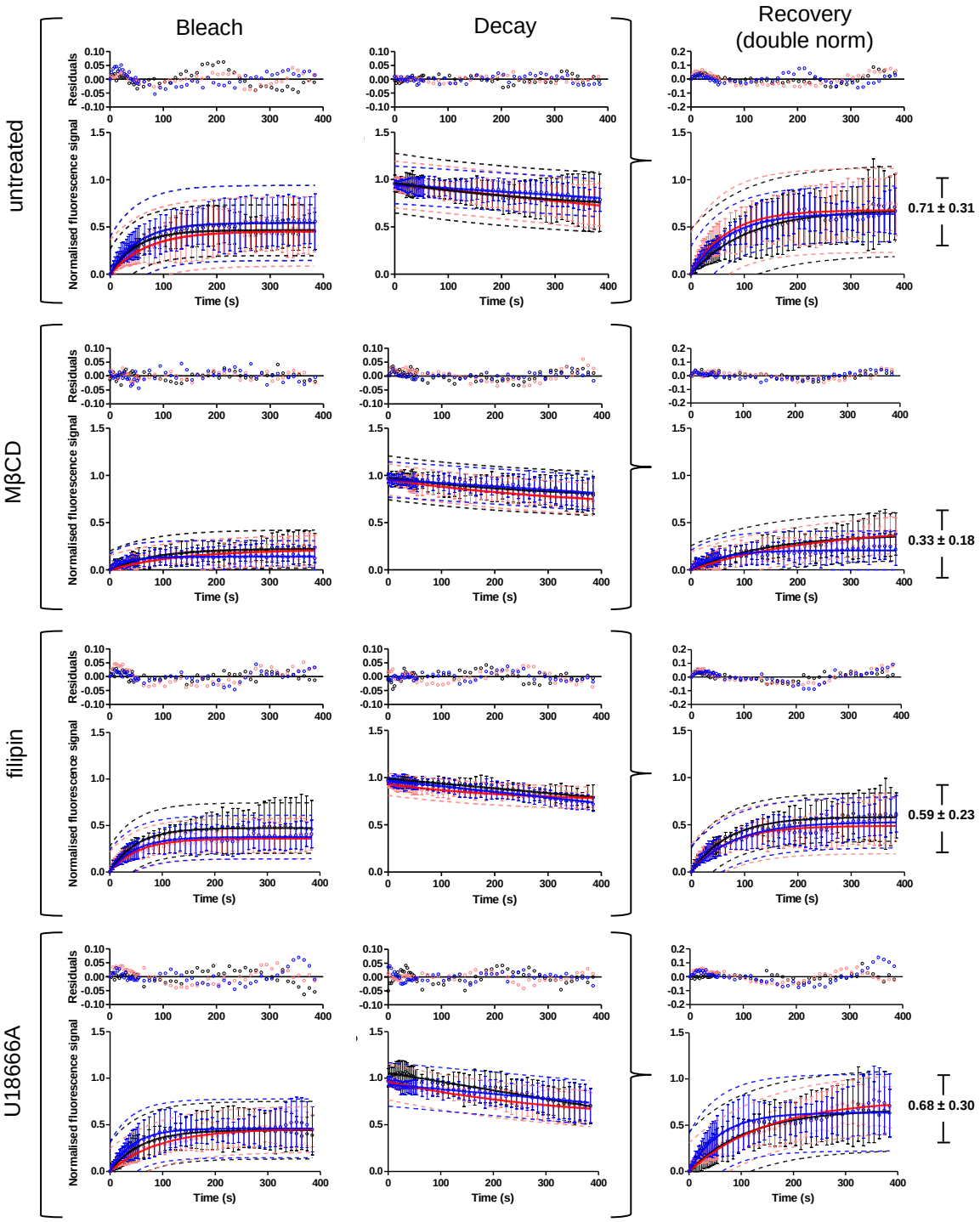

donor	treatment	Area under mean curve			$t_{1/2}$ (s)			mobile fraction (%)			R^2
		1-decay	bleach	dominance	mean	lower 95% CI	upper 95% CI	mean	lower 95% CI	upper 95% CI	
D2012006	untreated	62.17 (lin)	142.90	bleach	72.52	62.87	85.67	68.25	64.48	72.03	0.43
D2013001		47.74 (lin)	180.10	bleach	46.06	40.20	53.93	67.87	65.03	70.72	0.44
D2013002		59.85	156.40	bleach	47.43	42.51	53.64	64.21	61.99	66.42	0.64
D2013001	MβCD	47.51	67.31	bleach	101.20	78.73	141.70	37.37	33.08	42.38	0.42
D2013002		62.88	56.07	equal	161.30	123.00	234.40	45.13	37.24	53.02	0.57
D2013004		43.40 (lin)	49.41	equal	38.83	30.43	53.63	20.62	19.08	22.17	0.23
D2013004	filipin	41.90 (amb)	158.20	bleach	48.20	40.30	59.98	58.36	54.87	61.85	0.65
D2013005		61.78	118.00	bleach	48.38	40.40	60.29	48.93	46.09	51.77	0.47
D2013007		56.18 (amb)	126.20	bleach	55.40	48.28	64.96	52.88	50.47	55.30	0.57
D2013006	U18666A	50.45 (amb)	144.80	bleach	79.38	64.85	102.30	67.44	61.80	73.08	0.49
D2013007		80.39	134.10	bleach	103.50	88.31	125.10	78.01	72.13	83.89	0.67
D2013008		62.58 (lin)	157.60	bleach	41.58	35.45	50.27	63.70	60.65	66.76	0.45

Figure 5.10.2: The effect of cholesterol-disrupting drugs on mobility of CCR5 on MDMs. MDMs seeded in dishes were left untreated or were treated with 10 mM MβCD, 5 µg/mL filipin or

1 µg/mL U18666A, then labelled with MC5 and Fab^{488} and subjected to FRAP under identical conditions, as described in section 2.10.1. Single normalised bleach and decay curves, as well as double normalised recovery curves presented as the means of all curves acquired from each donor. Regression curves (solid line), 95% prediction bands (dotted line) and a plot of the mean residuals of the fit for each donor (n = 3) are shown. The average normalised fluorescence value at the final time-frame is shown on the double normalised recovery plot (mean ± SD). A corresponding table of values derived from single (area under curve values) and double ($t_{1/2}$ and mobile fraction values) normalised FRAP curves of untreated, MβCD, filipin and U18666A-treated MDMs is shown below. lin, linear fit; amb, ambiguous fit; CI, confidence interval.

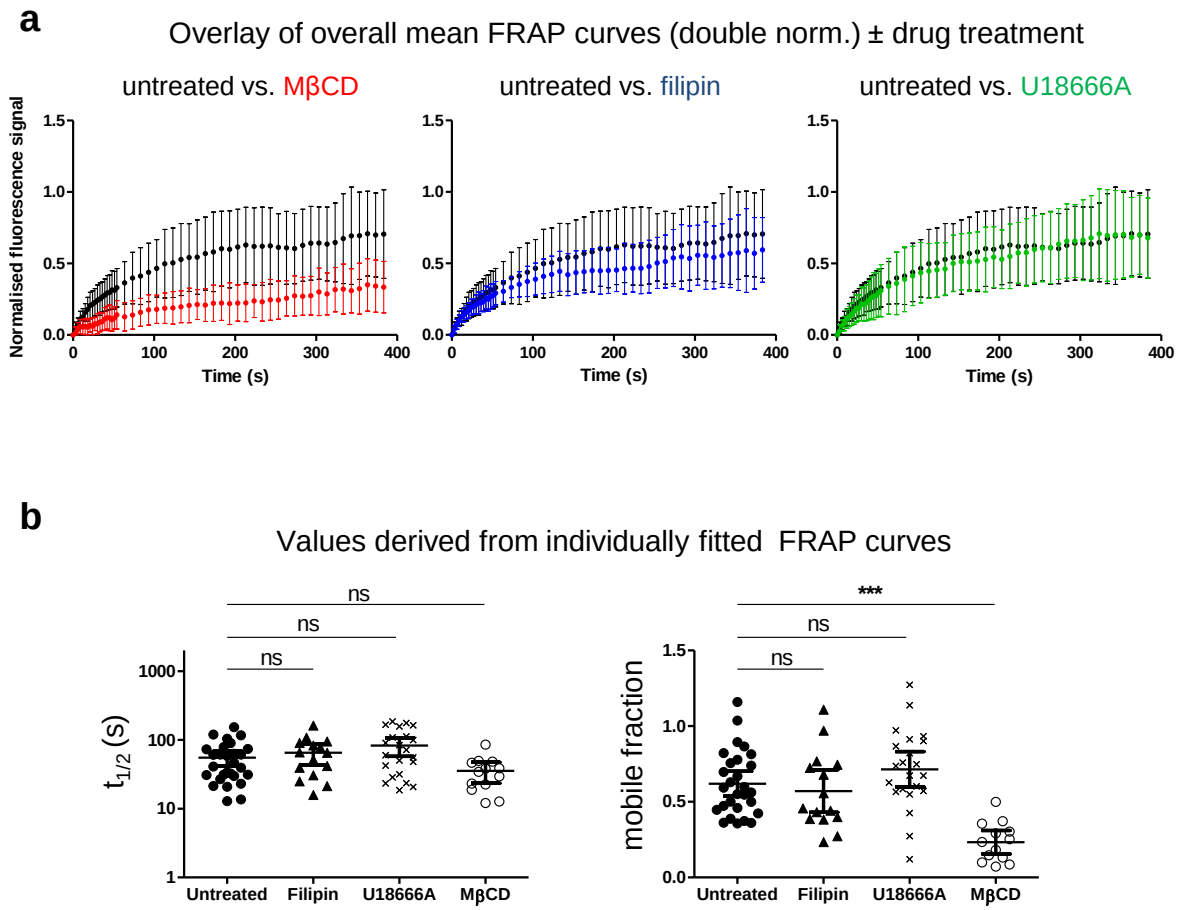

Figure 5.10.3: MβCD treatment causes a significant decrease in the mobile fraction of cell surface CCR5 on MDMs. (**a**) The mean FRAP curve of **untreated** MC5 Fab^{488}-labelled MDMs overlaid with the mean FRAP curves of **MβCD-**, **filipin-** or **U18666A**-treated MC5 Fab^{488}-labelled MDMs. Overall mean FRAP curves were calculated from the mean double normalised recovery curves of all donors (n = 3). Graphs show mean ± SD. (**b**) Plots showing $t_{1/2}$ and mobile fraction values, calculated by individually fitting FRAP curves from three donors, according to section 5.1.4, of untreated, filipin, U18666A or MβCD-treated MDMs acquired under identical conditions. Values were compared using a one-way ANOVA and a Tukey post-test. Bars, mean ± 95% confidence interval. ns, non-significant ***, $p < 0.001$.

5.3.4 Recovery of CCR5 on CHO-CCR5 cells vs. MDMs

FRAP was performed on CHO-CCR5 cells that were labelled indirectly with MC5, as described in section 2.8.1. Even though single normalised recovery curves appeared to indicate a higher level of recovery of CCR5 than of MDM, the decay curve for CHO-CCR5 cells was shallower (**Fig. 5.11a**). Consequently double normalised CCR5 recovery curves on CHO-CCR5 cells appeared to be very similar to those of MDMs. Indeed when CHO-CCR5 FRAP curves were individually fitted, the extracted $t_{1/2}$ and mobile fractions showed no significant difference to those of MDMs (**Fig. 5.11b**). Visually the similarity was illustrated by overlaying CHO-CCR5 and MDM mean CCR5 recovery curves (**Fig. 5.11b**). Note that bleaching at a lower laser power also yielded a similar recovery curve, meaning that CCR5 recovery was not perturbed due to photo-induced cross-linking at 26% laser power in CHO-CCR5 cells (data not shown). In general, the recovery of CCR5 on MDMs was analogous to that of CHO-CCR5 cells, indicating that this cell line suitably models CCR5 mobility.

5.3.5 Recovery of antibody-labelled CCR5 compared to GFP-CCR5

MDMs were transfected with one of two CCR5-GFP constructs in which GFP was located at either the N-terminus (GFP-CCR5) or the C-terminus (CCR5-GFP) of CCR5. As expected, successfully transfected MDMs appeared to express CCR5-GFP at the cell surface (**Fig. 5.12a**). FRAP was performed on transfected MDMs in the same way as MC5 Fab^{488}-labelled MDMs according to the method described in section 2.8.1. Single normalised recovery curves of MDMs expressing GFP-CCR5 showed a remarkably quick recovery with little or no decay over the course of analysis (**Fig. 5.12b**). Likewise, FRAP curves from MDMs transfected with CCR5-GFP showed a fast recovery, albeit to a lower final fluorescence level than seen for the GFP-CCR5 construct (**Fig. 5.12b**). This was reflected by the lower mobile fraction values calculated from regression of the double normalised curves for all of the CCR5-GFP FRAP curves, which lie outside of the 95% CIs of the higher values associated with GFP-CCR5. Despite this indication of difference, neither mobile fraction values nor $t_{1/2}$ values derived from individually fitted FRAP curves of MDMs expressing the two constructs were found to be significantly different (**Fig. 5.12c**). Thus, no overall difference between the GFP-CCR5 and the CCR5-GFP constructs was evident. As GFP in the latter construct is thought to mask the C-terminal PDZ recognition motif, this result demonstrates that this motif may not have any bearing on CCR5 mobility in this experimental setting.

Individually fitted FRAP curve $t_{1/2}$ values of MDMs expressing GFP-constructs were also compared with those of MDMs labelled indirectly with MC5 Fab^{488}. The $t_{1/2}$ values of both

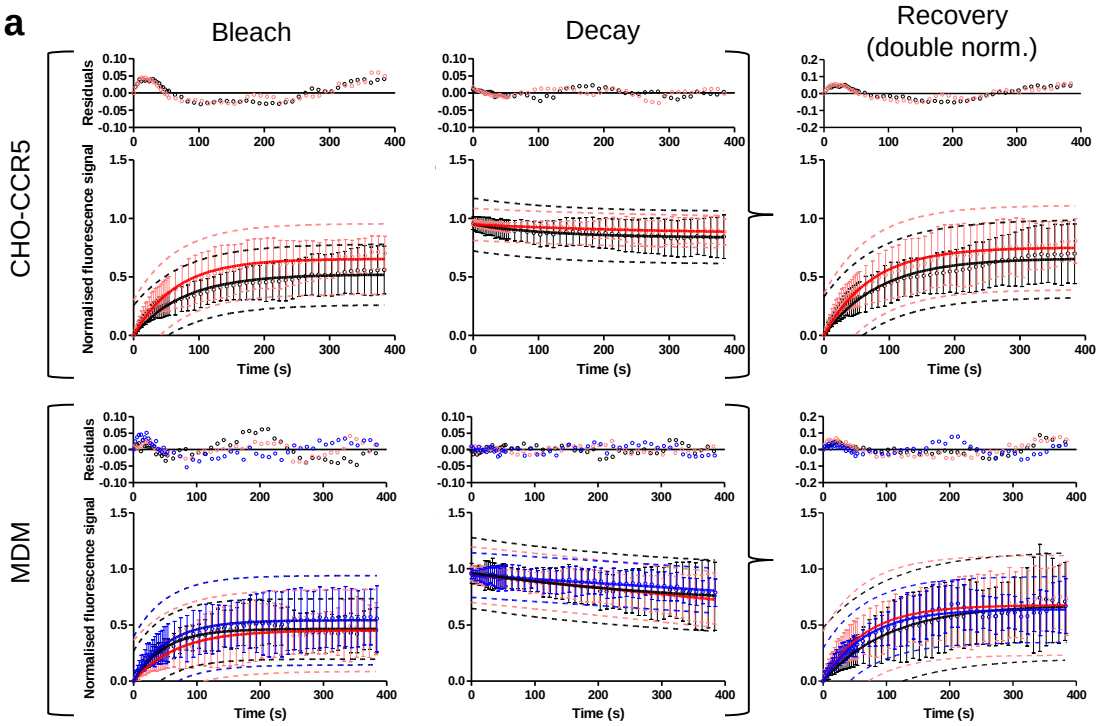

donor	cell type	marker	Area under mean curve			$t_{1/2}$ (s)			mobile fraction (%)			R^2
			1-decay	bleach	dominance	mean	lower 95% CI	upper 95% CI	mean	lower 95% CI	upper 95% CI	
rpt a	CHO-CCR5	CCR5 (MC5)	49.23	160.50	bleach	58.25	52.58	65.30	66.04	63.76	68.32	0.58
rpt b			33.74	209.10	bleach	49.78	43.58	58.03	75.26	72.03	78.49	0.61
D2012006	MDM		62.17 (lin)	142.90	bleach	72.52	62.87	85.67	68.25	64.48	72.03	0.43
D2013001			47.74 (lin)	180.10	bleach	46.06	40.20	53.93	67.87	65.03	70.72	0.44
D2013002			59.85	156.40	bleach	47.43	42.51	53.64	64.21	61.99	66.42	0.64

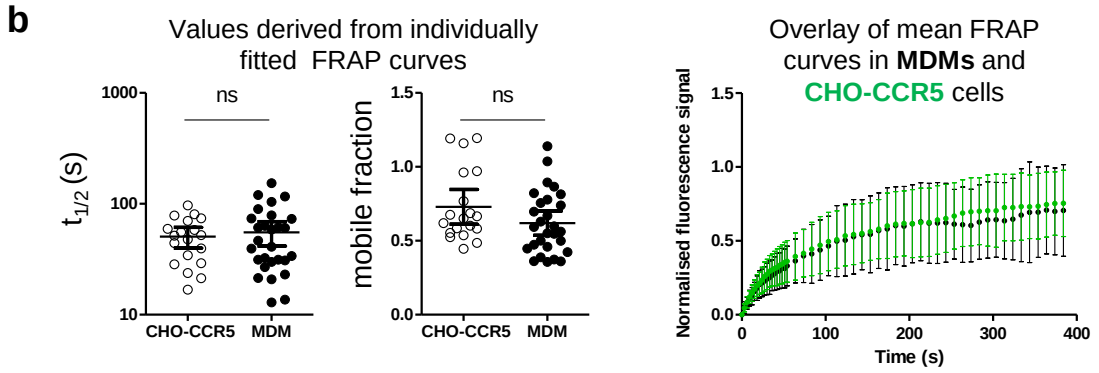

Figure 5.11: CCR5 mobility is similar between CHO-CCR5 cells and MDMs. FRAP was performed on CHO-CCR5 cells labelled with MC5 and Fab^{488}, as described in section 2.8.1, under identical imaging conditions to MDMs. (**a**) Single normalised bleach and decay curves, as well as double normalised recovery curves presented as the means of all FRAP curves acquired for CHO-CCR5 cells on two separate days (**repeat a**, **repeat b**). Data from MDMs are presented in the same format to aid direct comparison (**D2012006**, **D2013001**, **D2013002**). Regression curves (solid line), 95% prediction bands (dotted line) and a plot of the mean residuals of the fit for each donor are shown. A table of values derived from single (area under curve values) and double ($t_{1/2}$ and mobile fraction values) normalised FRAP curves of CHO-CCR5 cells and MDMs is shown below. (**b**) Plots show $t_{1/2}$ and mobile fraction values calculated by individually fitting FRAP curves from MDMs or from CHO-CCR5 cells that were acquired under identical conditions. Values were compared using an unpaired Student's t-test. Bars, mean ± 95% CI. Mean (± SD) FRAP curves from MC5 Fab^{488} labelled **MDMs** and **CHO-CCR5** cells were calculated from the average double normalised recovery curves of all donors (n=3) or days (n=2). CI, confidence interval; ns, non-significant.

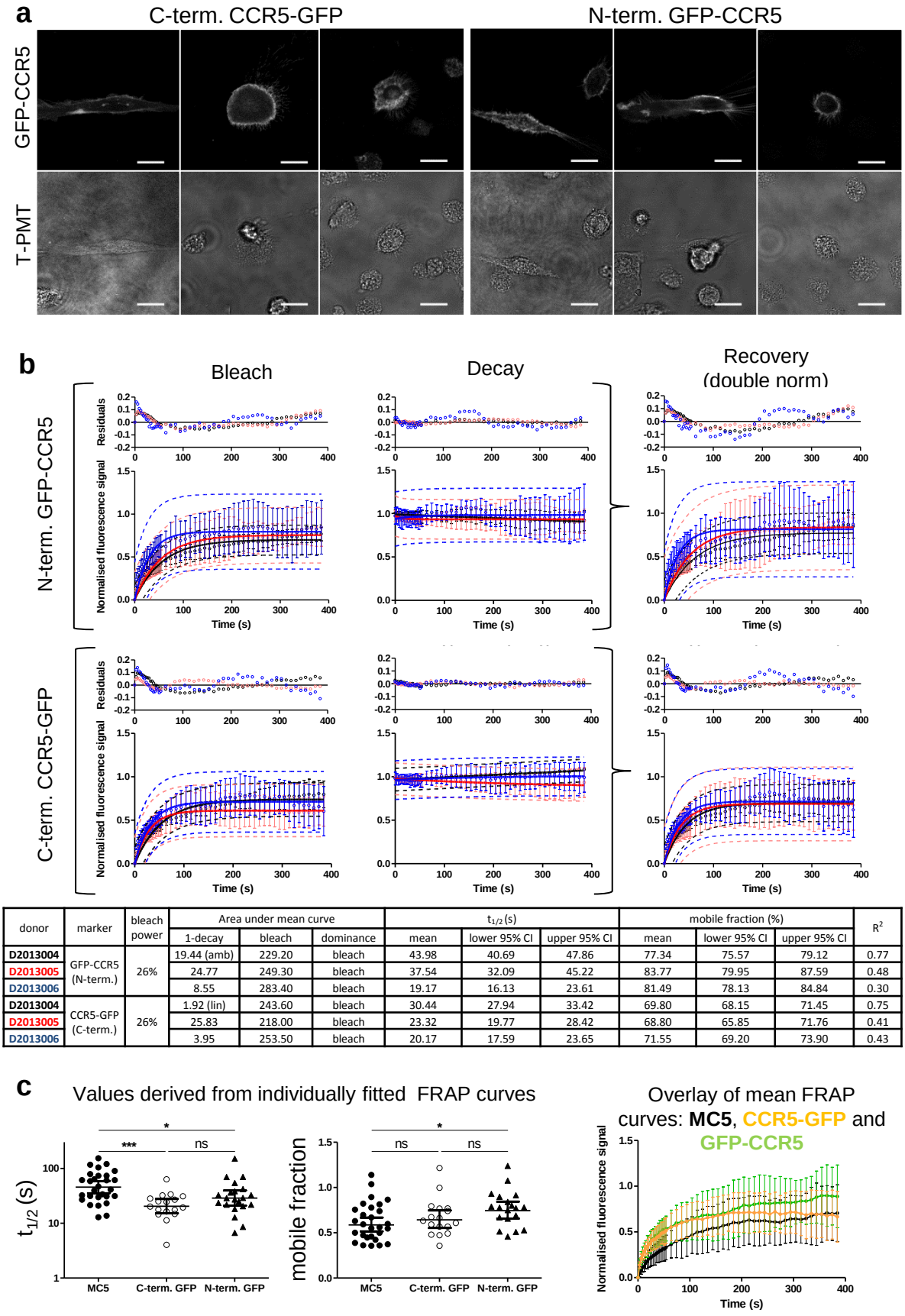

donor	marker	bleach power	Area under mean curve			$t_{1/2}$ (s)			mobile fraction (%)			R^2
			1-decay	bleach	dominance	mean	lower 95% CI	upper 95% CI	mean	lower 95% CI	upper 95% CI	
D2013004	GFP-CCR5 (N-term.)	26%	19.44 (amb)	229.20	bleach	43.98	40.69	47.86	77.34	75.57	79.12	0.77
D2013005			24.77	249.30	bleach	37.54	32.09	45.22	83.77	79.95	87.59	0.48
D2013006			8.55	283.40	bleach	19.17	16.13	23.61	81.49	78.13	84.84	0.30
D2013004	CCR5-GFP (C-term.)	26%	1.92 (lin)	243.60	bleach	30.44	27.94	33.42	69.80	68.15	71.45	0.75
D2013005			25.83	218.00	bleach	23.32	19.77	28.42	68.80	65.85	71.76	0.41
D2013006			3.95	253.50	bleach	20.17	17.59	23.65	71.55	69.20	73.90	0.43

Figure 5.12: MDM CCR5-GFP recovers significantly faster than endogenous CCR5 labelled with MC5 and Fab^{488}. MDMs were transfected with one of two CCR5-GFP constructs in which GFP is located at the C-terminus (CCR5-GFP) or the N-terminus (GFP-CCR5) of CCR5. FRAP was performed on transfected MDMs under conditions identical to those for MC5 Fab^{488}-labelled

MDMs, described previously. (**a**) Three representative fluorescence and bright-field images from each donor (n=3) show the PM expression of both constructs. Scale bars, 20 µm. (**b**) Single normalised bleach and decay curves, as well as double normalised recovery curves presented as means of all curves acquired for each donor (**2013004**, **2013005**, **2013006**) for both GFP-CCR5 and CCR5-GFP. Regression curves (solid line), 95% prediction bands (dotted line) and a plot of the mean residuals of the fit for each donor are shown. The table contains values derived from single (area under curve values) and double ($t_{1/2}$ and mobile fraction values) normalised FRAP curves (**c**) Plots showing $t_{1/2}$ and mobile fraction values, calculated by individually fitting FRAP curves from three donors, according to section 5.1.4, from FRAP of GFP-CCR5 and CCR5-GFP transfected or MC5 Fab^{488}-labelled MDMs acquired under identical conditions. Values were compared using a one-way ANOVA and a Tukey post-test. Bars, mean ± 95% CI. Mean (± SD) FRAP curves calculated from the mean double normalised recovery of all donors (n = 3) of **MC5** Fab^{488}-labelled MDMs, **GFP-CCR5** MDMs and **CCR5-GFP** MDMs. **, $p < 0.01$; ***, $p < 0.001$. lin, linear fit; amb, ambiguous fit; CI, confidence interval; ns, non-significant.

CCR5-GFP chimeras were found to be significantly smaller, signifying a faster recovery compared with the MC5 Fab^{488}-labelled MDMs (**Fig. 5.12c**). In addition, the fraction of mobile CCR5 molecules on MDMs transfected with the GFP-CCR5 construct was significantly greater than that of MC5-labelled MDMs, however the CCR5-GFP mobile fraction was not (**Fig. 5.12c**). Overlay of the mean FRAP curves shows the recovery of both GFP constructs to be similar, albeit diverging slightly at later time points (**Fig. 5.12c**). In contrast, the mean FRAP curve of the MC5-labelled MDMs consistently lies below the GFP-CCR5 recovery curves for most of the FRAP time course. Together these results indicate that the speed of CCR5 mobility in MDMs may be underestimated when using the MC5-labelling technique, perhaps as a direct result of antibody binding, or overestimated when using GFP-tagged CCR5 constructs.

5.4 Discussion

5.4.1 FRAP technique validation

The levels of endogenous CCR5 expressed on the cell surface of MDMs were known to be low at the outset of experimentation. Indeed, a previous report shows that MDMs differentiated in human serum and M-CSF have only 40-80 antibody binding sites for the prototypical anti-CCR5 mAb 2D7 (Lee et al., 1999b). A low level of fluorescence signal is often a problem for FRAP as typical solutions for confocal imaging, such as line averaging or increasing the laser power, can result in loss of dynamic information or high aquisitional bleaching, respectively, leading to systematic errors in FRAP results (Ishikawa-Ankerhold et al., 2012). Therefore other efforts were made to improve the signal. MC5 was found to have higher levels of binding and a greater affinity than 2D7 and CTC5 (**Fig. 5.2**) and was, therefore, deemed the most suitable mAb to label endogenous CCR5 on MDMs for FRAP.

In addition, MC5 was also a good candidate as it recognises a linear epitope that has been mapped to the extreme N-terminus of CCR5 and does not induce oligomerisation as evidenced by BRET (Blanpain et al., 2002). Yet use of MC5, which only recognises the form of CCR5 susceptible to ligand-induced downmodulation means that the FRAP results of the present study only represent one particular antigenic form of CCR5 (Signoret lab, unpublished data). Other forms of endogenous CCR5 may exhibit different mobility.

Conjugating MC5 with a fluorochrome (DyLight^{488}) to a D:P molar ratio of 5.4:1 resulted in a ~30-fold lower affinity and rendered fluorescence levels barely detectable above isotype control levels (**Fig. 5.4b**). In contrast, using an indirect immunolabelling procedure to detect MC5 with a monovalent Fab^{488} secondary yielded much higher fluorescence levels and did not alter the staining pattern. Thus, indirect immunolabelling for FRAP appears to be a useful method to detect low levels of proteins expressed at the cell surface.

In recent years, with the majority of FRAP studies utilising fluorescent proteins to label the molecule of interest, the notion that factors other than aquisitional photobleaching can influence the decay curve has become almost foreign. However, when using antibodies to study the mobility of a protein by FRAP they must be considered as an element that can contribute to the decay because the bound and unbound fractions will tend towards equilibrium. The present study showed that MC5 dissociates rapidly at 37°C compared to 4°C and that this results in a loss of the majority of fluorescence on MDMs after 15 min (**Fig. 5.5**). Thus, FRAP of a labelled sample did not begin until after 20 min at 37°C, after which the rate of loss of total fluorescence due to dissociation was expected to be less than 1% per minute. This gave greater consistency in decay and ensured that the percentage of CCR5 bound with fluorescent antibody was similar for sequential cells subjected to FRAP. Ishihara et al. (1987) also described the rate of decay (0.3%/6 s recovery) when investigating the mobility of the thymocyte/T-lymphocyte surface differentiation antigen (Thy-1) with fluorescently tagged anti-Thy-1 mAbs. They highlighted the need for other FRAP studies to state the levels of dissociation, as rapid dissociation can lead to artificially slow estimations of the diffusion constant (Ishihara et al., 1987). Whilst technological improvements now enable decay ROIs to be acquired simultaneously with bleaching, when using antibodies for FRAP care should be taken that a ROI of the same fluorescence level as the pre-bleach is used to model the decay. Such an approach was taken in the present study because the rate of antibody dissociation was expected to be higher in membrane regions of higher fluorescence/antibody concentration.

To minimise aquisitional photobleaching the image acquisition interval was changed from 3 s throughout, to 3 s for the first 40 cycles then 10 s for the remaining cycles. Despite this theoretical improvement and an appreciation of the MC5 dissociation factor that may

influence decay, the overall level of decay over comparable time-frames (316 s post-bleach) remained similar before ($MC5^{488}$-labelled MDMs on PEI: 0.74 ± 0.19) and after (MC5 Fab^{488}–labelled MDMs on collagen: 0.74 ± 0.16) technique development. This could indicate that other unknown factors are also components of the decay curve or that the technical improvements in the decay may not be apparent between these experimental situations because of the change in the immunolabelling procedure. Indeed, after determination of final imaging parameters (**Fig. 5.6b**) the level of decay was most likely due to factors associated with the immunolabelling procedure rather than the imaging technique. This is apparent from the lack of decay upon FRAP of CCR5-GFP-transfected MDMs (**Fig. 5.12b**).

5.4.2 Considerations for fitting CCR5 recovery

Another major consideration for FRAP is how best to represent the data that have been acquired. Variation in FRAP curves between cells from a single donor was evident (**Fig. 5.6.2a**), which can be caused by differences in the binding properties of proteins during the cell cycle (Phair et al., 2004). To obtain an overview of the mobility of CCR5 within the population of MDMs, the mean of the FRAP curves from each donor was calculated but SD rather than standard error of the mean (SEM) error bars were shown to provide a better representation of variation in the data. Regression of these mean curves, according to a simple exponential rise to maximum, yielded $t_{1/2}$ and mobile fraction values along with 95% CIs that could be compared between donors and experimental settings.

The R^2 value can be used as a measure of how well the curve describes the data. A value of 1.0 indicates that every point will lie along the regression line and a value of 0.0 indicates that the model fits no better than a horizontal line drawn through the data (Motulsky and Christopoulos, 2003). After experiments had been repeated numerous times under the final imaging conditions, R^2 values of regression for data sets composed of ≥10 individual FRAP curves became anticipated to be between 0.4 and 0.6. In comparison, under initial FRAP conditions the R^2 value for the generated data sets was much lower (~0.2; **Fig. 5.3.1a**). This indicates how improvements in the FRAP technique have led to generation of photometric data that can be more accurately described by the single exponential rise to maximum model.

The replicates test for lack of fit indicated that the single exponential rise to maximum model (section 2.9.3: Equation 5) was adequate, however, residuals were not found to be normally distributed, which is visually reflected by the fact that the majority of mean residuals at early time points are positive. This may indicate that the data do not fulfil the Gaussian assumptions of regression. To remedy this the data could be fit with a different

model, weighting applied, or outliers removed (Motulsky and Christopoulos, 2003). However, changing the model to a double exponential did not improve the fit according to R^2, nor yield normally distributed residuals according to D'Agostino's test. Further, weighting is not appropriate for use with normalised data, which is utilised in the present study (Motulsky and Christopoulos, 2003). Outliers can have an effect on fitting because of the underestimation of their occurrence by Gaussian distribution (cf. Poisson) (Press, 2007). Nevertheless, discrimination of outliers using the ROUT method (Motulsky and Brown, 2006) and subsequent removal from the data sets did not result in normality of residuals after fitting. Given the number of replicates acquired in the present study, other methods to identify outliers could be tested (Motulsky and Brown, 2006) in the future to provide further evidence as to whether outliers are causing the lack of normality seen in residuals. Overall, the least-squares single exponential rise to maximum fit was chosen as the replicates test indicated it was not inadequate and none of the alternatives tested appeared to solve the problem of lack of normality in residuals. Thus $t_{1/2}$ and mobile fraction parameters derived from regression of averaged data are understood to be rough indications rather than absolute values.

All FRAP curves were also 'individually fitted' as described in section 5.4.1. This approach was implemented to show the spread of $t_{1/2}$ and mobile fraction values in order to faithfully represent the range of CCR5 mobility in the cells analysed for all donors. One of the caveats of this approach was that fitting yielded very low 'Gamma-Q' values. These values are probabilities derived from the chi-squared (χ^2) distribution that can be mathematically calculated for the number of degrees of freedom in a particular experiment by subtracting the number of adjustable parameters from the number of data points to be fitted (Press, 2007). The Q probability is designed to indicate the likelihood that the χ^2 value obtained for the fit should exceed a particular χ^2 value by chance (Press, 2007). Values of $Q > 0.1$ indicate a convincing goodness-of-fit of the model but when $Q < 0.001$ the validity of the model is brought into question (Press, 2007).

Several models were applied to the individual FRAP curves, using the FRAPcalc plug-in, to determine whether any one fitted better than the other. The fitting procedures applied were: (A) single-exponential fit for double normalised data; (B) double-exponential fit for double normalised data; (C) single-exponential fit with back multiply normalisation. Details of how the fits are performed as well as the pros and cons of these models are summarised in **Technical Appendix 1a**. All fitting procedures gave similar percentages of FRAP curves associated with $Q < 0.001$ (**Technical Appendix 1b**), which may indicate a number of possibilities: (i) that none of the models tested appropriately describe the data; (ii) that the plug-in, which calculates χ^2 by approximating the SD at each time-point from the variance in intensity over the pre-bleach time, may be underestimating the errors; (iii)

that Gaussian assumptions of the fitting procedure are inappropriate for these FRAP data (Press, 2007). In addition, a number of Q values were found to be very close to 1.0 indicating a perfect fit, the cause of which is commonly attributed to overestimation of error (the opposite of possibility (ii) above) (Press, 2007).

Given the variability in the individual FRAP curves it is quite likely that χ^2 has been misrepresented by the program's estimations. For this reason the related Q value was not used as a measure of goodness-of-fit. Instead a single-exponential fit of double normalised data was chosen on the basis that this model was not found to be inadequate on averaged data. Despite the fact that this may oversimplify the parameters of recovery, no current evidence exists that suggests steady state mobility of CCR5 on MDMs is multiphasic. Ultimately this approach may not have modelled the data to the best degree but it has enabled a relatively unbiased estimation of the mobile fraction, which needs to be known to calculate $t_{1/2}$, so that these values can be used for comparison between drug treatments etc. Mobile fraction and $t_{1/2}$ values from individually fitted FRAP curves, therefore, supplement the rough indications given by regression of averaged data. A possible direction for future analysis would be to avoid fitting a model altogether and simply use the mode fluorescence value in the recovery curve as an estimation of the mobile fraction then use this to approximate the $t_{1/2}$ directly from the unfitted curve.

5.4.3 Influences of MDM mobility and PM topology

Cell migration and shape change are well documented phenomena that cause undesirable variations in intensity (Klein and Waharte, 2010). Investigations into adhesion and movement on different coverslip coatings were carried out in order to minimise these problems. MDMs were more spread (flattened shape) on collagen than on PEI (**Fig. 5.3.1b**), making the former coating more desirable. In addition, seeding MDMs on collagen was shown to be preferable to seeding on PDL which showed a higher cell drift (migration) (**Fig. 5.3.2b**). Therefore the collagen-coating was the best option to limit the mobility of MDMs. Even so, many MDMs still exhibited a degree of mobility and change in shape over the course of FRAP (**supplemental movie 17**), which may have contributed to variation in the data. Moreover, MDMs have recently been demonstrated to have complex, stable (present for over one hour) membrane domains called intracellular plasma-membrane connected compartments (IPMCs) (Mlcochova et al., 2013). FRAP of MDMs transfected with a GFP-tagged phospholipase Cδ pleckstrin homology domain (PH-GFP) showed that the mobility was comparable in the IPMCs and the PM, whilst fluorescence loss in photobleaching was used to show that PH-GFP exchanges between these compartments (Mlcochova et al., 2013). Combined with the notion that leukocyte ruffles are thought to double the spherical surface area of the cell (King, 2004), the

presence of IPMCs further convolutes the MDM membrane and, thus, the pathway of PM constituents, such as proteins and lipids. Accordingly, microscope measurements of CCR5 mobility will be influenced by topological features, particularly if CCR5 does in fact exist in clusters on MDM microvilli (Singer et al., 2001) or tetraspanin enrichment in IPMCs (Deneka et al., 2007) alters the hydrodynamic friction or trapping effects in these compartments. The mobility of soluble GFP in the lumen of the ER was modelled and diffusion coefficients were found to vary by up to 2.5 times, depending on the topology of the ER (Sbalzarini et al., 2005). Given the complex shape and mobility of the MDM PM it is unlikely that recovery observed in the present study is solely due to lateral CCR5 mobility in the PM. Ultimately this is the reason why diffusion coefficients were not calculated as they would misleadingly imply that the mobility measured in MDMs was directly due to CCR5.

Immobilisation of MDMs was achieved using CyGel (**supplemental movie 13**). However, the recovery of MC5-labelled CCR5 was perturbed in CyGel, therefore it was not deemed suitable for use with the labelling technique employed to investigate the mobility of endogenous CCR5 on MDMs. Nonetheless the effects of CyGel at the cell:gel interface were investigated in CHO-K1 cells transfected with CCR5-GFP constructs (CHO-K1.CCR5-GFP cells). Similarly to the MDMs, when CHO-K1.CCR5-GFP cells were labelled with MC5 the mobility of CCR5 was perturbed in the presence of CyGel (**Technical Appendix 2a**). The gel structure of CyGel allows diffusion of small molecules, such as chemokines (8–12 kDa) or cytokines but not of larger macromolecules such as antibodies (~150 kDa) (Roy Edwards, personal communication, 27 November, 2012). To investigate whether the antibody is responsible for immobilisation of CCR5, the mobility of CCR5-GFP or GFP-CCR5 was determined in the presence and absence of CyGel. Both GFP constructs showed recovery in both media and CyGel (**Technical Appendix 2a**), indicating that membrane protein mobility was not barred by the action of CyGel. Moreover, when FRAP was performed in two channels on dual-labelled cells ($MC5^{650}$ and CCR5-GFP) in the presence and absence of CyGel, the presence of $MC5^{650}$ in CyGel was observed to perturb the recovery of the CCR5-GFP (**Technical Appendix 2b**). This directly shows that the inhibition in recovery is due to trapping of the antibody-bound receptor by the CyGel.

Notice that recovery of CCR5-GFP in the presence of CyGel was slower, to a lower level and had less variation than in medium. This could be due to the presence of the gel-meshwork at the cell interface making the pathway of CCR5 movement from one membrane region to the next more tortuous. An interesting alternative hypothesis is that the gel immobilises submicron topological features (e.g. ruffles, wrinkles, protrusions, etc.) that occur on most cells (King, 2004), which could contribute to non-lateral recovery.

Thus, future investigation may show that CyGel has potential use as a tool to distinguish between truly lateral and membrane topology-driven recovery in FRAP.

The mobility of CCR5 on MDMs is slow in comparison to the lipid analogue DiO (**Fig. 5.9c**), however the majority of CCR5 exists as a mobile fraction (73 ± 10%) (**Fig. 5.8a & b**). The positive linear gradients fitted to the early time points post-bleach showed the mobility of CCR5 to be apparent even in raw uncorrected data. This reinforces that the recovery is not simply an artefact of the decay curve. Although the majority of CCR5 exists in the mobile fraction, a small immobile fraction is apparent. This is consistent with a study by Nakata et al. (2010) who showed CCR5 to have a mobile fraction of 84 ± 4.4% which, conversely, indicates that a small fraction of CCR5 is immobile. In the present study, double bleaching further implied the presence of an immobile fraction (Ishikawa-Ankerhold et al., 2012), as a second round of bleaching resulted in recovery that was higher than recovery after the initial bleach. Still, the term 'immobile' only applies to CCR5 over the FRAP time-frame (7–8 min) as a longer time-frame of analysis may show this fraction of CCR5 simply to be slowly exchanging.

5.4.4 Cholesterol depletion of MDMs appears to reduce PM CCR5 levels

Acute cholesterol depletion using MβCD resulted in a reduction in fluorescence levels detected by MC5, 2D7 and 45531 compared to controls (**Fig. 5.10.1a**). A previous study has also reported reduction in 2D7 levels after MβCD treatment (Venkatesan et al., 2003), whilst other reports have indicated that the 45531 and CTC5 epitopes are reduced after hydroxypropyl-β-cyclodextrin (HPCD) treatment (Berro et al., 2011; Nguyen and Taub, 2002). However, in contrast to Venkatesan et al. (2003) and the present study, Berro et al. (2011) did not observe a decrease in the 2D7 epitope upon HPCD treatment. Perhaps this relates to the differences between HPCD and MβCD treatment. Kline et al. (2010) directly compared the action of MβCD and HPCD on endothelial cells and, at a concentration of 10 mM, showed a greater level of cholesterol depletion by MβCD but also a higher cytoxicity (Kline et al., 2010). Perhaps more severe cholesterol depletion results in conformational changes in CCR5 that disrupt epitopes recognised by 2D7 and mask the linear MC5 epitope. This hypothesis is consistent with maintained levels of MDM cell surface CCR5 expression upon filipin and U18666A treatment, which sequester or reduce cholesterol rather than remove it from the membrane like MβCD. In contrast to the present study, Venkatesan et al. (2003) showed that filipin treatment reduced cell surface CCR5 expression on transfected HeLa cells. Perhaps this can be explained by the overexpression of CCR5, which may associate with a greater percentage of total PM cholesterol than is required by the lower number of CCR5 molecules on MDMs in order to

achieve correct conformation. Thus a greater proportion of CCR5 might become destabilised upon filipin treatment and unable to bind 2D7 compared to MDMs where cholesterol is in excess. An alternative explanation is the longer treatment of filipin at a higher concentration (10 µg/mL for 30 min) used by Venkatesan et al. (2003).

5.4.5 The differential effects of MβCD, filipin and U18666A

The mobility of CCR5 was significantly reduced upon MβCD treatment of MDMs, seemingly implicating a key role of cholesterol in CCR5 lateral mobility (**Fig. 5.10.3**). Note that the reduction in mobility is due to changes in fluorescence in the bleach ROI rather than being an artefact of differing fluorescence decay. This was shown by comparison of all area under curve values by two-way ANOVA and Tukey post-test, which showed significant differences between MβCD and all other treatments, whilst the same comparison of area under 1-decay curves yielded no significant difference in the decay (data not shown). Previous FRAP studies have described a similar type of decrease in CCR5 mobility upon MβCD treatment (Nakata et al., 2010; Steffens and Hope, 2004). However, simply concluding that cholesterol mediates CCR5 mobility contradicts why little or no reduction in mobility is seen with filipin or U18666A, which also have effects on cholesterol. The solution to these enigmatic results may be found by considering the mechanism of action of each drug.

5.4.5.1 MβCD extracts cholesterol from the PM

MβCD works by directly removing cholesterol from the PM through formation of soluble inclusion complexes with cholesterol (Ivanov, 2008). However, MβCD-treatment has also been reported to have a number of severe side effects, such as disruption of the cortical actin cytoskeleton, of multiple endocytic pathways and activation of Ras (Ivanov, 2008). In particular, adverse effects on the cortical cytoskeleton are likely to impact on topological features of the PM that would affect the result of FRAP. Through studying membrane protrusions, depletion of PM cholesterol content was shown to stiffen the membrane relative to higher cholesterol contents. Yet no such difference was observed when F-actin was disrupted at the same time (Khatibzadeh et al., 2013). This demonstrates how the interplay between the actin cytoskeleton with cholesterol can influence membrane topology. In addition, Kwik et al. (2003) reported that a number of mobile receptors (MHC class I and epidermal growth factor receptor) demonstrated a lower mobile fraction upon cholesterol depletion but they suggested that this was due to cytoskeletal deregulation rather than the properties of lipid rafts. Considered together, removal of cholesterol by MβCD will disrupt cytoskeletal regulation, increase membrane stiffness and reduce the length of membrane protrusions. This may account for the thinner lines of PM

fluorescence (**Fig. 5.10.1b**) and lower degree of membrane wrinkling (**supplemental movie 18**) observed in MβCD-treated MDMs. As MβCD-treatment also lowers the mobile fraction for several other receptors (Kwik et al., 2003) it is unlikely that the mobility of CCR5 is due to unique interactions with cholesterol. Rather, that PM cholesterol is required to maintain the PM dynamics that enable mobility of many membrane components.

5.4.5.2 Filipin sequesters cholesterol in the PM

Filipin acts mechanically on membranes by forming aggregates (~30 nm as measured by freeze-etched electron microscopy (EM) in erythrocyte membranes) that accrue cholesterol (Ivanov, 2008; Tillack and Kinsky, 1973). Under the assumption that CCR5 is tightly associated with cholesterol and considering that no change in the uniform distribution of CCR5 was observed upon filipin treatment, filipin/cholesterol aggregates are unlikely to be greater than the diffraction limit (~200 nm) (Ishikawa-Ankerhold et al., 2012). Due to the nature of oligomer-induced trapping and the fact that larger complexes will experience greater steric hindrance and hydrodynamic frictions (Kusumi et al., 2005) CCR5 in these aggregates would be expected to move slower but would not necessarily be immobile. Such subtle effects of filipin treatment may be reflected by the overall mean recovery curve of CCR5 lying lower than that of untreated MDMs (**Fig. 5.10.3a**). Equally, bundles of cholesterol not associated with CCR5 could slow movement of the receptor. Nevertheless, these differences are not significant in this system and would need to be investigated in a FRAP technique with much less error (e.g using synchronised cell line, GFP-CCR5 and CyGel) or with SPT methods. Note that filipin has also been reported to disrupt links with the actin cytoskeleton (Ivanov, 2008) thus SPT would be the favoured technique as it could also inform on any changes in PM compartment size as a result of drug treatment.

5.4.5.3 U18666A alters the trafficking of cholesterol

Unlike the other drugs, U18666A acts indirectly on cholesterol by inhibiting intracellular trafficking and exit of cholesterol from lysosomes (Cenedella, 2009). Treatment with U18666A has been shown to reduce PM cholesterol levels (Chen et al., 2011; Underwood et al., 1998), however other studies have shown no difference in the cholesterol content of the PM in U18666A treated cells (Appelqvist et al., 2011; Lange et al., 2000). Attempts were made to label U18666A–treated and untreated MDMs with filipin in order to visualise cholesterol levels at the PM but these were unsuccessful. Thus, as it is not certain that cholesterol is depleted in the PM of MDMs, U18666A treatment cannot inform about whether the mobility of CCR5 is dependent upon cholesterol. Nevertheless, as the

dynamics of cholesterol trafficking are known to be altered by U18666A (Cenedella, 2009) the lack of change in CCR5 recovery in U18666A treated vs. untreated MDMs (**Fig. 5.10.3**) shows that the speed of cholesterol replenishment/removal at the PM does not appear to impact CCR5 mobility. Even though U18666A treatment can induce autophagy and apoptosis as side effects (Cenedella, 2009), it is useful as a tool to study cholesterol dependence at the PM. The indirect effects exerted on cholesterol by U18666A make it a useful supplement to cholesterol depletion/sequestration by more direct means (e.g. filipin, nystatin and MβCD) provided that depletion of PM cholesterol is demonstrated.

5.4.6 Cholesterol is important in conferring CCR5 mobility in the PM

Although all three drugs have their side effects, the combined data indicates several effects of disrupting cholesterol with regard to endogenous CCR5 on MDMs. Firstly is that removal of cholesterol from the PM retards receptor mobility, as has been reported before in cell lines (Nakata et al., 2010; Steffens and Hope, 2004) and for other mobile PM receptors (Kwik et al., 2003). Secondly, when cholesterol is present at the PM but is sequestered, the mobility of CCR5 is not significantly slowed. Together this suggests that cholesterol is required to set the stage for CCR5 movement but may not be essential in the actual action of movement *per se*.

5.4.7 Influences of the labelling method

GFP-tagged CCR5 has a faster mobility than MC5 Fab^{488}-labelled CCR5 on MDMs (**Fig. 5.12c**). This difference in mobility between GFP and antibody -labelled CCR5 was also shown in FRAP studies of MC5^{650}-labelled CHO-K1.CCR5-GFP cells. The recovery of the GFP and DyLight^{650} signals after bleaching in the same ROI was found to be different despite the fact that both methods distinguish CCR5 (**Technical Appendix 1b**). This phenomenon cannot be explained by MC5 only recognising the ligand-inducible downmodulating cell surface pool of CCR5 on MDMs because the same results occur in transfected cells, which do not exhibit two pools of CCR5 distinguishable by downmodulation (Signoret lab, unpublished data).

There are a number of technical considerations that may help explain the differences observed between GFP and antibody-based CCR5 labelling methods. The simplest explanation for slower mobility of antibody-labelled CCR5 would be that MC5 stabilises CCR5 dimers and concurrent oligomerisation-induced trapping causes a decrease in lateral mobility of the receptor. However, a previous study used BRET to show that MC5 did not induce receptor dimerization (Blanpain et al., 2002). To confirm the conclusions of Blanpain et al. (2002) and rule out this explanation, FRAP could be performed on CHO-

CCR5 cells labelled with bivalent MC5 or a monovalent MC5 Fab fragment and the speed of recovery compared.

One of the major benefits of the antibody-labelling method is that only the cell surface receptors are identified. In contrast, even though the majority of CCR5-GFP fluorescence is apparent at the PM (**Fig. 5.12a**), *de novo* CCR5-GFP exists in the biosynthetic pathway (ER and trafficking vesicles) (**Fig. 5.13**). Consequently, as long as GFP is folded correctly, CCR5-GFP in non-PM organelles and vesicles will contribute to the fluorescence signal detected by confocal microscopy. Given that the lipid components of the PM differs vastly from that of the ER and other intracellular organelles (van Meer et al., 2008), the mobility of receptors is likely to vary between compartments. If such compartments were unintentionally included in the bleach ROI this could contribute to the faster recovery of CCR5-GFP compared to MC5-labelled CCR5 at the PM.

Another alternative could be differences in trafficking properties of GFP or antibody-bound CCR5. Endogenous CCR5, unlike CXCR4, does not undergo significant levels of internalisation in the absence of ligand (Borroni et al., 2010). Nevertheless there is potential for the CCR5-GFP chimera to exhibit altered trafficking properties due to the masking of a PDZ recognition motif. Indeed, the PDZ-recognition motif of beta-2-adrenergic receptor (β2AR) was found to be important in association of the receptor with actin that mediates an increased cell surface residence time of β2AR in clathrin-coated pits (Puthenveedu and von Zastrow, 2006). However since both GFP constructs showed faster mobility than antibody-labelled CCR5 in the present study, any possible effects of GFP on the PDZ recognition domain cannot explain the increased mobility. With regard to ligand induced internalisation, downmodulation in response to autocrine CCL5 would affect both antibody and GFP-labelled CCR5, although Gomez-Mouton et al. (2004) noted that ligand stimulated CCR5-GFP shows unusually sustained intracellular accumulation. Additionally, MC5-bound CCR5 cannot bind CCL3 or CCL4 (Blanpain et al., 2002), meaning that any autocrine effects of these chemokines may affect GFP chimeras but not antibody-bound CCR5. Overall, differences in chemokine binding and downmodulation might influence MC5-labelled and GFP-labelled CCR5 mobility or loss from the PM, however the extent of these effects are unclear as the level of CCR5 chemokine secretion by MDM during the FRAP procedure is unknown.

Overall, the main proportion of endogenous cell surface CCR5 appears to be mobile on the cell surface of MDMs. The speed of recovery and the mobile percentage of CCR5 on MDMs appear to be similar to that of CCR5 on CHO-CCR5 cells, however the complex topology of MDMs may mean that the true lateral mobility of CCR5 is underestimated. Future work would require single particle techniques (e.g. SPT and SFVI) in combination

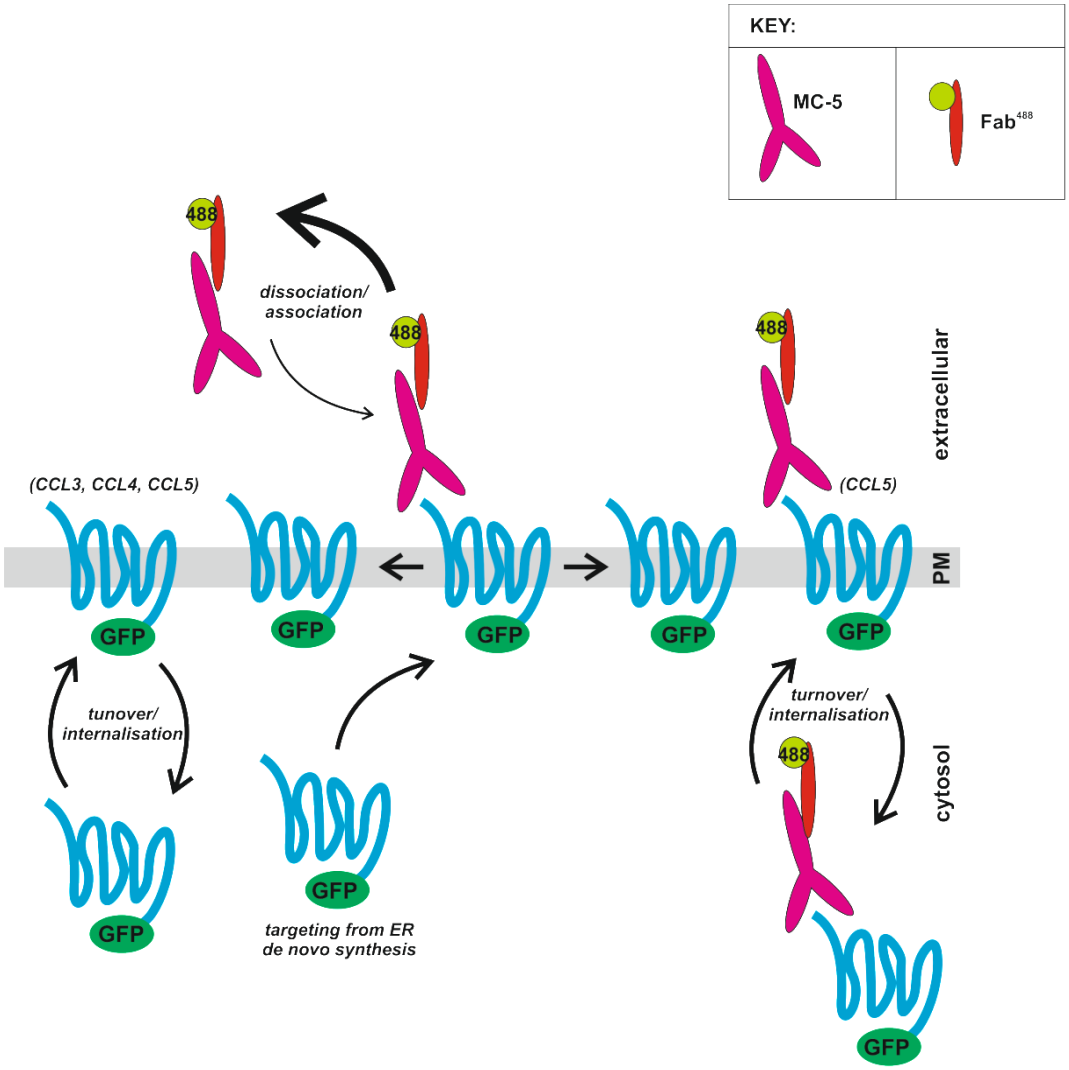

Figure 5.13: Cartoon summarising how antibody or GFP labelling methods can contribute to fluorescence that is perceived to be at the PM. Antibody (indirect labelling with MC5 followed by Fab^{488} that is bound to the PM will both associate and dissociate over the duration of FRAP, although the extent of dissociation is much greater than the extent of association. MC5 bound CCR5 permits binding of CCL5 and ligand-induced internalisation. Similarly the fluorescent signal of CCR5-GFP can also be removed from the PM in response to chemokine binding. Unlike antibody-associated fluorescence a contribution to apparent PM fluorescence within the bleach ROI would also be made from GFP present in the ER. All the indicated events would occur within the bleach ROI but, despite fluorescence (and thus CCR5) subsequently being associated with different cellular compartments, all events are treated as lateral mobility of CCR5 at the PM. This may help explain why GFP-tagged CCR5 can show a faster mobility by FRAP measurements than antibody-labelled CCR5.

with selective illumination of the sample in the plane of the PM only (e.g. using total internal reflection fluorescence microscopy) to supplement this FRAP study and decipher the lateral movement of CCR5. The presence of PM cholesterol was found to be important to enable CCR5 mobility, although cholesterol may not interact directly with CCR5 to facilitate movement. Finally, the labelling method is critical to the measurement of receptor mobility at the PM. Technological advances into ligand-directed covalent labelling may ultimately lead to stable-binding of fluorochromes to endogenous PM proteins (Fujishima et al., 2012). Until such methods become widespread and validated, researchers should use fluorescent proteins or antibodies in confocal FRAP studies with a mindfulness that these tools may over- or underestimate mobility measurements.

a

Process		Model Used		
Normalisation	transform name	**double normalisation** (according to Phair et al., 2004)		**back multiply**
	decay corrected	YES		NO
	data transformed	bleach curve		decay curve
	equation	$I_{frap-norm}(t) = \frac{I_{decay-pre}}{I_{decay}(t) - I_{bkgd}(t)} * \frac{I_{bleach}(t) - I_{bkgd}(t)}{I_{bleach-pre}}$		$I_{decay-norm}(t) = \frac{I_{decay}(t) - I_{bkgd}(t)\frac{I_{bleach-pre}}{I_{decay-pre}}}{I_{bleach-pre} - I_{bleach\ t=0}}$
Extracting parameters for final fitting		none required as $I_{frap-norm}$ will be fitted directly		fitting $I_{decay-norm}$ with exponential decay: $I_{decay-fit}(t) = A_{decay}e^{(\tau_{decay})t} + y_{0\ decay}$ to extract parameters (highlighted in red)
Fitting	fitting name	**single exponential**	**double exponential**	**single exponential**
	curve fitted	double normalised recovery curve ($I_{frap-norm}$)		un-corrected FRAP curve
	equation	$I_{frap}(t) = y_0 + Ae^{-\tau_1 t}$	$I_{frap}(t) = y_0 + A_1e^{-\tau_1 t} + A_2e^{-\tau_2 t}$	$I_{frap}(t) = A(1 - e^{-\tau_1 t})(y_{0\ decay} + A_{decay}e^{-\tau_{decay} t})$
Advantages		simple model that does not assume multiple interactions	better model cf. single exp. if protein of interest interacts with two components	simple model that does not assume multiple interactions
		---	---	un-corrected FRAP curve fitted so no amplification of error my multiplying decay curve therefore higher Gamma-Q
Disadvantages		double normalisation procedure amplifies error by multiplying bleach and recovery values at each timepoint = lowers Gamma-Q		flat or increasing decay curves are designated a horizonal line
		---	may overcomplicate an otherwise simple interaction model (but will still have similar or better goodness of fit)	---

b

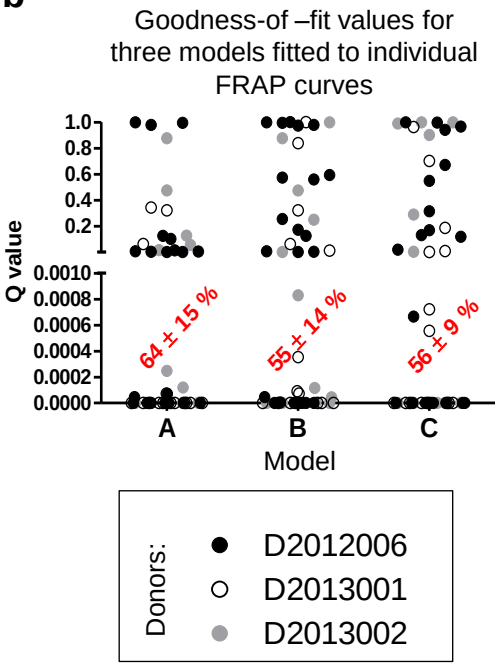

Technical Appendix 1: Details of the normalisation and fitting procedures used and the spread of Q probabilities when fitted to individual FRAP curves. (**a**) Table summarising the normalisation and fitting of FRAP data and advantages/disadvantages of each method, see Figure 1 for description of values used. Data summarised from FRAPcalc manual. (**b**) Spread of Q values when individual FRAP curves were fit with each model : A = double norm. single exponential; B = double norm. double exponential; C = back multiply single exponential. For each model the percentage (± SD) of FRAP curves giving Q<0.001 is shown in red.

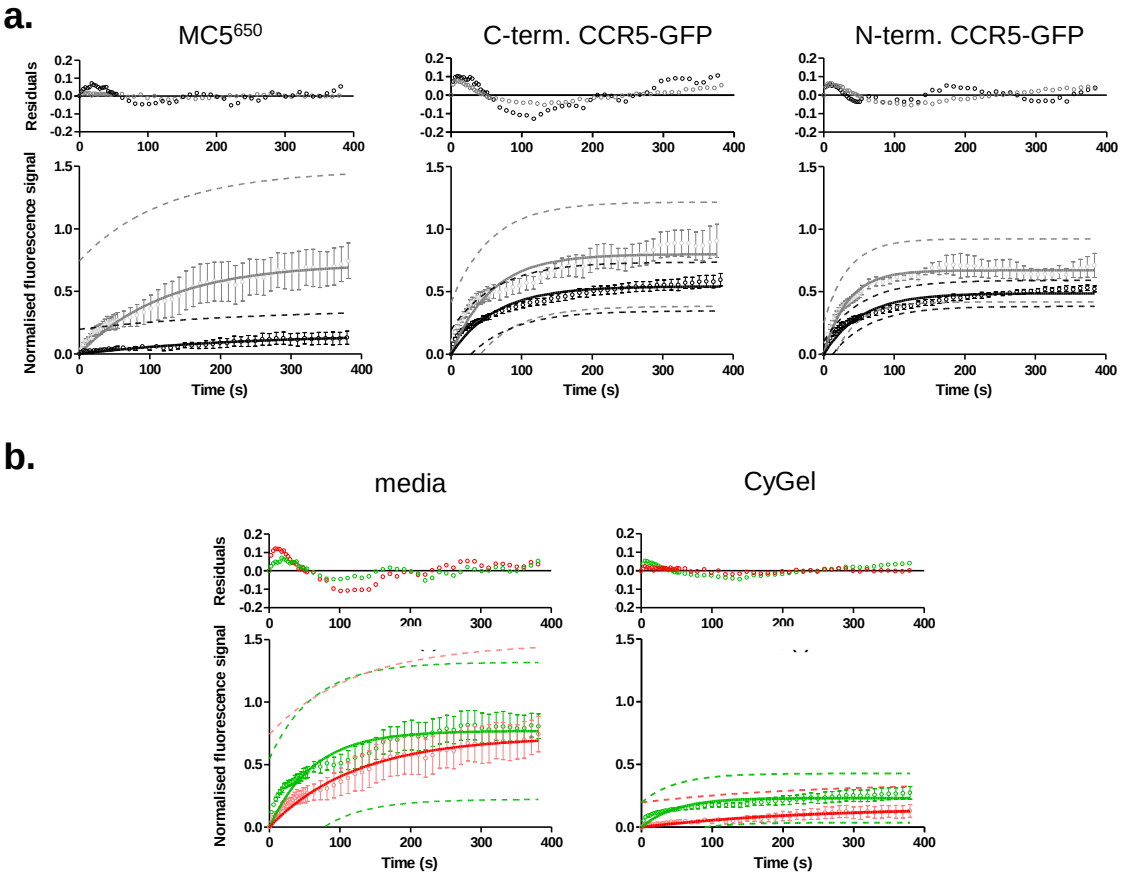

marker	imaging medium	Antibody used	# FRAP curves	Area under mean curve			$t_{1/2}$ (s)			mobile fraction (%)			R^2
				1-decay	bleach	dominance	mean	lower 95% CI	upper 95% CI	mean	lower 95% CI	upper 95% CI	
$MC5^{650}$	media	+	12	1.74	182.40	bleach	84.87	63.01	130.00	72.27	62.46	82.09	0.24
	CyGel	+	12	0.00	35.27	bleach	159.20	88.93	757.80	15.81	8.80	22.81	0.12
GFP-CCR5	media	-	8	11.80	220.60	bleach	23.51	21.07	26.59	67.05	65.23	68.87	0.65
	CyGel	-	5	0.00	164.80	bleach	36.65	33.99	39.76	48.74	47.72	49.75	0.87
CCR5-GFP	media	-	10	33.74	224.10	bleach	39.42	34.58	45.83	80.14	76.83	83.45	0.51
	CyGel	-	11	0.16	174.50	bleach	43.71	39.86	48.38	54.29	52.80	55.78	0.70
	CyGel	+	12	10.30 (lin)	71.93	bleach	33.28	27.79	41.46	23.26	22.05	24.47	0.25

Technical Appendix 2: CyGel strongly inhibits the mobility of MC5-bound CCR5. (**a**) FRAP was performed in either **medium** or **CyGel** on CHO-K1.CCR5-GFP cells labelled with $MC5^{650}$ or CHO-K1.CCR5-GFP cells generating by transfecting in GFP-CCR5 or CCR5-GFP. The fluorescence detected during FRAP was that associated with either the $MC5^{650}$ antibody (left graph), CCR5-GFP (middle graph) or GFP-CCR5 (right graph). (**b**) Dual channel FRAP was performed by simultaneous bleaching and imaging of the far-red fluorescence of **$MC5^{650}$** and the green fluorescence of **CCR5-GFP** when imaging cells in medium or CyGel. Plots show the mean recovery of CCR5 as detected by each fluorescent labelling tool. Graphs show mean ± SEM of experiments repeated on 2-3 separate days and are overlaid with regression curves (solid line), 95% prediction bands (dotted line) and a plot of the mean residuals of the fit. A table summarising values derived from the FRAP curves is shown below the graphs. lin, linear fit; CI, confidence interval.

Chapter 6: General Discussion

The chemokine receptors CCR5 and CXCR4 have been proposed to promote antigen-dependent cell-cell engagement by localising to the IS. Co-expression of CCR5 and CXCR4 occurs on macrophages and on subtypes of CD4+ T cells that primarily circulate in peripheral tissues. In these tissues, macrophages and CD4+ T cells can engage in dynamic antigen-dependent interactions that may involve IS formation. This thesis has considered, for the first time, the formation of an IS between primary human macrophages (MDMs) and CD4+ T cells and whether endogenous CCR5 redistributes to the CD4+ T cell or the macrophage side of this IS. Live cell calcium imaging and flow cytometry techniques were employed to show that sAgs induce the formation of productive MDM-CD4+ T cell conjugates, and to report on the frequency and signalling profiles of engaged CD4+ T cells. A correlative imaging technique identified that MDM-CD4+ T cell IS formation, as judged by CD3-capping, accounts for a subset of the productive conjugates. The presence or absence of CCR5 accumulation on the CD4+ T cell and MDM sides of the synapse, respectively, indicates a difference in the roles of CCR5 on T cells and APCs during synapse formation. This thesis also presents an analysis of the mobility of endogenous CCR5 at the cell surface of MDMs and the influence of cholesterol on its movement, as studied by FRAP. Overall the present study builds upon previous research in murine cells and takes us one step further in our understanding of the diverse nature of macrophage-CD4+ T cell interactions in human cells and how chemokine receptors may contribute to antigen-dependent interactions on either side of this synapse.

6.1 Investigating MDM-CD4+ T cell IS formation with human cells

6.1.1 Synapses and kinapses form between MDMs and CD4+ T cells

In chapters 3 and 4, live and fixed cell microscopy showed that IS formation can occur between primary human MDMs and CD4+ T cells. When high calcium signals were observed they were correlated with CD3 accumulation to the cell-cell interface, which is one of the prototypical markers of IS formation (Monks et al., 1998; Revy et al., 2001; Yokosuka et al., 2008). Additionally, although T cells appeared to be able to ‘arrest’ without demonstrating calcium signalling, the onset of high T cell calcium signalling consistently initiated ‘arrest’. T cells that sustained this calcium signalling maintained their position within the same cell-sized area, displaying a stable engagement with an MDM that is characteristic of IS formation (Dustin, 2009b). Note that in murine systems, stable

macrophage-CD4+ T cell interactions were reported at a low frequency *in vivo* and represented only 10% of the antigen-dependent interactions observed *in vitro* (Egen et al., 2011; Filipe-Santos et al., 2009; Underhill et al., 1999). In these studies the authors found that the vast majority of interactions were transient/dynamic, indicating that kinapses rather than synapses were the predominant type of macrophage-CD4+ T cell interactions. With regards to the present study, in support of kinapse formation correlative imaging suggested that a number of engaged T cells, which exhibited lower calcium signals, were lacking TCR clustering at the cell-cell interface (i.e. no CD3-accumulation). Together these factors might be indicative of a mobile cell-cell junction such as a kinapse (Azar et al., 2010; Beemiller et al., 2012; Kummerow et al., 2009). Typically, cells moving during calcium signalling is a sign of kinapses occurring *in vivo* (Moreau et al., 2012), however in the present study calcium signalling in moving cells was generally not detected. Overall we provide evidence of IS formation in human macrophage-CD4+ T cell interactions and our observations hint that kinapse formation may occur, although the extent of this latter type of interaction remains unknown.

6.1.2 Macrophage-CD4+ T cell interactions: deciding when to be stable

Among productively signalling conjugates, IS formation appears to occur more frequently than previously suggested by the limited occurrence of stable macrophage-CD4+ T cell interactions observed in mice *in vitro* or *in vivo* (Egen et al., 2011; Filipe-Santos et al., 2009; Underhill et al., 1999). A number of factors may contribute to this disparity.

Firstly, the *in vivo* studies found that antigen was presented in limited quantities, unlike the excess of sAg used to pulse MDMs in the present study (Egen et al., 2011; Filipe-Santos et al., 2009). Not only does a paucity of antigen result in fewer T cells exhibiting detectable rises in intracellular calcium (Reay et al., 2000), but lower levels of pMHC have also been correlated to an extended period of dynamic contacts between CD8+ T cells and DCs in lymph nodes (Henrickson et al., 2008). Thus, the mainly dynamic interactions observed *in vivo* are highly likely to be related to antigen availability. Speculatively this may represent a mechanism of immunological control by which CD4+ T cell effector action is limited to macrophages that are chronically infected and presenting greater quantities of antigen. However a different explanation must apply for the *in vitro* interaction studied by Underhill et al. (1999), where macrophages were pulsed with OVA peptide and so antigen is not likely to be limiting. Compared to an antigenic peptide the sAg SEA has previously been shown to be far more potent at inducing high T cell calcium signalling (Luxembourg and Grey, 2002). When compared to OVA pulsed macrophages, one may predict more stable cell-cell interactions in response to sAg considering that higher calcium signals

have been shown to be associated with less T cell mobility (Beemiller et al., 2012). Thus in the future, by titrating down the amount of sAg and/or switching to a peptide antigen to pulse the MDMs a more dynamic CD4+ T cell response repertoire may be achieved.

Secondly, the activation status of the APC can influence whether the antigen-dependent engagement is dynamic or static (Friedl et al., 2005). The IFNγ treatment of macrophages carried out by Underhill et al. (1999) was typical of classical activation (M1). In contrast, the present study generated MDMs by culture in M-CSF yielding an alternatively activated phenotype (M2), in contrast to the GM-CSF/IFNγ/LPS treated MDMs (M1). Perhaps M1 or M2 activation might influence the dynamics or formation of the macrophage-CD4+ T cell IS. This hypothesis is supported by evidence from chapter 4 in which M1 polarised MDMs demonstrated fewer synapses than M2 polarised MDMs. Additionally, a similar phenomenon occurs with other APCs; activated B cells or DCs show far more dynamic interactions with T cells than their naïve counterparts, which generally demonstrate prolonged, stable engagements (Friedl et al., 2005). Further, M1 and M2 polarised MDMs exhibit different chemokine receptor expression profiles (Mantovani et al., 2004), which may in turn affect the stability of the macrophage-CD4+ T cell interaction according to the chemokine hierarchy proposed by Bromley et al. (2000). Specifically, M1 cells show increased secretion of CXCL10, which although controversial (Dar and Knechtle, 2007), may overcome the TCR 'stop' signal and promote mobility (Bromley et al., 2000). In contrast, M2 macrophages are not generally associated with CXCL10 secretion but rather secrete an array of Th2-linked chemokines (Mantovani et al., 2004). Of these, only the action of CCL22 has been considered alongside TCR engagement but was found not to promote mobility over the TCR stop signal (Bromley et al., 2000). In this way the differing chemokine profiles of M2 versus M1 macrophages may promote more dynamic interactions of T cells with M1 macrophages but greater stability with M2 macrophages, a possible explanation as to why more synapses were formed with M2 cells. However this explanation is likely to be incomplete as M1 macrophages have been reported to preferentially secrete CCL3/4/5, which have been suggested to promote stability of the B cell-T cell IS (Mantovani et al., 2004; Molon et al., 2005). According to the distraction hypothesis, this effect is mediated by CCR5 recruitment to the IS (Molon et al., 2005). As chapter 4 suggests, CCR5 can be found to accumulate to the T cell side of the MDM-CD4+ T cell IS, implying that T cell CCR5 may similarly promote engagement in this synapse. Yet it remains unknown whether the recruitment of T cell CCR5 to the MDM-CD4+ T cell IS is mediated by chemokine secretion or via another mechanism, as was the case for TIL-tumour synapses (Franciszkiewicz et al., 2009). Nevertheless the different activation status of a macrophage is likely to contribute to whether a more dynamic or stable interaction can occur. In the future it would be useful to compare the relative

influence of M1 versus M2 macrophages on the mobility of the same population of clonal T cells in order to determine this relationship directly.

6.1.3 When would a stable macrophage-CD4+ T cell interaction be appropriate?

Macrophages typically integrate signals from interactions with resting or activated T cells, after they have been primed by DCs in lymph nodes (Biswas and Mantovani, 2010; Murphy et al., 2011). The different T cell effector functions of a T cell may dictate whether a synapse or a kinapse is formed. For example the gasket ring of actin formed in a stable IS with CTLs is thought to facilitate targeted secretion of lytic granules (Griffiths et al., 2010). On this basis a stable IS with an annular arrangement of actin can be imagined to assist CD4+ T cells to specifically instruct the activity of macrophages via cytokines such as IL-10 or IFNγ, which have been shown to be directionally secreted (Huse et al., 2006; Huse et al., 2008). On the other hand, a mobile junction makes teleological sense for effector action of other cytokines that show multidirectional secretion patterns such as IL-4 (Huse et al., 2006).

6.1.4 Calcium signalling

Chapter 3 demonstrates that a wide range of T cell intracellular calcium signals are induced in response to sAg-pulsed MDMs. This contrasts the fairly consistent, sustained calcium responses described for antigen-specific systems using clonal T cells (Wülfing et al., 1997), highlighting that the variation in calcium profiles likely comes from the use of a polyclonal T cell population being stimulated by a number of sAgs. There is potential that these calcium signals can result in selective activation of different transcription factors and thus influence the activation status or effector function of the T cells (Acuto et al., 2008; Dolmetsch et al., 1997). When calcium profiles were visually classified into groups, those that were high and sustained tended to correlate with IS formation which is consistent with the fact that stable contact yields sustained calcium signals *in vitro* (Negulescu et al., 1996). A recent report suggests that T cells are associated with oscillatory, rather than high, sustained calcium responses when contacting APCs (Salles et al., 2013). The T cell calcium profiles in the present study do not tend to support this hypothesis but rather demonstrate the presence of both high and low, sustained calcium rises, more than oscillatory profiles. Perhaps one of the reasons for this disparity is the analysis of naïve T cells by Salles et al. (2013), which have previously been demonstrated to undergo oscillatory signals that appear contact-independent and are maintained in the background of elevated baseline calcium signals even upon stable conjugate formation (Wei et al., 2007). Nevertheless this highlights that any future automated strategies to group similar

calcium profiles may need to be able to describe the oscillations as well as account for the general shape of the calcium response.

6.2 Chemokine receptor distribution at the MDM-CD4+ T cell IS

6.2.1 Factors triggering differential recruitment to the IS

Chapter 4 shows that endogenous CCR5 does not localise to the MDM side of the MDM-CD4+ T cell IS, but can localise to the T cell side. Evidently differences may exist in the way that CCR5 is regulated on the T cell or APC, which determines whether or not CCR5 is involved at the IS. Previously, recruitment of CCR5 to the IS has been suggested to be mediated by CD103 binding of E-cadherin (Franciszkiewicz et al., 2009), or via APC-secreted chemokine, possibly acting on a CCR5:CXCR4 heterodimer (Contento et al., 2008; Molon et al., 2005). Multidirectional secretion of chemokines by the MDM could act uniformly in an autocrine fashion on CCR5 present on the MDM cell surface, whilst simultaneously imposing a gradient on nearby, interacting T cells expressing CCR5. In the presence of a chemokine gradient CCR5 has been suggested to localise to the leading edge of T cells (Gomez-Mouton et al., 2004). Additionally, evidence from the B-T cell IS shows that if CCL5 or CXCL12 are present in the environment during IS formation then T cell CCR5 does not localise to the IS (Contento et al., 2008). This implies that without sensing a chemokine gradient CCR5 would not accumulate to the IS.

Expression of CD103 is not typically associated with macrophages but rather with T regulatory cells (Tregs) (Suffia et al., 2005), a subset of DCs in the small intestine (Zigmond and Jung, 2013), as well as the TILs identified by Franciszkiewicz et al. (2009). Thus the absence of CCR5 localisation to the IS on the MDM side may be related to the lack of CD103 expression on macrophages. Notably however, the ligand of CD103, E-cadherin is known to be a marker of M2 macrophages and so may be expressed by the MDMs (Biswas and Mantovani, 2010). Yet neither the expression of E-cadherin on the M2 MDMs nor CD103 on the CD4+ T cells was assessed in the present study. However recruitment of CCR5 to the T cell side of the MDM-CD4+T cell IS, as shown in chapter 4, could possibly be mediated by CD103+ Tregs, since staining of MDM-CD4+ T cell conjugates for FoxP3 hinted that a number of the synapses formed may involve Tregs (data not shown), but other markers would need to be tested to ascertain Treg involvement (Corthay, 2009).

In order to address why no accumulation of CCR5 was observed on the MDM side of the IS, we investigated whether there was an intrinsic inability of CCR5 to move across the MDM PM. The FRAP study presented in Chapter 5 demonstrated that the majority of endogenous CCR5 is present on MDMs as a mobile fraction in the PM. This is in agreement with the findings of previous studies using cell lines transfected with fluorescent protein-tagged CCR5 (Nakata et al., 2010; Steffens and Hope, 2004). This result implies that the non-accumulation of MDM CCR5 at the IS is not due to pre-existing restrictions on the mobility of CCR5 across the PM. Nevertheless, the organisation of proteins within the PM of MDMs engaged in the IS may be different to that of MDMs not interacting with T cells and this may alter the mobility of CCR5, a possibility that could not be tested in the present experimental system. Using the T cell side of the IS as an example, organisation within the PM is influenced heavily by the cortical actin cytoskeleton. Submicron features such as the dense cortical actin meshwork that emanates from TCR clusters have been found to corral proteins and lipids alike (Kusumi et al., 2005). CCR5 localised to the contact interface is unlikely to be exempt from F-actin mediated corralling and thus the mobility of CCR5 at the IS may be reduced. The influence of actin is particularly relevant to CCR5, which has been shown to accumulate in actin-rich PM structures and can align along actin filaments (Signoret et al., 2005; Steffens and Hope, 2003). It is conceivable that retrograde flow of the cortical actin cytoskeleton at the IS, which influences the centripetal movement of TCR (Dustin et al., 2010; Varma et al., 2006), might also have an influence on the mobility of CCR5 at the IS. As DCs have been reported to accumulate F-actin to the interface upon interaction with CD4+ T cells (Riol-Blanco et al., 2009), the cortical actin cytoskeleton may also play a key role in regulating membrane protein mobility at the APC-side of the synapse. Overall this implies that the mobility of PM CCR5 may differ on MDMs forming an IS, but a system in which the frequency of IS formation is much higher than that used in the present study would be required to test this hypothesis. Although treating MDMs with drugs that disrupt the cytoskeleton is useful to determine contributions of actin to the maintenance of MDM cell structures such as IPCMs (Mlcochova et al., 2013), such processes are unlikely to yield meaningful CCR5 mobility data by FRAP due to artefacts caused by drug-induced MDM detachment.

Lipid rafts are stabilised at the IS and represent dynamic platforms that are associated with actin filaments (Kusumi et al., 2005). It has been proposed that CCR5 associates with lipid rafts (Venkatesan et al., 2003). Since lipid rafts have been found to accumulate on both the T cell side (Burack et al., 2002) and the B cell side (Hiltbold et al., 2003) of the B-T cell IS, they potentially represent part of the mechanism by which CCR5 might become mobilised to either side of the IS. Chapter 5 shows that depletion but not sequestration of

membrane cholesterol, which is a constituent of lipid rafts, modulates the mobility of CCR5. The reduction in CCR5 mobility upon cholesterol depletion (using MβCD) corroborates the results of previous studies (Nakata et al., 2010; Steffens and Hope, 2004). However reduced mobility upon cholesterol depletion is common to a number of receptors and is thought to be caused by general cytoskeletal dysregulation in the absence of cholesterol (Kwik et al., 2003). This situation therefore is not thought to be representative of the spatial accumulation of cholesterol that occurs upon synapse formation. As CCR5 mobility was not significantly decreased when membrane cholesterol was sequestered (using filipin) it implies that the mobility of CCR5 on MDMs does not depend upon cholesterol. This suggests that CCR5 is not constitutively associated with lipid rafts in the PM of MDMs, perhaps unlike T cells on which CCR5 has been shown to cap in a cholesterol-dependent manner upon ligation with CD4-beads (Nguyen et al., 2005). Determining whether or not cholesterol sequestration affects CCR5 mobility on T cells would help to address this issue. However from a technical perspective this is unlikely to be possible at 37°C on activated T cells due to their constant mobility on glass. Instead the temperature could be lowered or resting T cells used in order to reduce the levels of mobility (Negulescu et al., 1996). Nonetheless a direct comparison of CD4+ T cell and MDM endogenous CCR5 mobility would be problematic due to differences in the PM topology of MDMs and CD4+ T cells, and the influence topological changes can have on measures of mobility (Sbalzarini et al., 2005).

6.2.2 Meaning of chemokine receptor localisation at the IS

Endogenous CCR5 and CXCR4 can localise to the T cell side of the MDM-CD4+ T cell IS, as shown in chapter 4, but what might be their function at this interface? Other studies analysing different synapses have suggested the distraction hypothesis, which reasons that in this position chemokine receptors are hidden away from chemotactic cues, which may otherwise distract from the cell-cell engagement (Contento et al., 2008; Franciszkiewicz et al., 2009; Molon et al., 2005). However even when accumulation of CCR5 or CXCR4 at the MDM-CD4+ T cell interface does occur, the fluorescence increase at the IS is generally not greater than two-fold that of the rest of the T cell. This indicates that a significant proportion of chemokine receptors remain distributed around the cell, available to distracting chemokines. Perhaps the level of chemokine receptor accumulation at the IS acts as a ‘rheostat’ that configures resistance of the T cell to distraction by environmental chemokine. Moreover, there is the potential that downstream signalling is altered by spatial segregation at the IS as lipid rafts have been shown to accumulate to the IS (Burack et al., 2002) and certain G proteins preferentially reside in lipid rafts (Oh and Schnitzer, 2001). G_i signalling downstream of chemokine receptors has

been implicated in inside-out activation of LFA-1 that leads to mitochondrial recruitment to the IS (Contento et al., 2010). However it is unknown whether this may be specific to chemokine receptors localised at the IS or globally around the cell. Furthermore, this may be an *in vitro* artefact considering the same effect is also mediated by TCR and that shear-flow has been shown to be required for chemokine-mediated integrin activation (Contento et al., 2010; Woolf et al., 2007). An additional hypothesis for an active functional role of chemokine receptors at the APC-T cell IS is that they may signal via $G_{11/q}$, thereby promoting cell-cell adhesion over chemotaxis (Molon et al., 2005). This is an attractive hypothesis given that the type of lipid domains stabilised at the IS contain caveolin, which is bound by G_q (Oh and Schnitzer, 2001). However it may not be possible to determine the extent of chemokine-receptor induced $G_{11/q}$ signalling using sAg-pulsed APC-T cell conjugates since TCR activation of G_{11} is induced by SEE binding (Bueno et al., 2006). Although Bueno et al. (2006) propose that sAgs may use a GPCR as a coreceptor during TCR triggering, they rule out CCR5 and CXCR4. This is supported by the present study as synapse formation was found to occur irrespective of whether CCR5 or CXCR4 localised to the interface. Without evidence that CCR5 and CXCR4 enhance cell-cell adhesion at the IS, their localisation to the T cell side of the MDM-CD4+ T cell IS is assumed to fit the distraction hypothesis as proposed for other synapses (Franciszkiewicz et al., 2009; Molon et al., 2005).

6.2.3 Chemokine receptor localisation in different states of T cell activation

Evidence in chapter 4 hints that T cell CXCR4 may be more faithfully accumulated to the MDM-CD4+ T cell IS when T cells are activated with CD3/CD28 beads in comparison to PHA/IL-2. As well as having a higher activation status than PHA/IL-2 stimulated CD4+ T cells, the lack of detectable cell surface CCR5 expression on CD3/CD28 activated CD4+ T cells indicates that CXCR4 accumulation to the IS is not necessarily co-dependent upon CCR5. This is in contrast to a previous study, which postulated that the recruitment of CXCR4 to the IS requires the presence of and heterodimerisation with CCR5 (Contento et al., 2008). However recruitment of endogenous CXCR4 to the T-B cell IS has also been shown to be mediated by an actin-binding protein, debrin, in a J77 T cell line (Perez-Martinez et al., 2010). Although a role for CCR5 cannot be excluded in these cells, the parental cell line (Jurkat T cells) has been used as a negative control for CCR5 expression (Shirvani et al., 2011), and shows no CCR5 expression in our hands. Thus, CD4+ T cells may switch to a dectin-dependent mechanism of CXCR4 recruitment to the IS after acute TCR stimulation, enabling recruitment independent from CCR5 cell surface expression. CXCR4 is thought to associate with the TCR to transduce signals in response to CXCL12 binding (Kumar et al., 2006; Patrussi et al., 2007). Specifically, CXCR4 is

thought to associate with pre-formed phosphorylated TCR-ZAP-70 complexes for signalling (Kumar et al., 2006), which may exist at greater levels in T cells that are continuously cultured with TCR stimulating beads and show higher levels of activation than the PHA/IL-2 T cells. Unlike classical TCR stimuli ZAP-70 has been reported not to be activated by sAg (Bueno et al., 2006; Morgan et al., 2001). This could represent a mechanism by which higher, more consistent CXCR4 recruitment to the MDM-CD4+ T cell IS occurs with the CD3/CD28 activated T cells. Moreover it is particularly intriguing that CXCR4 was found colocalising with debrin in the pSMAC, which is a region enriched in TCR-ZAP-70 complexes and actin, both of which CXCR4-TCR signalling depends upon (Dustin et al., 2010; Kumar et al., 2006; Perez-Martinez et al., 2010). Nevertheless, more repetition will need to be carried out in order to confirm this result.

In contrast to the CD3/CD28 activated T cells, the PHA/IL-2 activated T cells are thought to require co-expression of CXCR4 and CCR5, an MDM-secreted chemokine, or CD103 in order to mediate recruitment of CXCR4 and CCR5 to the IS (Contento et al., 2008; Franciszkiewicz et al., 2009; Molon et al., 2005). A mechanism that triggers recruitment is necessary to explain why in our study we observed less than half of the CD4+ T cells forming synapses to accumulate CCR5, and only a quarter to accumulate CXCR4. However pending future investigation, it is unknown what this trigger mechanism might be.

6.2.4 Role of the intracellular pool

In addition to the localisation of CCR5 to the IS on the surface of intact CD4+ T cells, in chapter 4 we also observed accumulation of internal CCR5. These internal pools of CCR5 could be found proximal to the MDM-CD4+ T cell interface even in the absence of IS formation. This type of chance distribution at the cell-cell interface in the absence of antigen was also demonstrated for the Golgi apparatus in the present study and has been reported previously for the MTOC (Meier et al., 2003). In line with previous reports we found that the Golgi was preferentially recruited to the cell-cell interface upon IS formation (Meier et al., 2003; Stinchcombe et al., 2006). The results of the present study show that this also appears to occur for the internal CCR5 pool. Although T cell CCR5 demonstrated more consistent polarisation towards the interface upon IS formation it is unclear whether the intracellular pool of CCR5 results from surface receptors that get internalised, or new CCR5 molecules transported along the biosynthetic pathway towards the cell-cell interface, or both. Partial colocalisation with TGN indicates that these pools of CCR5 are not the same as those identified by Achour et al. (2009), which were thought to reside in the ER. This pool could also result from sustained chemokine stimulation, which has previously been reported to cause accumulation of CCR5 in the TGN (Escola et al., 2010). However the MDMs are primarily of M2 phenotype, an unlikely source of CCR5 ligands

(Mantovani et al., 2004). Thus the origin of the intracellular pool of CCR5 in T cells remains unclear. Nevertheless, trafficking of CCR5 from an internal compartment may contribute to accumulation of surface CCR5 at the IS, whether this is the TGN, or even REs that have been shown to accumulate beneath the plane of the IS and to redirect internalised TCR to the cell-cell interface (Das et al., 2004).

6.3 General limitations of the experimental approach

6.3.1 Number of signalling MDM-CD4+ T cell conjugates

The major assay limitations were that conjugates form at an equal frequency in the presence and absence of sAg and that the numbers of MDM-CD4+ T cell interactions yielding detectable levels of calcium signalling were low. These observations are contrasted by previous reports of the high percentage (95%) of antigen-specific T cells undergoing calcium signals in the presence of cognate pMHC (Wülfing et al., 1997), or the increase in conjugate formation using SEE-pulsed B cells with Jurkat cells expressing Vβ8.1, which is recognised by sAg (Morgan et al., 2001). In both of these studies all T cells have the potential to productively engage MHC. Since there were no indications that the limited frequency of productive conjugate formation was caused by the activation status of the CD4+ T cells or the APCs used in the present study, one may postulate that the majority of the Vβ-regions of the CD4+ T cells were not recognised by the sAgs utilised. However, unless the different T cell activation methods used significantly skewed the distribution of the peripheral blood leukocyte Vβ profile (Geursen et al., 1993; Ochsenreither et al., 2008) this is unlikely to be the case. Nevertheless in the future, one may consider expanding sAg-specific T cells by culturing PBMCs in the presence of sAg followed by negative separation of CD4+ T cells and assessing conjugate formation. However whether these T cells also express CCR5 is another matter, as SEB expansion of CD4+ T cells reveals maximal CCR5 expression after 3 days followed by a rapid decline in expression levels (Maier et al., 2000). Ultimately cell-sorting utilising MC5, which was shown to rapidly dissociate at 37°C in chapter 5, may be required to isolate antigen-specific CCR5+ T cells.

6.2.2 Measuring arrest

One of the main difficulties in deciphering which CD4+ T cells were engaged in synapses or kinapses was that T cells that had not undergone any detectable rises in intracellular calcium were able to undergo ‘arrest’. Initially, the low activation status of PHA/IL-2 T cells was thought to cause this phenotype, since activated, but not resting human T cells

migrate at 37 °C (Negulescu et al., 1996). However CD3/CD28 activated T cells also demonstrated arrest in the absence of any detectable calcium signal (data not shown). Thus the cause of premature arrest may be due to the PDL coating of the coverslip used to promote attachment of the CFDA-SE labelled MDMs. In future work MDMs should be adhered to uncoated glass coverslips to avoid this potential systematic error. Yet as a consequence this meant that it was not possible to utilise the level of T cell mobility in order to identify kinapses, but rather productive signalling concomitant with a lack of molecular clustering (i.e. CD3 capping) was used (Azar et al., 2010).

So that the initial interactions between MDMs and CD4+ T cells could be observed, T cells were injected into the perfusion chamber immediately prior to imaging. Critically this enables early signalling events to be captured, as a rise in intracellular calcium occurs less than 10 s after TCR engagement (Acuto et al., 2008). However use of controlled rate injection, although critical to consistency between assays, means that initially the cells are exposed to shear-flow. Although this flow is not maintained the initial wave of T cells may be subject to a type of chemokine-mediated integrin-dependent arrest that would not normally occur in the tissue environment, thus influencing arrest (Lammermann et al., 2008; Woolf et al., 2007). To prevent this problem in the future use of a collagen gel would be the preferred solution to move towards. A collagen gel represents an appropriate model of the 3D solid tissue environments occupied by macrophages, yet still enables the early calcium signalling events and migration of infiltrating CD4+ T cells to be imaged using human cells (Dustin et al., 2001a).

6.4 Conclusions

In summary, the formation of an IS between MDMs and CD4+ T cells and the localisation of endogenous CCR5 to either side of the interface, has been explored for the first time using primary human cells, with the aim of assessing the impact of the native cellular environment of CCR5 on its behaviour. The accumulation of CXCR4 to the T cell side of this IS was also examined as an additional reference-point to other types of synapse previously studied *in vitro*. Additionally, the lateral mobility of endogenous CCR5 on MDMs was studied to determine whether CCR5 might be stationary within the PM and explain the lack of CCR5 interface-accumulation on the MDM side of the synapse. In performing this work, I also adapted an arsenal of imaging and cytometry-based techniques and developed computational approaches required to analyse large datasets, which will serve as a foundation for future *in vitro* studies of IS formation.

Work from this thesis established that a small number of MDM-CD4+ T cell conjugates can form in presence and absence of sAg, however the conjugates that form in the presence of sAg demonstrate higher T cell intracellular calcium levels. Typically, T cells that exhibited high, prolonged intracellular calcium signals were found to accumulate TCR-CD3 at the MDM-CD4+ T cell interface, a sign of IS formation. This observation would not have been possible using global analysis of the population by flow cytometry, thus highlighting the importance of observing calcium signalling at a single-cell level to distinguish how minor changes in the calcium profile might correlate with a specific outcome like IS formation. Furthermore our observations evidenced that synapse formation between human MDMs and CD4+ T cells is more common than might be suggested by the infrequent stable macrophage-CD4+ T cell interactions reported *in vitro* for murine cells (Underhill et al., 1999). Results from the present study indicate that a mix of both synapse and kinapse interactions can occur between human macrophages and CD4+ T cells. Whilst the IS:kinapse balance may change depending on antigen quality and abundance, the results presented here evidence that both these modes of antigen-dependent macrophage-CD4+ T cell engagements previously observed in murine systems may also exist in humans.

The characterisation of MDM-CD4+ T cell IS formation enabled me to establish that endogenous CCR5 does not localise to the MDM side of this synapse although can localise to the T cell side, as can endogenous CXCR4. Our observations on the T cell side are reminiscent of those previously reported by other studies (Contento et al., 2008; Franciszkiewicz et al., 2009; Molon et al., 2005; Perez-Martinez et al., 2010). Note that none of the studies had considered the macrophage-CD4+ T cell IS, or the APC side of a synapse, or the localisation of endogenous chemokine receptors on primary human CD4+ T cells. There is a general consensus that T cell CCR5 or CXCR4 localisation to the IS contributes to cell-cell engagement, be this by preventing distraction or via more active means. Thus localisation of endogenous CCR5 or CXCR4 on the T cell side of the MDM-CD4+ T cell IS, as shown in the present study, is also expected to contribute to engagement. In contrast, because of the lack of accumulation of CCR5 on the MDM side one may speculate that macrophage CCR5 may be inert in synapse formation or that the engagement of CCR5 is cell-type dependent (supported by: Signoret lab, unpublished data). Overall this is the first evidence indicating that the chemokine receptor CCR5 may play a different role on the APC compared to the T cell in promoting IS stability.

In the present study CXCR4 was also found to be able to be recruited to the IS of a highly activated (CD3/CD28 stimulated) CD4+ T cells that do not express cell surface CCR5. This indicates that co-dependence between CXCR4 and CCR5 for recruitment to the IS may not be the only mechanism of chemokine receptor mobilisation to the IS, and this is

further supported by the study by Franciszkiewicz et al. (2009) where CXCR4 was not recruited to the TIL-tumour IS despite the fact that CCR5 did accumulate to the interface. However some form of trigger for chemokine receptor recruitment to the IS appears to be required, since many of the CD4+ T cells demonstrating lower levels of activation (PHA/IL-2 activated) did not show recruitment of CCR5 or CXCR4 to the IS. The requirement for a trigger can be envisaged as a mechanism to prevent inappropriate receptor recruitment to the IS, which may otherwise render a T cell insensitive to environmental chemokines.

Pools of CCR5 in CD4+ T cells were identified in the present study and deemed intracellular due to partial colocalisation with markers of the TGN. Trafficking via intracellular compartments is a mechanism utilised by some components of the IS in order to facilitate accumulation to the cell-cell interface (Das et al., 2004; Griffiths et al., 2010). Thus the pools of CCR5 which may preferentially accumulate beneath the cell-cell interface upon the MDM-CD4+ T cell IS formation potentially represent an additional source from which CCR5 may accumulate to the IS upon the correct trigger.

This thesis demonstrates that endogenous CCR5 is largely present as a mobile fraction in the PM of MDMs. Thus, the lack of CCR5 accumulation to the MDM side of the IS does not appear to be a consequence of native immobility of CCR5 in the MDM membrane. Cholesterol depletion (using MβCD) resulted in inhibition of cell surface CCR5 movement, but milder treatment sequestering cholesterol (filipin) did not, which could be explained by an extensive loss of membrane cholesterol causing a cytoskeletal dysregulation (Kwik et al., 2003). Therefore, cholesterol may not be important for CCR5 mobility. This may potentially explain an apparent paradox reported for HIV, where CCR5 mobility is thought to be required for infection (Steffens and Hope, 2004; Viard et al., 2002), and HIV was shown to preferentially bind a cholesterol-independent form of CCR5. With regard to CCR5 behaviour at the IS, lipid rafts may account for the different recruitment of CCR5 on the MDM and CD4+ T cell sides of the IS.

This investigation also highlights the difficulty of working in human cells, as the unknown genetic and environmental background of donors can influence a wide range of features, from responses to recall antigen and the TCR Vβ profile through to the levels of CCR5 expressed by leukocytes. Yet these factors must be borne in order to examine the influences of the native cellular environment and gather more physiologically relevant information.

Overall this work contributes to our understanding of chemokine receptor cell surface function and regulation, and our findings may direct future research into how the involvement of chemokine receptors within a tissue can impact the function of macrophage-CD4+ T cell interactions in fighting disease.

6.5 Future perspectives

This study shows that CCR5 can localise to the CD4+ T cell side of an antigen-dependent junction with macrophages. Avenues of future investigation might explore whether chemokines and/or CD103 trigger the localisation of CCR5 at this IS. One exciting possibility to explore whether CCR5 localisation on CD4+ T cells at the MDM-CD4+ T cell IS might in fact be mediated by CD103, which is present on lymphocytes such as Tregs. The role of CD103 in reorganising CCR5 to the TIL-tumour IS (Franciszkiewicz et al., 2009) may be a mechanism employed to retain CCR5+ T cells in diseases involving CD4+ T cell interactions with macrophages, one primary candidate being *L. major* infection. At sites of cutaneous *L. major* infection Tregs enable the persistence of the pathogen by dampening the immune response (Suffia et al., 2005). Treg retention and homing to these sites is dependent upon CD103 and CCR5 expression, respectively (Bromley et al., 2008; Suffia et al., 2005). Considering that Treg action is antigen specific (Corthay, 2009) there might be coordination between CCR5 and CD103 to macrophage-Treg synapses that acts to promote retention via a mechanism reminiscent of that shown in TIL-tumour interactions (Franciszkiewicz et al., 2009). Additionally through promoting macrophage-Treg engagement, coordinated CD103 CCR5 action may stabilise the IS so as to facilitate targeted secretion of Treg IL-10, a cytokine which has previously been found to be directionally secreted (Huse et al., 2006).

Future studies may also consider a role for the intracellular pool of CCR5 on CD4+ T cells as was identified in this study and whether this pool may contribute to CCR5 recruitment to the IS. Due to its partial TGN colocalisation the present study considers this pool to consist of CCR5 sequestered downstream of receptor internalisation, rather than being akin to the pools of CCR5 previously observed earlier in the biosynthetic pathway (Achour et al., 2009), however this notion requires confirmation. In the absence of any potential chemokine source the intracellular levels of CCR5 would reduce if indeed this pool represents recycling receptors in a molecular bottleneck. Irrespective of the origin, a potential role of this pool may be examined by determining the levels of CCR5 recruitment to the IS with and without inhibitors of exocytosis, such as tetanus toxin, as was previously performed for TCR (Das et al., 2004). Additionally the concept of recycling to the IS may be examined by analysing the potential directional recovery of $MC5^{488}$ labelled chemokine-treated T cells with and without IS formation by time-lapse microscopy. An essential step in order to be able to perform a reliable study of CCR5 receptor trafficking at the MDM-CD4+ T cell IS is to improve the frequency of IS formation. Since the type of APC was not found to be a limiting factor in the present study, expansion of antigen or

sAg specific T cells prior to interaction with MDMs may be a starting-point to try and achieve an improved frequency of productive MDM-CD4+ T cell conjugates.

Further investigation into the mobility of CCR5 on MDMs via methods such as SFVI that are set up to focus specifically on the PM, may complement the supra-molecular FRAP data that is presented here. The improved time-resolution of these single-molecule techniques might give a better measurement of the true lateral mobility of CCR5 within the membrane in comparison to FRAP, which is likely to be highly influenced by the complex topological features of the MDM PM over the extended acquisition period. Nevertheless a number of lessons can be learnt from the FRAP study, including potential differences in the mobility using GFP-CCR5 and MC5-labelled CCR5, which would be best considered using CHO-CCR5 cells first. Single molecule techniques may distinguish differences in the mobility of CCR5 on MDMs and CD4+ T cells and when combined with cholesterol depletion/sequestration have the potential to correlate mobility to different forms of CCR5 that exist within the PM. Additionally, planar bilayers could be employed to study whether the mobility of CCR5 may differ at the contact interface between a T cell in the presence or absence of antigen and the effect chemokine ‘distraction’ might have on CCR5 mobility.

Appendix 1

```
/*****************************************************************************************************
plr2.c    Piecewise linear regression c-script.
Author: Dr J. Wilson (University of York, York, UK)
Positions of input file names are highlighted in red
*****************************************************************************************************/
#include <stdlib.h>
#include <stdio.h>
#include <math.h>
#include <string.h>
#include <ctype.h>

typedef struct dataArray{
  char name[1024];
  double *vars;
}SAMPLE;

double getparam(int i, SAMPLE *data, double *y, int length, int c1, int c2, double *slopes, double
*intercepts, double *jumps, int *nsections);

int main (int argc, char *argv[])
{
  int i, j, length;
  int dtmp, tmp;
  float ftmp, a;
  int c1, c2, d;

  double slopes[3];
  double bestbeta[3];
  double intercepts[3];
  double bestalpha[3];
  double jumps[2];
  double bestjumps[2];

  char name[1024];
  char dir[1024];

  int nsamples;
  int startlength = 100;

  double y[startlength];
  double besty[startlength];

  FILE *fp = NULL;
  FILE *fout = NULL;
  fp = fopen("inputfiles/ 340:380_calcium_data.csv", "r");
  tmp = fscanf(fp, "%d\n", &dtmp);
  nsamples = dtmp;
  printf("%d\n", nsamples);

  /* initialise array */
  SAMPLE *data = NULL;
  data = (SAMPLE*) malloc (nsamples * sizeof(SAMPLE));
  SAMPLE *time = NULL;
  time = (SAMPLE*) malloc (nsamples * sizeof(SAMPLE));
  for (i = 0; i < nsamples; i++)
  {
    data[i].vars = (double *) malloc (startlength * sizeof(double));
    time[i].vars = (double *) malloc (startlength * sizeof(double));
```

```
  for (j = 0; j < startlength; j++)
  {
    time[i].vars[j] = 0.0;
    data[i].vars[j] = 0.0;
  }
}

for (i = 0; i < nsamples; i++)
{
  /* read in data */
  for (j = 0; j < startlength; j++)
  {
    tmp = fscanf(fp, "%f,\n", &ftmp);
    data[i].vars[j] = ftmp;
          }
}
fclose(fp);

fp = fopen("inputfiles/time_data.csv", "r");
/* read in times */
for (i = 0; i < nsamples; i++)
{
  /* read in data */
  for (j = 0; j < startlength; j++)
  {
    tmp = fscanf(fp, "%d,\n", &dtmp);
    time[i].vars[j] = (float)dtmp;
          }
}
fclose(fp);

fp = fopen("segmentinfoNoAg", "w");
fout = fopen("test", "w");
double rsq, maxrsq;
int bestc1, bestc2, nsections, bestn;
for (i = 0; i < nsamples; i++)
{
  for (j = 0; j < startlength; j++)
  {
    besty[j] = 0.0;
  }
  /* find real length for this sample */
  length = startlength-1;
  while ((data[i].vars[length] == 0.0) && (length > 0)) length--;
  bestc1 = 0;
  bestc2 = 0;
  maxrsq = 0.0;
  d = 0;
  bestn = 0;
  if (length > 3)
  {
    for (c1 = 0; c1 < length; c1++)
    {
      for (c2 = c1; c2 < length; c2++)
      {
        rsq = getparam(i, data, y, length, c1, c2, slopes, intercepts, jumps, &nsections);
        if (rsq > maxrsq)
        {
          maxrsq = rsq;
          bestc1 = c1;
          bestc2 = c2;
          d = c2 - c1;
```

```
          bestn = nsections;
          for (j = 0; j < length; j++)
          {
            besty[j] = y[j];
          }
          for (j = 0; j < 3; j++)
          {
            bestbeta[j] = slopes[j];
            bestalpha[j] = intercepts[j];
          }
          for (j = 0; j < 2; j++)
          {
            bestjumps[j] = jumps[j];
          }
        }
      }
    }
  }
  else
  {
    for (j = 0; j < 3; j++)
    {
      bestbeta[j] = 0.0;
      bestalpha[j] = 0.0;
    }
    jumps[0] = 0.0;
    jumps[1] = 0.0;
  }
  for (j = 0; j < startlength; j++)
  {
    fprintf(fout, "%f ", besty[j]);
  }
  fprintf(fout, "\n");
  printf("%d %d %d %d %d %d %0.3f %0.3f %0.3f %0.3f %0.3f %0.3f %0.3f %0.3f %0.3f %0.3f %0.3f %0.3f %0.3f\n", i, bestc1, bestc2, d, length, bestn, maxrsq, time[i].vars[0], time[i].vars[bestc1], time[i].vars[bestc2], time[i].vars[length-1], bestbeta[0], jumps[0], bestbeta[1], jumps[1], bestbeta[2], bestalpha[0], bestalpha[1], bestalpha[2]);
  fprintf(fp, "%d %d %d %d %d %0.3f %0.3f %0.3f %0.3f %0.3f %0.3f %0.3f %0.3f %0.3f %0.3f %0.3f %0.3f %0.3f\n", bestc1, bestc2, d, length, bestn, maxrsq, time[i].vars[0], time[i].vars[bestc1], time[i].vars[bestc2], time[i].vars[length-1], bestbeta[0], jumps[0], bestbeta[1], jumps[1], bestbeta[2], bestalpha[0], bestalpha[1], bestalpha[2]);
 }
 fclose(fp);

 for (i = 0; i < nsamples; i++)
 {
  free(data[i].vars);
  free(time[i].vars);
 }
 free (data);
 free (time);

 return 0;
}

/*****************************************************************************************************************
Procedure:  slope
finds the slope from linear regression
*****************************************************************************************************************/
double slope(int n, double *data, int length)
{
 int j;
```

```
  double sx, sy, sxx, sxy;
  double beta;

  sx = 0.0;
  sxx = 0.0;
  sy = 0.0;
  sxy = 0.0;
  for (j = 0; j < length; j++)
  {
    sx += (n+j+1);
    sxx += (n+j+1)*(n+j+1);
    sy += data[j];
    sxy += data[j]*(n+j+1);
  }
  sxx = sxx - (sx*sx/(float)length);
  sxy = sxy - (sx*sy/(float)length);
  beta = sxy/sxx;

  return(beta);
}

/*****************************************************************************************************************
Procedure:  intercept
finds the intercept from linear regression
*****************************************************************************************************************/
double intercept(int n, double *data, int length, double beta)
{
  int j;
  double alpha;
  double sx, sy;
  sx = 0.0;
  sy = 0.0;
  for (j = 0; j < length; j++)
  {
    sx += (n+j+1);
    sy += data[j];
  }
  alpha = (sy -beta*sx)/(float)length;
  return(alpha);
}


/*****************************************************************************************************************
Procedure:  getparam
finds the 3 alphas and betas for a pair of breakpoints c1 and c2
*****************************************************************************************************************/
double getparam(int i, SAMPLE *data, double *y, int length, int c1, int c2, double *betas, double
*alphas, double *jumps, int *nsec)
{
  int j;
  double alpha1, beta1, alpha2, beta2, alpha3, beta3;
  int length1, length2, length3;
  int nsections = 3;

  if (c1 == 0)
  {
    c1 = c2;
  }
  if (c1 == c2)
  {
    c2 = length -1;
    nsections = 2;
```

```
 }
 if (c1 == length -1)
 {
   nsections = 1;
 }

 length1 = c1;
 length2 = c2 - c1;
 length3 = length - c2;

 beta1 = 0.0;
 alpha1 = 0.0;
 beta2 = 0.0;
 alpha2 = 0.0;
 beta3 = 0.0;
 alpha3 = 0.0;

 double section1[length1];
 for (j = 0; j < c1; j++)
 {
   section1[j] = data[i].vars[j];
 }
 beta1 = slope(0, section1, length1);
 alpha1 = intercept(0, section1, length1, beta1);

 if (nsections > 1)
 {
   double section2[length2];
   for (j = c1; j < c2; j++)
   {
     section2[j-c1] = data[i].vars[j];
   }
   beta2 = slope(c1, section2, length2);
   alpha2 = intercept(c1, section2, length2, beta2);

   if (nsections > 2)
   {
     double section3[length3];
     for (j = c2; j < length; j++)
     {
       section3[j-c2] = data[i].vars[j];
     }
     beta3 = slope(c2, section3, length3);
     alpha3 = intercept(c2, section3, length3, beta3);
   }
 }

 int n = 0;
 if (c1 != 0)
 {
   for (j = 0; j < c1; j++)
   {
     y[n] = alpha1 + beta1*(j+1);
     n++;
   }
 }
 if (c2 != c1)
 {
   for (j = c1; j < c2; j++)
   {
     y[n] = alpha2 + beta2*(j+1);
     n++;
```

```
    }
  }
  if (c2 != length -1)
  {
    for (j = c2; j < length; j++)
    {
      y[n] = alpha3 + beta3*(j+1);
      n++;
    }
  }
  jumps[0] = y[c1] - y[c1-1];
  jumps[1] = y[c2] - y[c2-1];

  alphas[0] = alpha1;
  betas[0] = beta1;
  alphas[1] = alpha2;
  betas[1] = beta2;
  alphas[2] = alpha3;
  betas[2] = beta3;

  /* get sst */
  double sst = 0.0;
  double sy = 0.0;
  double syy = 0.0;
  double sse = 0.0;
  for (j = 0; j < length; j++)
  {
    sy += data[i].vars[j];
    syy += data[i].vars[j]*data[i].vars[j];
    sse += (y[j]-data[i].vars[j])*(y[j]-data[i].vars[j]);
  }
  sst = syy - (sy*sy/(float)length);
  /* get R-squared */
  double rsq = 1.0 - sse/sst;
  double adjrsq = 1.0 - nsections*(1.0 - rsq)/3.0;
  *nsec = nsections;

  return (adjrsq);
}
```

Definitions

β2AR	Beta-2-adrenergic receptor
µg	Microgram
µL	Microlitre
µM	Micromolar
7TM	Seven transmembrane
AC	Adenylate cyclase
Ag	Antigen
ANOVA	Analysis of variance
APC	Antigen-presenting cell
BM	Binding media
BRET	Bioluminescence resonance energy transfer
CD	Cluster of differentiation
CFDA-SE	Carboxyfluorescein diacetate N-succinimidyl ester
CHO	Chinese hamster ovary
CI	Confidence interval
CO_2	Carbon dioxide
co-IP	Co-immunoprecipitation
CRAC	Calcium release activated channel
cSMAC	Central supramolecular activation cluster
CTL	Cytotoxic T lymphocyte
DAG	Diacylglycerol
DAPI	4',6-diamidino-2-phenylindole
DC	Dendritic cell

DCo	Direct coupled
DMSO	Dimethyl sulphoxide
DNA	Deoxyribonucleic acid
D:P	Dye:protein
dSMAC	Distal supramolecular activation cluster
DTP	Diptheria, tetanus and poliomyelitis
EBV	Epstein-Barr virus
ECL	Extracellular loop
ECM	Extracellular matrix
EDTA	Ethylenediaminetetraacetic acid
EM	Electron microscopy
ER	Endoplasmic reticulum
Fab	Monovalent antigen-binding fragment
FcR	Receptor for the Fc antibody region
FCS	Foetal calf serum
FoxP3	Forkhead box P3
FRAP	Fluorescence recovery after photobleaching
g	Gram
GaAsP	Gallium arsenide phosphide
GAG	Glycosaminoglycans
GAM	Goat anti-mouse
GDP	Guanosine diphosphate
GFP	Green fluorescent protein
GM-CSF	Granulocyte-macrophage colony-stimulating factor
GPCR	G protein coupled receptor

GRK	G protein receptor kinase
GTP	Guanosine triphosphate
HEK	Human embryonic kidney
HeLa	Henrietta Lacks human epithelial cell line
HEPES	4-(2-hydroxyethyl)-1-piperazineethanesulfonic acid
HIV	Human immunodeficiency virus
HLA-DR	Human leukocyte antigen-DR
HOS	Human osteosarcoma
HPCD	Hydroxypropyl-β-cyclodextrin
ICAM1	Intercellular adhesion molecule 1
ICL	Intracellular loop
IFNγ	Interferon gamma
IgG	Immunoglobulin G
IL	Interleukin
IPMCs	Intracellular plasma-membrane connected compartments
IP3	Inositol-1,4,5-triphosphate
IS	Immunological synapse
ITAM	Immunoreceptor tyrosine-based activation motif
kDa	Kilodaltons
LAT	Linker for activation of T cells
LBPA	Lysobisphosphatidic acid
Lck	Lymphocyte-specific protein tyrosine kinase
LFA	Lymphocyte function-associated antigen
Lf U	Limit of flocculation unit
LN	Lymph node

LPS	Lipopolysaccharide
LUT	Look-up table
Ly6C$^+$	Lymphocyte antigen 6C
mAb	Monoclonal antibody
MAGI	HeLa-CD4-LTR-beta-gal cell line
MßCD	Methyl-ß cyclodextrin
M-CSF	Macrophage colony-stimulating factor
MDM	Monocyte-derived macrophage
MEM	Minimum essential medium
MFI	Median fluorescence intensity
MHC	Major histocompatibility complex
mg	Milligram
mL	Millilitre
mM	Millimolar
mRNA	Messenger ribonucleic acid
MTOC	Microtubule-organizing centre
NFAT	Nuclear factor of activated T cells
ng	Nanogram
nm	Nanometre
nM	Nanomolar
ns	Non-significant
nsRPMI	RPMI without serum
OVA	Ovalbumin
PBL	Peripheral blood lymphocyte
PBMC	Peripheral blood mononuclear cell

PBS	Phosphate buffered saline
PC-12	Cell line derived from a pheochromocytoma (rat)
PCA	Principal component analysis
PDL	Poly-D-lysine
PDZ	Post synaptic density protein (PSD95), Drosophilia disc large tumour Suppressor (D1g1), and zonula occludens-1 protein (zo-1)
PE	R-phycoerythrin
PEI	Polyethylenimine
PFA	Paraformaldehyde
PH	Pleckstrin homology domain
PHA	Phytohaemagglutinin-M
PI3K	Phosphatidylinositol 3-kinase
PIP2	Phosphatidylinositol-4,5-bisphosphate
PIP3	Phosphatidylinositol-3,4,5,-trisphosphate
pMHC	Peptide-major histocompatibility complex
PKB	Protein kinase B
PKC	Protein kinase C
PLC	Phospholipase C
PM	Plasma membrane
PSC	Nα-(n-nonanoyl)-des-Ser1-[l-thioproline2, l-α-cyclohexyl-glycine3] RANTES
pSMAC	Peripheral supramolecular activation cluster
PTX	Pertussis toxin
PW	Pulse width
px	Pixels
RANTES	Regulated and normal T cell expressed and secreted

RE	Recycling endosome
ROI	Region of interest
rpm	Rotations per minute
RPMI	Roswell Park Memorial Institute
RT	Room temperature
sAg	Superantigen
SD	Standard deviation
SEA	Staphylococcal enterotoxin A
SEB	Staphylococcal enterotoxin B
SEE	Staphylococcal enterotoxin E
SEM	Standard error of the mean
SFVI	Single fluorescent molecule video imaging
SMAC	Supramolecular activation cluster
SP	Side-port
SPT	Single particle tracking
SSC	Side-scattered light
STIM1	Stromal interaction molecule 1
t	Timepoint
Treg	Regulatory T cell
TCR	T cell receptor
T_{CM}	T central memory
T_{EM}	T effector memory
TfR	Transferrin receptor
TGN	*trans*-Golgi network
Th	T helper

Thy-1	Thymocyte/ T-lymphocyte surface differentiation antigen
TIL	Tumour-infiltrating lymphocyte
TT	Tetanus toxoid
WASp	Wiskott-Aldrich syndrome protein
YFP	Yellow fluorescent protein
ZAP-70	ζ-chain-associated protein kinase of 70 kDa

References

Achour, L., Labbe-Jullie, C., Scott, M. G. and Marullo, S. (2008). An escort for GPCRs: implications for regulation of receptor density at the cell surface. *Trends Pharmacol Sci,* 29(10)**,** 528-35.

Achour, L., Scott, M. G., Shirvani, H., Thuret, A., Bismuth, G., Labbé-Jullié, C. and Marullo, S. (2009). CD4-CCR5 interaction in intracellular compartments contributes to receptor expression at the cell surface. *Blood,* 113(9)**,** 1938-47.

Acuto, O., Di Bartolo, V. and Michel, F. (2008). Tailoring T-cell receptor signals by proximal negative feedback mechanisms. *Nat Rev Immunol,* 8(9)**,** 699-712.

Adeboye, K. A. and Sangowawa, O. (2002). Tetanus prophylaxis in the A&E department. *J R Soc Med,* 95(3)**,** 113.

Albright, A. V., Shieh, J. T., Itoh, T., Lee, B., Pleasure, D., O'connor, M. J., Doms, R. W. and González-Scarano, F. (1999). Microglia express CCR5, CXCR4, and CCR3, but of these, CCR5 is the principal coreceptor for human immunodeficiency virus type 1 dementia isolates. *J Virol,* 73(1)**,** 205-13.

Alkhatib, G. (2009). The biology of CCR5 and CXCR4. *Curr Opin HIV AIDS*, 4(2), 96-103.

Allen, S. J., Crown, S. E. and Handel, T. M. (2007). Chemokine: receptor structure, interactions, and antagonism. *Annu Rev Immunol,* 25, 787-820.

Andreesen, R., Brugger, W., Scheibenbogen, C., Kreutz, M., Leser, H. G., Rehm, A. and Löhr, G. W. (1990). Surface phenotype analysis of human monocyte to macrophage maturation. *J Leukoc Biol,* 47(6)**,** 490-7.

Appelqvist, H., Nilsson, C., Garner, B., Brown, A. J., Kågedal, K. and Ollinger, K. (2011). Attenuation of the lysosomal death pathway by lysosomal cholesterol accumulation. *Am J Pathol,* 178(2)**,** 629-39.

Arrhenius, S. (1907). *The application of the principles of physical chemistry to the study of the biological antibodies.* New York: The Macmillan Company.

Asperti-Boursin, F., Real, E., Bismuth, G., Trautmann, A. and Donnadieu, E. (2007). CCR7 ligands control basal T cell motility within lymph node slices in a phosphoinositide 3-kinase-independent manner. *J Exp Med,* 204(5)**,** 1167-79.

Azar, G. A., Lemaître, F., Robey, E. A. and Bousso, P. (2010). Subcellular dynamics of T cell immunological synapses and kinapses in lymph nodes. *Proc Natl Acad Sci U S A,* 107(8)**,** 3675-80.

Baba, M., Nishimura, O., Kanzaki, N., Okamoto, M., Sawada, H., Iizawa, Y., Shiraishi, M., Aramaki, Y., Okonogi, K., Ogawa, Y., Meguro, K. and Fujino, M. (1999). A small-molecule, nonpeptide CCR5 antagonist with highly potent and selective anti-HIV-1 activity. *Proc Natl Acad Sci U S A,* 96(10)**,** 5698-703.

Bachelerie, F., Ben-Baruch, A., Burkhardt, A. M., Combadiere, C., Farber, J. M., Graham, G. J., Horuk, R., Sparre-Ulrich, A. H., Locati, M., Luster, A. D., Mantovani, A., Matsushima, K., Murphy, P. M., Nibbs, R., Nomiyama, H., Power, C. A., Proudfoot, A. E., Rosenkilde, M. M., Rot, A., Sozzani, S., Thelen, M., Yoshie, O. and Zlotnik, A. (2013). International Union of Pharmacology. LXXXIX. Update on the extended family of chemokine receptors and introducing a new nomenclature for atypical chemokine receptors. *Pharmacol Rev,* 66(1)**,** 1-79.

Beemiller, P., Jacobelli, J. and Krummel, M. F. (2012). Integration of the movement of signaling microclusters with cellular motility in immunological synapses. *Nat Immunol,* 13(8)**,** 787-95.

Beemiller, P. and Krummel, M. F. (2010). Mediation of T-cell activation by actin meshworks. *Cold Spring Harb Perspect Biol,* 2(9)**,** a002444.

Beemiller, P. and Krummel, M. F. (2013). Regulation of T-cell receptor signaling by the actin cytoskeleton and poroelastic cytoplasm. *Immunol Rev,* 256(1)**,** 148-59.

Bennett, L. D., Fox, J. M. and Signoret, N. (2011). Mechanisms regulating chemokine receptor activity. *Immunology,* 134(3)**,** 246-56.

Bermejo, M., Martín-Serrano, J., Oberlin, E., Pedraza, M. A., Serrano, A., Santiago, B., Caruz, A., Loetscher, P., Baggiolini, M., Arenzana-Seisdedos, F. and Alcami, J.

(1998). Activation of blood T lymphocytes down-regulates CXCR4 expression and interferes with propagation of X4 HIV strains. *Eur J Immunol,* 28(10)**,** 3192-204.
Berro, R., Klasse, P. J., Lascano, D., Flegler, A., Nagashima, K. A., Sanders, R. W., Sakmar, T. P., Hope, T. J. and Moore, J. P. (2011). Multiple CCR5 conformations on the cell surface are used differentially by human immunodeficiency viruses resistant or sensitive to CCR5 inhibitors. *J Virol,* 85(16)**,** 8227-40.
Berro, R., Yasmeen, A., Abrol, R., Trzaskowski, B., Abi-Habib, S., Grunbeck, A., Lascano, D., Goddard, W. A. 3rd, Klasse, P. J., Sakmar, T. P. and Moore, J. P. (2013). Use of G-protein-coupled and -uncoupled CCR5 receptors by CCR5 inhibitor-resistant and -sensitive human immunodeficiency virus type 1 variants. *J Virol,* 87(12)**,** 6569-81.
Biswas, S. K. and Mantovani, A. (2010). Macrophage plasticity and interaction with lymphocyte subsets: cancer as a paradigm. *Nat Immunol,* 11(10)**,** 889-96.
Blanpain, C., Doranz, B. J., Bondue, A., Govaerts, C., De Leener, A., Vassart, G., Doms, R. W., Proudfoot, A. and Parmentier, M. (2003). The core domain of chemokines binds CCR5 extracellular domains while their amino terminus interacts with the transmembrane helix bundle. *J Biol Chem,* 278(7)**,** 5179-87.
Blanpain, C., Vanderwinden, J.-M., Cihak, J., Wittamer, V., Le Poul, E., Issafras, H., Stangassinger, M., Vassart, G., Marullo, S., Schlndorff, D., Parmentier, M. and Mack, M. (2002). Multiple active states and oligomerization of CCR5 revealed by functional properties of monoclonal antibodies. *Mol Biol Cell,* 13(2)**,** 723-37.
Blanpain, C., Wittamer, V., Vanderwinden, J. M., Boom, A., Renneboog, B., Lee, B., Le Poul, E., El Asmar, L., Govaerts, C., Vassart, G., Doms, R. W. and Parmentier, M. (2001). Palmitoylation of CCR5 is critical for receptor trafficking and efficient activation of intracellular signaling pathways. *J Biol Chem,* 276(26)**,** 23795-804.
Bleul, C. C., Wu, L., Hoxie, J. A., Springer, T. A. and Mackay, C. R. (1997). The HIV coreceptors CXCR4 and CCR5 are differentially expressed and regulated on human T lymphocytes. *Proc Natl Acad Sci U S A,* 94(5)**,** 1925-30.
Bloom, O., Unternaehrer, J. J., Jiang, A., Shin, J. S., Delamarre, L., Allen, P. and Mellman, I. (2008). Spinophilin participates in information transfer at immunological synapses. *J Cell Biol,* 181(2)**,** 203-11.
Borroni, E. M., Mantovani, A., Locati, M. and Bonecchi, R. (2010). Chemokine receptors intracellular trafficking. *Pharmacol Ther,* 127(1)**,** 1-8.
Brewer, J. L. and Ericson, S. G. (2005). An improved methodology to detect human T cell receptor beta variable family gene expression patterns. *J Immunol Methods,* 302(1-2)**,** 54-67.
Bromley, S. K. and Dustin, M. L. (2002). Stimulation of naïve T-cell adhesion and immunological synapse formation by chemokine-dependent and -independent mechanisms. *Immunology,* 106(3)**,** 289-98.
Bromley, S. K., Mempel, T. R. and Luster, A. D. (2008). Orchestrating the orchestrators: chemokines in control of T cell traffic. *Nat Immunol,* 9(9)**,** 970-80.
Bromley, S. K., Peterson, D. A., Gunn, M. D. and Dustin, M. L. (2000). Cutting edge: hierarchy of chemokine receptor and TCR signals regulating T cell migration and proliferation. *J Immunol,* 165(1)**,** 15-9.
Bueno, C., Lemke, C. D., Criado, G., Baroja, M. L., Ferguson, S. S., Rahman, A. K., Tsoukas, C. D., Mccormick, J. K. and Madrenas, J. (2006). Bacterial superantigens bypass Lck-dependent T cell receptor signaling by activating a Galpha11-dependent, PLC-beta-mediated pathway. *Immunity,* 25(1)**,** 67-78.
Burack, W. R., Lee, K. H., Holdorf, A. D., Dustin, M. L. and Shaw, A. S. (2002). Cutting edge: quantitative imaging of raft accumulation in the immunological synapse. *J Immunol,* 169(6)**,** 2837-41.
Burchiel, S. W., Edwards, B. S., Kuckuck, F. W., Lauer, F. T., Prossnitz, E. R., Ransom, J. T. and Sklar, L. A. (2000). Analysis of free intracellular calcium by flow cytometry: multiparameter and pharmacologic applications. *Methods,* 21(3)**,** 221-30.
Busillo, J. M., Armando, S., Sengupta, R., Meucci, O., Bouvier, M. and Benovic, J. L. (2010). Site-specific phosphorylation of CXCR4 is dynamically regulated by

multiple kinases and results in differential modulation of CXCR4 signaling. *J Biol Chem,* 285(10)**,** 7805-17.
Busillo, J. M. and Benovic, J. L. (2007). Regulation of CXCR4 signaling. *Biochim Biophys Acta,* 1768(4)**,** 952-63.
Cahalan, M. D. and Parker, I. (2008). Choreography of cell motility and interaction dynamics imaged by two-photon microscopy in lymphoid organs. *Annu Rev Immunol,* 26, 585-626.
Camargo, J. F., Quinones, M. P., Mummidi, S., Srinivas, S., Gaitan, A. A., Begum, K., Jimenez, F., VanCompernolle, S., Unutmaz, D., Ahuja, S. S. and Ahuja, S. K. (2009). CCR5 expression levels influence NFAT translocation, IL-2 production, and subsequent signaling events during T lymphocyte activation. *J Immunol,* 182(1)**,** 171-82.
Cardaba, C. M., Kerr, J. S. and Mueller, A. (2008). CCR5 internalisation and signalling have different dependence on membrane lipid raft integrity. *Cell Signal,* 20(9)**,** 1687-94.
Castellino, F., Huang, A. Y., Altan-Bonnet, G., Stoll, S., Scheinecker, C. and Germain, R. N. (2006). Chemokines enhance immunity by guiding naive CD8+ T cells to sites of CD4+ T cell-dendritic cell interaction. *Nature,* 440(7086)**,** 890-5.
Catalfamo, M., Karpova, T., Mcnally, J., Costes, S. V., Lockett, S. J., Bos, E., Peters, P. J. and Henkart, P. A. (2004). Human CD8+ T cells store RANTES in a unique secretory compartment and release it rapidly after TcR stimulation. *Immunity,* 20(2)**,** 219-30.
Cenedella, R. J. (2009). Cholesterol synthesis inhibitor U18666A and the role of sterol metabolism and trafficking in numerous pathophysiological processes. *Lipids,* 44(6)**,** 477-87.
Chabre, M., Deterre, P. and Antonny, B. (2009). The apparent cooperativity of some GPCRs does not necessarily imply dimerization. *Trends Pharmacol Sci,* 30(4)**,** 182-7.
Chen, L. and Flies, D. B. (2013). Molecular mechanisms of T cell co-stimulation and co-inhibition. *Nat Rev Immunol,* 13(4)**,** 227-42.
Chen, Y., Li, X., Ye, Q., Tian, J., Jing, R. and Xie, Z. (2011). Regulation of alpha1 Na/K-ATPase expression by cholesterol. *JBiol Chem,* 286(17)**,** 15517-24.
Choi, S. and Schwartz, R. H. (2011). Impairment of immunological synapse formation in adaptively tolerant T cells. *J Immunol,* 187(2)**,** 805-16.
Choudhuri, K., Wiseman, D., Brown, M. H., Gould, K. and van der Merwe, P. A. (2005). T-cell receptor triggering is critically dependent on the dimensions of its peptide-MHC ligand. *Nature,* 436(7050)**,** 578-82.
Clapham, D. E. (2007). Calcium signaling. *Cell,* 131(6)**,** 1047-58.
Colin, P., Bénureau, Y., Staropoli, I., Wang, Y., Gonzalez, N., Alcami, J., Hartley, O., Brelot, A., Arenzana-Seisdedos, F. and Lagane, B. (2013). HIV-1 exploits CCR5 conformational heterogeneity to escape inhibition by chemokines. *Proc Natl Acad Sci U S A,* 110(23)**,** 9475-80.
Contento, R. L., Campello, S., Trovato, A. E., Magrini, E., Anselmi, F. and Viola, A. (2010). Adhesion shapes T cells for prompt and sustained T-cell receptor signalling. *EMBO J,* 29(23)**,** 4035-47.
Contento, R. L., Molon, B., Boularan, C., Pozzan, T., Manes, S., Marullo, S. and Viola, A. (2008). CXCR4-CCR5: a couple modulating T cell functions. *Proc Nat Acad Sci U S A,* 105(29)**,** 10101-6.
Cooper, G. M. (2000). *The Cell*. Sunderland (MA): Sinauer Associates.
Corse, E., Gottschalk, R. A. and Allison, J. P. (2011). Strength of TCR-peptide/MHC interactions and in vivo T cell responses. *J Immunol,* 186(9)**,** 5039-45.
Corthay, A. (2009). How do regulatory T cells work? *Scand J Immunol,* 70(4)**,** 326-36.
D'Amico, G., Frascaroli, G., Bianchi, G., Transidico, P., Doni, A., Vecchi, A., Sozzani, S., Allavena, P. and Mantovani, A. (2000). Uncoupling of inflammatory chemokine receptors by IL-10: generation of functional decoys. *Nat Immunol,* 1(5)**,** 387-91.

Dar, W. A. and Knechtle, S. J. (2007). CXCR3-mediated T-cell chemotaxis involves ZAP-70 and is regulated by signalling through the T-cell receptor. *Immunology,* 120(4)**,** 467-85.

Das, V., Nal, B., Dujeancourt, A., Thoulouze, M. I., Galli, T., Roux, P., Dautry-Varsat, A. and Alcover, A. (2004). Activation-induced polarized recycling targets T cell antigen receptors to the immunological synapse; involvement of SNARE complexes. *Immunity,* 20(5)**,** 577-88.

Deneka, M., Pelchen-Matthews, A., Byland, R., Ruiz-Mateos, E. and Marsh, M. (2007). In macrophages, HIV-1 assembles into an intracellular plasma membrane domain containing the tetraspanins CD81, CD9, and CD53. *J Cell Biol,* 177(2)**,** 329-41.

Disis, M. L., dela Rosa, C., Goodell, V., Kuan, L. Y., Chang, J. C., Kuus-Reichel, K., Clay, T. M., Kim Lyerly, H., Bhatia, S., Ghanekar, S. A., Maino, V. C. and Maecker, H. T. (2006). Maximizing the retention of antigen specific lymphocyte function after cryopreservation. *J Immunol Methods,* 308(1-2)**,** 13-8.

Dolmetsch, R. E., Lewis, R. S., Goodnow, C. C. and Healy, J. I. (1997). Differential activation of transcription factors induced by Ca2+ response amplitude and duration. *Nature,* 386(6627)**,** 855-8.

Duarte, R. F., Chen, F. E., Lowdell, M. W., Potter, M. N., Lamana, M. L., Prentice, H. G. and Madrigal, J. A. (2002). Functional impairment of human T-lymphocytes following PHA-induced expansion and retroviral transduction: implications for gene therapy. *Gene Ther,* 9(20)**,** 1359-68.

Dustin, M. L. (2004). Stop and go traffic to tune T cell responses. *Immunity,* 21(3)**,** 305-14.

Dustin, M. L. (2008). T-cell activation through immunological synapses and kinapses. *Immunological reviews,* 221**,**77-89.

Dustin, M. L. (2009a). The cellular context of T cell signaling. *Immunity,* 30(4)**,** 482-92.

Dustin, M. L. (2009b). Modular design of immunological synapses and kinapses. *Cold Spring Harb Perspect Biol,* 1(1)**,** a002873.

Dustin, M. L., Allen, P. M. and Shaw, A. S. (2001a). Environmental control of immunological synapse formation and duration. *Trends Immunol,* 22(4)**,** 192-4.

Dustin, M. L., Bromley, S. K., Davis, M. M. and Zhu, C. (2001b). Identification of self through two-dimensional chemistry and synapses. *Annu Rev Cell Dev Biol,* 17**,** 133-57.

Dustin, M. L., Chakraborty, A. K. and Shaw, A. S. (2010). Understanding the structure and function of the immunological synapse. *Cold Spring Harb Perspect Biol,* 2(10)**,** a002311.

Dustin, M. L., Tseng, S. Y., Varma, R. and Campi, G. (2006). T cell-dendritic cell immunological synapses. *Curr Opin Immunol,* 18(4)**,** 512-6.

Dziennis, S., Van Etten, R. A., Pahl, H. L., Morris, D. L., Rothstein, T. L., Blosch, C. M., Perlmutter, R. M. and Tenen, D. G. (1995). The CD11b promoter directs high-level expression of reporter genes in macrophages in transgenic mice. *Blood,* 85(2)**,** 319-29.

Egen, J. G., Rothfuchs, A. G., Feng, C. G., Horwitz, M. A., Sher, A. and Germain, R. N. (2011). Intravital imaging reveals limited antigen presentation and T cell effector function in mycobacterial granulomas. *Immunity,* 34(5)**,** 807-19.

El-Asmar, L., Springael, J.-Y., Ballet, S., Andrieu, E. U., Vassart, G. and Parmentier, M. (2005). Evidence for negative binding cooperativity within CCR5-CCR2b heterodimers. *Mol Pharmacol,* 67(2)**,** 460-9.

Escola, J. M., Kuenzi, G., Gaertner, H., Foti, M. and Hartley, O. (2010). CC chemokine receptor 5 (CCR5) desensitization: cycling receptors accumulate in the trans-Golgi network. *J Biol Chem,* 285(53)**,** 41772-80.

Filipe-Santos, O., Pescher, P., Breart, B., Lippuner, C., Aebischer, T., Glaichenhaus, N., Späth, G. F. and Bousso, P. (2009). A dynamic map of antigen recognition by CD4 T cells at the site of Leishmania major infection. *Cell Host Microbe,* 6(1)**,** 23-33.

Fooksman, D. R., Shaikh, S. R., Boyle, S. and Edidin, M. (2009). Cutting edge: phosphatidylinositol 4,5-bisphosphate concentration at the APC side of the

immunological synapse is required for effector T cell function. *J Immunol,* 182(9)**,** 5179-82.
Foucher, E. D., Blanchard, S., Preisser, L., Garo, E., Ifrah, N., Guardiola, P., Delneste, Y. and Jeannin, P. (2013). IL-34 induces the differentiation of human monocytes into immunosuppressive macrophages. antagonistic effects of GM-CSF and IFNɣ. *PLoS One,* 8(2)**,** e56045.
Fox, J. M., Letellier, E., Oliphant, C. J. and Signoret, N. (2011). TLR2-dependent pathway of heterologous down-modulation for the CC chemokine receptors 1, 2, and 5 in human blood monocytes. *Blood,* 117(6)**,** 1851-60.
Franchin, G., Zybarth, G., Dai, W. W., Dubrovsky, L., Reiling, N., Schmidtmayerova, H., Bukrinsky, M. and Sherry, B. (2000). Lipopolysaccharide inhibits HIV-1 infection of monocyte- derived macrophages through direct and sustained down-regulation of CC chemokine receptor 5. *J Immunol,* 164(5)**,** 2592-601.
Franciszkiewicz, K., Le Floc'h, A., Boutet, M., Vergnon, I., Schmitt, A. and Mami-Chouaib, F. (2013). CD103 or LFA-1 engagement at the immune synapse between cytotoxic T cells and tumor cells promotes maturation and regulates T-cell effector functions. *Cancer Res,* 73(2)**,** 617-28.
Franciszkiewicz, K., Le Floc'h, A., Jalil, A., Vigant, F., Robert, T., Vergnon, I., Mackiewicz, A., Benihoud, K., Validire, P., Chouaib, S., Combadière, C. and Mami-Chouaib, F. (2009). Intratumoral induction of CD103 triggers tumor-specific CTL function and CCR5-dependent T-cell retention. *Cancer Res,* 69(15)**,** 6249-55.
Friedl, P., den Boer, A. T. and Gunzer, M. (2005). Tuning immune responses: diversity and adaptation of the immunological synapse. *Nat Rev Immunol,* 5(7)**,** 532-45.
Fujishima, S.-H., Yasui, R., Miki, T., Ojida, A. and Hamachi, I. (2012). Ligand-directed acyl imidazole chemistry for labeling of membrane-bound proteins on live cells. *J Am Chem Soc,* 134(9)**,** 3961-4.
Gaertner, H., Cerini, F., Escola, J. M., Kuenzi, G., Melotti, A., Offord, R., Rossitto-Borlat, I., Nedellec, R., Salkowitz, J., Gorochov, G., Mosier, D. and Hartley, O. (2008). Highly potent, fully recombinant anti-HIV chemokines: reengineering a low-cost microbicide. *Proc Natl Acad Sci U S A,* 105(46)**,** 17706-11.
Gérard, A., Beemiller, P., Friedman, R. S., Jacobelli, J. and Krummel, M. F. (2013). Evolving immune circuits are generated by flexible, motile, and sequential immunological synapses. *Immunol Rev,* 251(1)**,** 80-96.
Geursen, A., Skinner, M. A., Townsend, L. A., Perko, L. K., Farmiloe, S. J., Peake, J. S., Simpson, I. J., Fraser, J. D. and Tan, P. L. (1993). Population study of T cell receptor V beta gene usage in peripheral blood lymphocytes: differences in ethnic groups. *Clin Exp Immunol,* 94(1)**,** 201-7.
Gharbi, S. I., Avila-Flores, A., Soutar, D., Orive, A., Koretzky, G. A., Albar, J. P. and Mérida, I. (2013). Transient PKCα shuttling to the immunological synapse is governed by DGKαζ and regulates L-selectin shedding. *J Cell Sci,* 126(Pt 10)**,** 2176-86.
Gómez-Moutón, C., Lacalle, R. A., Mira, E., Jiménez-Baranda, S., Barber, D. F., Carrera, A. C., Martínez-A, C. and Mañes, S. (2004). Dynamic redistribution of raft domains as an organizing platform for signaling during cell chemotaxis. *J Cell Biol,* 164(5)**,** 759-68.
Gong, J. H., Uguccioni, M., Dewald, B., Baggiolini, M. and Clark-Lewis, I. (1996). RANTES and MCP-3 antagonists bind multiple chemokine receptors. *J Biol Chem,* 271(18)**,** 10521-7.
Gordon, S. (2003). Alternative activation of macrophages. *Nat Rev Immunol,* 3(1)**,** 23-35.
Gordon, S. and Taylor, P. R. (2005). Monocyte and macrophage heterogeneity. *Nat Rev Immunol,* 5(12)**,** 953-64.
Gottfried, E., Kunz-Schughart, L. A., Weber, A., Rehli, M., Peuker, A., Muller, A., Kastenberger, M., Brockhoff, G., Andreesen, R. and Kreutz, M. (2008). Expression of CD68 in non-myeloid cell types. *Scand J Immunol,* 67(5)**,** 453-63.

Grakoui, A., Bromley, S. K., Sumen, C., Davis, M. M., Shaw, A. S., Allen, P. M. and Dustin, M. L. (1999). The immunological synapse: a molecular machine controlling T cell activation. *Science,* 285(5425)**,** 221-7.

Graziani-Bowering, G. M. and Filion, L. G. (2000). Down regulation of CD4 expression following isolation and culture of human monocytes. *Clin Diagn Lab Immunol,* 7(2)**,** 182-91.

Griffiths, G. M., Tsun, A. and Stinchcombe, J. C. (2010). The immunological synapse: a focal point for endocytosis and exocytosis. *J Cell Biol,* 189(3)**,** 399-406.

Groot, F., Van Capel, T. M., Schuitemaker, J., Berkhout, B. and de Jong, E. C. (2006). Differential susceptibility of naïve, central memory and effector memory T cells to dendritic cell-mediated HIV-1 transmission. *Retrovirology,* 3, 52.

Guglielmi, L., Gimenez, S., Larroque, M., Tong, X., Portalès, P. and Corbeau, P. (2011). Circulating human CD4+ T cells have intracellular pools of CCR5 molecules. *Blood,* 118(4)**,** 1177-8; author reply 1179.

Gurevich, V. V. and Gurevich, E. V. (2008). GPCR monomers and oligomers: it takes all kinds. *Trends Neurosci,* 31(2)**,** 74-81.

Hamann, D., Baars, P. A., Hooibrink, B. and van Lier, R. W. (1996). Heterogeneity of the human CD4+ T-cell population: two distinct CD4+ T-cell subsets characterized by coexpression of CD45RA and CD45RO isoforms. *Blood,* 88(9)**,** 3513-21.

Hamilton, J. A. and Achuthan, A. (2013). Colony stimulating factors and myeloid cell biology in health and disease. *Trends Immunol,* 34(2)**,** 81-9.

Harmon, B. and Ratner, L. (2008). Induction of the Galpha(q) signaling cascade by the human immunodeficiency virus envelope is required for virus entry. *J Virol,* 82(18)**,** 9191-205.

Hashimoto-Tane, A., Yokosuka, T., Sakata-Sogawa, K., Sakuma, M., Ishihara, C., Tokunaga, M. and Saito, T. (2011). Dynein-driven transport of T cell receptor microclusters regulates immune synapse formation and T cell activation. *Immunity,* 34(6)**,** 919-31.

Henrickson, S. E., Mempel, T. R., Mazo, I. B., Liu, B., Artyomov, M. N., Zheng, H., Peixoto, A., Flynn, M. P., Senman, B., Junt, T., Wong, H. C., Chakraborty, A. K. and von Andrian, U. H. (2008). T cell sensing of antigen dose governs interactive behavior with dendritic cells and sets a threshold for T cell activation. *Nat Immunol,* 9(3)**,** 282-91.

Herbein, G. and Varin, A. (2010). The macrophage in HIV-1 infection: from activation to deactivation? *Retrovirology,* 7, 33.

Hernanz-Falcón, P., Rodríguez-Frade, J. M., Serrano, A., Martínez-A, C. and Mellado, M. (2005). Response to "On the dimerization of CCR5". *Nat Immunol,* 6(6)**,** 535-536.

Hiltbold, E. M., Poloso, N. J. and Roche, P. A. (2003). MHC class II-peptide complexes and APC lipid rafts accumulate at the immunological synapse. *J Immunol,* 170(3)**,** 1329-38.

Hogan, P. G., Lewis, R. S. and Rao, A. (2010). Molecular basis of calcium signaling in lymphocytes: STIM and ORAI. *Annu Rev Immunol,* 28, 491-533.

Hogg, N., Patzak, I. and Willenbrock, F. (2011). The insider's guide to leukocyte integrin signalling and function. *Nat Rev Immunol,* 11(6)**,** 416-26.

Hoves, S., Krause, S. W., Schutz, C., Halbritter, D., Schölmerich, J., Herfarth, H. and Fleck, M. (2006). Monocyte-derived human macrophages mediate anergy in allogeneic T cells and induce regulatory T cells. *J Immunol,* 177(4)**,** 2691-8.

Huppa, J. B., Axmann, M., Mortelmaier, M. A., Lillemeier, B. F., Newell, E. W., Brameshuber, M., Klein, L. O., Schütz, G. J. and Davis, M. M. (2010). TCR-peptide-MHC interactions in situ show accelerated kinetics and increased affinity. *Nature,* 463(7283)**,** 963-7.

Huppa, J. B., Gleimer, M., Sumen, C. and Davis, M. M. (2003). Continuous T cell receptor signaling required for synapse maintenance and full effector potential. *Nat Immunol,* 4(8)**,** 749-55.

Huse, M., Lillemeier, B. F., Kuhns, M. S., Chen, D. S. and Davis, M. M. (2006). T cells use two directionally distinct pathways for cytokine secretion. *Nat Immunol,* 7(3)**,** 247-55.
Huse, M., Quann, E. J. and Davis, M. M. (2008). Shouts, whispers and the kiss of death: directional secretion in T cells. *Nat Immunol,* 9(10)**,** 1105-11.
Hüttenrauch, F., Pollok-Kopp, B. and Oppermann, M. (2005). G protein-coupled receptor kinases promote phosphorylation and beta-arrestin-mediated internalization of CCR5 homo- and hetero-oligomers. *J Biol Chem,* 280(45)**,** 37503-15.
Ishihara, A., Hou, Y. and Jacobson, K. (1987). The Thy-1 antigen exhibits rapid lateral diffusion in the plasma membrane of rodent lymphoid cells and fibroblasts. *Proc Natl Acad Sci U S A,* 84(5)**,** 1290-3.
Ishikawa-Ankerhold, H. C., Ankerhold, R. and Drummen, G. P. (2012). Advanced fluorescence microscopy techniques--FRAP, FLIP, FLAP, FRET and FLIM. *Molecules,* 17(4)**,** 4047-132.
Isik, N., Hereld, D. and Jin, T. (2008). Fluorescence resonance energy transfer imaging reveals that chemokine-binding modulates heterodimers of CXCR4 and CCR5 receptors. *PLoS One,* 3(10)**,** e3424.
Issafras, H., Angers, S., Bulenger, S., Blanpain, C., Parmentier, M., Labbé-Jullié, C., Bouvier, M. and Marullo, S. (2002). Constitutive agonist-independent CCR5 oligomerization and antibody-mediated clustering occurring at physiological levels of receptors. *J Biol Chem,* 277(38)**,** 34666-73.
Ivanov, A. I. (2008). Pharmacological inhibition of endocytic pathways: is it specific enough to be useful? *Methods Mol Biol,* 440, 15-33.
Jaguin, M., Houlbert, N., Fardel, O. and Lecureur, V. (2013). Polarization profiles of human M-CSF-generated macrophages and comparison of M1-markers in classically activated macrophages from GM-CSF and M-CSF origin. *Cell Immunol,* 281(1)**,** 51-61.
Jähnichen, S., Blanchetot, C., Maussang, D., Gonzalez-Pajuelo, M., Chow, K. Y., Bosch, L., De Vrieze, S., Serruys, B., Ulrichts, H., Vandevelde, W., Sunders, M., De Haard, H. J., Schol, D., Leurs, R., Vanlandschoot, P., Verrips, T. and Smit, M. J. (2010). CXCR4 nanobodies (VHH-based single variable domains) potently inhibit chemotaxis and HIV-1 replication and moilize stem cells. *Proc Natl Acad Sci U S A*, 107(47), 20565-70.
Jinquan, T., Quan, S., Jacobi, H. H., Madsen, H. O., Glue, C., Skov, P. S., Malling, H. J. and Poulsen, L. K. (2000). CXC chemokine receptor 4 expression and stromal cell-derived factor-1alpha-induced chemotaxis in CD4+ T lymphocytes are regulated by interleukin-4 and interleukin-10. *Immunology,* 99(3)**,** 402-10.
Johnson, Z., Schwarz, M., Power, C. A., Wells, T. N. and Proudfoot, A. E. (2005). Multi-faceted strategies to combat disease by interference with the chemokine system. *Trends Immunol,* 26(5)**,** 268-74.
Johnstone, R. W., Andrew, S. M., Hogarth, M. P., Pietersz, G. A. and Mckenzie, I. F. (1990). The effect of temperature on the binding kinetics and equilibrium constants of monoclonal antibodies to cell surface antigens. *Mol Immunol,* 27(4)**,** 327-33.
Jolliffe, I. T. (2002). *Principal component analysis. 2nd* edn. New York: Springer.
Kallikourdis, M., Trovato, A. E., Anselmi, F., Sarukhan, A., Roselli, G., Tassone, L., Badolato, R. and Viola, A. (2013). The CXCR4 mutations in WHIM syndrome impair the stability of the T-cell immunologic synapse. *Blood,* 122(5)**,** 666-73.
Kasai, R. S., Suzuki, K. G. N., Prossnitz, E. R., Koyama-Honda, I., Nakada, C., Fujiwara, T. K. and Kusumi, A. (2011). Full characterization of GPCR monomer-dimer dynamic equilibrium by single molecule imaging. *J Cell Biol,* 192(3)**,** 463-80.
Kelly, E., Bailey, C. P. and Henderson, G. (2008). Agonist-selective mechanisms of GPCR desensitization. *Br J Pharmacol,* 153(Suppl 1), S379-88.
Khanam, N., Mikoryak, C., Draper, R. K. and Balkus, K. J. Jr. (2007). Electrospun linear polyethyleneimine scaffolds for cell growth. *Acta Biomater,* 3(6)**,** 1050-9.

Khatibzadeh, N., Spector, A. A., Brownell, W. E. and Anvari, B. (2013). Effects of plasma membrane cholesterol level and cytoskeleton F-actin on cell protrusion mechanics. *PLoS One,* 8(2)**,** e57147.

King, M. R. (2004). Apparent 2-D diffusivity in a ruffled cell membrane. *J Theor Biol,* 227(3), 323-6.

Klein, C. and Waharte, F. (2010). Analysis of molecular mobility by fluorescence recovery after photobleaching in living cells. In: A. Méndez-Vilas, and J. Díaz, (Eds.) *Microscopy: Science, Technology, Applications and Education.* Badajoz, Spain: FORMATEX, pp. 772-83.

Kline, M. A., O'connor Butler, E. S., Hinzey, A., Sliman, S., Kotha, S. R., Marsh, C. B., Uppu, R. M. and Parinandi, N. L. (2010). A simple method for effective and safe removal of membrane cholesterol from lipid rafts in vascular endothelial cells: implications in oxidant-mediated lipid signaling. *Methods Mol Biol,* 610, 201-11.

Kobayashi, T., Beuchat, M. H., Lindsay, M., Frias, S., Palmiter, R. D., Sakuraba, H., Parton, R. G. and Gruenberg, J. (1999). Late endosomal membranes rich in lysobisphosphatidic acid regulate cholesterol transport. *Nat Cell Biol,* 1(2)**,** 113-8.

Koltsova, E. K., Garcia, Z., Chodaczek, G., Landau, M., Mcardle, S., Scott, S. R., von Vietinghoff, S., Galkina, E., Miller, Y. I., Acton, S. T. and Ley, K. (2012). Dynamic T cell-APC interactions sustain chronic inflammation in atherosclerosis. *J Clin Invest,* 122(9)**,** 3114-26.

Krakauer, T. (2013). Update on staphylococcal superantigen-induced signaling pathways and therapeutic interventions. *Toxins (Basel),* 5(9)**,** 1629-54.

Krummel, M. F. and Cahalan, M. D. (2010). The immunological synapse: a dynamic platform for local signaling. *J Clin Immunol,* 30(3)**,** 364-72.

Krummel, M. F., Sjaastad, M. D., Wülfing, C. and Davis, M. M. (2000). Differential clustering of CD4 and CD3zeta during T cell recognition. *Science,* 289(5483)**,** 1349-52.

Kumar, A., Humphreys, T. D., Kremer, K. N., Bramati, P. S., Bradfield, L., Edgar, C. E. and Hedin, K. E. (2006). CXCR4 physically associates with the T cell receptor to signal in T cells. *Immunity,* 25(2)**,** 213-24.

Kumar, A., Kremer, K. N., Dominguez, D., Tadi, M. and Hedin, K. E. (2011). Gα13 and Rho mediate endosomal trafficking of CXCR4 into Rab11+ vesicles upon stromal cell-derived factor-1 stimulation. *J Immunol,* 186(2)**,** 951-8.

Kummerow, C., Junker, C., Kruse, K., Rieger, H., Quintana, A. and Hoth, M. (2009). The immunological synapse controls local and global calcium signals in T lymphocytes. *Immunol Rev,* 231(1)**,** 132-47.

Kusumi, A., Ike, H., Nakada, C., Murase, K. and Fujiwara, T. (2005). Single-molecule tracking of membrane molecules: plasma membrane compartmentalization and dynamic assembly of raft-philic signaling molecules. *Semin Immunol,* 17(1)**,** 3-21.

Kwik, J., Boyle, S., Fooksman, D., Margolis, L., Sheetz, M. P. and Edidin, M. (2003). Membrane cholesterol, lateral mobility, and the phosphatidylinositol 4,5-bisphosphate-dependent organization of cell actin. *Proc Natl Acad Sci U S A,* 100(24)**,** 13964-9.

Lämmermann, T., Bader, B. L., Monkley, S. J., Worbs, T., Wedlich-Soldner, R., Hirsch, K., Keller, M., Förster, R., Critchley, D. R., Fässler, R. and Sixt, M. (2008). Rapid leukocyte migration by integrin-independent flowing and squeezing. *Nature,* 453(7191)**,** 51-5.

Lando, P. A., Olsson, C., Kalland, T., Newton, D., Kotb, M. and Dohlsten, M. (1996). Regulation of superantigen-induced T cell activation in the absence and the presence of MHC class II. *J Immunol,* 157(7)**,** 2857-63.

Lange, Y., Ye, J., Rigney, M. and Steck, T. (2000). Cholesterol movement in Niemann-Pick type C cells and in cells treated with amphiphiles. *J Biol Chem,* 275(23)**,** 17468-75.

Langmead, C. J. and Christopoulos, A. (2014). Functional and structural perspectives on allosteric modulation of GPCRs. *Curr Opin Cell Biol,* 27, 94-101.

Lee, B., Sharron, M., Blanpain, C., Doranz, B. J., Vakili, J., Setoh, P., Berg, E., Liu, G., Guy, H. R., Durell, S. R., Parmentier, M., Chang, C. N., Price, K., Tsang, M. and Doms, R. W. (1999a). Epitope mapping of CCR5 reveals multiple conformational states and distinct but overlapping structures involved in chemokine and coreceptor function. *J Biol Chem,* 274(14)**,** 9617-26.

Lee, B., Sharron, M., Montaner, L. J., Weissman, D. and Doms, R. W. (1999b). Quantification of CD4, CCR5, and CXCR4 levels on lymphocyte subsets, dendritic cells, and differentially conditioned monocyte-derived macrophages. *Proc Natl Acad Sci U S A,* 96(9)**,** 5215-20.

Lemay, J., Marullo, S., Jockers, R., Alizon, M. and Brelot, A. (2005). On the dimerization of CCR5. *Nat Immunol,* 6(6)**,** 535; author reply 535-6.

Levental, I., Byfield, F. J., Chowdhury, P., Gai, F., Baumgart, T. and Janmey, P. A. (2009). Cholesterol-dependent phase separation in cell-derived giant plasma-membrane vesicles. *Biochem J,* 424(2)**,** 163-7.

Levental, I., Lingwood, D., Grzybek, M., Coskun, U. and Simons, K. (2010). Palmitoylation regulates raft affinity for the majority of integral raft proteins. *Proc Natl Acad Sci U S A,* 107(51)**,** 22050-4.

Libby, P., Lichtman, A. H. and Hansson, G. K. (2013). Immune effector mechanisms implicated in atherosclerosis: from mice to humans. *Immunity,* 38(6)**,** 1092-104.

Lillemeier, B. F., Pfeiffer, J. R., Surviladze, Z., Wilson, B. S. and Davis, M. M. (2006). Plasma membrane-associated proteins are clustered into islands attached to the cytoskeleton. *Proc Natl Acad Sci U S A,* 103(50)**,** 18992-7.

Lim, H. W., Lee, J., Hillsamer, P. and Kim, C. H. (2008). Human Th17 cells share major trafficking receptors with both polarized effector T cells and FOXP3+ regulatory T cells. *J Immunol,* 180(1)**,** 122-9.

Lingwood, D. and Simons, K. (2010). Lipid rafts as a membrane-organizing principle. *Science,* 327(5961)**,** 46-50.

Lioudyno, M. I., Kozak, J. A., Penna, A., Safrina, O., Zhang, S. L., Sen, D., Roos, J., Stauderman, K. A. and Cahalan, M. D. (2008). Orai1 and STIM1 move to the immunological synapse and are up-regulated during T cell activation. *Proc Natl Acad Sci U S A,* 105(6)**,** 2011-6.

Luxembourg, A. and Grey, H. (2002). Strong induction of tyrosine phosphorylation, intracellular calcium, nuclear transcription factors and interferongamma, but weak induction of IL-2 in naïve T cells stimulated by bacterial superantigen. *Cell Immunol,* 219(1)**,** 28-37.

Mack, M., Luckow, B., Nelson, P. J., Cihak, J., Simmons, G., Clapham, P. R., Signoret, N., Marsh, M., Stangassinger, M., Borlat, F., Wells, T. N., Schlondorff, D. and Proudfoot, A. E. (1998). Aminooxypentane-RANTES induces CCR5 internalization but inhibits recycling: a novel inhibitory mechanism of HIV infectivity. *J Exp Med,* 187(8)**,** 1215-24.

Maier, R., Bartolomé-Rodríguez, M. M., Moulon, C., Weltzien, H. U. and Meyerhans, A. (2000). Kinetics of CXCR4 and CCR5 up-regulation and human immunodeficiency virus expansion after antigenic stimulation of primary CD4(+) T lymphocytes. *Blood,* 96(5)**,** 1853-6.

Mantovani, A., Biswas, S. K., Galdiero, M. R., Sica, A. and Locati, M. (2013). Macrophage plasticity and polarization in tissue repair and remodelling. *J Pathol,* 229(2)**,** 176-85.

Mantovani, A., Sica, A., Sozzani, S., Allavena, P., Vecchi, A. and Locati, M. (2004). The chemokine system in diverse forms of macrophage activation and polarization. *Trends Immunol,* 25(12)**,** 677-86.

Mantovani, A., Sozzani, S., Locati, M., Allavena, P. and Sica, A. (2002). Macrophage polarization: tumor-associated macrophages as a paradigm for polarized M2 mononuclear phagocytes. *Trends Immunol,* 23(11)**,** 549-55.

Mariotti, S. and Nisini, R. (2009). Generation of human T cell clones. *Methods Mol Biol,* 514, 65-93.

Martinez, F. O., Gordon, S., Locati, M. and Mantovani, A. (2006). Transcriptional profiling of the human monocyte-to-macrophage differentiation and polarization: new molecules and patterns of gene expression. *J Immunol,* 177(10)**,** 7303-11.
Martinez, F. O., Helming, L. and Gordon, S. (2009). Alternative activation of macrophages: an immunologic functional perspective. *Annu Rev Immunol,* 27, 451-83.
Meier, C. L., Svensson, M. and Kaye, P. M. (2003). Leishmania-induced inhibition of macrophage antigen presentation analyzed at the single-cell level. *J Immunol,* 171(12)**,** 6706-13.
Mlcochova, P., Pelchen-Matthews, A. and Marsh, M. (2013). Organization and regulation of intracellular plasma membrane-connected HIV-1 assembly compartments in macrophages. *BMC Biol,* 11**,** 89.
Molon, B., Gri, G., Bettella, M., Gómez-Moutón, C., Lanzavecchia, A., Martínez-A, C., Mañes, S. and Viola, A. (2005). T cell costimulation by chemokine receptors. *Nat Immunol,* 6(5)**,** 465-71.
Monks, C. R., Freiberg, B. A., Kupfer, H., Sciaky, N. and Kupfer, A. (1998). Three-dimensional segregation of supramolecular activation clusters in T cells. *Nature,* 395(6697)**,** 82-6.
Morales-Tirado, V., Johannson, S., Hanson, E., Howell, A., Zhang, J., Siminovitch, K. A. and Fowell, D. J. (2004). Cutting edge: selective requirement for the Wiskott-Aldrich syndrome protein in cytokine, but not chemokine, secretion by CD4+ T cells. *J Immunol,* 173(2)**,** 726-30.
Moreau, H. D., Lemaitre, F., Terriac, E., Azar, G., Piel, M., Lennon-Dumenil, A. M. and Bousso, P. (2012). Dynamic in situ cytometry uncovers T cell receptor signaling during immunological synapses and kinapses in vivo. *Immunity,* 37(2)**,** 351-63.
Morgan, M. M., Labno, C. M., Van Seventer, G. A., Denny, M. F., Straus, D. B. and Burkhardt, J. K. (2001). Superantigen-induced T cell:B cell conjugation is mediated by LFA-1 and requires signaling through Lck, but not ZAP-70. *J Immunol,* 167(10)**,** 5708-18.
Moriuchi, M., Moriuchi, H., Turner, W. and Fauci, A. S. (1997). Cloning and analysis of the promoter region of CXCR4, a coreceptor for HIV-1 entry. *J Immunol,* 159(9)**,** 4322-9.
Morone, N., Fujiwara, T., Murase, K., Kasai, R. S., Ike, H., Yuasa, S., Usukura, J. and Kusumi, A. (2006). Three-dimensional reconstruction of the membrane skeleton at the plasma membrane interface by electron tomography. *J Cell Biol,* 174(6)**,** 851-62.
Morris, D. L., Cho, K. W., Delproposto, J. L., Oatmen, K. E., Geletka, L. M., Martinez-Santibanez, G., Singer, K. and Lumeng, C. N. (2013). Adipose tissue macrophages function as antigen-presenting cells and regulate adipose tissue CD4+ T cells in mice. *Diabetes,* 62(8)**,** 2762-72.
Morris, G. P. and Allen, P. M. (2012). How the TCR balances sensitivity and specificity for the recognition of self and pathogens. *Nat Immunol,* 13(2)**,** 121-8.
Motulsky, H. J. and Brown, R. E. (2006). Detecting outliers when fitting data with nonlinear regression - a new method based on robust nonlinear regression and the false discovery rate. *BMC Bioinformatics,* 7**,** 123.
Motulsky, H. J. and Christopoulos, A. (2003). *Fitting models to biological data using linear and nonlinear regression. A practical guide to curve fitting.* San Diego CA: GraphPad Software Inc.
Mrass, P., Petravic, J., Davenport, M. P. and Weninger, W. (2010). Cell-autonomous and environmental contributions to the interstitial migration of T cells. *Semin Immunopathol,* 32(3)**,** 257-74.
Mueller, A., Kelly, E. and Strange, P. G. (2002). Pathways for internalization and recycling of the chemokine receptor CCR5. *Blood,* 99(3)**,** 785-91.
Murdoch, C. (2000). CXCR4: chemokine receptor extraordinaire. *Immunol Rev,* 177, 175-84.

Murphy, K., Travers, P., Walport, M. and Janeway, C. (2011). *Janeway's immunobiology. 8th* Edn. New York: Garland Science.
Murray, P. J. (1999). Defining the requirements for immunological control of mycobacterial infections. *Trends Microbiol,* 7(9)**,** 366-372.
Murray, P. J. and Wynn, T. A. (2011). Protective and pathogenic functions of macrophage subsets. *Nat Rev Immunol,* 11(11)**,** 723-37.
Naif, H. M., Li, S., Alali, M., Sloane, A., Wu, L., Kelly, M., Lynch, G., Lloyd, A. and Cunningham, A. L. (1998). CCR5 expression correlates with susceptibility of maturing monocytes to human immunodeficiency virus type 1 infection. *J Virol,* 72(1)**,** 830-6.
Nakata, H., Kruhlak, M., Kamata, W., Ogata-Aoki, H., Li, J., Maeda, K., Ghosh, A. K. and Mitsuya, H. (2010). Effects of CC chemokine receptor 5 (CCR5) inhibitors on the dynamics of CCR5 and CC-chemokine-CCR5 interactions. *Antivir Ther,* 15(3)**,** 321-31.
Negulescu, P. A., Krasieva, T. B., Khan, A., Kerschbaum, H. H. and Cahalan, M. D. (1996). Polarity of T cell shape, motility, and sensitivity to antigen. *Immunity,* 4(5)**,** 421-30.
Nguyen, D. H., Giri, B., Collins, G. and Taub, D. D. (2005). Dynamic reorganization of chemokine receptors, cholesterol, lipid rafts, and adhesion molecules to sites of CD4 engagement. *Exp Cell Res,* 304(2)**,** 559-69.
Nguyen, D. H. and Taub, D. (2002). Cholesterol is essential for macrophage inflammatory protein 1 beta binding and conformational integrity of CC chemokine receptor 5. *Blood,* 99(12)**,** 4298-306.
Nogueira, E., Hamour, S., Sawant, D., Henderson, S., Mansfield, N., Chavele, K. M., Pusey, C. D. and Salama, A. D. (2010). Serum IL-17 and IL-23 levels and autoantigen-specific Th17 cells are elevated in patients with ANCA-associated vasculitis. *Nephrol Dial Transplant,* 25(7)**,** 2209-17.
Ochsenreither, S., Fusi, A., Busse, A., Nagorsen, D., Schrama, D., Becker, J., Thiel, E. and Keilholz, U. (2008). Relative quantification of TCR Vbeta-chain families by real time PCR for identification of clonal T-cell populations. *J Transl Med,* 6, 34.
Oh, P. and Schnitzer, J. E. (2001). Segregation of heterotrimeric G proteins in cell surface microdomains. G(q) binds caveolin to concentrate in caveolae, whereas G(i) and G(s) target lipid rafts by default. *Mol Biol Cell,* 12(3)**,** 685-98.
Omoe, K., Nunomura, W., Kato, H., Li, Z. J., Igarashi, O., Araake, M., Sano, K., Ono, H. K., Abe, Y., Hu, D. L., Nakane, A., Kiyono, H., Takakuwa, Y., Shinagawa, K., Uchiyama, T. and Imanishi, K. (2010). High affinity of interaction between superantigen and T cell receptor Vbeta molecules induces a high level and prolonged expansion of superantigen-reactive CD4+ T cells. *J Biol Chem,* 285(40)**,** 30427-35.
Opalek, J. M., Ali, N. A., Lobb, J. M., Hunter, M. G. and Marsh, C. B. (2007). Alveolar macrophages lack CCR2 expression and do not migrate to CCL2. *J Inflamm (Lond),* 4, 19.
Oppermann, M. (2004). Chemokine receptor CCR5: insights into structure, function, and regulation. *Cell Signal,* 16(11)**,** 1201-10.
Parish, C. R., Glidden, M. H., Quah, B. J. and Warren, H. S. (2009). Use of the intracellular fluorescent dye CFSE to monitor lymphocyte migration and proliferation. *Curr Protoc Immunol,* Chapter 4, Unit 4 9.
Patrussi, L., Ulivieri, C., Lucherini, O. M., Paccani, S. R., Gamberucci, A., Lanfrancone, L., Pelicci, P. G. and Baldari, C. T. (2007). p52Shc is required for CXCR4-dependent signaling and chemotaxis in T cells. *Blood,* 110(6)**,** 1730-8.
Pelchen-Matthews, A., da Silva, R. P., Bijlmakers, M. J., Signoret, N., Gordon, S. and Marsh, M. (1998). Lack of p56lck expression correlates with CD4 endocytosis in primary lymphoid and myeloid cells. *Eur J Immunol,* 28(11)**,** 3639-47.
Percherancier, Y., Planchenault, T., Valenzuela-Fernandez, A., Virelizier, J. L., Arenzana-Seisdedos, F. and Bachelerie, F. (2001). Palmitoylation-dependent control of

degradation, life span, and membrane expression of the CCR5 receptor. *J Biol Chem,* 276(34)**,** 31936-44.
Pérez-Martínez, M., Gordon-Alonso, M., Cabrero, J. R., Barrero-Villar, M., Rey, M., Mittelbrunn, M., Lamana, A., Morlino, G., Calabia, C., Yamazaki, H., Shirao, T., Vázquez, J., González-Amaro, R., Veiga, E. and Sánchez-Madrid, F. (2010). F-actin-binding protein drebrin regulates CXCR4 recruitment to the immune synapse. *J Cell Sci,* 123(Pt 7)**,** 1160-70.
Phair, R. D., Gorski, S. A. and Misteli, T. (2004). Measurement of dynamic protein binding to chromatin in vivo, using photobleaching microscopy. *Methods Enzymol,* 375**,** 393-414.
Pike, L. J. (2006). Rafts defined: a report on the Keystone symposium on lipid rafts and cell function. *J Lipid Res,* 47(7)**,** 1597-8.
Pike, L. J. (2009). The challenge of lipid rafts. *J Lipid Res,* 50(Suppl),S323-8.
Pilch-Cooper, H. A., Sieg, S. F., Hope, T. J., Koons, A., Escola, J. M., Offord, R., Veazey, R. S., Mosier, D. E., Clagett, B., Medvik, K., Jadlowsky, J. K., Chance, M. R., Kiselar, J. G., Hoxie, J. A., Collman, R. G., Riddick, N. E., Mercanti, V., Hartley, O. and Lederman, M. M. (2011). Circulating human CD4 and CD8 T cells do not have large intracellular pools of CCR5. *Blood,* 118(4)**,** 1015-9.
Press, W. H. (2007). *Numerical recipes : the art of scientific computing. 3rd* Edn. Cambridge, UK: Cambridge University Press.
Proudfoot, A. E., Buser, R., Borlat, F., Alouani, S., Soler, D., Offord, R. E., Schröder, J. M., Power, C. A. and Wells, T. N. (1999). Amino-terminally modified RANTES analogues demonstrate differential effects on RANTES receptors. *J Biol Chem,* 274(45)**,** 32478-85.
Puthenveedu, M. A. and von Zastrow, M. (2006). Cargo regulates clathrin-coated pit dynamics. *Cell,* 127(1)**,** 113-24.
Rahimpour, R., Mitchell, G., Khandaker, M. H., Kong, C., Singh, B., Xu, L., Ochi, A., Feldman, R. D., Pickering, J. G., Gill, B. M. and Kelvin, D. J. (1999). Bacterial superantigens induce down-modulation of CC chemokine responsiveness in human monocytes via an alternative chemokine ligand-independent mechanism. *J Immunol,* 162(4)**,** 2299-307.
Rawat, S. S., Zimmerman, C., Johnson, B. T., Cho, E., Lockett, S. J., Blumenthal, R. and Puri, A. (2008). Restricted lateral mobility of plasma membrane CD4 impairs HIV-1 envelope glycoprotein mediated fusion. *Mol Membr Biol,* 25(1)**,** 83-94.
Reay, P. A., Matsui, K., Haase, K., Wulfing, C., Chien, Y. H. and Davis, M. M. (2000). Determination of the relationship between T cell responsiveness and the number of MHC-peptide complexes using specific monoclonal antibodies. *J Immunol,* 164(11)**,** 5626-34.
Réthi, B., Detre, C., Gogolák, P., Kolonics, A., Magócsi, M. and Rajnavölgyi, E. (2002). Flow cytometry used for the analysis of calcium signaling induced by antigen-specific T-cell activation. *Cytometry,* 47(4)**,** 207-16.
Revy, P., Sospedra, M., Barbour, B. and Trautmann, A. (2001). Functional antigen-independent synapses formed between T cells and dendritic cells. *Nat Immunol,* 2(10)**,** 925-31.
Rey-Giraud, F., Hafner, M. and Ries, C. H. (2012). In vitro generation of monocyte-derived macrophages under serum-free conditions improves their tumor promoting functions. *PLoS One,* 7(8)**,** e42656.
Richardson, M. W., Jadlowsky, J., Didigu, C. A., Doms, R. W. and Riley, J. L. (2012). Kruppel-like factor 2 modulates CCR5 expression and susceptibility to HIV-1 infection. *J Immunol,* 189(8)**,** 3815-21.
Ringnér, M. (2008). What is principal component analysis? *Nat Biotechnol,* 26(3)**,** 303-4.
Riol-Blanco, L., Delgado-Martín, C., Sánchez-Sánchez, N., Alonso, C. L., Gutiérrez-López, M. D., Del Hoyo, G. M., Navarro, J., Sánchez-Madrid, F., Cabañas, C., Sánchez-Mateos, P. and Rodríguez-Fernández, J. L. (2009). Immunological synapse formation inhibits, via NF-kappaB and FOXO1, the apoptosis of dendritic cells. *Nat Immunol,* 10(7)**,** 753-60.

Rot, A. and von Andrian, U. H. (2004). Chemokines in innate and adaptive host defense: basic chemokinese grammar for immune cells. *Annu Rev Immunol,* 22, 891-928.
Ruardij, T. G., Goedbloed, M. H. and Rutten, W. L. C. (2003). Long-term adhesion and survival of dissociated cortical neurons on miniaturised chemical patterns. *Med Biol Eng Comput,* 41(2)**,** 227-32.
Salles, A., Billaudeau, C., Sergé, A., Bernard, A. M., Phélipot, M. C., Bertaux, N., Fallet, M., Grenot, P., Marguet, D., He, H. T. and Hamon, Y. (2013). Barcoding T cell calcium response diversity with Methods for Automated and Accurate Analysis of Cell Signals (MAAACS). *PLoS Comput Biol,* 9(9)**,** e1003245.
Sallusto, F., Geginat, J. and Lanzavecchia, A. (2004). Central memory and effector memory T cell subsets: function, generation, and maintenance. *Annu Rev Immunol,* 22, 745-63.
Sallusto, F., Lenig, D., Förster, R., Lipp, M. and Lanzavecchia, A. (1999). Two subsets of memory T lymphocytes with distinct homing potentials and effector functions. *Nature,* 401(6754)**,** 708-12.
Sbalzarini, I. F., Mezzacasa, A., Helenius, A. and Koumoutsakos, P. (2005). Effects of organelle shape on fluorescence recovery after photobleaching. *Biophys J,* 89(3)**,** 1482-92.
Scholer, A., Hugues, S., Boissonnas, A., Fetler, L. and Amigorena, S. (2008). Intercellular adhesion molecule-1-dependent stable interactions between T cells and dendritic cells determine CD8+ T cell memory. *Immunity,* 28(2)**,** 258-70.
Scholten, D. J., Canals, M., Maussang, D., Roumen, L., Smit, M. J., Wijtmans, M., de Graaf, C., Vischer, H. F. and Leurs, R. (2012). Pharmacological modulation of chemokine receptor function. *Br J Pharmacol,* 165(6)**,** 1617-43.
Schubert, D. A., Gordo, S., Sabatino, J. J., Vardhana, S., Gagnon, E., Sethi, D. K., Seth, N. P., Choudhuri, K., Reijonen, H., Nepom, G. T., Evavold, B. D., Dustin, M. L. and Wucherpfennig, K. W. (2012). Self-reactive human CD4 T cell clones form unusual immunological synapses. *J Exp Med,* 209(2)**,** 335-52.
Schulz, C., Gomez Perdiguero, E., Chorro, L., Szabo-Rogers, H., Cagnard, N., Kierdorf, K., Prinz, M., Wu, B., Jacobsen, S. E., Pollard, J. W., Frampton, J., Liu, K. J. and Geissmann, F. (2012). A lineage of myeloid cells independent of Myb and hematopoietic stem cells. *Science,* 336(6077)**,** 86-90.
Shamri, R., Grabovsky, V., Gauguet, J. M., Feigelson, S., Manevich, E., Kolanus, W., Robinson, M. K., Staunton, D. E., von Andrian, U. H. and Alon, R. (2005). Lymphocyte arrest requires instantaneous induction of an extended LFA-1 conformation mediated by endothelium-bound chemokines. *Nat Immunol,* 6(5)**,** 497-506.
Shen, R., Meng, G., Ochsenbauer, C., Clapham, P. R., Grams, J., Novak, L., Kappes, J. C., Smythies, L. E. and Smith, P. D. (2011). Stromal down-regulation of macrophage CD4/CCR5 expression and NF-κB activation mediates HIV-1 non-permissiveness in intestinal macrophages. *PLoS Pathog,* 7(5)**,** e1002060.
Shen, R., Richter, H. E., Clements, R. H., Novak, L., Huff, K., Bimczok, D., Sankaran-Walters, S., Dandekar, S., Clapham, P. R., Smythies, L. E. and Smith, P. D. (2009). Macrophages in vaginal but not intestinal mucosa are monocyte-like and permissive to human immunodeficiency virus type 1 infection. *J Virol,* 83(7)**,** 3258-67.
Shirvani, H., Achour, L., Scott, M. G., Thuret, A., Labbé-Jullié, C., Bismuth, G. and Marullo, S. (2011). Evidence for internal stores of CCR5 in blood cells. *Blood,* 118(4)**,** 1175-6.
Sica, A. and Mantovani, A. (2012). Macrophage plasticity and polarization: in vivo veritas. *J Clin Invest,* 122(3)**,** 787-95.
Signoret, N., Christophe, T., Oppermann, M. and Marsh, M. (2004). pH-independent endocytic cycling of the chemokine receptor CCR5. *Traffic,* 5(7)**,** 529-43.
Signoret, N., Hewlett, L., Wavre, S., Pelchen-Matthews, A., Oppermann, M. and Marsh, M. (2005). Agonist-induced endocytosis of CC chemokine receptor 5 is clathrin dependent. *Mol Biol Cell,* 16(2)**,** 902-17.

Signoret, N., Oldridge, J., Pelchen-Matthews, A., Klasse, P. J., Tran, T., Brass, L. F., Rosenkilde, M. M., Schwartz, T. W., Holmes, W., Dallas, W., Luther, M. A., Wells, T. N., Hoxie, J. A. and Marsh, M. (1997). Phorbol esters and SDF-1 induce rapid endocytosis and down modulation of the chemokine receptor CXCR4. *J Cell Biol,* 139(3)**,** 651-64.

Signoret, N., Pelchen-Matthews, A., Mack, M., Proudfoot, A. E. and Marsh, M. (2000). Endocytosis and recycling of the HIV coreceptor CCR5. *J Cell Biol,* 151(6)**,** 1281-94.

Signoret, N., Rosenkilde, M. M., Klasse, P. J., Schwartz, T. W., Malim, M. H., Hoxie, J. A. and Marsh, M. (1998). Differential regulation of CXCR4 and CCR5 endocytosis. *J Cell Sci,* 111(Pt 18), 2819-30.

Simons, K. and Ikonen, E. (1997). Functional rafts in cell membranes. *Nature,* 387(6633)**,** 569-72.

Simons, K. and Vaz, W. L. (2004). Model systems, lipid rafts, and cell membranes. *Annu Rev Biophys Biomol Struct,* 33, 269-95.

Singer, I., Scott, S., Kawka, D. W., Chin, J., Daugherty, B. L., DeMartino, J. A., DiSalvo, J., Gould, S. L., Lineberger, J. E., Malkowitz, L., Miller, M. D., Mitnaul, L., Siciliano, S. J., Staruch, M. J., Williams, H. R., Zweerink, H. J. and Springer, M. S. (2001). CCR5, CXCR4, and CD4 are clustered and closely apposed on microvilli of human macrophages and T cells. *J Virol,* 75(8)**,** 3779-90.

Singer, S. J. and Nicolson, G. L. (1972). The fluid mosaic model of the structure of cell membranes. *Science,* 175(4023)**,** 720-31.

Springael, J. Y., de Poorter, C., Deupi, X., Van Durme, J., Pardo, L. and Parmentier, M. (2007). The activation mechanism of chemokine receptor CCR5 involves common structural changes but a different network of interhelical interactions relative to rhodopsin. *Cell Signal,* 19(7)**,** 1446-56.

Steffens, C. M. and Hope, T. J. (2003). Localization of CD4 and CCR5 in living cells. *J Virol,* 77(8)**,** 4985-91.

Steffens, C. M. and Hope, T. J. (2004). Mobility of the human immunodeficiency virus (HIV) receptor CD4 and coreceptor CCR5 in living cells: implications for HIV fusion and entry events. *J Virol,* 78(17)**,** 9573-8.

Steinbach, F. and Thiele, B. (1994). Phenotypic investigation of mononuclear phagocytes by flow cytometry. *J Immunol Methods,* 174(1-2)**,** 109-22.

Stinchcombe, J. C., Majorovits, E., Bossi, G., Fuller, S. and Griffiths, G. M. (2006). Centrosome polarization delivers secretory granules to the immunological synapse. *Nature,* 443(7110)**,** 462-5.

Suffia, I., Reckling, S. K., Salay, G. and Belkaid, Y. (2005). A role for CD103 in the retention of CD4+CD25+ Treg and control of Leishmania major infection. *J Immunol,* 174(9)**,** 5444-55.

Takahashi, A., Camacho, P., Lechleiter, J. D. and Herman, B. (1999). Measurement of intracellular calcium. *Physiol Rev,* 79(4)**,** 1089-125.

Tan, Q., Zhu, Y., Li, J., Chen, Z., Han, G. W., Kufareva, I., Li, T., Ma, L., Fenalti, G., Li, J., Zhang, W., Xie, X., Yang, H., Jiang, H., Cherezov, V., Liu, H., Stevens, R. C., Zhao, Q. and Wu, B. (2013). Structure of the CCR5 chemokine receptor-HIV entry inhibitor maraviroc complex. *Science,* 341(6152)**,** 1387-90.

Tarasova, N. I., Stauber, R. H. and Michejda, C. J. (1998). Spontaneous and ligand-induced trafficking of CXC-chemokine receptor 4. *J Biol Chem,* 273(26)**,** 15883-6.

Thelen, M. (2001). Dancing to the tune of chemokines. *Nat Immunol,* 2(2)**,** 129-34.

Thelen, M. and Stein, J. V. (2008). How chemokines invite leukocytes to dance. *Nat Immunol,* 9(9)**,** 953-9.

Tillack, T. W. and Kinsky, S. C. (1973). A freeze-etch study of the effects of filipin on liposomes and human erythrocyte membranes. *Biochim Biophys Acta,* 323(1)**,** 43-54.

Tseng, S. Y., Liu, M. and Dustin, M. L. (2005). CD80 cytoplasmic domain controls localization of CD28, CTLA-4, and protein kinase Ctheta in the immunological synapse. *J Immunol,* 175(12)**,** 7829-36.

Tuosto, L., Parolini, I., Schröder, S., Sargiacomo, M., Lanzavecchia, A. and Viola, A. (2001). Organization of plasma membrane functional rafts upon T cell activation. *Eur J Immunol,* 31(2)**,** 345-9.

Tybulewicz, V. L. J. (2002). Chemokines and the immunological synapse. *Immunology,* 106(3)**,** 287-8.

Underhill, D. M., Bassetti, M., Rudensky, A. and Aderem, A. (1999). Dynamic interactions of macrophages with T cells during antigen presentation. *J Exp Med,* 190(12)**,** 1909-14.

Underwood, K. W., Jacobs, N. L., Howley, A. and Liscum, L. (1998). Evidence for a cholesterol transport pathway from lysosomes to endoplasmic reticulum that is independent of the plasma membrane. *J Biol Chem,* 273(7)**,** 4266-74.

van Meer, G., Voelker, D. R. and Feigenson, G. W. (2008). Membrane lipids: where they are and how they behave. *Nat Rev Mol Cell Biol,* 9(2)**,** 112-24.

Vancha, A. R., Govindaraju, S., Parsa, K. V. L., Jasti, M., González-García, M. and Ballestero, R. P. (2004). Use of polyethyleneimine polymer in cell culture as attachment factor and lipofection enhancer. *BMC Biotechnol,* 4, 23.

Varma, R., Campi, G., Yokosuka, T., Saito, T. and Dustin, M. L. (2006). T cell receptor-proximal signals are sustained in peripheral microclusters and terminated in the central supramolecular activation cluster. *Immunity,* 25(1)**,** 117-27.

Venkatesan, S., Petrovic, A., Locati, M., Kim, Y. O., Weissman, D. and Murphy, P. M. (2001). A membrane-proximal basic domain and cysteine cluster in the C-terminal tail of CCR5 constitute a bipartite motif critical for cell surface expression. *J Biol Chem,* 276(43)**,** 40133-45.

Venkatesan, S., Rose, J. J., Lodge, R., Murphy, P. M. and Foley, J. F. (2003). Distinct mechanisms of agonist-induced endocytosis for human chemokine receptors CCR5 and CXCR4. *Mol Biol Cell,* 14(8)**,** 3305-24.

Viard, M., Parolini, I., Sargiacomo, M., Fecchi, K., Ramoni, C., Ablan, S., Ruscetti, F. W., Wang, J. M. and Blumenthal, R. (2002). Role of cholesterol in human immunodeficiency virus type 1 envelope protein-mediated fusion with host cells. *J Virol,* 76(22)**,** 11584-95.

Viola, A. and Luster, A. D. (2008). Chemokines and their receptors: drug targets in immunity and inflammation. *Annu Rev Pharmacol Toxicol,* 48, 171-97.

Wang, J., Alvarez, R., Roderiquez, G., Guan, E. and Norcross, M. A. (2004). Constitutive association of cell surface CCR5 and CXCR4 in the presence of CD4. *J Cell Biochem,* 93(4)**,** 753-60.

Wang, J., Guan, E., Roderiquez, G., Calvert, V., Alvarez, R. and Norcross, M. A. (2001). Role of tyrosine phosphorylation in ligand-independent sequestration of CXCR4 in human primary monocytes-macrophages. *J Biol Chem,* 276(52)**,** 49236-43.

Weber, M., Hauschild, R., Schwarz, J., Moussion, C., De Vries, I., Legler, D. F., Luther, S. A., Bollenbach, T. and Sixt, M. (2013). Interstitial dendritic cell guidance by haptotactic chemokine gradients. *Science,* 339(6117)**,** 328-32.

Wei, S. H., Safrina, O., Yu, Y., Garrod, K. R., Cahalan, M. D. and Parker, I. (2007). Ca2+ signals in CD4+ T cells during early contacts with antigen-bearing dendritic cells in lymph node. *J Immunol,* 179(3)**,** 1586-94.

Weissman, D., Dybul, M., Daucher, M. B., Davey, R. T. Jr., Walker, R. E. and Kovacs, J. A. (2000). Interleukin-2 up-regulates expression of the human immunodeficiency virus fusion coreceptor CCR5 by CD4+ lymphocytes in vivo. *J Infect Dis,* 181(3)**,** 933-8.

Wetzel, S. A., Mckeithan, T. W. and Parker, D. C. (2002). Live-cell dynamics and the role of costimulation in immunological synapse formation. *J Immunol,* 169(11)**,** 6092-101.

Woolf, E., Grigorova, I., Sagiv, A., Grabovsky, V., Feigelson, S. W., Shulman, Z., Hartmann, T., Sixt, M., Cyster, J. G. and Alon, R. (2007). Lymph node chemokines promote sustained T lymphocyte motility without triggering stable integrin adhesiveness in the absence of shear forces. *Nat Immunol,* 8(10)**,** 1076-85.

Wu, B., Chien, E. Y., Mol, C. D., Fenalti, G., Liu, W., Katritch, V., Abagyan, R., Brooun, A., Wells, P., Bi, F. C., Hamel, D. J., Kuhn, P., Handel, T. M., Cherezov, V. and Stevens, R. C. (2010). Structures of the CXCR4 chemokine GPCR with small-molecule and cyclic peptide antagonists. *Science,* 330(6007)**,** 1066-71.

Wülfing, C. and Davis, M. M. (1998). A receptor/cytoskeletal movement triggered by costimulation during T cell activation. *Science,* 282(5397)**,** 2266-2269.

Wülfing, C., Rabinowitz, J. D., Beeson, C., Sjaastad, M. D., Mcconnell, H. M. and Davis, M. M. (1997). Kinetics and extent of T cell activation as measured with the calcium signal. *J Exp Med,* 185(10)**,** 1815-25.

Yokosuka, T., Kobayashi, W., Sakata-Sogawa, K., Takamatsu, M., Hashimoto-Tane, A., Dustin, M. L., Tokunaga, M. and Saito, T. (2008). Spatiotemporal regulation of T cell costimulation by TCR-CD28 microclusters and protein kinase C theta translocation. *Immunity,* 29(4)**,** 589-601.

Yokosuka, T., Sakata-Sogawa, K., Kobayashi, W., Hiroshima, M., Hashimoto-Tane, A., Tokunaga, M., Dustin, M. L. and Saito, T. (2005). Newly generated T cell receptor microclusters initiate and sustain T cell activation by recruitment of Zap70 and SLP-76. *Nat Immunol,* 6(12)**,** 1253-62.

Zaunders, J. J., Munier, M. L., Seddiki, N., Pett, S., Ip, S., Bailey, M., Xu, Y., Brown, K., Dyer, W. B., Kim, M., de Rose, R., Kent, S. J., Jiang, L., Breit, S. N., Emery, S., Cunningham, A. L., Cooper, D. A. and Kelleher, A. D. (2009). High levels of human antigen-specific CD4+ T cells in peripheral blood revealed by stimulated coexpression of CD25 and CD134 (OX40). *J Immunol,* 183(4)**,** 2827-36.

Zheng, C. Y., Petralia, R. S., Wang, Y. X. and Kachar, B. (2011). Fluorescence recovery after photobleaching (FRAP) of fluorescence tagged proteins in dendritic spines of cultured hippocampal neurons. *J Vis Exp,* 50.

Zigmond, E. and Jung, S. (2013). Intestinal macrophages: well educated exceptions from the rule. *Trends Immunol,* 34(4)**,** 162-8.